Imperial College London

Department of Chemical Engineering

TAR REMOVAL IN HOT GAS STREAMS

Anthony Odongo

Thesis Submitted for degree of Doctor of Philosophy (PhD) of

Imperial College London

September 2015

Declaration of Originality

I certify that all the work contained in this thesis is my own and all else is appropriately referenced.

Anthony Odongo

Copyright Declaration

The copyright of this thesis rests with the author and is made available under a Creative Commons Attribution Non-Commercial No Derivatives licence. Researchers are free to copy, distribute or transmit the thesis on the condition that they attribute it, that they do not use it for commercial purposes and that they do not alter, transform or build upon it. For any reuse or redistribution, researchers must make clear to others the licence term of this work.

Abstract

Thermal conversion of organic materials through gasification yields gaseous fuel. The fuel gas often requires cleaning and upgrading ahead of combustion in advanced technologies such as gas engines, fuel cells and turbines. Tar is one of the major impurities found in streams, and can foul and block equipment.

This study focuses on catalytic destruction of tar in a hot gas stream, at different operating conditions to improve the gas yield and quality. Steam gasification and reforming of tar involves thermal decomposition of tar and the reaction of tar with steam and fuel gases. These processes contribute to complex kinetics of the overall process involving a series of reactions, including: $CO + H_2O \leftrightarrow CO_2 + H_2$, $CO + 3H_2 \rightarrow CH_4 + H_2O$, $C + H_2O \rightarrow CO + H_2$, $CH_4 + 2H_2O \rightarrow CO_2 + 4H_2$, $CO_2 + 4H_2 \rightarrow CH_4 + 2H_2O$, $C + 2H_2O \rightarrow 2H_2 + CO_2$, $CO + 2H_2 \rightarrow CH_3OH$, $C + CO_2 \rightarrow 2CO$, $2C + H_2 \rightarrow C_2H_2$, & $C + 2H_2 \rightarrow CH_4$.

The concentration of each component affects the rate of reaction for each product. Introducing a catalyst to these processes increases the rate reactions and hence the number of successful reactions. The operating temperature, residence time and type of feedstock are other factors that can also affect the gas yield and quality.

In this work, a continuous fixed bed-reactor was developed and assembled at Imperial College London, and used to investigate the activity of Pt-, Rh- and Ni-based catalysts, provided by Johnson Matthey. Experiments were performed at temperatures from 700 ^oC to up to 950 ^oC. The carrier gas flow rate, the steam-to-carbon ratio and feed gas composition were also varied to investigate the reaction kinetics and reaction pathways.

Rh- and Pt-based catalysts had a better activity, thermal durability and corrosion resistance than the Ni-based catalyst. The Rh-catalyst results at considered conditions and above 800 ^oC were just about the same as the equilibrium results. Rh- had a better longevity and a tar conversion to syngas as high as 98% at 750 ^oC and S/C of 3. Ni deactivated within initial 30 minutes whereas the Rh- and Pt-catalyst activity remained steady.

Acknowledgments

I would like to express my sincere gratitude to my supervisors: Dr Marcos Millán-Agorio and Professor Klaus Hellgardt, who gave me the opportunity to pursue this PhD. Your knowledge, guidance and motivations were invaluable throughout my project. I am privileged to have been your student. I would also like to thank Dr. Andreas Kogelbauer my collaborating academic for being there to support me.

I thank my industrial supervisors: Dr. Liz Rowsell, Dr Stephen Poulston, Dr Andrew Steele and Dr Sonia Garcia at Johnson Matthey plc for the catalysts I have used in my project. You are remarkably amazing to work with. Thank you for sharing your views in support of my project, thank you for inviting me to JM centre for my industrial visits and also for inviting me to the conferences.

Thank you to Dr Nigel Paterson and Dr Cesar Berrueco for the constructive ideas throughout my project. You have been very supportive from the very beginning to the end. Your knowledge in gasification and in operating the Hot-Rod reactor was extremely inspiring. I also thank my PhD group whom together we have worked in the same labs, motivated each other and helped one another.

Thank you to Ms Susi Underwood, Ms Aleksandra Szymanska, Ms Anusha Sri-Pathmanathan, Ms Vani Thuvaragan, Ms Sarah Payne, Ms Patricia Carry and Mr Andrew Macey for your sustained support together with Mr Chin Lang, Mr Richard Wallington, Mr Tony Meredith, Mr Andrew Macey and James (from BOC).

Finally, I would like to thank Dr Christine Fernando, Dr Majella Fernando, The Winchcombe family, The Forbes family, Ms Helen Johnson, Dr Richard Taylor and Ms Hannah Edwards who have exceptionally been there to encourage and support me over the many years of my studies.

Contents

Declaration of Originality ii

Abstract iii

Acknowledgments iv

Contents v

Abbreviations & Nomenclature xvii

1. INTRODUCTION 1

1.1. Project aims 5

1.2. Thesis structure 6

2. LITERATURE REVIEW 8

2.1. Tar 8

2.2. Tar formation 12

2.3. Factors linked with tar characteristics 13

2.3.1. Reaction temperature 13

2.3.2. Feedstock (biomass composition) 16

2.3.3. Gasifier design 16

2.3.4. Fixed bed gasifiers 17

2.3.5. Fluidised-Bed Gasifier 20

2.3.6. Reactor pressure 23

2.3.7. Residence time 23

2.3.8. Gasifying agents 24

2.4. Tar removal 25

2.4.1. Primary measures 26

2.4.2. Secondary measures 27

2.5. Catalytic activity 28
2.5.1. Potential metallic catalysts for tar reduction 30
2.5.2. Potential Non-Metallic oxides 34
2.5.3. Other Tar cracking catalysts 39
2.6. Summary of the Literature review 40
3. EXPERIMENTAL PROCEDURE & ANALYTICAL TECHNIQUES 41
3.1. Materials and Experimental Procedure 41
3.1.1. Materials 41
3.1.2. Equipment Description 44
3.1.3. Reactor and Trap Description 47
3.1.4. Process Stages 50
3.1.5. Experimental Procedure 53
3.1.6. Analytical Techniques 61
3.2. Sources of errors, uncertainties and accuracy of materials 67
4. THERMODYNAMIC EQUILIBRIUM MODELLING AND PRELIMINARY TESTS 69
4.1. Thermodynamic Modelling in Aspen Plus 69
4.2. Thermodynamic Modelling and Equilibrium Results 70
4.2.1. Product Gas ratios 73
4.2.2. Conclusion Drawn from Equilibrium Data: 75
4.3. Preliminary Tests 76
4.3.1. Preliminary Tests Using Model Compounds 76
4.3.2. Preliminary Tests on Biomass Derived Tar 78
4.4. Summary 84
5. REACTOR DEVELOPMENT 86
5.1. Review of Previous Reactor 86

5.1.1. Original Reactor 86
5.1.2. Original method for steam generation 88
5.1.3. Original method used for cooling, extracting and analyzing products. 88
5.2. Modification to the reactor 91
5.2.1. Introduction to causes for modification 91
5.2.2. Objectives for the reactor modification 91
5.2.3. Material feeding / Introduction of Syringe Pumps 92
5.2.4. Introduction of a Pre-conditioning Chamber 95
5.2.5. Relocating the Bed Thermocouple 95
5.2.6. Determining the Bed Position 97
5.2.7. Determining the effect of CO_2 on the Hydrogen analyser 99
5.2.8. Determining an Appropriate Cooling Agent for the Second Trap 100
5.2.9. Introducing a Quartz Glass Liner inside the Metallic Reactor Tube 102
5.3. Summary 103
6. RESULTS AND DISCUSSION I: CONTRUST BETWEEN THE REACTOR BEFORE AND AFTER, AND TESTS AT HIGHER TEMPERATURES 106
6.1. The Contrast between the Reactor with and Without a Quartz Liner 108
6.2. Catalytic effect at 850 °C, 900 °C and 950 °C with an S/C 2 in a quartz reactor 109
6.2.1. Hydrogen formation at 850 – 950 °C with S/C of 2 111
6.2.2. Carbon monoxide formation at 850 – 950 °C with S/C of 2 112
6.2.3. Carbon dioxide formation at 850 – 950 °C with S/C of 2 113
6.2.4. Methane formation at 850 – 950 °C with S/C of 2 114
6.2.5. Carbon conversion at 850 – 950 °C and S/C of 2 in a Quartz Reactor 115
6.3. Thermal-Cracking and Reforming of Tar at 700 – 950 °C with an S/C of 2. 117

6.4. Conclusions 119

7. RESULTS AND DISCUSSION II: TAR REFORMING IN A QUARTZ LINED REACTOR AT 700 AND 750 °C UNDER DIFFERENT OPERATING VARIABLES 121

7.1. Thermodynamic Equilibrium Calculations to Validate the Operating Window 121

7.2. Pt-, Rh- and Ni-catalytic Reforming of Guaiacol and Toluene Mixture at 750 °C 122

7.3. Thermal- and Catalytic Cracking and Reforming of Tar 124

7.4. The Effects of Adding Steam to the Reactants in a Quartz Reactor at 750 °C125

7.5. Effects of Changing Residence Time 127

7.6. Effects of Adding Hydrogen 131

7.7. Effects of Adding a Syngas Mixture 134

7.8. Summary 138

8. RESULTS AND DISCUSSION III: THE ANALYSIS FOR SPENT CATALYSTS AND BY-PRODUCTS 140

8.1. Analytical Techniques Employed 140

8.1.1. Thermogravimetric Technique 140

8.1.2. Scanning Electron Microscopy, Raman and GC-MS techniques 141

8.2. Spent Catalysts and Trapped Liquids 141

8.2.1. Trapped Liquids 141

8.2.2. GC-MS analysis of Liquid Products 142

8.2.3. Analysis of the Fresh Pt, Rh and Ni-catalyst 143

8.2.4. Results Analysis of By-products from Model Compounds. 146

8.2.5. Results Analysis of Biomass Tar By-products when Using Pt-catalyst 148

8.2.6. Results Analysis of Biomass Tar By-products when Using Rh-catalyst 154

8.2.7. Results Analysis of Biomass Tar By-products when Using Ni-catalyst 157

8.2.8. Carbon conversion to Gas in a Quartz Reactor at 750 °C with Steam at an S/C of 3 160

8.3. Raman Analysis 161

8.4. FTIR analysis 162

9. CONCLUSIONS. 163

REFERENCES 174

Appendix 184

Appendix 1: Compounds Detected from GC-MS Analysis of Fresh Tar 184

Appendix 2: GC-MS Sample Emitted Spectra 199

Appendix 4: Fatigue Assessment of Reactor Vessel 205

Appendix 5: General Arrangement of Thermocouples Along the Reactor 208

Appendix 6: Heat conduction in the gas inside the heated reactor tube. 209

Appendix 7: Hydrogen Analyser Calibration 212

Appendix 8: Graphs Illustrating Gas Formation 214

Appendix 9: Graphical representation for data from Increasing S/C and Temperature. 216

List of Tables

Table 2:1: Classification of quantitatively analysed tar compounds 9

Table 2:2: List of tar compounds that are considered in classes 1, 2, to 5 [10] 11

Table 2:3: Typical compositions of tar generated from biomass gasification [12] 12

Table 2:4: Typical tar levels in various biomass gasifiers [4]. 20

Table 2:5: Classification of physical gas cleaning equipment [10] 26

Table 2:6: The typical reactions in the conversion of tar: [22]. 27

Table 2:7: Catalysts with related advantages and disadvantages 37

Table 3:1: The Ultimate Analysis of the Tar 42

Table 3:2: The Composition of the Fresh Catalyst..... 43
Table 3:3: The BET and BJH Analysis of the Fresh Catalyst Measured using a Micro-meter Accusorb 2100E 43
Table 3:4: The key operational process variables 55
Table 3:5: Multi-Gas Analyser Ranges..... 64
Table 3:6: Calibration and Producer Gas degree of accuracy 68
Table 3:7: Absolute Gas limits of gas accuracy..... 68
Table 4:1: Specified conditions for Aspen modelling 70
Table 4:2: Thermodynamic Modelling of Products from 850 ^{o}C, 900 ^{o}C and 950 ^{o}C and 1 bar reactor conditions and feed at 100 g/Nm^{3} of Tar in N_2 with an S/C of 3..... 73
Table 4:3: Carbon Balance: Non-catalysed test at 850 – 950, S/C 2 in an Incoloy Reactor 81
Table 4:4: Blank Repeated Tar Cracking with S/C 2 at 850, 900 and 950 ^{o}C in Quartz.... 83
Table 4:5: Fuel Gas Composition upon Tar Reforming With Platinum-Based Catalyst.... 83
Table 4:6: Fuel Gas Composition upon Tar Reforming With Rhodium-Based Catalyst ... 84
Table 4:7: Fuel Gas Composition upon Tar Reforming With Nickel-Based Catalyst 84
Table 5:1: Table describing the feeding times, feed composition and coolant in the Dewar 101
Table 6:1: Summary of Gas Composition Formed During the Reactions of 100 g/Nm^{3} of Tar in 0.209 L/min of N_2 with Steam at an S/C of 2 under Pt-, Rh- and Ni-Based Catalyst at 850, 900 and 950 °C in a Quartz Reactor. 110
Table 7:1: Thermodynamic Equilibrium Calculated Gas Data at 700°C, 750°C and 900°C at Different Steam-to-Carbon Ratios..... 122
Table 7:2: Product Formation from Tar Cracking at 750 °C without Steam 126
Table 7:3: Products Formation from Tar Reforming Without Steam and With Steam of an S/C Ratios of 1 -3 and Catalyst at 750 °C..... 126
Table 7:4: Gas formation and Carbon Balance at Different Flow Rate 128
Table 7:5: Gas and Carbon Formation in an Increased H_2 Concentration environment 131
Table 7:6: Product gas and Carbon Formation at 750 ^{o}C, S/C 3 in 0.627 l/min N_2 133
Table 7:7: Reforming tar at S/C of 3 in 0.209 l/min and 0.409 l/min N_2 at 750 °C 137

List of Figures

Figure 1:1: Left- Primary Inputs to Power, and Right - Energy and Emissions forecast..... 1
Figure 1:2: Illustration of some of the Tar molecules. [3] 4
Figure 2:1: Variation in primary, secondary and tertiary tar products with temperature [13]..... 15
Figure 2:2: The effects of maximum gasification temperature on tar yield [4]. 16
Figure 2:3: Tar production in an updraft gasifier correlated to temperature variation. . 18
Figure 2:4: Tar generation in a downdraft gasifier correlated to temperature variation 20
Figure 2:5: Principles Of Single And Circulating Fluid Bed Gasifiers. [27] 22
Figure 3:1: The sample weight at increasing temperature; from TGA analysis of feed tar 42
Figure 3:2: Conceptual Process Block Flow Diagram. 45
Figure 3:3: The Process Flow Diagram 46
Figure 3:4: Final Reactor Configuration..... 48
Figure 3:5: U-shaped Condensate Traps 49
Figure 3:6: Gas Line filter..... 53
Figure 3:7: The Reactor Temperature Controller..... 57
Figure 3:8: Process Control Diagram 60
Figure 3:9: The MGA Series Analyser – Basic gas flow arrangement..... 65
Figure 4:1: Equilibrium composition as a function of Temperature on a Dry-Basis. Feed at 100 g/Nm³ of Tar in N_2 and an S/C of 3..... 71
Figure 4:2: Thermodynamic Modelling of Products from a Feed on a Wet-Basis. Feed at 100 g/Nm³ of Tar in N_2 with an S/C of 3..... 72
Figure 4:3: Thermodynamic Modelling of Product Gases from a Feed on a Wet-Basis, excluding water in the Products. Feed at 100 g/m³ of Tar in N_2 with an S/C of 3 72
Figure 4:4: Syngas Ratios as a Function of Temperature. Feed at 100 g/Nm³ of Tar in N_2 with an S/C of 3. 74
Figure 4:5: Thermodynamic Equilibrium Product Gas Concentration from 100 g/Nm³ of Tar in N_2, at 750 ^{o}C with Increasing Steam in the Feed..... 75

Figure 4:6: Process Flow Diagram at JM Technical Centre reproduced from a shared document between JM and Imperial College. 77
Figure 4:7: Catalytic Conversion of Benzene and Methane at 900 °C (between 0 – 90 minutes) and 850 °C (Between 140 minutes to the end) with an S/C of 2.5 using Ph-, Pt- and Ni-Based Catalysts. 78
Figure 4:8: A Normalised Gas Composition With Steady Concentrations Obtained and a Fairly Good Signal Throughout the Entire Period of the Test. 79
Figure 4:9: Gas Formation in Non-catalysed test at 850 – 950 ^{O}C in an Incoloy reactor. 81
Figure 4:10: Tar Concentration in the Gas Products as a Function of Temperature from Reactions of 100 g/Nm³ of Tar with steam to carbon ratio of 3 in 0.209 L/min of N_2 at 850 °C, 900 ^{O}C and 950 °C 82
Figure 5:1: The initial arrangement of the first stage reactor. 87
Figure 5:2: Lay-out of the Tow-stage Reactor in the Configuration used by Dabai [75] . 90
Figure 5:3: Initial Feedings Set-up 92
Figure 5:4: Tar Clots Deposited on the Inner Walls of the Feed Tube. 93
Figure 5:5: Recovered Carbon from the Feed Nozzle at 500 $^{\circ}$C 93
Figure 5:6: Signal to the Gas Analyser as Gas Concentration with Time during a Reaction at 600 °C with S/C =2 and Tar at 30g/Nm^3. 94
Figure 5:7: The signal to the Gas Analysers as Gas Concentration with Time during a Reaction at 600 °C with an S/C of 2 and Feed at 100 g/Nm³ of Tar. 94
Figure 5:8: Reactor Design After the Primary Modifications. 96
Figure 5:9: Temperature distribution Along the Vertical Axis of the Reactor Tube, with 0.209 L/min N2 Flow at 900 °C Bed Temperature. 97
Figure 5:10: Reactor Tube with Multiple Thermocouple Points Distributed along Its Vertical Length. 98
Figure 5:11: Calibration curve to estimate the hydrogen content in CO_2 and H_2 gas environment. 99
Figure 5:12: Calibration curve to Estimate the Hydrogen content in CO_2 and N_2 gas environment. 100

Figure 5:13: Calibration Gas Concentration in N_2 Detected by Analysers after Passing through Liquid Nitrogen or a Dry-Ice Condensate Trap 101
Figure 5:14: Final Design of the Process Reactor 103
Figure 5:15: Quartz and Incoloy Reactor Tubes separately 104
Figure 5:16: Quartz Tube Lined Inside the Incoloy Tube..... 104
Figure 5:17: To the left is are the control equipment and to the right is the non lagged reactor connected to the condensate traps..... 105
Figure 6:1: Comparisons of results from reaction in Incoloy & Quartz reactors at 900 °C with an S/C of 2. 108
Figure 6:2: Hydrogen concentrations as a Function of Temperature, Formed during the Reactions of 100 g/Nm³ of Tar in 0.209 L/min N_2 with Steam at an S/C of 2 under Pt-, Rh- and Ni-catalysts at 850, 900 and 950 °C..... 111
Figure 6:3: CO concentrations as a Function of Temperature, Formed during the Reactions of 100 g/Nm³ of Tar in 0.209 L/min N_2 with Steam at an S/C of 2 under Pt-, Rh- and Ni-catalysts at 850, 900 and 950 °C..... 112
Figure 6:4: CO_2 Concentrations as a Function of Temperature, Formed during the Reactions of 100 g/Nm³ of Tar in 0.209 L/min N_2 with Steam at an S/C of 2 under Pt-, Rh- and Ni-catalysts at 850, 900 and 950 °C..... 113
Figure 6:5: CH_4 concentrations as a Function of Temperature, Formed during the Reactions of 100 g/Nm³ of Tar in 0.209 L/min N_2 with Steam at an S/C of 2 under Pt-, Rh- and Ni-catalysts at 850, 900 and 950 °C..... 114
Figure 6:6: Carbon Converted to Gas Products in a Quartz Reactor as a Function of Temperature, Formed during the Reactions of 100 g/Nm³ of Tar in 0.209 L/min N_2 with Steam at an S/C of 2 under Pt-, Rh- and Ni-catalysts at 850, 900 and 950 °C 116
Figure 6:7: Gas Formation in 0.209 L/min of N_2 at 700 - 950 ^{o}C from Tar Reactions with Steam at an S/C of 2. 118
Figure 7:1: Reforming of 100 g/Nm³ of 50% Guaiacol and 50% Toluene with an S/C of 3 in 0.209 L/min at 750 °C 123
Figure 7:2: Thermal reaction 130
Figure 7:3: Rh-catalyst activity 130

Figure 7:4: Pt-catalyst activity 130
Figure 7:5: Ni-catalyst activity 130
Figure 7:6: Gas Product and Catalytic Activity in H_2 Rich N_2 Environment 132
Figure 7:7: Reforming of Tar in Syngas and N_2 at 0.209 l/min 135
Figure 7:8: Reforming in Syngas at 0.402l/min 136
Figure 7:9: Carbon Conversion to Carbon in Product gas in a syngas mixture and in N_2 only 138
Figure 8:1: Liquid Products in Collected in Tar Traps; Orange - Yellowish from the first trap and Dark Brown to Black in the Second Trap, from Reforming Tar at 750 °C with S/C of 3 in 0.209 L/min of N_2. 142
Figure 8:2: Liquids FTIR Transmission Spectra 143
Figure 8:3: TGA for carbon decomposition from Fresh Pt-, Rh- and Ni-catalyst 143
Figure 8:4: SEM Imaging of Fresh Pt-catalyst 144
Figure 8:5: SEM Imaging of Fresh Rh-catalyst 145
Figure 8:6: SEM Imaging of Fresh Ni-catalyst 145
Figure 8:7: TGA for carbon decomposition from Spent Pt-, Rh- and Ni-catalyst in Model Compounds 146
Figure 8:8: Gas Concentration in 0.209 L/min of N_2 under Pt-catalyst Activity at 750 °C from 50% Guaiacol / Toluene Reforming Reactions with Steam at an S/C of 3 147
Figure 8:9: Gas Concentration in 0.209 L/min of N_2 under Rh-catalyst Activity at 750 °C from 50% Guaiacol / Toluene Reforming Reactions with Steam at an S/C of 3 147
Figure 8:10: Gas Concentration in 0.209 L/min N_2 under Ni-catalyst Activity at 750 °C from 50% Guaiacol/Toluene Reforming Reactions with Steam at an S/C of 3 148
Figure 8:11: TGA for Carbon Decomposition from Spent Pt-Catalyst from Reactions of Biomass-Derived Tar at 750 °C and an S/C Of 3 149
Figure 8:12: TGA for Carbon Decomposition from Spent Pt-Catalyst from Reactions of Biomass-Derived Tar at 750 °C and an S/C of 2 149
Figure 8:13: TGA for Carbon Decomposition from Spent Pt-Catalyst from Reactions of Biomass-Derived Tar at 700 °C and an S/C Of 3 150

Figure 8:14: TGA for Carbon Decomposition from Spent Pt-Catalyst from Reactions of Biomass-Derived Tar at 750 °C and an S/C of 3 in Syngas Mixture 151
Figure 8:15: Gas Concentration in 0.209 L/min of N_2 under Pt-catalyst Activity at 750 °C from Biomass-derived Tar Reforming Reactions with Steam at an S/C of 3 152
Figure 8:16: TGA for Carbon Decomposition from Spent Pt-Catalyst from Reactions of Biomass-Derived Tar at 900 °C and an S/C of 2 Direct Feed without Pre-conditioning 153
Figure 8:17: SEM Analysis Showing Carbon Deposition on Pt-catalysts at 750 °C, an S/C of 3 154
Figure 8:18: SEM Analysis Showing Fouling in Pt-catalysts at 900 °C and an S/C of 2 (without a preconditioning chamber) 154
Figure 8:19: TGA for Carbon Decomposition from Spent Rh-Catalyst from Reactions of Biomass-Derived Tar at 750 °C and an S/C of 3 154
Figure 8:20: TGA for Carbon Decomposition from Spent Rh-Catalyst from Reactions of Biomass-Derived Tar at 750 °C and No Steam 155
Figure 8:21: Gas Concentration in 0.209 L/min of N_2 under Rh-catalyst Activity at 750 °C from Biomass-derived Tar Reforming Reactions with Steam at an S/C of 3 156
Figure 8:22: SEM Analysis for Recovered Rh-catalysts after Biomass-derived Tar Reforming Reactions with Steam at an S/C of 3 in 0.209 L/min N_2 at 750 °C. 156
Figure 8:23: TGA for carbon decomposition from Spent Ni-catalyst from reactions of biomass-derived tar at 700 °C and an S/C of 3 157
Figure 8:24: TGA for Carbon Decomposition from Spent Ni-Catalyst from Reactions of Biomass-Derived Tar at 750 °C and an S/C Of 3 157
Figure 8:25: Gas formation in 0.209 L/min N_2 at 750 °C with an S/C of 3 with Ni-catalyst 158
Figure 8:26: SEM Analysis Showing Carbon growth on Ni-catalysts at 750 °C, with an S/C of 3 159
Figure 8:27: SEM Analysis Showing Fouling in Pt-catalysts at 900 °C and an S/C of 2 (without a preconditioning chamber) 159
Figure 8:28: Mass Conversion of Carbon to Gas at 750 ^{O}C from Reforming 100 g/Nm^3 of Tar with Steam at an S/C of 3 160

Figure 8:29: Raman Analysis for Carbon Deposited on the Individual Catalyst Recovered from the Reactions of Biomass-Derived Tar Reforming with Steam of an S/C of 3 in 0.209 L/min N2 at 750 °C..... 161
Figure 8:30: FTIR Spectra of Tar Analysis from Feedstock and By-Products Collected In the Identified Condensate Traps 162
Figure 0:1: GC-MS Analysis of Biomass Tar for the Reactants Feed 199
Figure 0:2: GC-MS Analysis of Liquid Products Recovered in the Dry-Ice Condensate Trap from Reforming Guaiacol and Toluene in an S/C of 3 at 750 °C using Rh-catalyst. 200
Figure 0:3: GC-MS Analysis of Liquid Products Recovered in the Ice-Water Condensate Trap from Reforming Guaiacol and Toluene in an S/C of 3 at 750 °C using Rh-catalyst 201
Figure 0:4: GC-MS Analysis of Liquid Products Recovered in the Dry-Ice Condensate Trap from Reforming Tar in an S/C of 3 and 1%CO_2, 5%CO, 1%CH_4 and 20%H_2 at 750 °C using Rh-catalyst 202
Figure 0:5: GC-MS Analysis of Guaiacol only Before Reaction 203
Figure 0:6: Heated Cylindrical Tube for Gas Heating 211
Figure 0:7: Gas Formation in N_2 due to the Effects of steam –to-carbon ratio at 700 °C 216
Figure 0:8: Gas Formation in N_2 due to the Effects of steam –to-carbon ratio at 750 °C 216
Figure 0:9: Gas Formation in N_2 due to the Effects of steam –to-carbon ratio at 900 °C 217

Abbreviations & Nomenclature

Carbon, Hydrogen and Nitrogen analysis	CHN
Carbon-to-Carbon bond	C-C
Carbon-to-Oxygen bond	C-O
Chromatography-Mass Spectrometry	GC-MS
Concentration	Conc.
Design stress at working temperature	σ_d
Equivalent ratio	E.R
Flow rate	υ
Gas density	ρ
Gas thermal conductivity	k
Heat capacity	C_p
High Temperature	HT
Infrared gas analysis	IRGA
Inlet temperature	T_o
Inside diameter	I.D
Internal pressure	P
Johnson Matthey	JM
Lengths	z
Mass of Carbon	C_i
Molecular mass	MM_i
Multigas Analyser	MGA
Number of samples	N
Outside diameter	O.D
Overall heat transfer coefficient	h

Pipe outside diameter	d
Polyaromatic Hydrocarbons	PAH
Polytetrafluorothalene	PTFE
Safe working pressure	P_s
Safe working stress	σ_s
Sample mean	M
Sample measurement	X_i
Scanning Electron Microscopy	SEM
Seconds	sec.
Silicon Carbide	SiC
Standard Deviation	SD
Standard Error	SE
Steam-to-Biomass ratio	S/B
Steam-to-Carbon ratio	S/C
Temperature	T
Thermogravimetric Analyser	TGA
Thickness	t
Volume	vol.
Volumetric flow rate	q
Volumetric fraction or concentration	X_i
Wall Temperature	T_w.
Weight	wt

1. INTRODUCTION

The availability of affordable energy is fundamental to the stability of societies with both developed and developing economies, but there are conflicting pressures in providing this. The world population and the energy demand are increasing, particularly in countries with recently developing economies. Energy supply has so far kept up with demand, but it has had a negative impact on the environment and there is now considered to be potential for far greater impacts.

For over 150 years most energy has been provided from fossil fuels. Some of this energy is used in its found state (coal and gas), whereas others require to be converted to a more usable state. Later in the 1900s, the predominant use of fossil fuels for transport and power generation became recognised as the principle drivers for climate change due to their emissions of CO_2. Irrespective of its nature, the fossil fuels release compounds, in particular CO_2, back into the environment that were locked up as fossil fuels 100s of millions of years ago. Figure 1:1 shows the normalised primary inputs to power since 1965 and predictions for until 2035 and the energy and CO_2 emission outlook reported in BP energy-outlook report-2015 [1].

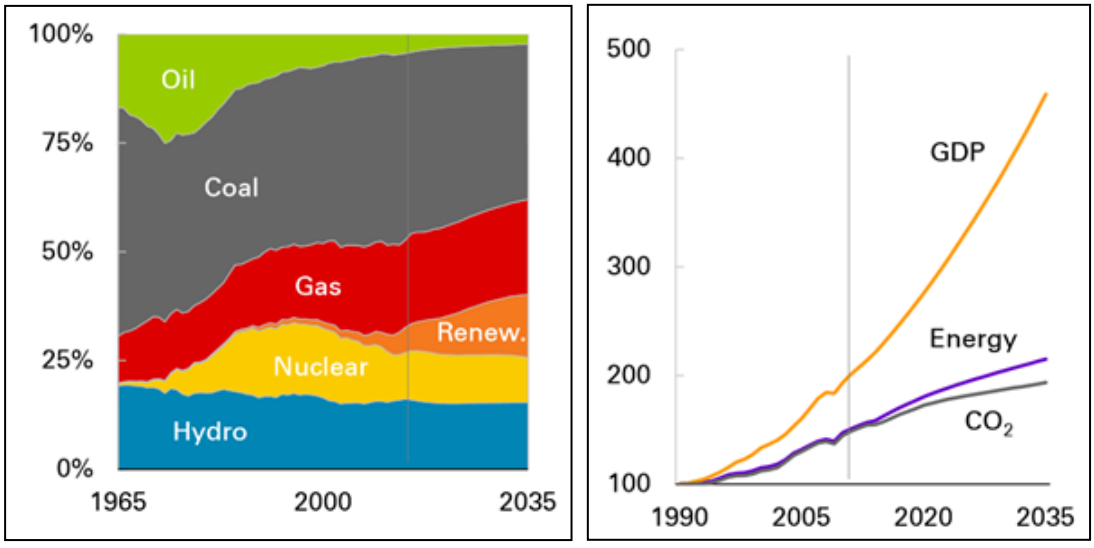


Figure 1:1: Left- Primary Inputs to Power, and Right - Energy and Emissions forecast

Awareness of the problems that CO_2 emission causes has been growing and for several decades there has been much discussion and research on ways of either cleaning up the fossil fuels technologies or developing new technology options that are less damaging. Cleaning-up fossil fuels, in particular coal, is complex and severely impacts on the economics of its use. Because of this some countries are moving away from being highly dependent on coal energy. This is one of the driving factors for developing technologies based on biomass which is CO_2 neutral, and other renewable sources.

Also, to cut the carbon emissions, a number of countries including members of the European Community, the United States, Canada and Australia have put efforts into developing policies to reduce emissions and finding alternative solutions to fuel sources. For instance, in 1990s the European Union agreed to reduce its emissions by 40% in 2030, measured against the 1990 emissions levels. As a result, the EU and national governments have provided support for research in developing alternative environmentally friendly fuel sources, among which, renewable sources such as biomass, wind and solar have significant potential in providing energy on a large scale and in reducing greenhouse gas emissions. Unlike wind and solar sources, biomass can be processed and converted directly into liquid or gas fuels for various energy uses. In recent years, there has been a rapid expansion in biomass energy processes; including gasification and pyrolysis to improve both syngas and bio-liquid fuel products.

Gasification of biomass produces a primary gaseous product that can be used either directly as a fuel gas or used as synthesis gas for further product conversions [2]. The process is carried out at relatively high temperatures and involves a reaction of fuel products that produce a gas, solids and liquid impurities through a complex kinetically-controlled process. The fuel gas is separated from the solids and liquids and used in downstream equipment or converted into liquid fuel or transformed into chemical products.

Syngas (hydrogen and carbon monoxide) is a product from gasification processes used for heat / power production and chemical synthesis. In the 1800s, it was used as town gas in Australia to produce electricity for industrial use and in the UK it was used as a

supply for domestic use. During the mid-1900s, it was used in generators to power motor vehicles and trains. In the course of the Second World War, the Germans used it to produce synthetic fuel to compensate for shortages in the supply of crude petroleum. The gasification process was later used by Sasol in South Africa to produce liquid fuels, because of shortages of crude oil owing to sanctions imposed during Apartheid. By using the Fischer-Tropsch process, Sasol produced economically viable mixture of gases and liquid hydrocarbons. The technologies developed for coal can be adapted to gasify biomass and other waste materials. At present, syngas from gasification of renewable is used to produce automotive fuels, chemicals, heat/power and electricity and various synthesised chemical.

The production of syngas from gasification of biomass is currently at a relatively low scale due to the widespread availability of fossil fuels which enjoy a mature and highly developed infrastructure and huge economies of scale. While there are currently fewer commercial operations in biomass gasification, the process potentially has an important role to play in combating climate change. A good example of this is the gasification plant in Gussing, Austria, currently gasifying biomass at the core of an 8MW system of combined heat and power, which has been reproduced at other locations.

One of the big challenges encountered during syngas production is that most of the current technologies generate tar products in the gas stream, which cause major blockages and other damage to downstream equipment.

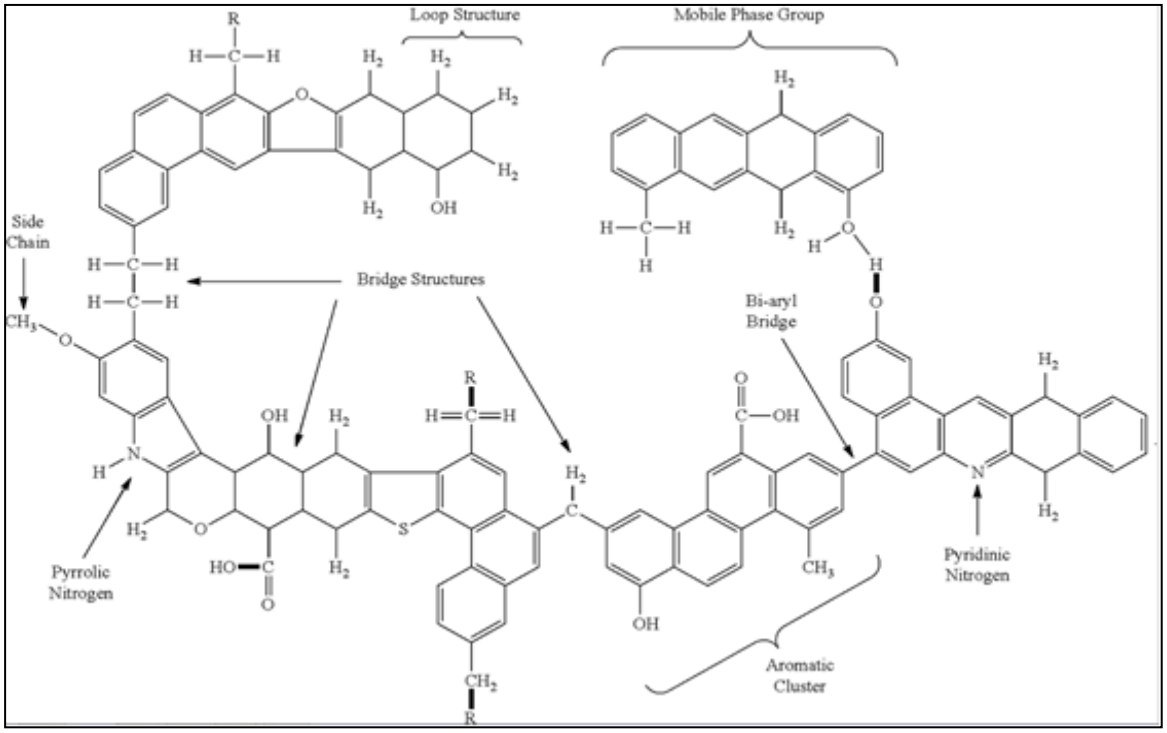


Figure 1:2: Illustration of some of the Tar molecules. [3]

Tars are condensable organic compounds made of mostly polyaromatic hydrocarbons, containing toluene, and other one ring aromatic hydrocarbons, naphthalene and other two ring aromatic compounds, heterocyclic compounds, phenolic compounds and larger ring aromatic compounds. To prevent tar problems from occurring, the use of syngas for fuel gas requires cleaning and upgrading before it can be fed into downstream equipment which can include gas engines, fuel cells or gas turbines. To reduce heat loses, it is preferable to clean-up the syngas at high temperatures. One potential way of achieving this is to catalytically crack the tar. Numerous studies show that different catalysts can be developed to crack tars, but at the same time other fuel contaminants, such as sulphur and carbon, poison the catalysts and reduce their activity and some catalysts developed can only work at low temperatures. It is therefore highly desirable to develop and test catalysts that can resist poisoning and able to remove tars at high temperature operations.

1.1. Project aims

A major emphasis of this project is to study a range of suitable operating parameters and three types of catalysts developed by Johnson Matthey Plc at Johnson Matthey Sonning Common Technical Centre, intended for use for hot gas clean up and fuel upgrading to reduce or eliminate tar in a syngas stream and improve the syngas yield to conditions suitable for downstream equipment. This project was carried out in collaboration with Johnson Matthey Plc, who provided funding with specific interests incorporated in the project goals below.

Project goals:

Develop, design and build a catalytic reactor based on modifications made to an existing high temperature fixed bed reactor suitable for tar destruction processing, including:

I. Modifying an existing fixed bed reactor

    a. set up a reactor with a quartz liner tube

    b. identifying a suitable technique for continuous feeding of biomass-derived tar into the reactor while using a quartz liner to prevent any background reactions as a result of the reactor metal material, and

    c. designing a suitable system of traps to condense the tars still present after the catalytic bed and the quartz liner tube, in order to explicitly identify and distinguish the activity of the catalysts.

II. Establish the effect of Nickel, Platinum and Rhodium based catalysts in tar reforming, as part of a hot gas cleaning process.

III. Assess the effects of various operating conditions on hydrocarbon reactions and study the reforming reactions, which include developing a thermodynamic equilibrium model that is instrumental in assessing the process performance, conducting experimental tests at different temperatures and steam to carbon

(S/C) ratios with both tars and model compounds and calculating the process material balance.

1.2. Thesis structure

Abstract summarising ideas on the effects of tar, the theoretic ideas from literature and the nature of work performed in this study to contribute towards the solution of eliminating tar.

Chapter 1 gives an introduction as a keynote for why syngas is of interest and why this study focuses on removing tar in processes. This chapter also presents the project aims.

Chapter 2 provides a discussion on literature findings, the ideas developed towards syngas production and the relevant technologies developed to date.

Chapter 3 describes the methodology employed to perform this projects' experimental work, including a description of the materials and equipment used and the analytical techniques utilised.

Chapter 4 details the thermodynamic equilibrium modelling used to predict the products formation at different temperatures and steam-to-carbon ratios. The chapter also gives details on preliminary work performed using a reactor built at Imperial College London set-up purposely for this work and in another reactor built at the collaborating company's (Johnson Matthey plc) technical site.

Chapter 5 guides the reader through the development of the reactor (built at Imperial College London), from its initial design, and gives a detailed description of the rig and reactor modifications achieved for the current studies.

Chapter 6 presents a contrast between products formed in an incoloy reactor to those from a quartz lined reactor. It also gives a set of results obtained from

operations at temperatures between 850 °C and 950 °C with steam-to-carbon ratio of 2:

Chapter 7 presents a contrast between the thermodynamic equilibrium results and the products formed within a selected range of variables in quartz lined reactor. Variables include:

- presence and type of catalyst,
- varying steam flowrate,
- varying temperature
- Varying feedstock: bio-tar or model tar compounds.

Chapter 8 provides details from the analysis of the spent catalysts, liquid and solid products.

Finally, chapter 9 summarises the whole research project with conclusions drawn from this work and future recommendations.

2. LITERATURE REVIEW

2.1. Tar

By definition, “tar is a complex mixture of condensable hydrocarbons, aromatic and complex polyaromatic hydrocarbons” [4]. This definition seems to be comprehensive enough; however, currently there is no universally accepted definition of tar. A number of authors define tar in slightly different ways. For instance, in one reference tar was defined as ‘ the organic impurities with high molecular weight aromatic hydrocarbons’ [5]. Another reference described tar as ‘undesirable materials with a complex mixture of condensable hydrocarbons, which include single- to multiple-ring aromatic compounds along with other oxygen-containing hydrocarbons that easily condense in ambient conditions’ [6].

Tars are typical compounds among the products from either gasification or pyrolysis processes of either biomass or coal. In either of these processes, tars are produced in a wide range of temperatures from just above 200 ^{o}C to 1100 ^{o}C. Many articles suggest that tar compounds are classified into primary, secondary and tertiary tars as shown in Table 2:1. Other authors classified tars produced at temperatures below 500 ^{o}C as primary tars and those above 500 ^{o}C as secondary and tertiary tars [7]. Literature also shows other categorisations in terms of tertiary tars as; alkyl tertiary and condensed tertiary tars.

Tar can also contain other elements such as O, N, Cl and S. Typical tar is considered to contain about 78% C, 12% O, 6% H, 0.7% N, less than 0.5% S and the rests are solids [8]. However, there is a range of discrepancies in the ultimate data [9] and it is established that the composition varies enormously with the primary sources and conditions. Some suggested there are yet more tar components to be identified. Some authors classified these hydrocarbon compounds into five classes, depending on (a) chemistry, (b) condensability and (c) solubility [10]. Table 2:2 gives a summary of the five classes drawn from a collection of different authors.

Table 2:1: Classification of quantitatively analysed tar compounds

Tar Class	**Primary tar compounds**				
Compound type	Acids	Ketones	Phenols	Guaiacols	Furans
Compound name	Acetic acid Propionic acid Butyric acid	Acetol (1-hydroxy-2-propanone)	Phenol 2,3-Dimethylphenol 2,4/2,5- Dimethylphenol 2,6- Dimethylphenol 3,4- Dimethylphenol 3,5- Dimethylphenol	Guaiacol 4-methylguaiacol	Furfural Furfural alcohol 5-Methylfurfural

Tar Class	**Secondary tar compounds**			
Compound type	Mono-aromatic hydrocarbons		Miscellaneous hydrocarbons	Methyl derivatives of aromatics
Compound name	Benzene Etheylbenzene a-Methylstyrene 3&2-Methylstyrene	4-Methylstyrene 3-Ethyltoluene 4-Ethyltoluene 2-Ethyltoluene	2,3-Benzofuran Dibenzofuran Biphenyl Indene	2-Methylnaphthalene 1-methylhaphthalene Toluene

Tar Class	**Tertiary tar compounds**				
Compound type	PAH: 2-ring	3-ring	4-ring	5-ring	6-ring
Compound name	Acenaphthylene Acenaphthene Fluorene Naphthalene	Phenanthrene Anthracene Fluoranthene Pyrene	Benz[a]anthracene Chrysene Benz[e]acephenanthene	Benzo[a]pyrene Perylene Dibenzo[ah]anthracene Indeno[1,2,3-cd]pyrene	Benzo[ghi]perylene

Table 2:2: List of tar compounds that are considered in classes 1, 2, to 5 [10]

Class	Class name	Property	Representative compounds
1	GC-undetectable	• Very heavy tars, cannot be detected by GC	Determined by subtracting the GC-detectable tar fraction from the total gravimetric tar.
2	Heterocyclic	• Tars containing hetero atoms; highly water soluble compounds.	Pyrideine, phenol, cresols, quinoline, isoquinoline, dibenzophenol.
3	Light aromatic (1 ring)	• Usually light hydrocarbons with single ring; do not pose a problem regarding condensability and solubility.	Toluene, ethylbenzene, xylenes, styrene
4	Light PAH compounds (2-3 rings)	• 2 and 3 rings compounds; condense at low temperature even at very low concentration.	Indene, naphthalene, methylnaphthalene, biphenyl, acenaphthalene, fluorene, phenanthrene, anthracene
5	Heavy PAH compounds (4-7 rings)	• Larger than 3-ring, these components condense at high-temperatures at low concentrations.	Fluoranthene, pyrene, chrysene, coronene, benzo-fluoranthene, benzopyrene, perylene.

Table 2:2, suggests that the most relevant organic compounds identified in the heavy tar residue were poly-aromatic hydrocarbons (PAH) with an estimated weight composition of 20% of which, naphthalene occupied the biggest percentage and among

the heavy tar residue, 6% weight was phenolic nature [11]. It is reported that 70% of the heavy tars were unidentified and only a negligible amount of the solvent anisole remained in the heavy tar residue. A typical compositions of tar components, is listed in the Table 2:3 below, however, comparing different sources data, there are significant differences [12]. The treads in Table 2:3 below indicate that the composition of tar varies particularly in different types of fuel feedstock but, also the composition varies depending on the gasifier.

Table 2:3: Typical compositions of tar generated from biomass gasification [12]

Component	Weight (%) [13]	Weight % [12]
Benzene	37.9	
Toluene	14.3	24
Other 1-ring aromatic hydrocarbons	13.9	22
Naphthalene	9.6	15
Other 2-ring aromatic hydrocarbons	7.8	13
Heterocyclic compounds	6.5	10
Phenol compounds	4.6	7
3-ring aromatic hydrocarbons	3.6	6
4-ring aromatic hydrocarbons	0.8	1
Others	1.0	2

2.2. Tar formation

Tar forms in a range of four different bands of temperature, and tar from each band was characterized as primary, secondary, alkyl tertiary or condensed tertiary tar, [13]. The primary tar develops between 200 – 500 ^{o}C, consists of lignin, cellulose and hemicelluloses derived products; the secondary tar (formed at temperatures within 500 – 1000 ^{o}C) is essentially olefins and phenolics; the alkyl tertiary tars are the methyl derivatives of aromatic compounds formed at temperatures above 650 ^{o}C, and the

condensed tertiary tar group, forms at temperatures above 750 ^{o}C, consists of the PAH chains without substituent.

During gasification, once fuel biomass is fed into a gasifier, it undergoes the drying stage and then the pyrolysis stage before the gasification stage. Pyrolysis starts to occur at a relatively low temperature of about 200 ^{o}C and completes at 500 ^{o}C, [8]. In this temperature range, the lignocellulose components; lignin, cellulose and hemicelluloses break down into primary tars and at the same time, char is formed. At temperatures above 500 ^{o}C the primary tar components start reforming into heavier molecules, the secondary tars, and along with smaller lighter non-condensable gases, CO, CO_2 and H_2O.

When temperatures exceed 650 ^{o}C, alkyl tertiary tars started to develop, and at 750 ^{o}C the condensed tertiary tars build up at a relatively high rate. If these temperatures are maintained, these tars remain in vapour phase until they condense on contact with cool surfaces [14]. Once they are condensed, they subsequently plug equipment streams, they polymerise into more complex structures and /or form tar aerosols [14] [4].

2.3. Factors linked with tar characteristics

2.3.1. Reaction temperature

In gasification, the reaction temperature influences the chemical reactions involved as well as the amount and composition of tar formed. By increasing the reaction temperature, the amount of tars from a reactor is expected to reduce [15]. The same effect is expected for impurities: O, S and N containing compounds with the exception of an increase in NH_3 during the thermochemical conversion of NH_3 [16]. The temperature effect is firstly thought to promote the pyrolysis stage, secondly the endothermic reaction of char gasification and finally promote the cracking and reforming processes [17]. Several literature sources show that increase in temperature reduces tar recovery. One good example was is described in gasifying tar using a two-stage fixed bed reactor [15]. This study involved using a two-stage fixed-bed downdraft gasifier to pyrolyse 1 g of biomass in the first stage operated at 500 ^{o}C and a heating

rate of 1 ^{o}C/s, using helium as a sweep gas at 0.1 m/s, and cracked tar in the second stage at temperatures between 700 to 1000 ^{o}C. The results suggested that tar recovery decreased when temperatures were increased, methane quantity increased between 700 ^{o}C to 800 ^{o}C but remained constant above 800 ^{o}C, and the release of CO increased throughout the observed temperature range (700 ^{o}C to 1000 ^{o}C). Another study reports on gasification of waste material in an updraft fixed bed reactor at 1400 ^{o}C and adding a mixture of air and steam at 102 Nm^3/h with 4% to 82% steam [18]. This studied suggested use of high temperatures sufficient to investigate the effect of other operating conditions on gasification of waste. Another example employed a fluidized bed gasifier for continuous operation to study the effects of temperature, equivalent ratio and residence time [18, 19]. This study required feeding sawdust biomass at 3.4 kg/h and varying the operating temperature between 700 to 900 ^{o}C, equivalent ratio 0.22 – 0.32 and residence time 3.0 – 5.0s at increments of 0.4s. These studies reported a strong link between tar cracking and temperature variation after observing that at high temperatures, primary tars such as phenolic compounds, olefins and alkylated aromatics cracked and relatively high amounts of tertiary tars such as aromatics were spotted. A typical variation of tar with temperature is illustrated in Figure 2:1 below and in Figure 2:2 is an illustration of the effect of maximum gasification temperature on tar yield [20]; [21]. Between 200 ^{o}C to 500 ^{o}C, the primary tars increase due to the breakdown of lignin, cellulose and hemicelluloses components. At this stage, primary tar organics begin to formulate.

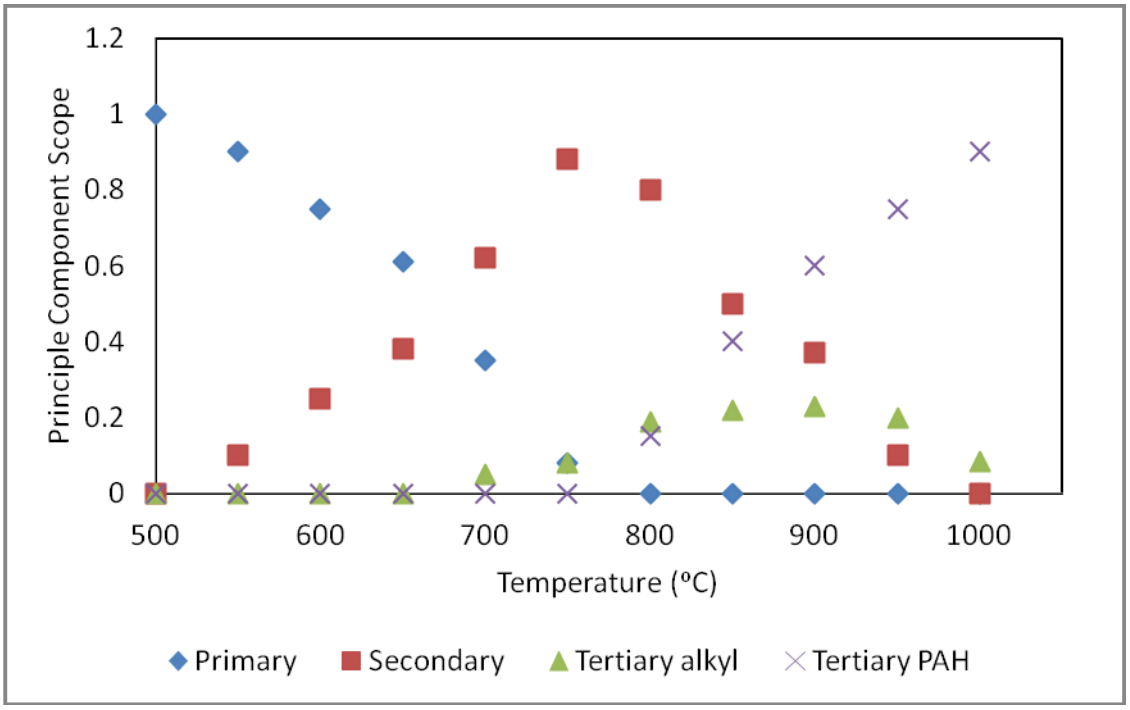


Figure 2:1: Variation in primary, secondary and tertiary tar products with temperature [13]

In Figure 2:1, at about 500 ^{o}C, the primary tars started to decompose and continued almost gradually to decompose with increased temperatures above 500 ^{o}C. Simultaneously, at 500 ^{o}C and above the secondary tars started to formulate from the rearrangement of the primary ones, increasingly forming more non-condensable gases and heavier molecules, whereas the quantity of primary tars decreased accordingly. A previous research study shows that at about 700 ^{o}C, the tar concentration increased and above 750 ^{o}C it started to drop with a sharper decrease at roughly 850 ^{o}C [19]. Even though the graph in Figure 2:1 indicates that tertiary tars start to form before the primary tars are completely destroyed, one study suggested that "Primary products are destroyed before the tertiary products appear" [10]. Another study supported the above findings by focussing on phenol behaviours, and concluded that at 900 ^{o}C, phenols are completely thermally converted [22].

An demonstration on the effect of temperature on tar concluded that increasing the temperature at the bottom of the reactor in a fluidised bed reduces the tar quantity and

a more rapid tar reduction occurs by increasing the temperature at the top of the reactor [23]. See Figure 2:2 below.

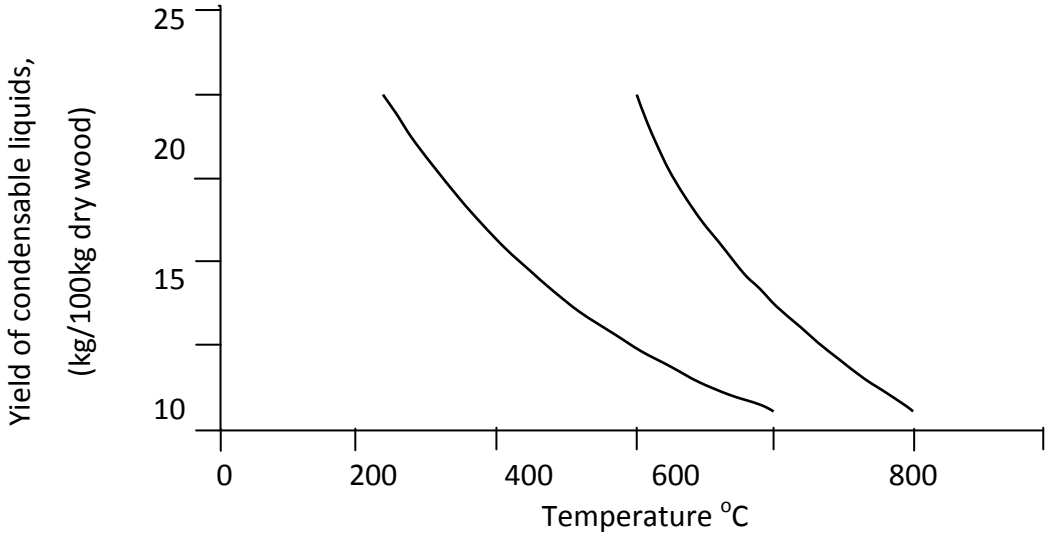


Figure 2:2: The effects of maximum gasification temperature on tar yield [4].

2.3.2. Feedstock (biomass composition)

Feedstock composition varies depending on the type of biomass and particle size feed fuel used. For instance, in a study of ten residual fuels, [24], it was identified that different fuels resulted in different fuel gas properties and a diversity of tars were detected. More evidence was shown [25] when experimenting on different biomass particle sizes, which indicated that a reduction in feed particle size improved the gasification parameters and product gas of a higher heat value. This research also illustrated that small feed particles improved the quality of fuel conversion and the producer gas composition, with maximum conversion [25].

2.3.3. Gasifier design

The design of gasifiers is another major factor that influences the net quantity of tar in the product gas [10]. It determines where pyrolysis takes place, the temperature influencing the reactions and how the tar reacts with the oxidants. As mentioned in

section 2.2, primary tar is produced at fairly low temperatures during the pyrolysis stage. This is defined by the design of the gasifier. For example, studies of design parameters such as the bed height, [26] suggested that an increase in the bed height increased the gas residence time, and significantly reduced the tar concentration as well as improving the product gas quality. Therefore, gasifiers designs may have unique features that vary between one and another, accountable for the overall reactor design, gasifier pressure and gasification agent. Among different designs, there are, the moving bed gasifiers (updraft and downdraft), entrained and fluidised bed gasifiers with distinctive tar formation [27]. The amount and chemical making of tar in the gas is a function of the temperature, residence time, thoroughness of circulation and mixing, degree of channelling, feed particle size distribution, uniformity of the bed, etc. which influence the choices of gasification configuration [28]. In view of the thoroughness of mixing and good gas-solid contact, the use of fluidised bed gasifiers is common place. With the fluidised bed, some of the tars produced in downdraft gasifiers and some of the char produced in updraft gasifiers can be oxidised, thus generating a moderate level of tar in the gas produced. A comprehensive comparison between various types of gasifier configurations was discussed in design studies covered in literature [29]. The design interests of the primary gasifiers and their interaction in tar formation is discussed in the following section.

2.3.4. Fixed bed gasifiers

Fixed bed gasifiers generally operate with a long solid residence time, high carbon conversion, low ash carry-over and low gas velocity. They are designed with a fuel feeding unit, a cylindrical space for fuel and gasifying zone, a gas exit and an ash removing unit. The design allows the gasifying media and gas to either move up or down or are introduced from one side of the reactor and are released from the other side on the same horizontal level.

2.3.4.1. Updraft gasifier

An updraft gasifier is typically made up of a fixed bed with an open-core where biomass is fed from the top and the gasifying medium from the bottom as in Figure 2:3. The gas and biomass feedstock move counter-currently, the gas leaves at the top while solids leave from the bottom, with reactions far from equilibrium [27]. The consumption of biomass is governed by the gasifying medium flow, usually air/oxygen that blows the gas, tar and other gas contaminants through the pyrolysis and drying zones before living the gasifier. The highest temperature is achieved close to the grate. Here oxygen burns the char and the hot gas travels up, providing heat to the endothermic gasification reaction. The hot gas meets the pyrolysing biomass at relatively low temperatures of roughly 200-500 ^{o}C, where primary tar is formed. While the produced gas travels upwards, it travels through cooler regions and/or making contact with cooler surfaces which reduce the likelihood of secondary or tertiary tar formation and tar cracking for gas formation, and as a result, larger amounts of tars are produced. The product gas exits the gasifier at temperatures between 100 ^{o}C – 400 ^{o}C, with a very high level of tar content (30-150 g/Nm^{3}) but low particulates relative to those from a downdraft gasifier [30].

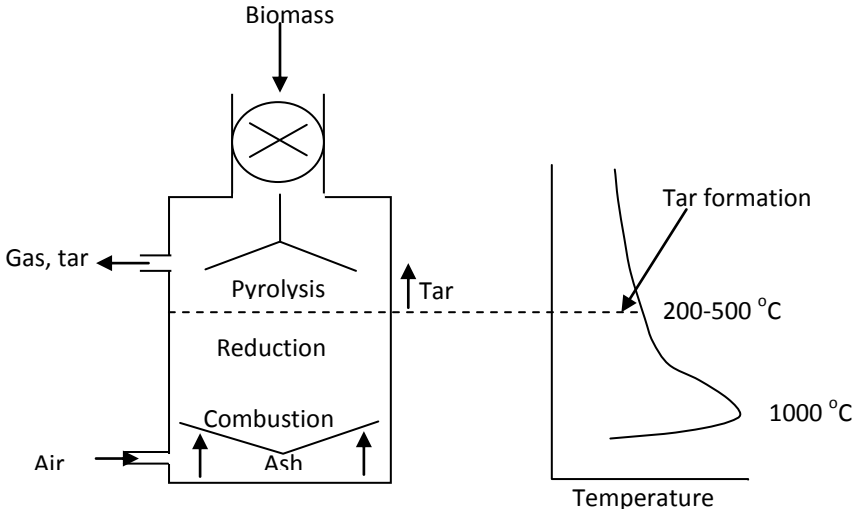


Figure 2:3: Tar production in an updraft gasifier correlated to temperature variation.

2.3.4.2. Downdraft gasifier

This is a usually throated but can as well be of an open-core shape. Both biomass and gas travel co-currently downwards at a typical the ratio of air used to stoichiometric air, (also known as the equivalent ratio – E.R) of 0.25 – 0.3 [27]. Similarly, to the updraft design, biomass consumption in downdraft is governed by the air flow, and unlike the updraft, the downdraft product gas leaves the gasifier after the charcoal bed at temperatures between 500 ^{o}C and 900 ^{o}C. The reactions in such gasifiers tend to reach equilibrium and the product gas leaves as a good quality gas with medium particulates. The process starts with the fuel undergoing through the combustion, pyrolysis and gasification stages. Tar is produced close to the gasifier feed point at lower temperatures (200-500 ^{o}C) after drying. Then air drives the tar downwards to the hotter zone. In the presence of oxygen, tar burns in a flame rising the gas temperature to 1000 ^{o}C or above and tar reforms into non-condensable gases. Bridgewater [27] indicated that the temperature is highest in the downstream combustion zone and the reactions approach equilibrium. The gas leaves after the charcoal bed as a good quality gas (compared to updraft design), with a low tar content in a range of 0.015-3.0 g/Nm^3 [30]. Updraft gasifiers produce a gas containing roughly 10% tars and, 10% methane and higher hydrocarbons whereas downdraft gasifiers products commonly contain no more than 1% tars and up to 2% CH_4 content in the overall gas product [17]. Table 2:4 shows a comparison of typical tar levels from individual designs. Slightly different concentrations were reported elsewhere, showing that tars in updraft are several hundred g/Nm^3, less than 2 g/Nm^3 in downdraft and approximately 15 g/Nm^3 for fluidized gasifiers [21].

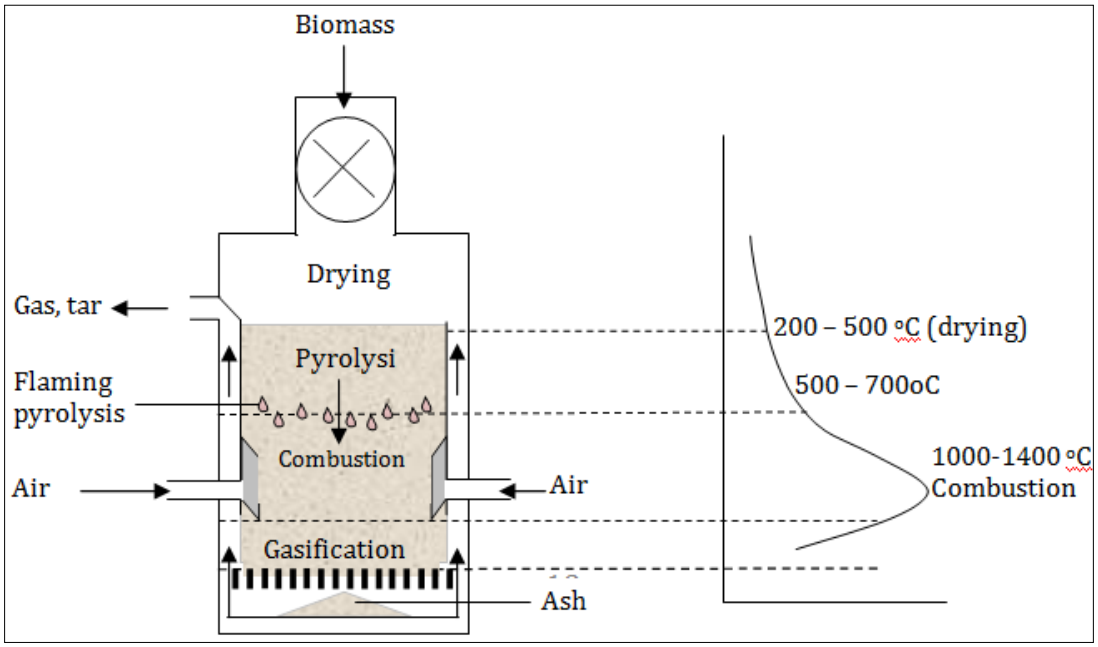


Figure 2:4: Tar generation in a downdraft gasifier correlated to temperature variation

Table 2:4: Typical tar levels in various biomass gasifiers [4].

	Typical levels of tar in a range of biomass gasifiers	
Gasifier type	Average tar concentration in product gas (g/Nm^3)	Tar as % of biomass feed
Updraft	50	10 – 20
Downdraft	<1.0	<2.0
Fluidised-bed	10	1 – 5
Entrained	Negligible	

2.3.5. Fluidised-Bed Gasifier

The fluidised-bed design considerations are primarily established from the fluidising velocity of the bed, which is determined by the size of the bed media used so that mixing occurs. There are three typical designs of fluidised-bed gasifiers; bubbling, circulating and twin fluidised bed, of which the circulating bed designs are most commonly used [27]. In all three designs, the fuel is fed into the bed from the sides or

top whereas the fluidising gas flows vertically upwards from the bottom. The flow of air upwards through the fuel forms a fluidised bed at a range of velocities of the fed air and causes fluidisation conditions up to the point at which particle elutriation occurs.

The process starts with setting up a gasifier partially filled with a heat conducting solid, usually sand, as bed material. This is followed by feeding a fluidising gas entering the bottom of the gasifier, in a plug-flow mode, into the bed at a sufficient velocity to fluidise the bed and cause a back-mixing of the solid. While the fluidising gas mixes up with the solid bed, fuel biomass particles are introduced into a preheated hot solid bed. The particles rapidly dry and pyrolyse and, the oxygen in the fluidising gas undergo fast exothermic reactions with the char mixed in the bed solid. Immediately at the point of these reactions, heat is dispersed from the bed and released to the entire fluidised bed achieving uniform temperatures. The gases along with contaminants are driven off and the spent char is oxidised and burnt (partially), providing heat for drying and for continuation of de-volatilising reactions. As the gas rises further up the gasifier, gasification reactions take place. The pyrolysis products come into contact with the hot solid and crack into non condensable gases.

Circulating fluidised gasifiers are designed to circulate the solid around a loop subjected to intensive mixing and long solid residence time within its solid circulation loop (Figure 2:5). A gasification of a range of residual biomass fuels in a fluidised gasifier [24] indicated that different fuels resulted in different fuel gas properties and a large range of tars were identified with a mean weight per volume of 270 mg/Nm^3. Another study carried out in a circulating fluidised bed, [8], describes a gasifier bed operated at a range of temperatures from 700 to 850 ^{o}C using sawdust, suggested that the tar yield decreased exponentially with increasing operating temperature within a temperature range of 700 – 850 ^{o}C and the performance of the gasifier deviated away from the chemical equilibrium due to the kinetic limitations.

In the case of bubbling fluidised bed, vibrant mixing of solids takes place, which initiates a uniform temperature but the back-mixing of the solids restrains the complete conversion of char. The principles of this operation are indicated in Figure 2:5 below

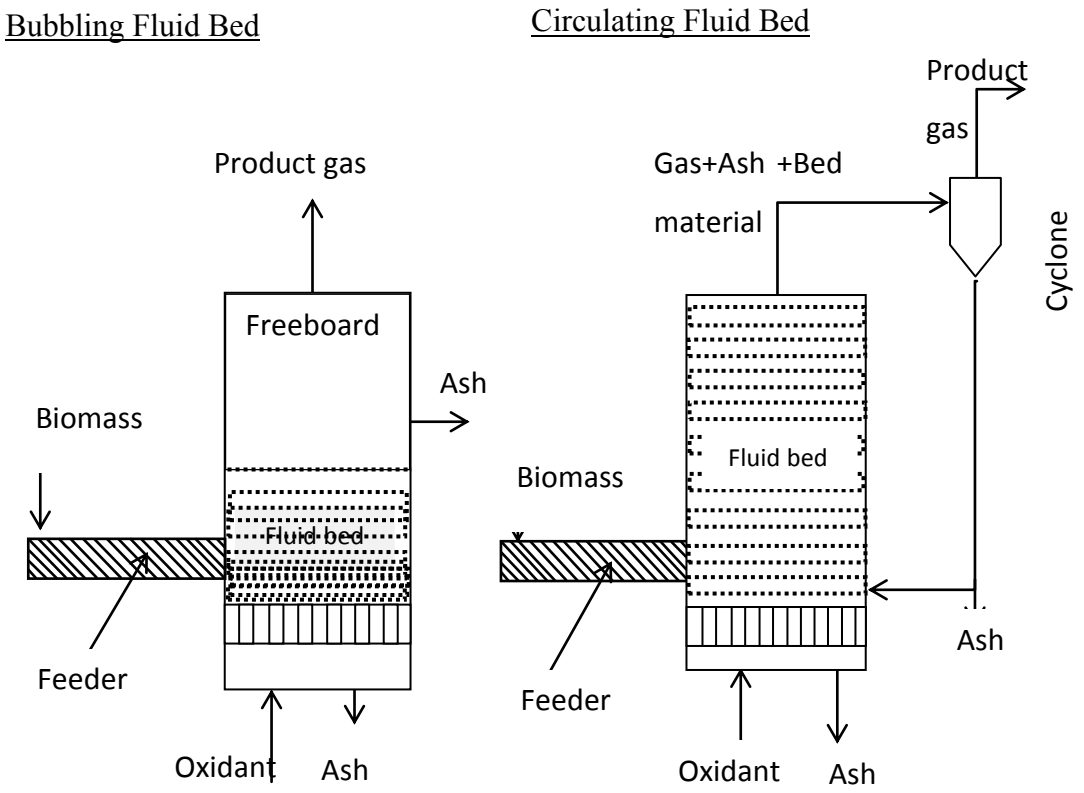


Figure 2:5: Principles Of Single And Circulating Fluid Bed Gasifiers. [27]

In general, fluidised bed gasifiers can be characterised to have a range of feedstock [31], - they can be very well mixed, - they can be operated at atmospheric or higher pressure, - air and fuel flows independently through their bed mater, - they have a low residence time and a high heat transfer and - they are operated at temperatures between 800 to 1000 ^{o}C to avoid agglomeration. The gas quality generated in the fluidised gasifier systems is influenced by the fuel characteristics, gasifier configuration, and the fluidizing agent used [32]. The amount of heat released near the bottom grid additionally depends on the oxygen content in the fluidising gas and the amount of char that come in contact with it. Between the circulating and bubbling gasifiers, the circulating gasifier is mostly preferred due to its compatibility, ease to control and potential to have a high carbon conversion.

2.3.6. Reactor pressure

Increased decreases the amount of tar, but the percentage of the PAH increased [33]. This can be explained by the fact that increasing pressure increases the reactants residence time in the bed, as a result this allows sufficient time for plenty of cracking [34]. In catalytic reactions, higher pressures above 10 bar lead to a rise in the partial pressure of CO_2 which would lead to carbonisation of a catalyst. Studies with increased H_2O pressure showed an increase in char gasification, but this reaction reduced when CO_2 pressure was increased [14]. Generally, pressurised process decreased the overall reduction in the amount of light hydrocarbons.

2.3.7. Residence time

There has been a significant research in investigating the biomass gasification residence time. Despite of attracting a lot of researchers in gasification residence time, most authors suggest that there is little impact of residence time on tar conversion. Residence time is indirectly proportional with the feed velocity in a sense that an increase in velocity reduces the residence time and vice versa. At higher velocities, there is little contact between tar and the reactor bed to allow sufficient cracking for equilibrium reactions and results in obtaining tars in the product streams [35]. Experiments to investigate the influence of gas residence time on the air gasification of dried sewage in a bubbling fluidised bed expressed that an increase in the bed height consequently increased the residence time, and these modifications played a key role in the gasification process efficiency [26], in addition, it was identified that there were concerns to study the tar trend. Elsewhere, it was suggested that a longer residence time inside a gasifier improved all process parameters; CO and H_2 content, cold gas efficiency, and fuel conversion [25]. Studies of biomass gasification at 1050 ^{o}C showed a constant H_2/CO ratio of around 0.5 [25]. The H_2/CO ratio increased with increase in both residence time and temperature above 1000 ^{o}C and decreased with residence time for lower temperature. It is also suggested elsewhere [36] that an increase in residence time increased the carbon conversion efficiency but a longer residence time would lead

to unsteady feeding and reduced efficiency of the whole system. Based on these limitations it was suggested that the best residence time would be about 1.6 s [36]. However, this suggestion can be argued from a range of reasons and on average, most articles suggest a range between 0.2 to 0.4 s when a catalyst is applied in a secondary reactor.

2.3.8. Gasifying agents

Gasifying agents include: air, oxygen, carbon dioxide, and steam [37]. Each of these gasifying agents has different outcomes on gasification reactions as well as the influence on the product gas composition and heating value. The defining parameter in gasifying medium is the ratio of the gasifying agent to the fuel biomass in the feed [8]. The following section describes some of the works of other researchers with a particular interest in the ratio of gasifying agent to feed biomass.

Adding air to a gasifier reduces the tar concentration in the product gas and it has a significant impact on the heating value of the product gas [37]. Air has a large composition of nitrogen as a result; an air gasifying media dilutes the product gas with nitrogen, which reduces the product gas heat value. As the volumetric ratio of air used to stoichiometric air increases, it increases the amount of oxygen, sufficient to react with the volatiles in the flaming pyrolysis zone to decrease the tar concentration in the product stream [19] . Even though increasing the volumetric E.R decreases tar concentration, above a certain limit a very high ratio encourages a higher carbon dioxide concentration, lower hydrogen and carbon monoxide and a slight increase in nitrogenous products, and because of nitrogen dilution from air, the product gas heat value is reduced and the fraction of PAH, Benzene, Naphthalene, and other 3- and 4-ring aromatics increases. Above a volumetric E.R of 0.27 phenols are nearly converted and less tar is formed [4]. It was also similarly suggested elsewhere that increasing the equivalence ratio to 0.27 also stimulated the formation of polyaromatic compounds, for instance, the yields of single-ring compounds excluding benzene, increased slightly while increasing the E.R above 0.27, the single-ring compounds decreased and the two-

ring, three-ring and four-ring compounds increased [19]. With steam addition in the gasification product gas influences the structure of compounds with molecular mass from 130 to 200 amu compounds and at 800 ^{o}C it decreases the tar aromaticity [38]. Addition of steam causes almost similar effects as air gasifying medium however, comparisons of the two suggest that an oxygen/air medium was more effective in tar reduction than the addition of steam [39]. In studies of tar reforming reactions using dolomite catalysts, it was suggested that a carbon dioxide medium generates a faster rate of reforming reaction than a steam medium [34]. In case a steam medium is used, the steam/carbon ratio is considered to be the sole parameter that affects the gas composition and the water-gas shift reactions to control the gas composition and reducing the quantity of tars. Also, a higher steam level and high temperatures improve the water-gas shift reactions [34]. The studies on sawdust tar yield evaluating the effects of temperature and Steam/Biomass ratio, showed that tar yield using air-steam gasification, decreased with the increase in of S/B ratio [38]. In a separate study it is suggested that a ratio of steam to biomass fuel in a range of 0.5 to 2.5 results in a larger reduction in tar yield [4]. An increase in S/B ratio was observed to increase the H_2 and CO_2 content, to slightly decreased CH_4 content and sharply decrease the CO content [17].

2.4. Tar removal

Tar is removed from syngas in either a primary or secondary reactor by wet and/or hot gas cleaning techniques, which involve: (1) physical, (2) thermal and (3) catalytic processes. Physical processes use a range of equipment (Table 2:5), to remove tar from the producer gas through gas/liquid or gas/solid interactions. The thermal process reduces tars by cracking them into lighter and less problematic species at raised temperatures. This process is often employed in secondary reactors and together with the addition of a gasifying agent such as air; added to provide a rise in temperature for an effective residence time. The catalytic cracking process involves the application of catalysts such as nickel-based, dolomite and Silica, which reduce tar at a relatively lower

temperature than in thermal processes. The selected catalysts must have the potential to increase the syngas conversion efficiencies and simultaneously eliminating the waste.

All three processes (Physical, Thermal and Catalytic) have been used during wet or dry cleaning techniques. These techniques are commonly identified as (1) the primary – (in-situ) and (2) the secondary (/post-gasification) tar removal methods, both named after their target locations.

Table 2:5: Classification of physical gas cleaning equipment [10]

Basic type	Equipment
Dry	Cyclone, electrostatic precipitators, fabric/tube filters, baffle filters, sand bed filters, bag filters, ceramic filters, barrier filters, absorbers, rotating particle separators,
Wet	Wet cyclone, wet electrostatic precipitators, venture scrubbers, impingement scrubbers, packed column scrubber and spray towers.

2.4.1. Primary measures

The primary methods are treatments carried out during gasification to prevent the formation or to remove tar. This method is designed and optimised for treatments inside a gasifier. This optimisation process involve: (I) making proper selection of operating parameters, (II) an addition of effective catalysts (III) and making appropriate modifications to the gasifier [4, 14]. The gasifier operating parameters; the gasifying agent, residence time, equivalence ratio, temperature and pressure, play an important role in the reforming and decomposition of tar as discussed in the sections earlier. The best results for primary treatment are obtained from fluidised bed gasifiers [27].

During primary tar reductions, the reforming and thermal cracking reactions are two most important operations that convert tar into other smaller and lighter hydrocarbons including CO, CO_2, H_2, CH_4 and Coke. Reforming takes place in either a CO_2 or steam medium producing more H_2 and CO (Table 2:6). Where thermal cracking dominates, tars are exposed to an oxygen rich environment and high temperatures (i.e. above 1000 ^{o}C),

and pressure, which break down the molecular bonds to form free radicals that reform into smaller and lighter molecules. The other process is steam cracking; uses steam to dilute tars that are then briefly heated in a furnace in the absence of oxygen.

2.4.2. Secondary measures

The secondary methods are treatments carried out in a separate reactor independent of the type of gasifier used and can be operated at different conditions from those in the gasifier. The secondary methods are commonly used as hot gas cleaning techniques, involving chemical, thermal or physical treatments [4, 14]; [10]. The physical treatments as described earlier (section 2.4), involve using equipment such as cyclones, filters and separators. The chemical treatment, conventionally involves hydrocarbon and methane reforming catalysts. This treatment has attracted many authors because it is economically feasible, effective in tar cracking, and it simultaneous increases the quantity and quantity of syngas. Section 2.5 following below, describes some of the catalysts used with emphasis on the ones that are most commonly. It has also been known as gathered from literature that typical tar reactions in the conversion of tar, the dry and steam reforming reactions are particularly governed by H_2O and CO_2 compounds [41]; [22].

Table 2:6: The typical reactions in the conversion of tar: [22].

Stoichiometry	Reaction	Reaction N^{o}
$C_nH_m + (n/2)O_2 \rightarrow nCO + (m/2)H_2$	Partial oxidation	9
$C_nH_m + nCO_2 \rightarrow 2nCO + (m/2)H_2$	Dry reforming	10
$C_nH_m + nH2O \rightarrow (m/2 + n)H_2 + nCO_2$	Steam reforming	11
$C_nH_m + (2n - m/2)H_2 \rightarrow nCH_4$	Hydrogenation	12
$C_nH_m \rightarrow (m/4)CH_4 + (n - m/4)C$	Thermal cracking	13

2.5. Catalytic activity

A catalyst is “a substance that increases the rate of approach to equilibrium of a chemical reaction without being substantially consumed in the reaction” [35]. Catalysts can play a significant role in (a) removing tar and (b) reducing the methane content in the product gas where syngas is the desired product and hence improving the desired product composition [34]. Their activity is subject to the idea of the reaction rate, and therefore fundamental in the reaction kinetics, while the size and shape of small metal particles determine the geometry in which the atoms are available in the reacting environment [42].

The catalytic interaction often involves adsorption or formation of intermediate compounds and the transfer of ions (often hydrogen ions), electrons, and radicals. The catalytic mechanisms, initiates with (1) dissociative adsorption of hydrocarbons including methane (2) the dissociation of H_2O, which is adsorbed, hydroxylating the surface, (3) the dehydrogenation course of the catalysed metal, creating the adsorbed hydrocarbon-derived fragments (4) the formed fragments, the OH radicals on the surface migrate to the metal site, activated by temperature and (5) they immediately form intermediates leading to carbon oxides. This process would carry on until all adsorbent molecules are used up but, the presence of impurities; sulphur, chlorine and alkali metals, coat on the surface of the catalyst, restricting the catalytic activity.

Tars at high temperatures are concentrated in the gas phase, so as they flow through the reactor, they are channelled for catalytic activity. Depending on the composition and type of the catalysts, the catalytic reactions take place on the ion surface. The catalyst surface activity may differ depending on its (1) surface area, (2) pore side and (3) pore distributions [34]. The rate of reaction also depends on how fast the tar is transported on to the surface active sites and how fast the products are transported away [4]. The catalytic intervention promotes the reforming, water-gas shift and reactions 16, 17 and 18 below, and consequently reduces tar in the product gas [43].

$$C_nH_mO_k + (n-k)H_2O \rightarrow nCO + \left(\frac{n+m}{2-k}\right)H_2 \ldots\ldots\ldots\ldots\ldots\ldots\ldots\ldots (16)$$

$$CO + H_2O \leftrightarrow CO_2 + H_2 \ldots\ldots\ldots\ldots\ldots\ldots\ldots\ldots\ldots\ldots\ldots\ldots\ldots\ldots\ldots\ldots (17)$$

$$C + H_2O \leftrightarrow CO + H_2 \ldots\ldots\ldots\ldots\ldots\ldots\ldots\ldots\ldots\ldots\ldots\ldots\ldots\ldots\ldots\ldots (18)$$

A catalysts must be (a) cheap (b) strong, (c) effective in tar removal, (d) capable of reforming methane in case of syngas production, (e) provide a suitable syngas ratio for the intended process, (f) easy to regenerate and (g) resistant to deactivation as a result of carbon fouling and sintering [34].

A number of authors grouped the catalysts on the basis of (1) method of application (primary or secondary), (2) material nature (metallic or non-metallic), (3) extractions source (synthetic or natural minerals) and some other authors reviewed groups of: nickel-based catalyst; alkali-metal catalysts; alkaline earth metal oxides; natural ores dolomite and olivine; and acid catalysts such as zeolite, silica and alumina. Between these classifications, metallic, non-metal oxides, and alkali metal catalysts have been predominantly studied, where the metallic and non-metallic oxides such as Nickel and Dolomite respectively, are repeatedly suggested for secondary applications in downstream reactors. For gasification processes involving fluidised bed reactors, non-metallic oxides have as well been used as primary catalysis. Most commonly, alkali metal and dolomite catalysts have been used as primary catalysts in either fixed and/or fluidised bed reactors.

Use of alkali metal catalyst has attracted less interest as they are associated with the increase in ash content and are not easy to recover. The difference between alkali metal catalysts and the metallic / non-metallic catalysts is that alkali metals are used to boost the process of biomass gasification instead of promoting tar reforming. Literature shows that alkali salts were fed directly into the gasifier where they influenced the raise of char formation reactions during thermochemical conversions in the pyrolysis stage, [44].

A lot of interest has attracted the use of metallic catalyst since they are easier to regenerate particularly the Ni-based catalyst, whereas the alkali and most non-metallic catalysts are hardy regenerated. The key features in these catalysts are based on their composition, which involve (a) an active catalytic metal, (b) a promoter and (c) a support. 'Promoters' increase the activity and stability of the catalyst activity, and the 'supports' facilitate the dispersion of the active phase/catalyst activity by the influence of; the surface area, the pore structure, the electronic structure and the acidity potential. These additives are used to facilitate the catalytic mechanisms; adsorption and desorption although generally, the catalyst mechanism may remain the same, but the products' behaviour of an individual active metal catalyst may vary from one promoter and/or support to another. The following sections describe the potential catalysts, grouped into; metallic and non-metallic catalysts.

2.5.1. Potential metallic catalysts for tar reduction

Studies in catalytic tar cracking, in particular, steam reforming of hydrocarbons indicate that there have been multiple catalysts employed containing base metals, such as Cu, Co and Ni, or noble metals, such as Ir, Rh, Pt, Pd and Ru [30]. Metal-based and noble metal-based catalysts are usually dispersed on supports such as alumina, aluminate, alpha-alumina, gamma-alumina, calcium aluminate spinals, magnesium aluminate and pervoskites as well as oxide ion-conducting substrates including CeO_2 and ZrO_2.

Nickel (Ni)-Based Catalysts

Ni-based catalysts have been tremendously published in most literature for biomass gasification hot gas cleaning processes, and allegedly considered to be excellent for the steam and dry reforming of hydrocarbons. Considerably, they are the most broadly used and perhaps ranked as the economically best catalysts in tar cracking [45]; [34]; [34] and [12].

The activity of Ni-based catalysts is credited to be very effective in tar cracking plus simultaneously valuable in removing ammonia from both coal and biomass gasification

products [46]; [34]; and [10]. Some studies suggested that Ni-based catalyst have been extensively used for reforming and NH_3 decomposition in both coal and biomass gasification at temperatures above 800 ^{o}C [47]. Elsewhere, Ni was combined with other catalysts either to improve its effectiveness or to improve the activity of its precedent catalyst. For instance, in cracking of toluene, a combination of 1.5-5.7 wt% Ni with Austrian Olivine catalyst was prepared by wet impregnation using excess nitrate, chloride and acetate aqueous solutions and reduced at 400, 900, 1100 and 1400 ^{o}C, was used to demonstrate its efficiency in removing tar from gasification gas and its resistance to carbon deactivation [48]. The same catalyst was tested in a fluidised bed gasifier at 560 – 850 ^{o}C for 7 hours which led to conclusions that catalysts reduced at higher temperatures with larger nickel content had a better activity except that carbon deposition also increased proportionally.

Other differences in Ni activity are particularly due to use of different additives, the supports and promoters. The commonly used additives include transition metals, alkaline earth metal and phosphorous. For instance, a nickel catalyst with various contents of Fe, Mg, Mn, and Ce additives added on palygorskite-support, and the catalysts were prepared by incipient wetness impregnation were investigated for their effectiveness in tar cracking in a fixed bed reactor [49]. The reactor was operated at 700 ^{o}C, for a reaction time of 20 minutes, 10g of a catalyst, nitrogen as a carrier gas at 80 ml/min and a tar concentration of 0.45 g/min. The results were divergent from the other literature but there was a general trend in the addition of additives which improved the performance of the Ni/PG catalyst that produced good results for both tar conversion and H_2 yield. In particular, Ni/PG with Fe addition had better results than the other additives. Observations show a conversion of 64% in tar concentration and it was recommended that high addition of additives weakened the catalyst promoters. A study on the effectiveness of using Ni-based catalyst for tar cracking [50] using additives; BASF G1-51, ICI 46-1 and Topsoe R-67 operated at 840 ^{o}C and a gas residence time 0.2 to 0.3s shows that all these three catalysts were effective and reached a 99.8% cracking efficiency. A different study investigated the effect of NiMo, and comparing it to Al_2O_3, CaO, CuMn and SiO_2 catalyst using 1-Methylnaphthalene as a model tar compound [51].

NiMo was observed to be more effective than the others and less coking appeared as opposed to the other supports in the group. Unlike other catalysts discussed in this report, Ni-based catalysts are capable of adjusting a methane rich gas product to syngas of preferred composition [34]. More studies on Ni are reported elsewhere in literature [10], which outlined the nickel catalytic operating conditions under the influence of different additives.

Platinum catalyst

The performance of platinum and platinum-rhenium catalysts, prepared on alumina supports by impregnation and sequential impregnation was conducted during the reforming of n-heptane [52]. The detailed description of the catalyst synthesis can be found in literature [52]. The catalysts were tested in an internal recycle reactor at a temperature of 500 ^{o}C, a pressure of 1.2MPa and liquid hourly space velocity of 3.0 v/v/h; having been reduced with hydrogen at 9 l/h at 480 ^{o}C for 2 hrs. 3 ml of catalyst was used for each test with 1000:1 vol. of hydrogen/n-heptane. The same catalyst was tested at extreme conditions (500 ^{o}C, 0.4MPa and 700:1 vol. H_2/nC_7) for 3 hours. Over the period of 3 hours, the conversion of n-heptane was observed to decrease from above 80% to below 55% for either catalyst. Other analysis illustrated that platinum-rhenium catalyst had a better stability due to the presence of rhenium, and had a higher product distribution, with a selectivity of 6% aromatised compounds more than the conventional platinum catalyst. The increase in selectivity of the platinum-rhenium catalyst was explained to be a result of dispersing carbon on the catalyst. The stability and selectivity observations supported conclusions linked to literature that stability and selectivity are enhanced by dispersing higher metal compounds on a catalyst surface [53]. Another study of platinum supports titania and alumina was conducted to determine the resistance to sulphur poisoning [54] during a process of oxidising hydrogen. Pt/TiO catalyst was prepared by hydrolysis of $Ti(SO_4)_2$ while Pt/Al_2O_3 catalyst was prepared by impregnation (details of preparations can be found in literature [54]) were employed in a pulse reaction process that involved the oxidation of hydrogen and carbon monoxide at 200 ^{o}C.

Rhodium Catalyst

Rhodium is known to be responsible for reduction of NO by CO and it has also been used for the conversion of synthesis gas (carbon monoxide and hydrogen) to oxo-products including acetaldehyde and ethanol [42]. In its uses, rhodium is known to form a strong metal support interaction after high temperature treatment in hydrogen [55]. For instant the thermal stability of rhodium oxide on pure alumina and Ce-ZrO_2-modified alumina-supported catalyst was investigated during its reduction and it was shown that the catalyst synergistic effect on the alumina support stabilised the rhodium against the formation of a reduction-resistive oxide phase at 300 ^oC, whereas rhodium on Ce-ZrO_2-conataining catalyst reduced, formed more pronounced growth of the noble metal particle size [55]. The undesirable effect with Ce-ZrO_2 occurs when operations require use of very high temperatures. When rhodium on Ce-ZrO_2 was reduced at high temperature, it is thought that the water vapour it forms, from the reaction of hydrogen with the oxygen it releases, forms localised humidity in the catalyst pores which eventually would cause sintering of the catalyst [55]. For this reason, very high temperature operations are rather preferable for operation with rhodium on alumina. Analysis of alumina –supported rhodium model catalysts, using TEM, XPS, SIMS, EXAFS and infrared spectroscopy, showed that rhodium catalysts used in the three-way catalyst reduction of NO by CO were significantly larger particle sizes and mostly those of 10 nm and above were more active at NO reaction with CO (NO + CO) because of the large ensembles of rhodium surface atoms needed for the reaction [42]. In these studies, rhodium on alumina catalyst was prepared by impregnating the Al2O3 support with a solution of rhodium trichloride. It is indicated that in water $RhCl.xH_2O$ forms a range of neutral and ionic complexes. In such complexes, the Rh^{3+} ion was found to be surrounded by six ligands including hydroxide ions (OH^-), chloride ions (Cl^-) and H_2O. A detailed description of this formulation can be found in literature [42]. In preparation for the usage of the catalyst, rhodium reduction / activation was investigated using TPR methods where it was shown that the catalyst was reduced at relatively low temperatures even below 200 ^oC [42].

Alkali metal catalysts

These are commonly used in primary techniques; they are directly added to the biomass by wet impregnation or by dry mixing. They dramatically increase the rate of gasification and have a significant impact on methane reforming reactions in the product gas.

Iron-based catalysts

These are natural minerals containing Iron and with the potential to decompose tar compounds. Among these mineral, you will find compounds such as; olivine (Fe_2SiO_4 or Mg_2SiO_4), limonite and ankerite (as a ferrous dolomite) [47]. Olivine is a natural mineral made up of ion, silicon and magnesium, of which the compositions of these amalgamated minerals fluctuate based on originality. More information on olivine can be found among the non-metallic catalysts. Limonite is mainly composed of goethite (FeOOH). Its activity was reported to increase with increase in the α-FeOOH content [47]. For instance, it was used on studies of Australian limonite, which demonstrated that high contents α-FeOOH were very effective in ammonia decomposition [47]. Activation of FeOOH was found to be at temperatures above 400 ^{o}C and FeOOH reduces to Fe_3O_4. In other applications Iron was used in Ni-Fe alloys to serve as the oxygen supplier, a process that promoted the reaction of tar destruction and suppressed the formation of coke [40].

2.5.2. Potential Non-Metallic oxides

Dolomite

Dolomite also known as calcium magnesium is a naturally occurring ore, $CaMg(CO_3)_2$, is widely used in both; gasification and steam reforming reactions for tar destruction. It is the most commonly used catalyst among the non-metallic oxide catalyst because it is inexpensive and has potential to eliminate tar [4]. The dolomite chemical composition typically contains approximately 45 wt.% CO_2, 30 wt.% CaO, 21 wt.% MgO and with 4 wt.% minor mineral impurities including traces of SiO_2, Fe_2O_3 and Al_2O_3, but this

composition varies from source to source [34]. It is reported that the Fe_2O_3 content in different types of dolomite catalysts plays a key role and dictate how effective dolomite can behave during tar reduction in oxygen/steam gasification [34].

In natural occurrence, dolomites are inactive for tar destruction and therefore, they are activated by reduction. Its reduction process involves decomposing the carbonate mineral and eliminating CO_2 at temperatures of 800-900 ^oC to form MgO-CaO for optimum tar cracking, [34]. However, this process reduces the surface area of the catalyst and transforms it into a very friable product [56], which attracts it for use in fluidised bed reactors. From this point of view, dolomites of different types are thought to vary in surface area, pore sizes and pore size distribution. The applications of the dolomite catalysts require relatively high temperatures as a result of its reduction conditions and ability to maintain its activity, the catalyst equilibrium decomposition pressure should at all-time be greater than the partial pressure of the CO_2. In case of pressure increase in the reactor during the process, the operating temperature of a reduced dolomite reactor must be increased to maintain its activity. Principally dolomite catalyst is effective when reduced and used at temperatures above 800 ^oC [34]. Some advantages associated with dolomite can be found in table in Table 2:7.

Studies conducted on conditions for activation of dolomite (composition: 24.07% Ca, 12.69% Mg, 0.02% Na, 0.02% K and 0.002% Cr) showed that dolomite activation required processing in a mill for 10h and using 5 bars, and activation occurs at 200 ^oC [57]. At higher temperatures dolomite decomposed in two distinctive steps, one between 590-810 ^oC with a mass loss of 12.5% and the other at 810-900 ^oC with a mass loss of 29.5%. Addition of quartz in the mill during the activation of dolomite accelerated the deformation and amorphization of dolomite, and reduced the activation temperature to 880 ^oC [58]. A combination of Ni/Dolomite and a mixture of dolomite and commercial nickel catalyst indicated a very good performance with an effectiveness of nearly 100% tar conversion [59]. Dolomite was also used in gasification of coal and found to reduce H_2S by promoting a reaction of H_2S with which resulted in generation of additional water and altered the equilibrium of the reaction [60]. In 1992, dolomite was

used in cracking of tar from pyrolysis liquids where remarks made show that dolomite had a high activity in increasing gas yield and reducing tars [61]. Comparison between product gases obtained using a reduced dolomite at 800 ^{o}C and unreduced dolomite in 86% N_2 and 16% CO_2 showed that using the reduced dolomite increased H_2 yield by nearly 81%, CO by 46% while CO_2 decreased by 71% and CH_4 by 81% [34].

Olivine

Olivine consists mainly of silicate minerals which contains oxides of iron and magnesium that give its characteristics features for cracking tars. As with dolomite, natural olivine (represented by the formula $(Mg, Fe)_2SiO_4$) can be reduced to modification suitable for its activity and even in higher temperatures. In a study of olivine [12], the catalytic activity of olivine in tar removal was considered to be similar to that of reduced rocks (CaO and MgO) in the same process. In the study of olivine, a combination of three Ni/olivine catalysts prepared by wet impregnation were investigated [62] to determine their performance in cracking tar compounds; benzene and toluene during the production of producer gas through biomass gasification steam reforming process. The results indicated that 3.0% NiO/olivine with 1.0% CeO2 had a better performance of catalytic activity and coking resistance than the other two. However, the use of catalysts in cracking tars has attracted other listed catalysts than the Olivine [47].

Comparison of reduced olive and dolomite in the potential of hydrogen production reported [56], showed that reduced dolomite has approximately twice the potential of producing hydrogen, with results indicating the ratio of the sum of H_2 and CO to the total product gas between reduced dolomite and alumina was much higher in the dolomite catalyst. A comparison of dolomite catalyst with zeolite catalyst in cracking tar from gasification of lignite and a sub-bituminous coal indicated that dolomite catalyst had a 50% effectiveness higher than zeolite [63].

Table 2:7: Catalysts with related advantages and disadvantages

Catalyst	Description	Advantage	Disadvantage
Dolomite	- Used at temperatures; 800-900 ^{o}C. - Effective by calcining - CO_2 partial pressure should be less than that of dolomite's equilibrium decomposition pressure.	- Effective in removing tar content in product gas [34]. - Relatively inexpensive - Disposable and cheap to dispose off - For both: primary and secondary applications. - Can be used in primary techniques but commonly as a guard bed in secondary cleaning techniques [34].	- Hardly recovered - Calcination reduces surface area. - High temperature limits are restricted by calcination temperature. - Inactive for methane reforming, hence not suitable for syngas production [34]
Nickel	- Have high activity for tar destruction, reforming of methane and water-gas shift activity to adjust the H_2:CO ratio - Operated at about 800 ^{o}C. - Also reduces NH_3 in	- Can be regenerated and have a longer lifetime. - Effective in hot gas conditions. - Effective in the water-gas shift activity to adjust the H_2:CO ratio of the product gas - Promotes methane reforming gasification reaction. - Valuable in increasing the H_2 and CO content in product. - Suits higher temperatures than dolomite.	- Toxic for disposal as waste - Deactivated by carbon (Coke) depositing on the catalyst surface. - Relatively expensive

	product gas.	- Reduce the content of NH_3 in the product gas by catalysing the reverse reaction of NH_3. - Can be used in both primary and secondary treatment but best as secondary catalysts.	
Olivine	-	- Relatively cheap (similarly to dolomite) - High attrition resistance relative to that of dolomite [12]. - Better performance due to its high mechanical strength relative to that of dolomite [12].	- Lower potential of tar conversion, even relative to that of dolomite [12].
Alkali	-	- Effective for methane reforming reactions - Commonly used in primary techniques but can also be used in secondary processes.	- A lot expensive relative to dolomite. - Difficult to recover. - Poor tar conversion (<80%) relative to that of dolomite or Nickel catalyst. [34]

2.5.3. Other Tar cracking catalysts

Other catalysts include Char, Zeolites and Fluid catalytic cracking catalysts (FCC). Commercial FCC catalysts to a limited extent have been used to crack tars and enhance the heating value of the gas. They are considered to be less effective and deactivate rapidly but more suitable in a fluidised beds [17]. Char is a non-metallic catalyst and plays a key role in reforming reactions of the CO_2 reforming of CH_4 and water-gas shift reactions [64]. Its activity relies on its pore size, surface area and pore size distribution together with its ash or mineral content. Char reactions may involve interactions with catalysts to boost the steam reforming reactions of tar [65] but also can be affected during steam and dry reforming reaction, and by coke deposition.

Gasification reactions with steam or CO_2 may consume char, which may result in a need for its continuous external supply. Generally, biomass char is continuously produced during gasification [22]. This idea is supported elsewhere where coal char was used as a support of NiO for tar removal, since char has the potential reduce tars and it is inexpensive [66]. NiO loading with 5-20wt% char support at 0.1-1.2 s residence time and 800 ^{o}C reforming temperature, removed more than 97% of the tar in syngas [66].

A research on the potential use of char in reducing compounds phenol and naphthalene compared to using other catalysts (dolomite, olivine, fluid catalytic cracking, silica sand and commercial nickel) showed that at 900 ^{o}C all sample catalyst produced full conversions of which 98% phenol was alleged to have been thermally converted, whereas at 700 ^{o}C, char was found to have a higher tar conversion of phenol relative to the conversions with silica sand and olivine. This study was performed at 700-900 ^{o}C; 1 atmospheric pressure; a gas residence time of 0.3 s; a catalyst bed volume of 25 cm^3; initial tar concentration of 8-13 g/Nm^3 phenol and 40 and 90 g/Nm^3 Naphthalene; and a feed gas compositions of 6, 10 and balance Volume% for CO_2, H_2O and N_2 respectively [22]. The conversions of naphthalene indicated that only Nickel had a better conversion than char.

2.6. Summary of the Literature review

Tar is a complex mixture of condensable hydrocarbons, and commonly a by-product from gasification or pyrolysis of biomass, coal and other waste matter. It can contain compounds with one to several carbon rings and traces of: O, N, Cl and S. It can be categorised into primary, secondary and tertiary tars and classified as: GC-undetectable, heterocyclic, light and heavy PAH compounds. The majority of biomass or coal originated tars are benzene, toluene and naphthalene.

Mostly the operational factors including temperature, gasifier design, pressure, residence time and gasifying agents influence the nature and amount of tar products. The temperature distinctly influences the heating rate, and higher heating rates result in decrease of tar and CO_2, and increase of H_2 and CO contents. Tars are believed to form between 200 ^{o}C to 1100 ^{o}C. At increasing temperature primary tars crack first followed on by the secondary and then tertiary. The entrained and downdraft gasifiers are thought to be the most effective gasifiers. On average, downdraft gasifiers have an output of < 1 g/Nm^3 tar and a typical gas product of 15% H_2, 24% CO, 11% CO_2, 2% CH_4 and 48% N_2 on dry basis. Operating pressures < 10 bars are more suitable since high pressures result in high PAH concentrations in products, and a conversion shift to higher temperatures. Among the possible gasifying agents, steam is thought to influence the production of gas with a relatively higher heating value (i.e. higher H_2 and CO content).

In the interest of reducing costs during tar cracking, catalysts are preferable over higher temperatures. The catalyst so far used can be applied either in the gasifier matter (primary catalyst) or in a separate reactor as secondary catalysts. Secondary catalysts are preferable over the primary ones because it is hard to recover the primary catalysts. Among the catalysts explored, the ones containing Co, Ni and Rh are thought to have a better performance but commonly, Ni-based catalysts are mostly utilised due to nickel's sufficient performance, abundance and low cost. Carbon formation on Ni-based catalysts can be minimised using alkali promoters such as CaO, MgO and K_2O.

3. EXPERIMENTAL PROCEDURE & ANALYTICAL TECHNIQUES

Upon completing the modification and commissioning tests of the reactor an experimental procedure for the entire process was developed. The methodology underpinning the experimental work in this project was done in a “hot-rod” fixed bed reactor. This is a fixed bed reactor with joule heating. This chapter describes the detailed procedure followed during experiments and the analytical techniques used together with the analysis of the feed materials.

3.1. Materials and Experimental Procedure

In this work the objective was to apply, at the laboratory scale, the procedure of removing tar using hot gas cleaning techniques. The experiments carried out were focussed on verifying the possibility of reforming biomass tars using special catalysts developed for reforming hydrocarbons. The tars were obtained liquids from pyrolysis of wood biomass at 600 °C. The catalysts used are anticipated to increase the rates of tar reforming reactions that are thermodynamically feasible. During these experiments all the critical qualitative and quantitative parameters of both input material and generated products were determined.

3.1.1. Materials

Biomass tar, model compounds of tar; guaiacol and toluene, a syngas mixture, hydrogen, nitrogen, water and Pt-, Rh- and Ni-based catalysts were the materials used in this study. The tar and the catalysts were analysed to determine their compositions and established their properties. The materials used and how the conditions were integrated into the process are described below.

3.1.1.1. Tar

Tar was brought in from Australia, identified to have been produced from the pyrolysis of Birchwood at 500 °C. The CHN analysis was conducted, with the results of the elemental analysis shown in Table 3**:1**.

Table 3:1: The Ultimate Analysis of the Tar

Compound	C	H	S	N	O	Total
% Mass/g	44.03	7.05	0.04	0.36	48.0	100

This tar was further characterised using a Thermogravimetric Analyser (TGA) and a Gas Chromatography-Mass Spectrometry (GC-MS). The TGA analysis was carried out to determine the vaporising temperature of the sample by studying the rate of change in the weight of the sample as a function of temperature in a controlled atmosphere. TGA results of the raw tar are shown in Figure 3:1. The graph indicates that 70% and 80% of the sample evaporated at temperatures of 300 °C and 400 °C respectively.

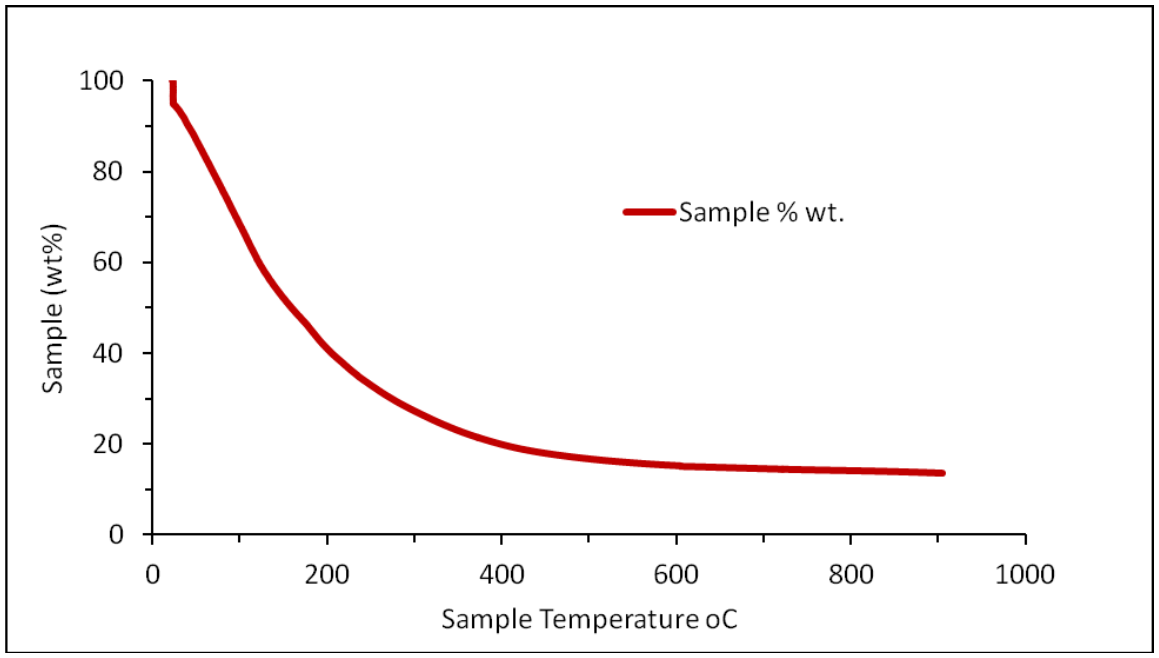


Figure 3:1: The sample weight at increasing temperature; from TGA analysis of feed tar

GC-MS analysis

A GC-MS analysis of the tar sample was carried out to identify and quantify the nature of compound in the sample. A group of the compounds identified during the analysis is given in Appendix 1.

3.1.1.2. Catalysts

Three types of transition metal-based catalysts: Rhodium Oxide on alumina, Platinum Oxide on alumina, and Nickel Oxide on alumina were tested for their performance. All were considered to be good catalysts for reforming hydrocarbons and to be able to withstand high temperatures. The mixture composition of these three catalysts is shown in Table 3:2 and the BET analysis of Each Catalyst is shown in Table 3:3. All catalysts were prepared / developed by Johnson Matthey plc who holds confidentiality of the procedure followed during catalyst preparation.

Table 3:2: The Composition of the Fresh Catalyst

Catalyst mixture composition (wt %)				
Catalyst / Mixtures	Alumina	Zirconium (IV) Oxide	Metal Oxide	Physical description
Rhodium oxide on Alumina	60 – 99%	1 – 5%	Rhodium (III) Oxide < 1%	Brown pellets.
Platinum Oxide on Alumina	60 – 99%	1 – 5%	Platinum (IV) Oxide < 1%	Brown pellets.
Nickel Oxide on Alumina	60 – 99%	1 – 5%	Nickel Monoxide<1%	White pellets.

Table 3:3: The BET and BJH Analysis of the Fresh Catalyst Measured using a Micro-meter Accusorb 2100E

Catalyst	BET Surface area	Micro pore area	Single point surface area at P/Po	Total pore volume	BJH Adsorption	BJH desorption
	(m^2/g)			(cm^3/g)	Av. pore diameter (nm)	
$Rh_2O_3/ZrO_2/Al_2O_3$	193	5.02	186	0.49	8.20	7.07
$Pt_2O_3/ZrO_2/Al_2O_3$	192	5.64	185	0.49	8.16	7.00
$Ni_2O_3/ZrO_2/Al_2O_3$	196	5.49	189	0.50	8.07	6.93

3.1.1.3. Producer gas (syngas mixture) and span (calibration) gas mixture.

The producer gas was a special gas mixture containing 20% hydrogen, 1% carbon dioxide, 1% methane and 5% carbon monoxide, with balance nitrogen. The span gas (for calibrating the gas analyser) contained 20% hydrogen, 5% carbon dioxide, 1% methane and 20% carbon monoxide in nitrogen. Other individual gases comprised of the 99.99% hydrogen and the 99.995% nitrogen. Nitrogen free of oxygen was used for purging the process lines and as the main carrier gas throughout the experiments. Dry nitrogen gas was also used as the zero calibration gas to set the zero concentration condition of the gas analysers.

3.1.2. Equipment Description

To perform the catalysts tests, the system equipment was classified into five main processing stages. These processing stages were: the material feeding, feed preconditioning, reacting (catalytic and thermal cracking), tar collection and gas measurement. These are shown in the block diagram in Figure 3:2 and explained in the following paragraphs. The process flow diagram is shown in Figure 3:3.

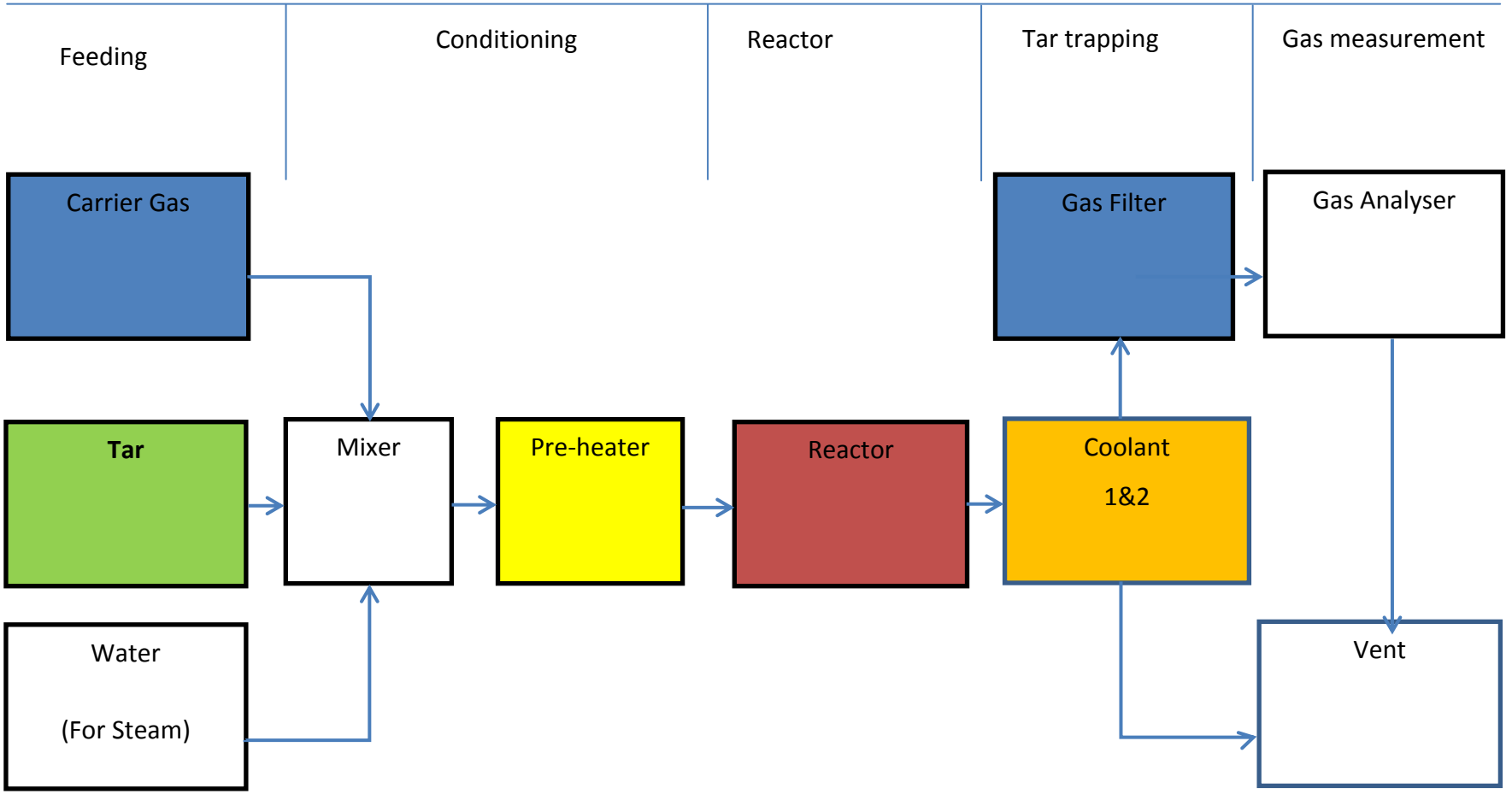


Figure 3:2: Conceptual Process Block Flow Diagram.

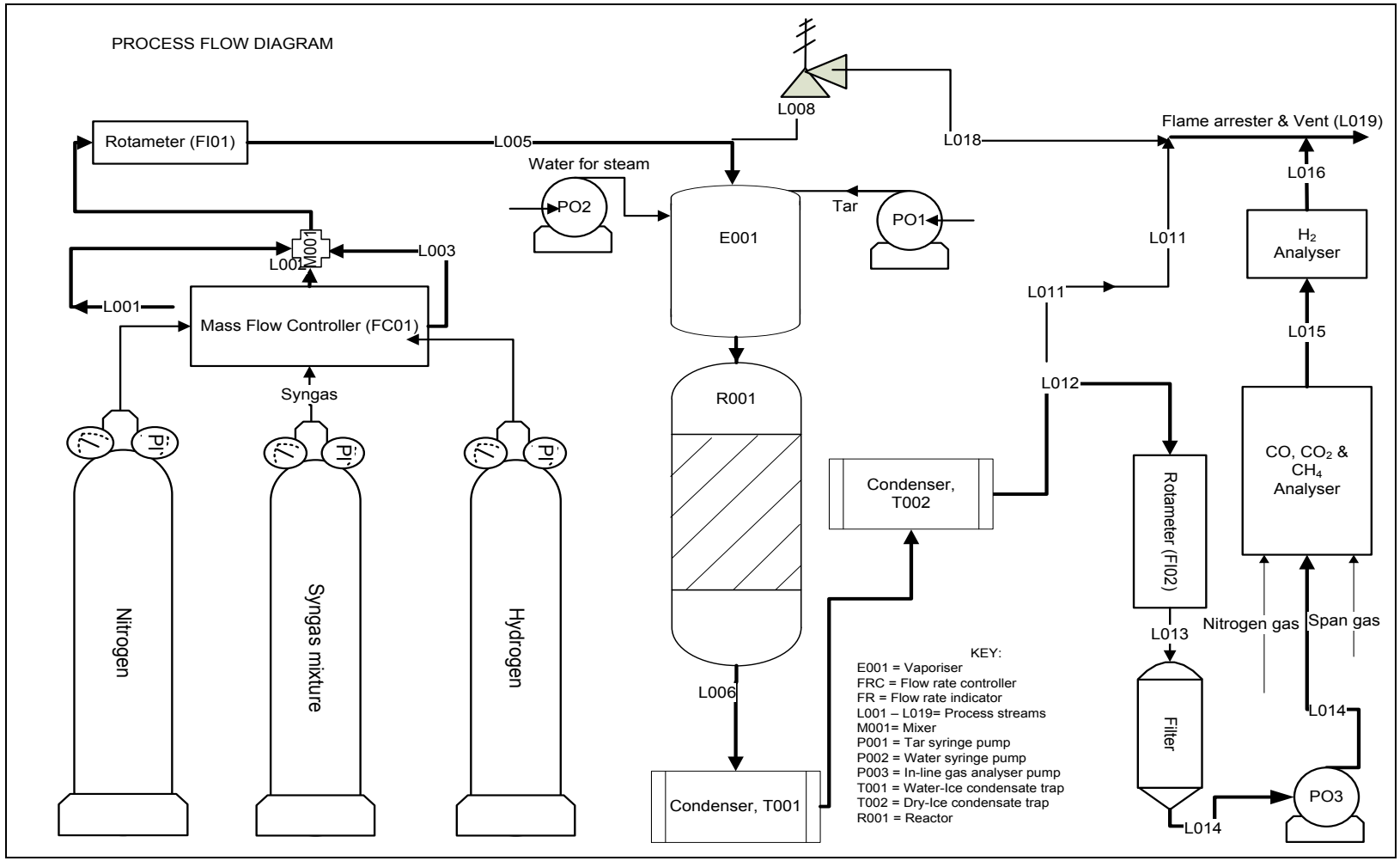


Figure 3:3: The Process Flow Diagram

3.1.3. Reactor and Trap Description

The reactor is a tubular reactor made out of an Incoloy material. The Incoloy reactor was 12 mm i.d, 2 mm wall thickness and 253 mm long as shown in Figure 3:4. A quartz tube of 9 mm i.d, 1 mm thick and 300 mm long, was added inside the Incoloy tube to prevent the Incoloy material from playing a part in the reactions. A quartz liner from a continuous fibre was used because of its physical and mechanical properties. Quartz is inert and has good stiffness, strength and thermal stability that it can withstand high temperatures as high as 1050^{o}C for long-term working and if it's in a form of a continuous fibre it maximises its achievable stiffness and strength as desired [67]. The quartz tube stretched from the top to the bottom pockets of the stainless steel fittings. Inside the bottom pocket, a high temperature spring was installed to suspend the quartz tube in a fixed position. The design of the reactor is shown in Figure 3:4.

At the inlet of the reactor a preconditioning chamber is attached using a 9.53 mm Swagelok-316 male union fitting as in Figure 3:4. The preconditioning section was constructed using Incoloy tube with 12 mm inside diameter, 2 mm wall thickness and length 50 mm. The inlet into the preconditioning tube was connected to a reducer from 9.53 mm tube fitting to a 6.35 mm tube adapter. The adapter was linked to a 6.35 mm Swagelok-316 Stainless Steel union cross fitting using a 25 mm long tube with a 6.35 mm tube diameter. The other three ends of the cross union fitting had inlets for tar at the top, steam and the carrier gas from the sides.

At the bottom end, the reactor tube is fitted with a reducing union that connects to the condensate traps and a connection to the inside thermocouple. There are two condensate traps placed in baths containing water-ice (first trap) and dry-ice (second trap). Both traps are U-shaped stainless-steel tubes with 12mm (i.d) and are connected to the bottom end of the reactor. The traps were made out of stainless steel 316 because it contains slightly increased nickel content and contains 2% - 3% molybdenum, making the metal more corrosion resistant. The exit of the dry-ice trap is connected to the gas analysers as illustrated in Figure 3:5.

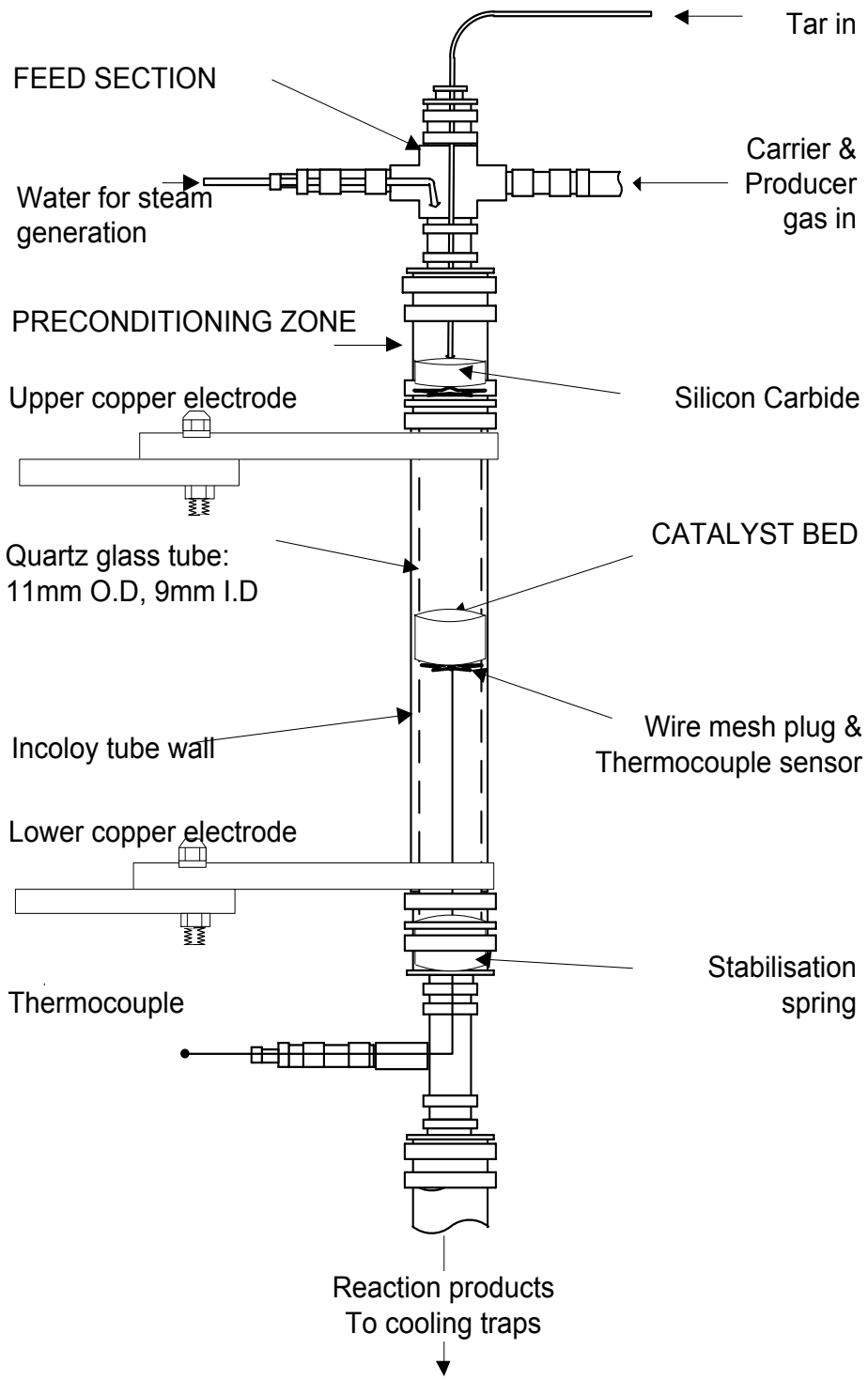


Figure 3:4: Final Reactor Configuration

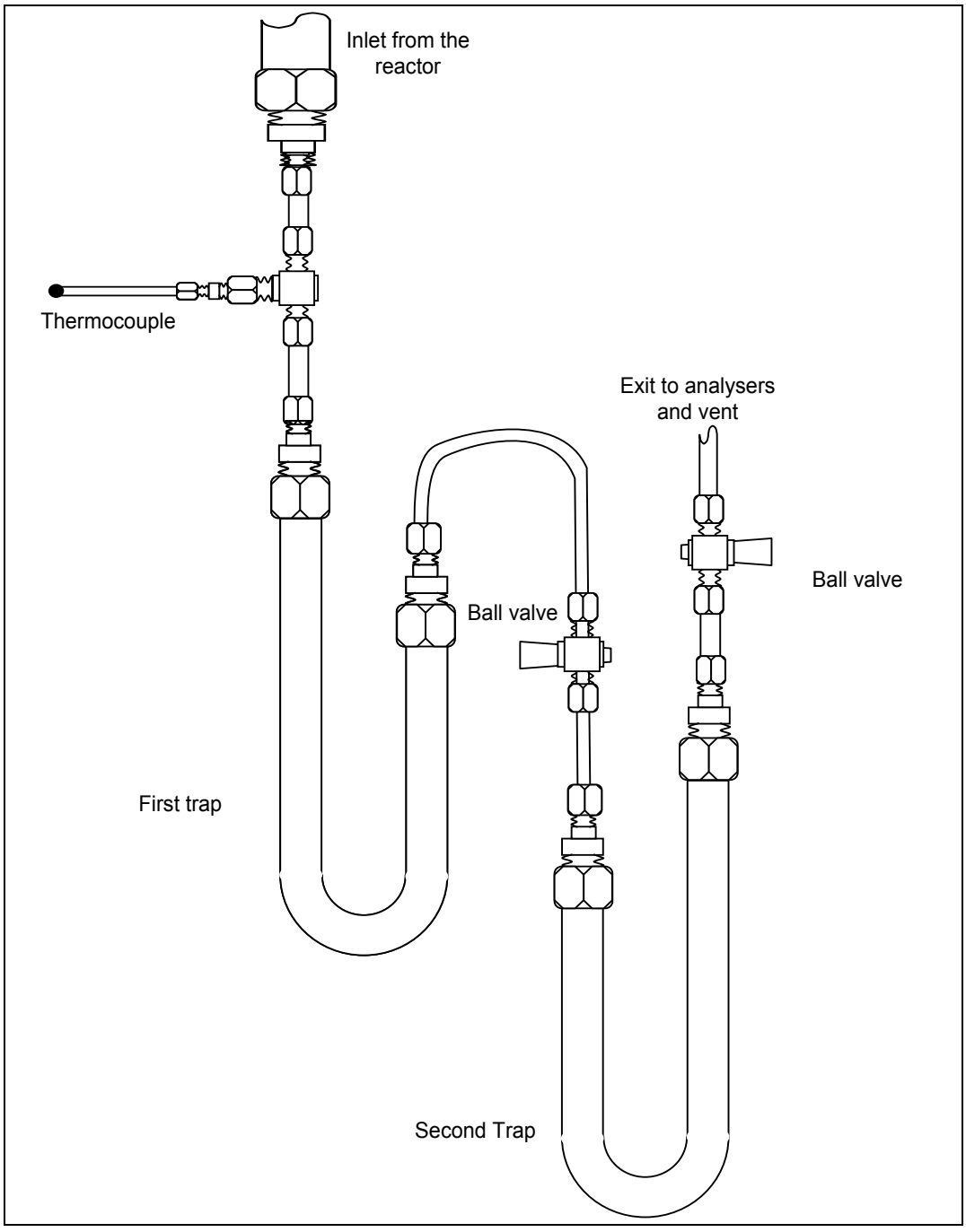


Figure 3:5: U-shaped Condensate Traps

3.1.4. Process Stages

3.1.4.1. Material Feeding

In the feeding section, nitrogen, hydrogen carbon monoxide, water and biomass tar are injected into the main stream flowing into the pre-conditioner. Gases nitrogen, hydrogen and carbon monoxide are primarily supplied from gas cylinders at one bar gauge pressure. A flashback arrester was fitted to the hydrogen stream for safety. All gases passed through a series of valves and a Microprocessor-based Brooks Smart Mass Flow Meter and Controller, where the flows were regulated to the desired rates. After the mass flow controllers, the gases were mixed together in the main stream to the reactor. A flow rotameter was installed to measure off the overall inlet gas flow-rate before the water and tar were added. The water and tar feed were steadily and precisely injected to the process line using KD Scientific programmable syringe pumps. Water was injected horizontally into the gas stream where it was immediately mixed and swept down the pre-conditioner along with the feed gas. Tar was injected vertically directly into the SiC bed in the pre-conditioning chamber where it was vaporised at 350 °C. Both the tar and water nozzles were 1mm in diameter. The arrangement of the feed nozzle and the design of the pre-conditioning chamber are illustrated in Figure 3:4.

3.1.4.2. Material Mixing and Pre-conditioning

Sweep gas (also referred to as the carrier gas) and pyrolysis gas from the cylinders was carried down the main stream with aerosols of water and the tar feed stream placed in the centre of the sweep gas line into the preconditioning chamber. The tip of the tar feed steam was positioned on top of a silicon carbide packing weighing 0.2g which was placed in the preconditioning chamber attached at the top of the reactor tube.

The pre-conditioning chamber was wrapped in an HT7 Glass Fibre heating tape code, which was spiralled around the entire pre-conditioning tube length. The tape was completely insulated with ceramic fibre and tightly wrapped with a woven ceramic tape to minimise heat losses. During each experiment, the heating tape was heated to a constant temperature of 350 °C. At this temperature, when tar and water were injected

the volatile material was evaporated and all feed materials mixed together. After the preconditioning chamber, the materials emerged as a mixture of gaseous reacts in the inert carrier gas. This gaseous mixture was then steadily and continuously carried down into the reactor by the flow of the sweep gas. Additional joints in the preconditioning zone were minimised to avoid risks of leaks, and the SiC packing was kept as small as possible to minimize risks of tar clots in the packing. A preconditioning temperature within this range was chosen after TGA tests confirmed it was a suitable range to vaporise the tar with minimal risks of carbonisation and tar clots in the preconditioning chamber. In addition, at these temperatures the volatile material would not thermally decompose for further reactions to occur before reaching the reactor zone.

3.1.4.3. Reaction Section

The reactor tube was tightly clamped and heated by two electrodes one at the top and the other at the bottom on the outer wall of the metal tube. A quartz liner tube was placed inside the metallic tube and a catalyst bed was place inside the quartz liner tube supported on a stainless steel wire-mesh plug. The temperature along the length of the tube was significantly different between the top and middle point. So, the bottom of the catalyst bed was placed at 12 cm (midway) down the reactor tube. The thermocouple was introduced into the reactor from the bottom through at Tee piece, tailing up the tube with its tip just touching the bottom of the reactor.

3.1.4.4. Tar Collection and Liquid Extraction

The organic contaminants tar and water were collected by condensation in two traps. The traps were designed as U-shaped stainless steel tubes with an inside diameter of 12mm. These traps were connected in series and placed in condensate baths to gradually holdup the liquid products at ambient temperature, separating the liquids from the producer gas.

Condensation of the liquid effluent was directly achieved by immersing the first trap in an ice-water bath to condense and collect the water, whereas the second trap was

immersed in dry ice, contained in a Dewar, to condense and collect the remaining liquid effluent. The second trap contained a coiled wire mesh net to act as a filter to retain liquid effluent. This coiled wire mesh effectively enhanced both mass and heat transfer across the length of the tap, dispersed the gas flow and trapped the condensed tar. The effectiveness of the trap was also checked to ensure there was no tar escaping by measuring tar and checking there was no tar in the filter after the trap outlet.

At the end of each experiment, the traps and lines that were at low temperature were left to warm to room temperature. At room temperature, the first trap was rinsed with chloroform to extract solvents such as water and reformed tars. All other surfaces of the lines and second trap were rinsed with 4:1 chloroform and methanol solvent mixture; to recover/ extract the condensed materials. Chloroform was preferred for extracting solvents in the first trap because it can easily be separated from water.

3.1.4.5. Gas Measurement

The gas leaving the traps was fed through a PTFE hose which connected to a rotameter. The flow was then split to the gas analysers, with the remaining flow being vented to a safe place. A quartz wool filter was placed in the line before the analysers. This was partially filled with the wool and partially with silica gel beads (as seen in Figure 3:6). The quartz wool was essentially employed to trap any particles. And the silica gel beads removed residual moisture before the gas analysers. Without the filter, low moisture and particulate contents would affect the analysis.

The flow of the sample gas was aided by an internal pump in the gas analyser. The overall flow rate to the analyser cells was regulated by an adjustable flow meter, which was located between the pump and the gas detector cells. During experiments, the product gas was sampled throughout the entire period of each experiment. The sample gas flow rate in the gas analysers was maintained at 0.1L/s. As the gas discharged out of the gas analyser, it was directed to the vent together with the by-pass and immediately burnt on a flare stack, before the combusted gases were safely vented off to the atmosphere.

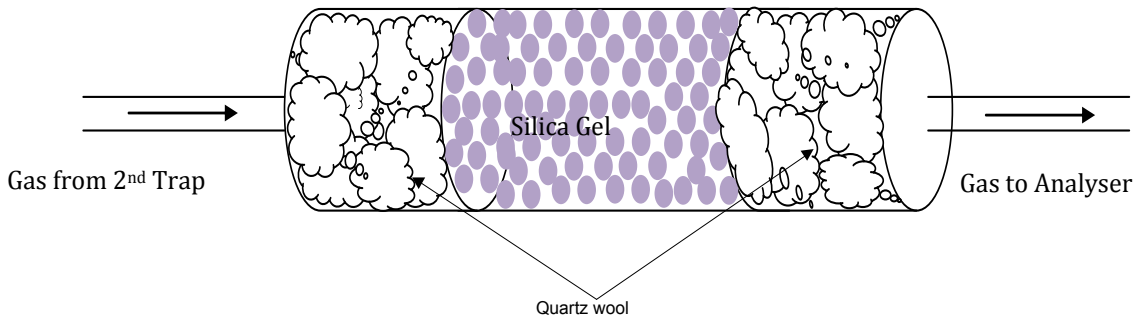


Figure 3:6: Gas Line filter

3.1.5. Experimental Procedure

Two similar procedures were followed during experiments. The first procedure was followed to conduct tests without a catalyst bed while the second procedure was followed to conduct tests with a catalyst bed inside the reactor. The procedures followed during experiments are given below.

3.1.5.1. Experiments Without Catalysts

A strip of a circular wire mesh was weighed and firmly placed in the preconditioning chamber forming a plug. The preconditioning chamber was tightly attached on top of the reactor metal tube and a weighed quantity of silicon carbide crystals was placed on the surface of the mesh plug. A weighed quartz tube with a mesh plug placed halfway down the tube was inserted inside the metal reactor tube. At the bottom of the reactor, the quartz tube was supported by a high temperature spring. A thermocouple used to maintain a steady and uniform bed temperature was fitted with its sensor positioned at the centre of the reactor mesh plug. The reactor body was then placed between two electrodes, and the whole reaction unit was set up with controlled electric power connections, feed stream connections and condensate trap connections. The moisture condensate trap was fitted directly below the reactor and its other exit was connected to the tar trap. The outlet from the second trap was connected on the vent and online

analyser stream. The moisture and the liquid tar collector traps were successively immersed in a water-ice bath and dry-ice Dewar respectively to condense the effluents.

The process lines, reactor and traps were leak tested to prevent any gas escaping to the surroundings and purged with nitrogen to create an inert atmosphere by remove any accumulation of unwanted materials that may otherwise build up in the streams. Although the process was purged with excessive quantity of nitrogen gas, the amount of nitrogen gas required using design standards had been calculated using the displacement equations below. If, however, had the process involved a large reservoir vessel, an alternative equation for pressurisation purging is also shown below.

Displacement of unwanted materials; purging equation:

$$V = Vo*P/14.7$$

Where: V = Total nitrogen volume required (scf), V_o = Water volume of pipeline (cf) and P = absolute pressure of nitrogen in the pipeline during purging (psia)

Otherwise; Pressurization Purging – where conditions do not permit a sweeping action of nitrogen through the vessel:

$$V = 1.2nV_o*P/P_a$$

Where: P = absolute pressure after pressurization with nitrogen (psia), P_a = absolute pressure after exhaust (psia), n = number of purges = C log C_o/(logP_a log$P$), C_o = initial content of gas to be removed, C = final content of gas to be removed.

After leak testing, a controlled flow of nitrogen was started and the reactor heated to the desired temperature. Once a steady set temperature was reached, simultaneously, water for steam generation and tar were injected into the preconditioning chamber. The vaporised gases were heated to the set temperature in the nitrogen environment, whilst no catalysts were used or increased pressure applied. Thereafter, the product gas drawn off downstream of the reactor and the condensate traps was analysed in the gas analysis units. At the end of the test time, the electric heating was switched off and the

equipment was cooled to room temperature. Nitrogen flowing through the process lines was maintained and the traps were kept immersed in their coolants until the reactor had cooled down to room temperature. At room temperature the rig was dismantled to remove the reactor and the traps were removed from the coolants to warm up to room temperature. Water and tar were recovered from the traps and carbon products were recovered from the reactor and the preconditioning chamber.

3.1.5.2. Catalytic Experiment Procedure

Where a catalyst was used, the procedure to set up the process was similar to that followed during the non-catalytic tests, with the main differences described below. A weighed wire mesh was placed 16 cm from the top the quartz reactor tube forming a plug to hold the catalyst bed. The plug was held in position by the quartz tube wall but also its bottom was supported by the thermocouple. At the top of this plug, a weighed quantity of catalyst was placed on top of the plug and the quartz tube was placed inside the reactor metal tube. Once set-up, with gaseous nitrogen passing through, the reactor was heated to 900 °C and the gas passing through the tube was adjusted to a mixture of 45% hydrogen and 55% nitrogen (by volume) to reduce the catalyst. The catalyst was reduced for one hour then; the nitrogen flow rate was restored while the hydrogen was stopped. The reactor was left to acclimatise to a nitrogen environment. After a further 10 minutes, steam and tar were injected into the process. At the end of the experiment the catalyst was recovered; the carbon content on the catalyst was obtained by gravimetric analysis, while the equipment was cleaned to recover the tar as described for non-catalytic operation.

3.1.5.3. Process Control

The key process variables during the reactor operation are temperature, gas flow rate, reactant flow rate, feed material and pressure. Most of these variables are manually monitored during the rig operation.

Table 3:4: The key operational process variables

Process variable	Control gauge	Control measure
Temperature	Thermocouple	Temperature control box
Flow rate	Flow meter	Automatic mass flow meter
Pressure	Pressure gauge	Relief value
Reactants	Feed syringe	Syringe pumps
Residence time	Bed size & Flow rate	Bed size

Reactor Temperature Control

The reactor was heated by two electrodes from an electric transformer which generated heat by the resistance it encountered during its passage along the reactor wall. The input supply to the transformer is 240 volts to 250 volts and a maximum current of 16 amps. The output of this transformer is 2.5 volts and provides a current of up to 1600 amps. The desired test temperature was pre-set up in a temperature control box, which is connected to the voltage and power control box. The temperature control system consisted of a temperature controller box, a voltage controller box and a transformer with two joule heated electrodes. The temperature controller box was used to pre-set the desired temperature. It communicated the set parameters to the voltage controller box which, in response, it induced a regulated voltage to the transformer. The transformer supplied an equal amount of power into the two electrodes that clamped the top and bottom ends of the reactor and subsequently heated it up.

The temperature in the reactor is controlled using a thermocouple placed inside the reactor with a feedback loop to the transformer and back to the electrodes. The reactor outside wall temperature was monitored using a separate thermocouple which at the same time was used as the power cut-off thermocouple, in case the reactor temperature reached the set high-high temperature alarm level.

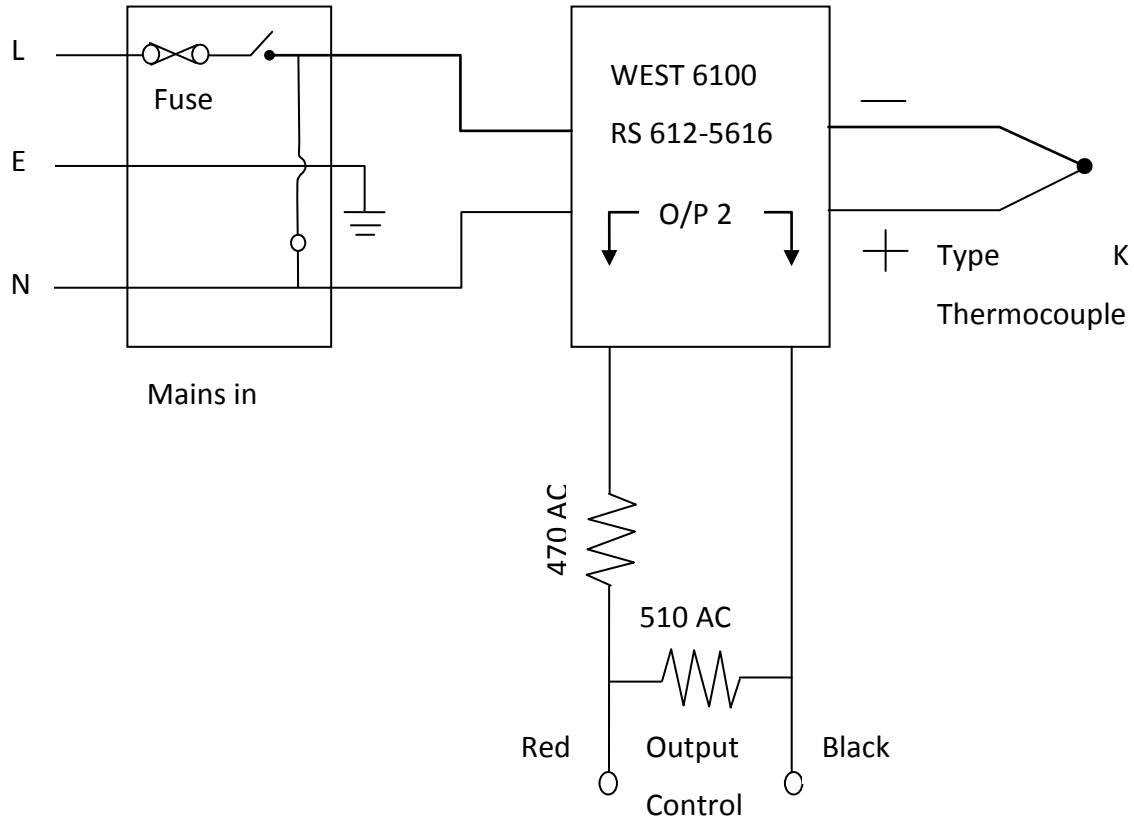


Figure 3:7: The Reactor Temperature Controller

Pressure control

At the top of the reactor, a high temperature resistant pressure gauge was installed. This pressure gauge was used to monitor the pressure in the system and ensure it was within the desired operating limits. In all experiments, the rig was operated at a pressure of 1.1 barg. Before each experiment, the reactor was leak tested by pressurising the system at 5 bar using nitrogen.

A pressure relief valve was installed in the feed line just above the pressure gauge and closer to the reactor. This was set to vent to a safe place at 1.32bars (20% over the normal operating condition) and prevented excessive pressure build up in the reactor under unplanned conditions. During leak tests, the pressure relief value was isolated off using a high temperature valve between the top of the reactor and the relief valve.

Flow control

All gases were supplied from pressurised cylinders using the flow arrangement presented in Figure 3:3. Each cylinder was fitted with a 2-stage pressure regulator connecting to a 3.18 mm stainless tube supplying the gas into the process. Each of the lines from the hydrogen cylinder, span gas cylinder and producer gas cylinder was fitted with a flashback arrester to prevent any potential risks. On each of the pressure regulators, the outlet pressure gauge was regulated to feed the supply lines (stainless tubes) at 1bar. The span gas, directed to the gas analyser, was fitted with a 2-stage pressure regulator. This cylinder outlet pressure regulator was maintained between 0 – 0.3 barg and was set to give a normal nominal outlet pressure of 0.2 barg.

The gas flow rates through the system were precisely controlled by three mass flow valves and a meter controller. The mass flow valves were installed in the line between the gas cylinders and the T-piece that combined the lines flowing with the various process gases. These mass flow valves were in a loop together with a mass flow meter and controller. The desired process flow rates were manually entered into the flow controller that automatically controlled the mass flow valves. In case of any blockage or high pressure build up in the line beyond the mass flow valves, these valves would automatically trip and interlock, cutting-off the flow and preventing any further pressure build up in the process. In addition, if any over flow had occurred, a by-pass line was connected to a pressure relief valve discharging directly to the vent.

During flow in pipe-lines, static pressure and dynamic loss of flow due to friction in the pipe, and pressure loss through the equipment or for miscellaneous reasons were

accounted for. To overcome these uncertainties, the flow was measured before and after the reactor.

Based on design principles, the process was designed to handle flow pressures of several times higher than 10% over the desired maximum pressure (1 barg) calculated for each experiment. All pipes were chosen to meet British Standard 5500 using the formulas: $t = (Pd/(20\sigma_d + P)$ for pressurised pipes and Schedule number = $(P_s \times 1000)/\sigma_s$ for unpressurised process pipes.

Where t = pipe thickness, P = internal pressure (bar), d = pipe outside diameter (mm), σ_d = design stress at working temperature (N/mm^2), P_s = safe working pressure (N/mm^2), and σ_s = safe working stress (N/mm^2). A schedule number of 40 was used in all applications.

3.1.5.4. Alarms and safety indicators

Carbon monoxide and hydrogen gas detectors were placed at various points around the rig including the gas cylinders and the gas analysers. Pressure indicators were placed after the mixer of the feed gases, above the reactor and at the exit of the second condensate trap. Additional thermocouples were installed on the outside wall of the reactor to indicate temperature readings and cut off temperatures at 30 °C (high – high level) above the normal wall operating temperature.

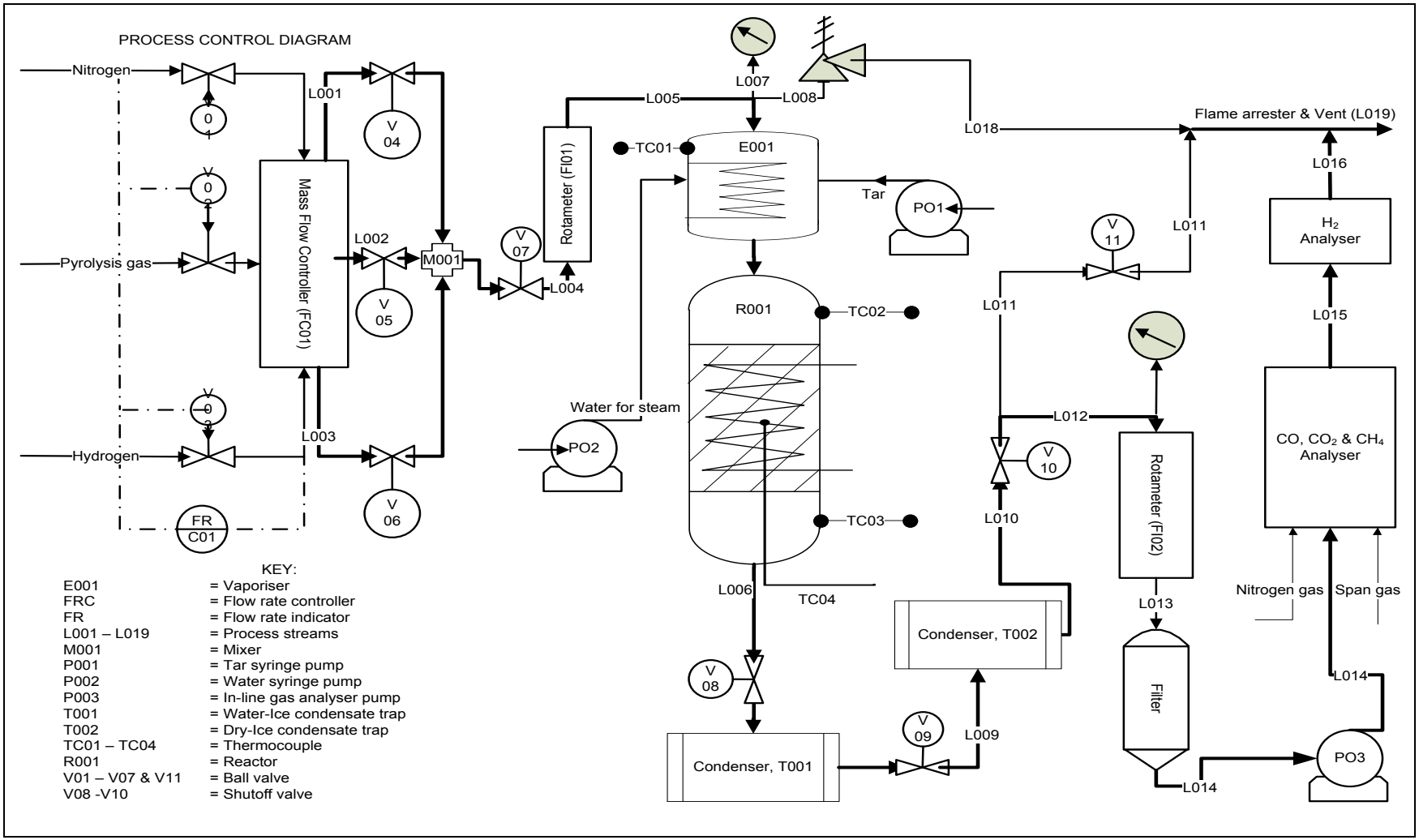


Figure 3:8: Process Control Diagram

3.1.6. Analytical Techniques

Different analytical techniques were used to characterize the products of reaction and the used catalysts. The methods used gravimetric and thermogravimetric (TGA) analysis, chromatogram analysis, on-line gas analysis, SEM analysis and Raman spectroscopy for carbon analysis. The methods are described below.

3.1.6.1. Gravimetric Analysis

Gravimetric analysis was used to determine the total amount of organic compounds recovered in the traps and the amount of carbon deposits on the spent catalysts. To recover the organic tar in the traps, firstly, water was extracted from the first trap by rinsing the trap with chloroform. The chloroform and water mixture was then emptied into a volumetric flask where it was left to settle forming two immiscible liquids. The volume of water was given by the volume of the aqueous layer.

Recovery and determination of reformed/unconverted tar

After rinsing the first trap with Chloroform, the two traps were then washed with 4:1 chloroform and methanol mixture to extract the organic tar compounds. The recovered mixture and the chloroform fraction from water extraction were emptied into a small beaker and placed in a circulating oven set at 35 °C for 5 hours to evaporate the solvent. After drying, the tar in the beaker was then left for 5 minutes to cool to room temperature. The weight of the organic tar left in the beaker after drying was determined by weighing the beaker and its contents on an analytical balance.

Alternatively, (a method tested during the preliminary tests), the extracted solvent was emptied into a conical flask and placed on a standard rotary evaporator, set up in a fume cupboard at 40 revolutions / minute for vacuum distillation. The flask was then placed into a water bath set at a temperature of 45 °C and left to operate for 25 minutes. The remaining solvent from the reduced sample, after distillation, was evaporated in a circulating oven at 35 °C for 30 minutes. After drying, the tar which was left at the bottom of the flask was left for 5 minutes to acclimatise at room temperature

and then weighed on the analytical balance. Both methods adapted proved to give reproducible results that agree.

TGA analysis

A thermogravimetric analyser (Pyris 1 TGA, PerkinElmer) was used to measure the weight of carbon deposits on the catalysts. For other uses, the TGA was used to monitor mass loss of tar with increasing temperature.

A. To monitor the mass of carbon on the catalyst:

A sample of catalyst was placed on the TGA pan and followed the steps below:

In Nitrogen at 40.0 mL/min,

1. Hold for 15.0 min at 50 °C.
2. Switch the gas to air at 40.0 mL/min and immediately heat from 50 °C to 900 °C at 10 °C /min.
3. Hold for 30 minutes at 900 °C.
4. Switch the gas to Nitrogen at 40 mL/min.
5. Immediately cool from 900 °C to 30 °C.

B. To evaporation tar and measure the relative weight of tar with temperature,

The TGA was set to the following programme steps

In Nitrogen at 40 mL/min,

1. Hold for 15.0 minutes at 40 °C.
2. Heat from 40 °C to 600 °C at 2 °C/min.
3. Hold for 15.0 minutes at 600 °C.

4. Heat from 600 °C to 900 °C at 2 °C per minute.

5. Hold for 10.0 minutes at 900 °C.

The change in weight of the sample was obtained as a function of temperature.

The analysed data for both the tar weight and catalyst weight as a function of temperature (*and time*) give the idea of the boiling point distribution of the collected organics but also gave the residual moisture after the evaporation and separation procedures and quantify the lost carbon from the catalyst.

3.1.6.2. Gas Chromatographic Analysis

A GC-MS was used to identify the organic compounds in the tar, before and after reacting. This analytical equipment has two main blocks: the gas chromatograph and the mass spectrometer, which can characterise each of the components. In this project, GC-MS analysis was done by the laboratory assistant from the department of chemistry in Imperial College London at the South Kensington Campus. The equipment used was described as an Agilent HP6890 GC using a BPX5 column of 30 mm long x 0.25 mm diameter. Samples were run using Helium as a carrier gas at 1 mL/min. The column oven temperature was programmed from 50 °C, held for 0.5 minutes, then ramped up at 10 °C/min to 300 °C and then held for 2 minutes.

3.1.6.3. Online Gas Analysis

To analyse the gases in the product stream, a multi-gas analyser and a hydrogen gas analyser were added in series at the end of the product stream, after the gas had been cleaned.

Multi-gas analyser

The concentrations of gases: carbon dioxide, carbon monoxide and methane were analysed online using an MGA3000 Multi-Gas Analyser. Its output was calibrated with a gas of known composition.

The analyser unit consisted of infrared gas analysis (IRGA) benches that generated signals which were proportional to the infrared absorption of the CO_2, CO and CH_4 gases. The analyser absorption system was designed based on two key principles that: (1) all hetero-atomic gases absorb or transmit light energy in the infrared region at specific wavelengths that are dependent upon the chemical structure of each type of gas. (2) The level of absorption was proportional to the mass of the gas present. This level of absorption measurement was relative against the references for zero gas and a calibration gas concentration.

The MGA3000 analyser was designed specifically with the ability of detecting the identified gases within the ranges presented in the table below. The output gas concentrations were displayed and the absorption measurement was recorded though an analogue and digital signal outputs on to a computer as a percentage concentration.

Table 3:5 shows the gas concentration ranges specified for the MGA3000 multi-gas analyser employed.

Table 3:5: Multi-Gas Analyser Ranges

Gas	Detection range 1	Detection range 2	Accuracy
CO_2 (%)	0 – 1	0 – 5	+/- 0.01
CO (%)	0 – 5	0 – 20	+/- 0.01
CH_4 (%)	0 – 1	0 – 5	+/- 0.01

The flow rate of the gas sample to the analyser was set using a diaphragm pump which was internally fitted into the analyser box. The gas circulated through the analyser through a series of polytetrafluorothalene tubes to the various analyser subunits.

The overall flow rate of the sample gas in the tubes would affect the response time of the measurement; for this reason, the analyser was fitted with an adjustable display flow meter (flow sensor). This flow meter was used to monitor and control the flow rate

through the infrared sensors. The performance of the analyser unit was optimised by adding a filter (consist of wool and silica gel) in the sample line, which kept the inlet gas sample dry, free of moisture and particulates.

In addition, all line entries to the analyser were fitted with in-line filters that stopped any foreign matter entering the analyser unit. It was also necessary to switch off the sample pump during standby conditions but keep the analyser running for most of the time to prevent vapour condensation in the unit which would deteriorate the analyser performance. Figure 3:9 illustrates the basic gas flow arrangement in the MGA3000 analyser.

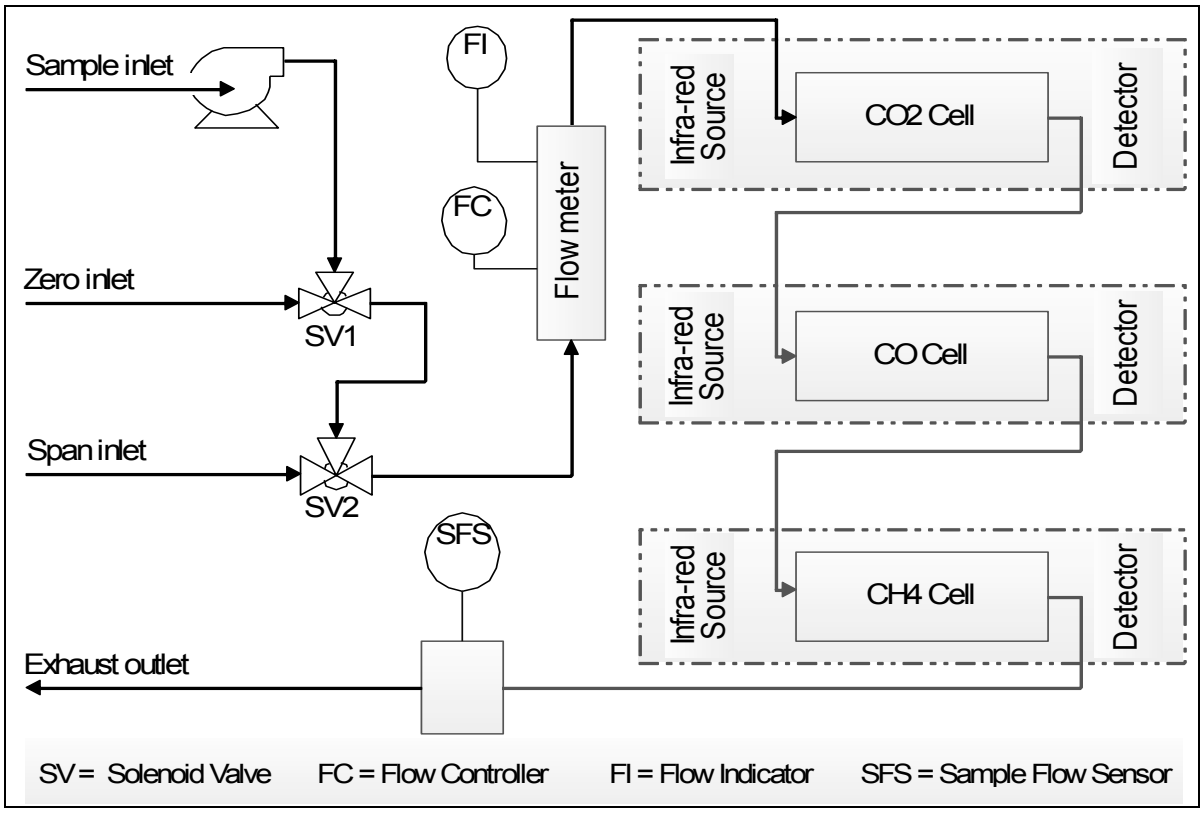


Figure 3:9: The MGA Series Analyser – Basic gas flow arrangement

NB: The IR analysers are pressure sensitive, so all procedures were done at the same, near atmospheric pressure.

Hydrogen analyser

To measure the H_2 concentration, a K1550 series Hydrogen analyser was installed on the rig. This analyser works on the principle of thermal conductivity and suitable for measurements in a binary or pseudo-binary mixture. Of all the gases that were present in the products stream, hydrogen has a relatively higher thermal conductivity, which meant that the analyser could measure H_2 selectively. However, CO_2, CH_4 and CO gas concentrations still caused a noticeable impact on the H_2 reading due their thermal conductivity. This impact was investigated and a correlation factor was developed to contemplate for the H_2 content in the fuel gas. This was achieved by deduce a hydrogen calibration curve shown in Appendix 7. Overall, the effect of CO_2, CH_4 and CO on hydrogen analysis was relatively low, presumably due to a relative higher H_2 thermal conductivity characteristic and the low concentrations of CO_2, CH_4 and CO in the stream.

The hydrogen analyser also featured a measurements of hydrogen purity in various ranges, from 0 – 20% to 0 – 100% but in this project it was used in a range of 0 – 100%.

3.1.6.4. Scanning Electron Microscopy (SEM)

SEM was used to observe the morphological features of the fresh and spent catalyst samples. This technique uses a beam of electrons passing through an evacuated column to form an image with a greater depth of field. It was hence used to obtain information about the structural and elemental changes of the catalyst.

The SEM operates by using built-in electromagnetic lenses which focus a beam of electron onto the specimen surface. While the electron beam is focused onto the specimen, a beam from a cathode ray tube display screen is also scanned over the sample. When the electron beam hits the atoms of the sample, secondary and back scattered electrons are emitted from the sample. A scintillator collects the emitted electrons forming a signal that is used to modulate the brightness of the cathode ray tube.

In this analysis, a JEOL model JSM-5610LV microscope, with an accelerating voltage of 20 keV and working distance of 20 mm was used. Catalyst samples were adhered to gold plated stickers which were then mounted on to a 10 mm diameter aluminium JEOL type stub. The stubs were then introduced into the evacuation chamber for imaging and elemental analysis.

3.2. Sources of errors, uncertainties and accuracy of materials

Calibration gas and producer gas: The calibration and producer gases used were a mixture of gases as described in section 3.1.1.3. The accuracy of the mixture specified by the supplier was +/-2% of the certified values. The cylinders for both calibration and producer gas were kept the same throughout the entire project in order to maintain consistency. The level of accuracy is presented in Table 3**:6**.

Mass flow controller: The mass flow controller itself is given an accuracy of +/-1%, however this mass flow controller had been calibrated for a specific gas. For this reason, it was recalibrated for the gas used in this project and a maximum error was estimated. The other source of inaccuracy on the mass flow controller was the interface used to control the mass flow controller. The controller was specified with a 0 – 5 V signal and theoretical resolution of 12 bit which would give an accuracy of +/-1.2 mV but practically, having conducted tests with a bubble column, the controller was found to give an error of approximately +/-0.001 L/min of the set point.

Rotameter: Two identical rotameters, of the same make using a freely moving float in tapered, housed and scaled tube, were used to measure the gas volumetric flow. One rotameter was vertically installed in the main process line before the preconditioning chamber and the other in the main process line between the exit of the traps and the split for vent and analyser line. These rotameters gave repeatable measurements but it was always necessary to clean them regularly, particularly the one at the exit of the traps. Each of these rotameters measured to have an accuracy of +/- 2.5%.

Tar feed and water fee syringe pumps: Two identical kd-Scientific Legato 100 syringe pumps were used. One pump was used to inject tar and the other to inject water for

steam generation. Calibration on these pumps by measuring the mass of water against time led to conclusions that they had an accuracy of +/-0.5% and a reproducibility of +/-0.05%. For various syringes this accuracy is likely to change, hence, the same syringes and pumps were used throughout this project. For tar fed at 1.05 mL/h this gives an error of +/-0.00525 mL/h and for water injected at 1.7 mL/h (S/C = 2) and 2.5 mL/h (S/C = 3) this gives an error of +/-0.0085 mL/h and +/-0.0125 mL/h respectively.

Temperature measurement: Both the preconditioning chamber and reactor temperatures were measure using K-Type thermocouples specified with an accuracy of 2% of the reading. During the design of the process, the temperatures from the bed centre to the top and to the bottom were identified to have low temperature difference at lower temperatures and a higher temperature difference at higher temperatures.

Online gas analysers. The precision of each of the analysers used was given as 1% but this was affected by the accuracy of the calibration gas, which introduced additional inaccuracy. The overall error induced in the analysers was therefore estimated to be the summation of error from the calibration gas and the analyser. The overall estimated absolute error in for each gas is shown in the Table 3**:7**.

Cylinder		CO_2 (%)	CO (%)	CH_4 (%)	H_2 (%)
Calibration gas	Conc.	5	20	1	20
	Accuracy	0.1	0.4	0.02	0.4
Producer gas	Conc.	1	5	1	20
	Accuracy	0.02	0.1	0.02	0.4

Table 3:6: Calibration and Producer Gas degree of accuracy

Gas measured	CO_2	CO	CH_4	H_2
Absolute limits of accuracy	+/-0.011	+/-0.014	+/-0.012	+/-0.014

Table 3:7: Absolute Gas limits of gas accuracy

4. THERMODYNAMIC EQUILIBRIUM MODELLING AND PRELIMINARY TESTS

In this chapter, Aspen plus simulation was used to model and predict the equilibrium composition of the gas. Once the process was modelled, preliminary experiments were carried out for training purposes using the hot-rod reactor. The reactor system was modified to improve its performance and tested for its reliability by performing repeated tests. The results from both simulations and preliminary results are reported in this chapter and chapter 5 where they are compared with the experimental data.

4.1. Thermodynamic Modelling in Aspen Plus

Aspen plus is a computer-aided software used to build model and simulate processes. The software can be used to create simulation models, define a process flowsheet with property data such as components, streams and physical data, and run the simulation to generate a product composition. It works by specifying the desired values for flowsheet variables and uses the underlying physical relationships including rate equations, thermodynamic equilibrium and material and energy balances to predict process performance. With this software, it is also possible to define design specifications, sensitivity, convergence, property analysis, optimization and data regressions.

The key advantage of using Aspen plus software is that; one can simulate actual experimental behaviour and rapidly predicts the products behaviour at equilibrium. In aspen plus one can interactively change specifications, including the process flowsheet configuration, feed compositions and operating conditions. With such flexibility, one can run new cases, generate results and analyse alternatives within a short period. In this project Aspen plus software was used because it simulates the input data, such that the results can be compared with the experimental data. A replicated model of tar was simulated to examine the process parameters and generate the process mass balance, products and equilibrium relationships. The equilibrium analysis is compared with experimental results in subsequent chapters.

In order to emulate the experimental variables, the process feed flow rates were firstly calculated based on some guide taken from the literature and the reactor dimensions. By specifying the feed conditions and using a range of variables, the Aspen model input parameters could be specified and these are presented in Table 4:1.

Table 4:1: Specified conditions for Aspen modelling

Feed input components	**Total Flow (L/min.)**
44.03%C, 7.05H, 0.36%N & 48.56%O (density 1200kg/m^3)	1.745E-05 – 6.109E-05
H_2O(l)	1.386E-05 - 1.455E-04
Carrier gas N_2	0.209 – 0.627
Streams and block data	**Temperature (^oC)**
Conditioning Heat exchanger	350
Reactor	350 - 1000
Feed streams and condenser output	25

4.2. Thermodynamic Modelling and Equilibrium Results

The RGibbs reactor model was selected for this modelling, which uses Gibbs free energy minimization with phase splitting to calculate equilibrium. In literature there are no defined reactions for the tests performed in this work, and for this reason the RGibbs reactor model was appropriate since it does not require specifying the reactions. A similar approach was undertaken elsewhere in a study of heat integration strategy for economic production of combined heat and power from biomass waste [28] to model a single phase (vapour) chemical equilibrium. In order to do this, the reactor operating conditions and phase for equilibrium calculations were specified. Also, the possible products, inert, temperature and pressure for equilibrium restrictions were specified.

The variables and data points as inputs into the simulation package were manipulated and optimised in order to validate the practical experimental work. A range of results from the simulation output were then compared with the output from the experimental

work. To make a rational comparison, the specified conditions in the simulation package were similarly the same as set for the experimental work. The results from a series of simulation models are plotted in Figure 4**:1**, Figure 4**:2** and Figure 4:3.

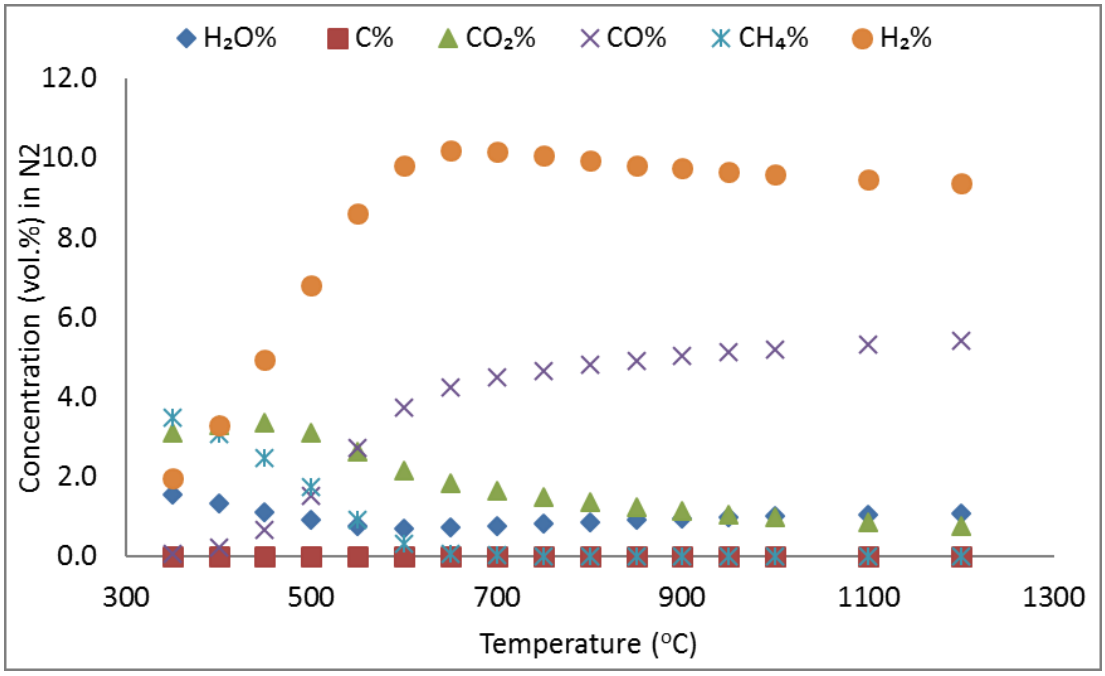


Figure 4:1: Equilibrium composition as a function of Temperature on a Dry-Basis. Feed at 100 g/Nm³ of Tar in N_2 and an S/C of 3.

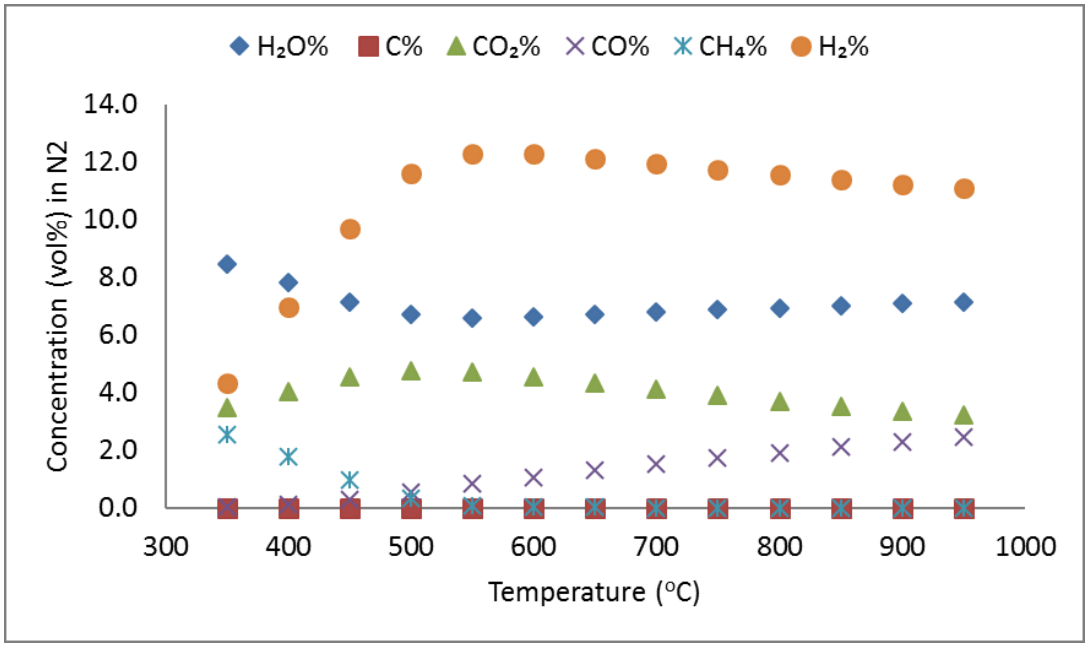


Figure 4:2: Thermodynamic Modelling of Products from a Feed on a Wet-Basis. Feed at 100 g/Nm³ of Tar in N_2 with an S/C of 3.

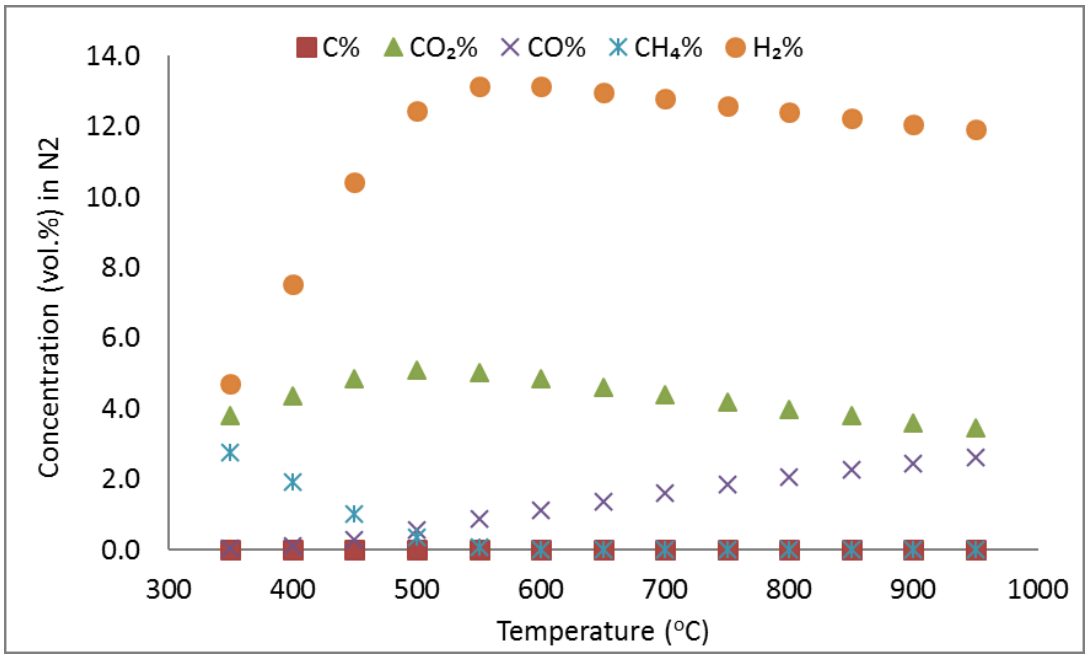


Figure 4:3: Thermodynamic Modelling of Product Gases from a Feed on a Wet-Basis, excluding water in the Products. Feed at 100 g/m³ of Tar in N_2 with an S/C of 3

The results plotted in Figure 4**:1**, illustrate the gas concentration obtained from a feed specified without any additional steam to the process. Figure 4**:2** and Figure 4:3 show the gaseous composition of the products formed from a feed specified with added steam to promote the steam reforming reactions. The main difference between Figure 4:2 and Figure 4:3 is that the product stream in Figure 4:2 takes into account for steam in the products whereas Figure 4:3 excludes steam in the product stream, and the rest of the gaseous are normalised to reflect what will be seen from the gas analysers after condensing of water during experiments. In all three plots, the gaseous concentrations of the predicted product compounds are shown for over a temperature range covering between 350°C to 950°C at equilibrium. In each simulation, 100g/Nm³ of tar in nitrogen were introduced into the reactor with a 1 bar pressure.

Observations of the represented data in Figure 4**:1**, Figure 4**:2** and Figure 4:3 show that at temperatures below 500 °C the gas produced has a low heat value because of the

products composition, which is of less interest. At 600 ^{o}C and above, a syngas rich product with a higher heating value was obtained. From these simulations and guide from literature, the operating temperatures of the preliminary tests were selected for a range between 850 and 950 ^{o}C, given that at these temperatures the feed is carbon is predicted to reach high conversions, the products are predicted to reach a steady state and a high heating value gas would be formed. Table 4**:2** shows the predicted gas concentrations at equilibrium. The simulations were performed at a S/C of 3, in nitrogen specified as a carrier gas and tar concentration at 100g/Nm^{3}.

Table 4:2: Thermodynamic Modelling of Products from 850 ^{o}C, 900 ^{o}C and 950 ^{o}C and 1 bar reactor conditions and feed at 100 g/Nm³ of Tar in N_2 with an S/C of 3

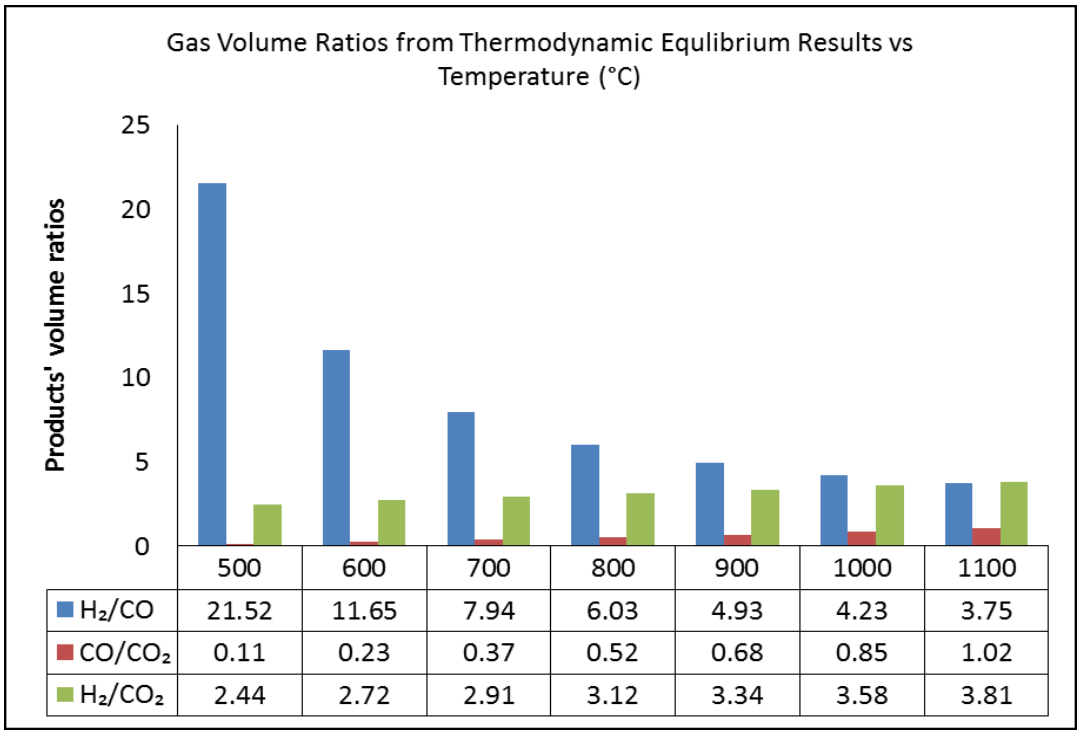
Operating conditions Using 1 bar, S/C of 3		Concentration (vol. %) balance with N_2				
	Temperature (^{o}C)	CO_2	CO	CH_4	H_2	H_2O
Equilibrium modelling	850	3.52	2.10	0.00	11.38	7.00
	900	3.35	2.28	0.00	11.22	7.07
	950	3.20	2.44	0.00	11.07	7.23

The tabulated data representing the simulations at 850 ^{o}C, 900 ^{o}C and 950 ^{o}C in Table 4**:2**, suggest that the H_2 concentration is approximately four times the concentration of CO. The CO concentration is slightly lower than CO_2 at 850 ^{o}C but slightly higher as the temperature was raised to 900 ^{o}C and 950 ^{o}C. There is no CH_4 gas is left in the system at these temperatures. These observations match with what is reported in literature of biomass gasification. Later in this chapter and the following chapters, these results are compared with the experimental figures obtained from tests run at similar conditions.

4.2.1. Product Gas ratios

In chemical synthesis, syngas is used at specific ratios to optimise the production of a variety of products. For instance in methanation and in Fischer Tropsch processes,

H_2:CO_2 or H_2:CO or H_2:CO_2 ratios are adjusted to achieve a selected product by either adding or striping out excess H_2. Figure 4:4 shows the calculated ratios obtained from the simulation results at temperatures between 500 ^{o}C and 1100 ^{o}C. It is important to note here that the total number of moles of each gas at each individual temperature is different but Figure 4:4 only adds emphasis on the gas ratios as they association with temperature.



	500	600	700	800	900	1000	1100
H_2/CO	21.52	11.65	7.94	6.03	4.93	4.23	3.75
CO/CO_2	0.11	0.23	0.37	0.52	0.68	0.85	1.02
H_2/CO_2	2.44	2.72	2.91	3.12	3.34	3.58	3.81

Figure 4:4: Syngas Ratios as a Function of Temperature. Feed at 100 g/Nm^3 of Tar in N_2 with an S/C of 3.

At lower temperatures, H_2/CO is significantly higher than at higher temperatures. For instance, from 500 °C to 900 ^{o}C H_2/CO drops from 21.52 to 4.93 respectively. At 900 ^{o}C CO/CO_2 is six times more than CO/CO_2 at 500 ^{o}C. H_2/CO_2 only slightly increases as temperature increases. While the H_2/CO ratio is observed to decrease with increasing temperatures, the CO/CO_2 and H_2/CO_2 increase. This can suggest a shift in equilibrium position of the water gas shift reaction with temperature. Based on Figure 4**:1**, Figure 4**:2** and Figure 4:3, it can be concluded that H_2 and CO_2 gradually decrease as temperatures increased above 500 ^{o}C while CO rapidly increases.

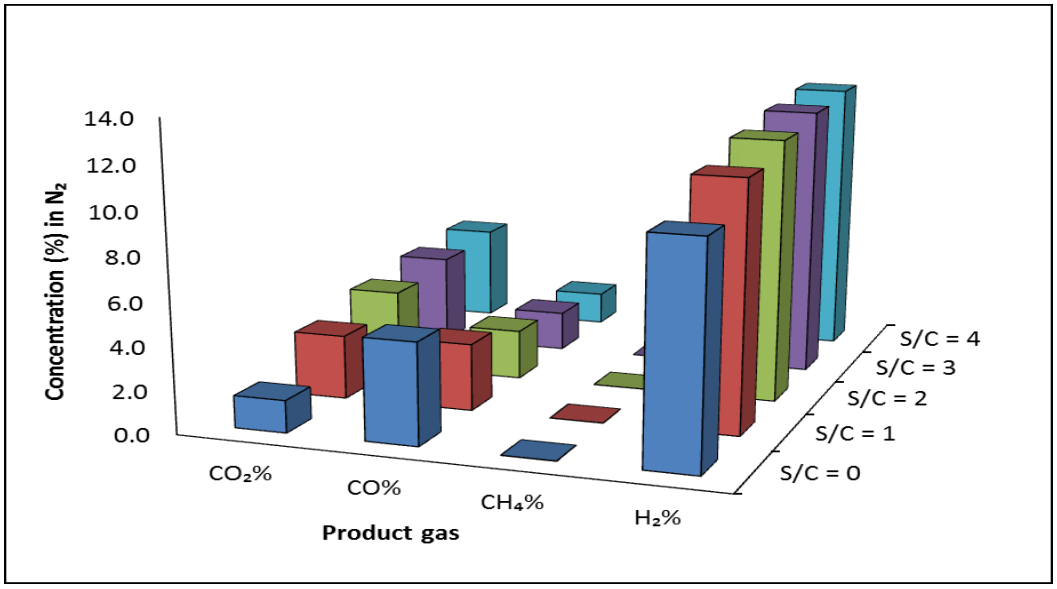


Figure 4:5: Thermodynamic Equilibrium Product Gas Concentration from 100 g/Nm³ of Tar in N_2, at 750 ^{o}C with Increasing Steam in the Feed.

Figure 4:5 shows the variation in gas formation with steam addition. The results indicate that steam can be varied to alter the gas ratios or composition. At low steam to carbon ratio larger amounts of CO is formed while at higher steam to carbon ratios less and less CO is formed. On the contrary, CO_2 and H_2 increase as steam increases while no CH_4 is formed. This reflects a shift in the equilibrium for the water gas shift reaction meaning that more steam reacts with CO, CO reduces while more CO_2 and H_2 are formed.

4.2.2. Conclusion Drawn from Equilibrium Data:

The chosen range of temperatures and steam to carbon ratios demonstrate a significant process flexibility and the results show a significant gas concentration sensitivity when a variable was altered. Higher conversions of the tar to CO_2 and H_2 were achieved at 500 - 600 ^{o}C but this can be altered by changing the steam to carbon ratio. At all temperatures, H_2 concentration was higher than the other predicted products and CO production increased with temperature. Adding more steam to would increase the formation of CO_2 and H_2 but reduces CO formation, shifting the equilibrium position of the water gas shift reaction towards the formation of more and more CO_2 and H_2.

4.3. Preliminary Tests

Preliminary tests were carried out to familiarise with the process control and later assess the suitability of the reactor for performing the reforming reactions under the range of conditions established by the thermodynamics equilibrium study. Two sets of preliminary studies were carried out. The first set was carried out at Johnson Matthey Sonning Common Technical Centre, which involved studying the reforming of model compounds; benzene and methane. The second set of preliminary tests was performed at Imperial College London, studying the gasification and reforming of biomass tar using the Hot Rod reactor.

4.3.1. Preliminary Tests Using Model Compounds

A set of preliminary tests was carried out at Johnson Matthey (JM) Sonning Common Technical Centre aimed at familiarizing with the process design and operation, and developing a preliminary understanding of the reforming reactions. The process rig was built by JM technicians purposely for testing catalyst performance. The reactor used on the rig was a quartz tube housed in a tubular furnace. The quartz tube was packed with catalyst beads in the centre and the bed the bed was supported on a ceramic plug. The process was remotely controlled on a computer software providing a platform to vary the process conditions. The physical instrumentation of the rig included mass flow controllers used to regulate the carrier gas flow rate, K-type thermal couples to temperature transmission and controlling the bed temperature, syringe pumps for regulating water and tar feed stock flow rates, and a GC-analyser to measure the feed and product composition.

At start of each test, the process lines were purged with nitrogen to remove any contaminants. After purging the reactor bed was progressively heated to a uniform temperature and the catalyst was reduced in situ under 300ml/min of 40% H_2 with N_2 balance at 900 ^{o}C for 30 minutes. After activating the catalyst for, the process streams were purged with 300ml/min of nitrogen gas for 15 minutes. Thereafter, model compounds of benzene and methane were injected into the reactor feed stream

together with steam at a steam-to-carbon (S/C) ratio of 2.5. At continuous material feeding, the catalyst bed temperature was maintained at a steady temperature of 900 °C and after a few hours the temperature was switched to 850 °C. At both temperatures, the concentrations of residual benzene and methane in the product stream all together with the formed permanent gases were measured.

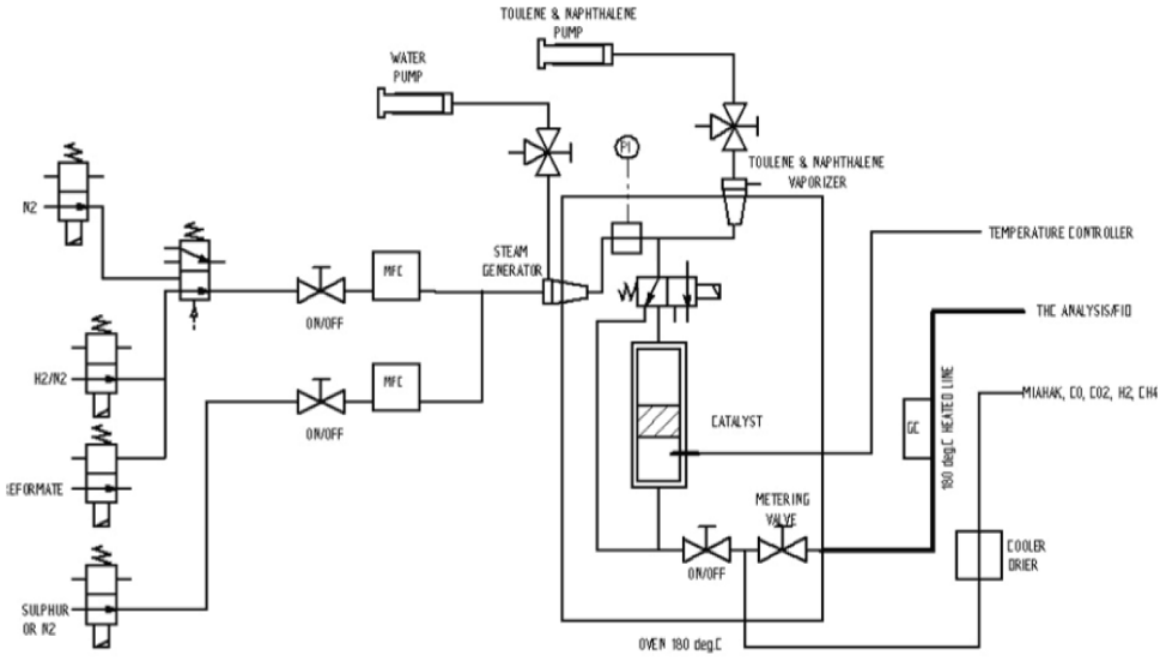


Figure 4:6: Process Flow Diagram at JM Technical Centre reproduced from a shared document between JM and Imperial College.

Figure 4:7 illustrates the results obtained from tests conducted at bed temperatures 900 °C and 850 °C with three different catalysts, for approximately 90 minutes at each temperature. Between 90 and 140 minutes, the temperature was dropping from 900 °C to a steady 850 °C.

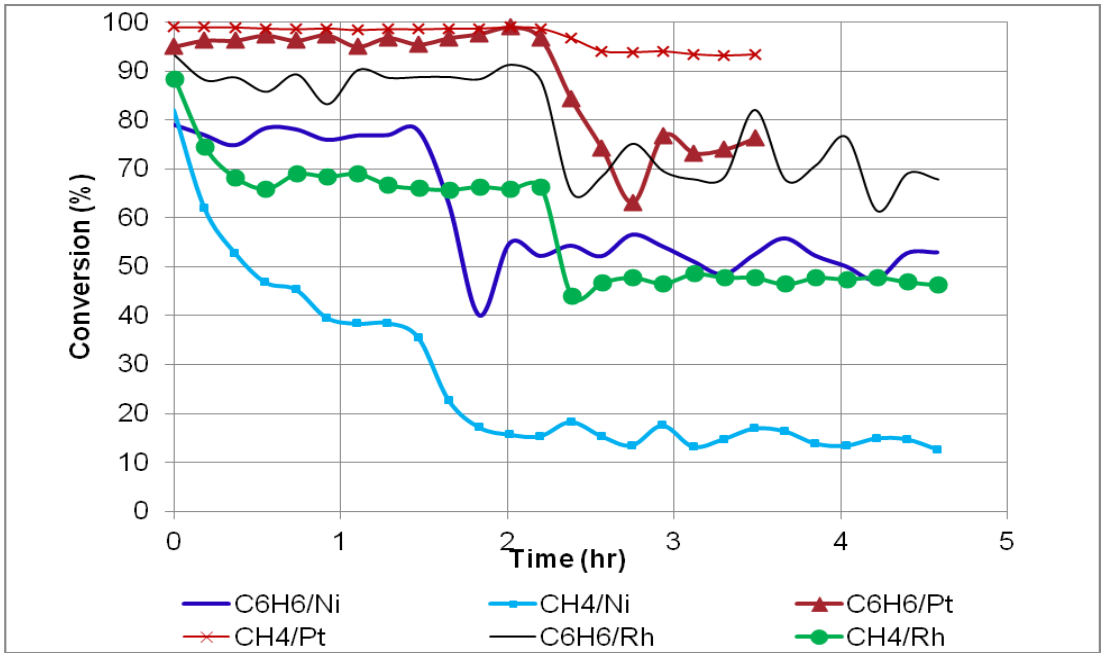


Figure 4:7: Catalytic Conversion of Benzene and Methane at 900 °C (between 0 – 90 minutes) and 850 °C (Between 140 minutes to the end) with an S/C of 2.5 using Ph-, Pt- and Ni-Based Catalysts.

The results show significant differences in conversions with the different reactants, catalysts and bed temperatures. Between the catalysts, platinum and rhodium gave more steady results and higher conversions for both feeds than the nickel catalyst. Process operation at 900 °C gave higher conversions than at 850 °C. At 900 °C, the conversion with the Pt catalyst was over 90%.

4.3.2. Preliminary Tests on Biomass Derived Tar

The second set of the preliminary studies was performed at Imperial College London using the rig designed and built during this project. The study involved gasifying and reforming biomass tar following the procedure described in Chapter 3. The initial set-up of the reactor system was developed with an Incoloy reactor, which was used for the majority of the preliminary tests. After developing the reactor with control over the variables, a series of reproducible runs were performed and successfully integrated in the discussion. In this section, the results are discussed and later compared to the thermodynamics equilibrium calculations.

4.3.2.1. Stability, Repeatability and Error Measurements

In order to monitor the improvements from the modifications, a new set of preliminary tests was conducted. The results are shown in Figure 4**:8** and Table 4:4. All the following preliminary results were obtained from tests performed with an S/C ratio of 2 in nitrogen, while changing one parameter at a time.

To analyse the reliability and repeatability of the experimental set-up and determine whether there was sufficient control over the process, each test was repeated at least twice to identify the trends and deviations in the measured data. Most importantly, at this stage the tests without catalyst were useful to certify the quality of the signal integrity, a continuous flow and steady product trends were achievable and that the results were reproducible. The tests with the catalysts were used to assess the catalysts' impact on the performance. At this stage, all three catalysts described in Chapter 3 were tested at 850 °C, 900 °C and 950 °C, same as the blank.

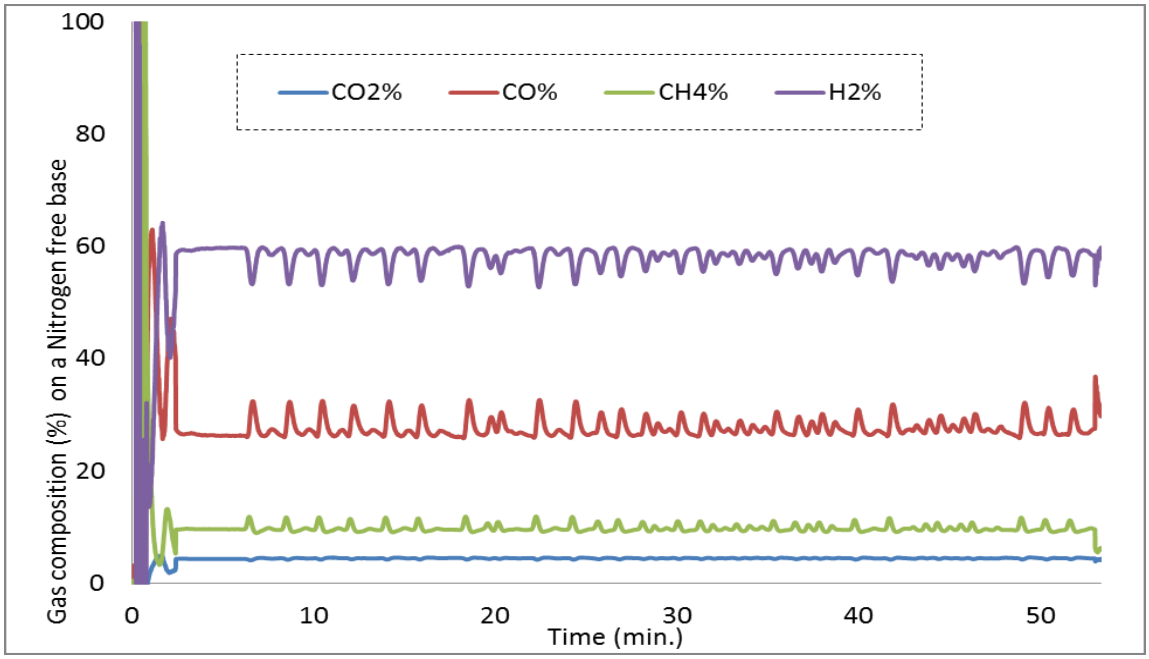


Figure 4:8: A Normalised Gas Composition With Steady Concentrations Obtained and a Fairly Good Signal Throughout the Entire Period of the Test.

Figure 4:8 presents a test conducted in a blank reactor at a steady temperature of 850 ^{o}C for 50 minutes. After the initial 2 minutes, the gas contents remained mostly steady throughout the 50 minutes of injecting the reactants. This demonstrates the controllability and reliability of the feed conditions. Virtually identically steady results (tabulated Table 4:4) were obtained from each of the repeated tests under the same conditions.

The standard deviation, standard error and error percentages were calculated using Equation 4**:1**, Equation 4**:2** and Equation 4:3.

Equation 4:1:

$$\text{Standard Deviation (SD)} = \sqrt{\left(\sum (X_i - M)^2 / (N-1)\right)}.$$

Equation 4:2:

$$\text{Standard Error (SE)} = +/- (SD/\sqrt{N})$$

Equation 4:3:

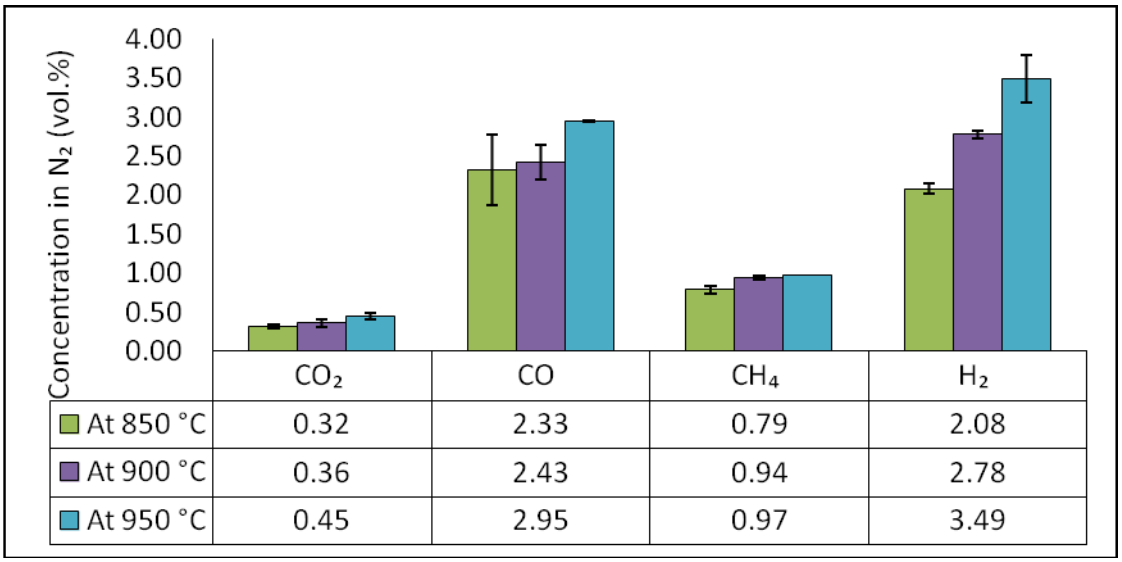
$$\text{Error (\%)} = +/- (SE*100/M)$$

Where, X_i is the sample measurement, M is mean and N is the number of samples

4.3.2.2. Blank tests

Two sets of blank tests were performed in the preliminary tests, one set in an Incoloy tube reactor and the other in a quartz lined reactor. Initially, tests were performed in the Incoloy tube reactor but later in the project development the reactor was modified, adding a quartz glass liner. In the early stages of developing the operating conditions, only observation of the gas trends was monitored and some results were not recorded. Experiments that were performed with 100 g/Nm³ of tar at 850 and 900 °C with an S/C of 1 in an Incoloy reactor showed minimal carbon conversion and a relatively large amount of soot was formed in the reactor. These experimental conditions were carried over with increasing the S/C to 2, matching the conditions adapted from JM and

amalgamating them with the understanding of the thermodynamic equilibrium. Figure 4:9 shows the gas formed from non-catalysed tests in an S/C of 2 at 850 - 950 °C.



	CO_2	CO	CH_4	H_2
At 850 °C	0.32	2.33	0.79	2.08
At 900 °C	0.36	2.43	0.94	2.78
At 950 °C	0.45	2.95	0.97	3.49

Figure 4:9: Gas Formation in Non-catalysed test at 850 – 950 ^{o}C in an Incoloy reactor

Each experiment was repeated at least twice to establish control from repeatability. The results show rational trend in gas formation with changes in temperature. The gas formation from individual tests performed at identical conditions is just about the same, and the largest error seen was 9%, in CO at 850 °C. These results show good control and ability to reproduce data. More preliminary tests were performed at various conditions and after the final modification. The results are shown in Table 4:3 to Table 4:7 and Figure 4:10.

Table 4:3: Carbon Balance: Non-catalysed test at 850 – 950, S/C 2 in an Incoloy Reactor

	Carbon conversion in an Incoloy reactor at S/C 2		
Temperature (^{o}C)	850	900	950
Carbon to gas	54% +/- 11.5%	58% + 9.3%	68% +/- 2.7%
Carbon Trapped	41% +/- 15.0%	33% +/- 13%	22 % +/- 17.0%
Difference in carbon balance	+5%	-9%	-10%

Figure 4:10 shows the unconverted tar concentration in the gas stream to the traps at the reactor outlet.

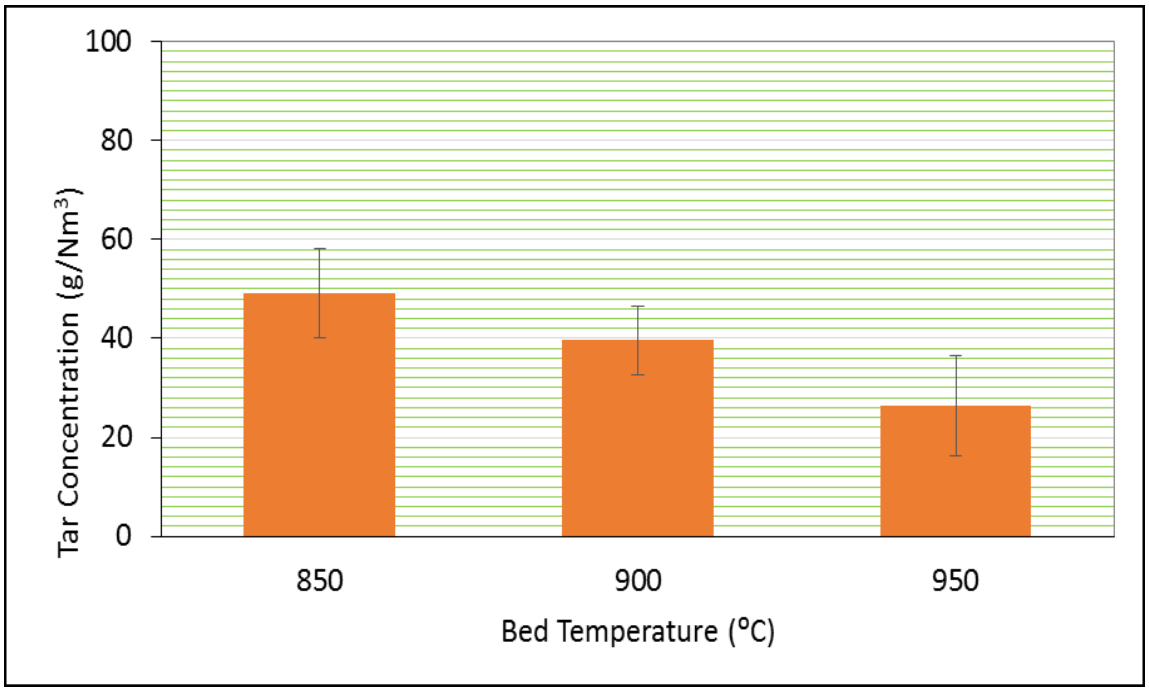


Figure 4:10: Tar Concentration in the Gas Products as a Function of Temperature from Reactions of 100 g/Nm³ of Tar with steam to carbon ratio of 3 in 0.209 L/min of N_2 at 850 °C, 900 °C and 950 °C

In Figure 4:10 at 850 °C the tar concentration was reduced from 100 g/Nm^3 in the feed to 49 g/Nm^3 in the product stream. When the temperature was increased to 900 °C and 950 °C, the tar concentration was further reduced to 40 g/Nm^3 and 26 g/Nm^3 respectively. Most noticeable, less tar was in the product stream when the temperature was raise but 50 °C from 900 °C than from 850 °C. This behaviour is the same as reported in the literature and similarly observed in the equilibrium simulations, with the only exception that in simulations, there is no tar left at these temperatures. The outlet tar composition in would be different from the inlet composition as some conversion towards volatile and possibly heavier compounds would have occurred.

Table 4:4: Blank Repeated Tar Cracking with S/C 2 at 850, 900 and 950 ^{o}C in Quartz

Temp.		Product Gases (Conc. %)				Recovered	
(^{o}C)	Run	CO_2	CO	CH_4	H_2	C (g %)	H_2O (ml)
850	(i)	0.25	1.58	0.59	3.41	62	0.8
	(ii)	0.27	1.54	0.57	3.36	54	1.3
	Av.	0.26	1.56	0.58	3.39	58	1.1
	+/- Error	0.01	0.02	0.01	0.03	0.03	0.1
900	(i) F	0.29	1.77	0.41	3.49	56	1.1
	(ii)	0.28	1.82	0.45	3.46	54	1.2
	Av.	0.29	1.80	0.43	3.48	55	1.2
	+/- Error	0.00	0.03	0.02	0.02	0.00	0.1
950	(i)	0.39	2.67	0.35	3.93	42	1.2
	(ii)	0.44	2.64	0.36	3.88	41	1.2
	Av.	0.42	2.66	0.36	3.91	42	1.2
	+/- Error %	0.03	0.01	0.01	0.03	0.00	0.1

With such small errors, the results reflect considerable ability to reproduce the gas formation and approach to experiments.

4.3.2.3. Catalytic tests in a Quartz Reactor with S/C 2 at 850 ^{o}C – 950 ^{o}C.

Table 4:5: Fuel Gas Composition upon Tar Reforming With Platinum-Based Catalyst

Operating conditions; S/C =2		Average Fuel gas formation (Vol. %) in nitrogen			
Catalyst	Temperature (^{o}C)	CO_2	CO	CH_4	H_2
Pt-	850	2.11	1.85	0.03	8.78
	900	1.93	1.87	0.01	8.99
	950	1.95	2.02	0.00	9.08

Table 4:6: Fuel Gas Composition upon Tar Reforming With Rhodium-Based Catalyst

Operating conditions; S/C =2		Average Fuel gas formation (Vol. %) in nitrogen.			
Catalyst	Temperature (^{o}C)	CO_2	CO	CH_4	H_2
Rh-	850	2.07	1.66	0.03	8.50
	900	2.04	1.97	0.00	9.54
	950	2.01	2.07	0.00	9.43

Table 4:7: Fuel Gas Composition upon Tar Reforming With Nickel-Based Catalyst

Operating conditions; S/C =2		Average Fuel gas formation (Vol. %) in nitrogen			
Catalyst	Temperature (^{o}C)	CO_2	CO	CH_4	H_2
Ni-	850	0.82	2.10	0.57	5.28
	900	1.12	2.74	0.42	6.41
	950	1.49	2.41	0.49	7.19

4.4. Summary

- A fixed bed lab scale reactor has been constructed and modified to simulate the conditions in a downdraft gasifier and an operating protocol has been developed. The performance of the equipment has been tested using biomass tar and was successfully commissioned. All three catalysts were effective in tar reforming based

on the judgement of gas formation between the non-catalysed and the catalysed results.

- Where CH_4 gas formation is favoured, H_2 decreases in response possibly the two compete for the dissociated hydrogen, but at high temperatures the thermodynamic stability of CH_4 decreases in most cases favouring the water gas shift reaction.

- Reactions in an Incoloy tube lead to different reaction pathways compared with the reactions performed in a quartz tube. This would suggest Incoloy would affect the reactions results to a different specification of gas formation. When the product distribution was investigated, there was a strong linking pattern between products formed and those from Ni-catalyst in a quartz tube. This suggests the Ni in the Incoloy would play a role in the reforming reactions.

- The main body of results chapter will include tests at lower temperatures than those covered in the preliminary tests in order to investigate the kinetics, and the results obtained from tar gasification and reforming in the preliminary tests will be discussed further.

5. REACTOR DEVELOPMENT

5.1. Review of Previous Reactor

The reactor was adapted from previous work on gasification studies at Imperial College London. It had been designed to allow operation as a single or two stage reactor connected in series. In this work it has been modified to a single pass tube with a newly developed preconditioning process unit, to simulate a continuous flow downdraft reformer.

5.1.1. Original Reactor

The "Hot-Rod" reactor was designed by O'Brien [75], but as work progressed over several research projects, its design has undergone a number of alterations carried out sequentially by Gonenc, Pindoria, Collot, Monteiro and Dabai [75]. In the earlier studies, the first stage reactor was used for both the gasification and pyrolysis of biomass and the second stage for thermal cracking of tars. Both stages were heated by copper electrodes clamped at the bottom and top of each stage. The electrode heating was controlled using computer software that communicated to both the reactor and the power controller.

The design used in this work was adapted from that of Dabai [75]. The principal features of this reactor are;

- Incoloy 800 reactor body
- Inner diameter (i.d) of 12 mm
- Wall thickness of 2 mm
- Single tubes pass with a length of 250 mm.

The reactor used by Dabai [75] had a "T"-piece connection at the top with connections for a control thermocouple and a stream for the feed carrier gas. In this arrangement, a

weighed biomass sample was placed inside the centre of the reactor as shown in Figure 5:1.

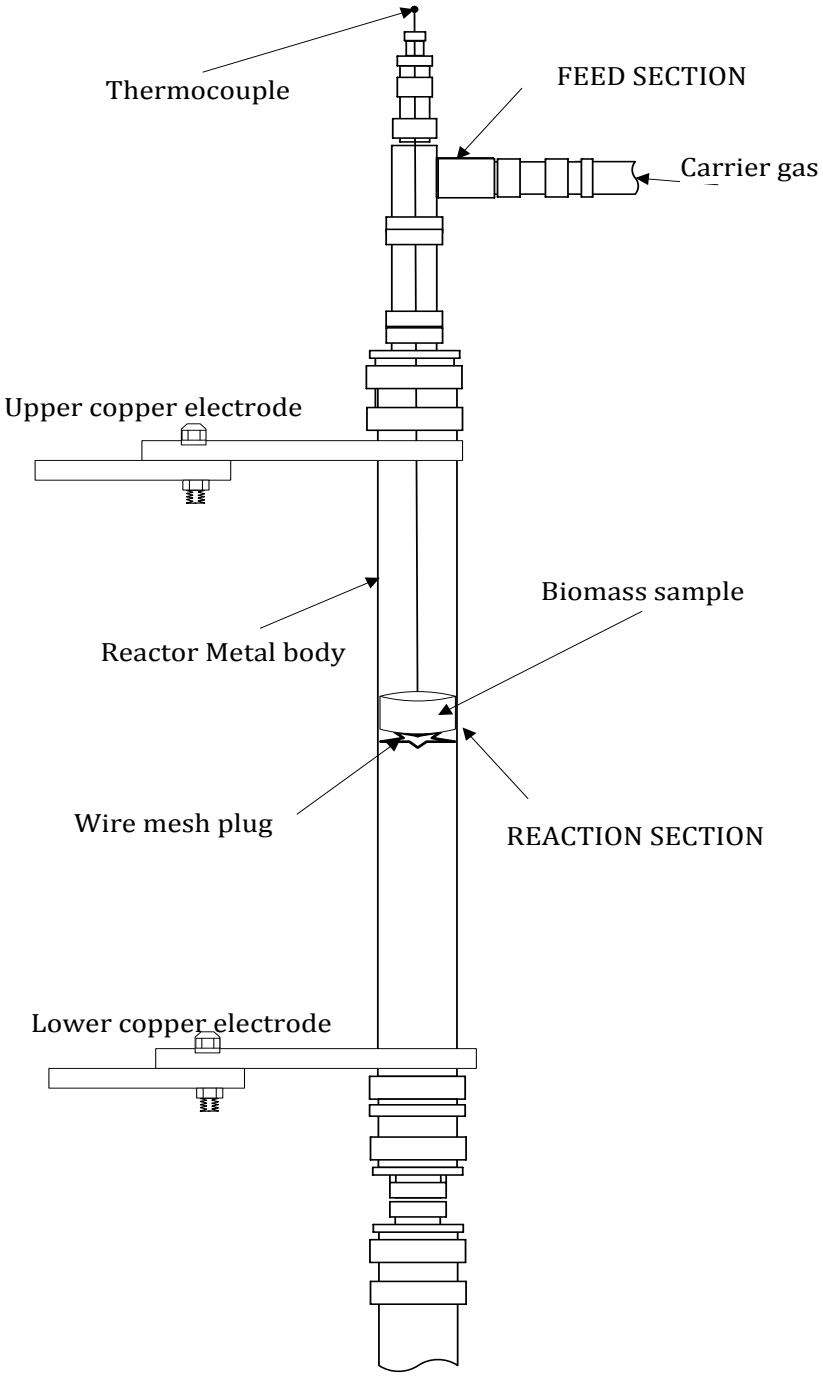


Figure 5:1: The initial arrangement of the first stage reactor.

Earlier users of the “Hot-Rod” used only the single stage, so that when the sample was heated, the carrier gas swept the formed products into the traps and analysers. Other user in particular those just before this project used the two-stage reactor tubes. The second stage was connected to the bottom of the first stage using welded flanges at the end of each reactor. The two flanges were held together by six cap head bolts, with a copper gasket disc/rings used to seal the flanges and prevent leaks. The first and second stage reactor arrangement is shown in Figure 5:2.

The top flange of the second stage had three drilled and threaded nozzles for connections to additional gas feeds. A thermocouple was located in the middle of the reactor tube, independently controlling and monitoring the temperature in the second stage.

5.1.2. Original method for steam generation

Steam was generated using a high pressure liquid metering pump, driven by a piston with the ability to pump water against pressures up to 350 bars. The flow of water induced was controlled by changing the length of the stroke of the piston. The waster was introduced was mixed with the carrier and evaporated as it passed through an electric heater set at a desired temperature. The heated mixture of the carrier gas and steam was then fed into the reactor for contact with the sample for reactions.

5.1.3. Original method used for cooling, extracting and analyzing products.

Two condensate traps were used to cool the gas and capture the tars at the outlet from the reactor. Both condensate traps were U-shaped stainless-steel tubes with 12 mm inside diameter. The first trap was immersed in a water-ice bath and the second trap was placed in liquid nitrogen. The outlet of the second condensate trap was connected to a vinyl tube with a split connection to the gas analysers and the vent. Occasionally the tar trap could get blocked due to freezing of water in the product stream as a result of using liquid nitrogen.

The tar yields from the reactants were recovered from the traps by washing each trap with 1:4 methanol chloroform solution into a pre-weighted beaker. The tar was separated from the solvent by evaporating off the solvent using a light blown nitrogen gas into the beaker while gently heating it. Alternatively, the tar was transferred into a conical flask and placed on a rotavapor with a heated water bath where most of the solvent was evaporated off and the tar was transferred into a small weighted beaker. The tar recovered was then dried at 50 °C in a circulating oven for 30 to 45 minutes. The remaining tar in was then weighed in a beaker and the mass off tar recovered was obtained by weight difference. A sample of the product tar was then analysed in a size exclusion chromatography to determine the molecular mass distribution of the reformed tar.

The gases H_2, and CO were analysed on line. Some of the CO_2 and CH_4 were detected in the analysers but not all as some of the gas was trapped in the liquid nitrogen trap. To collect for the gas concentration in the online analysis, the traps were locked off at the end of each experiment and left to warm up to room temperature. At room temperature, a sample of gas was extracted in a syringe and analysed on a gas chromatogram (GC).

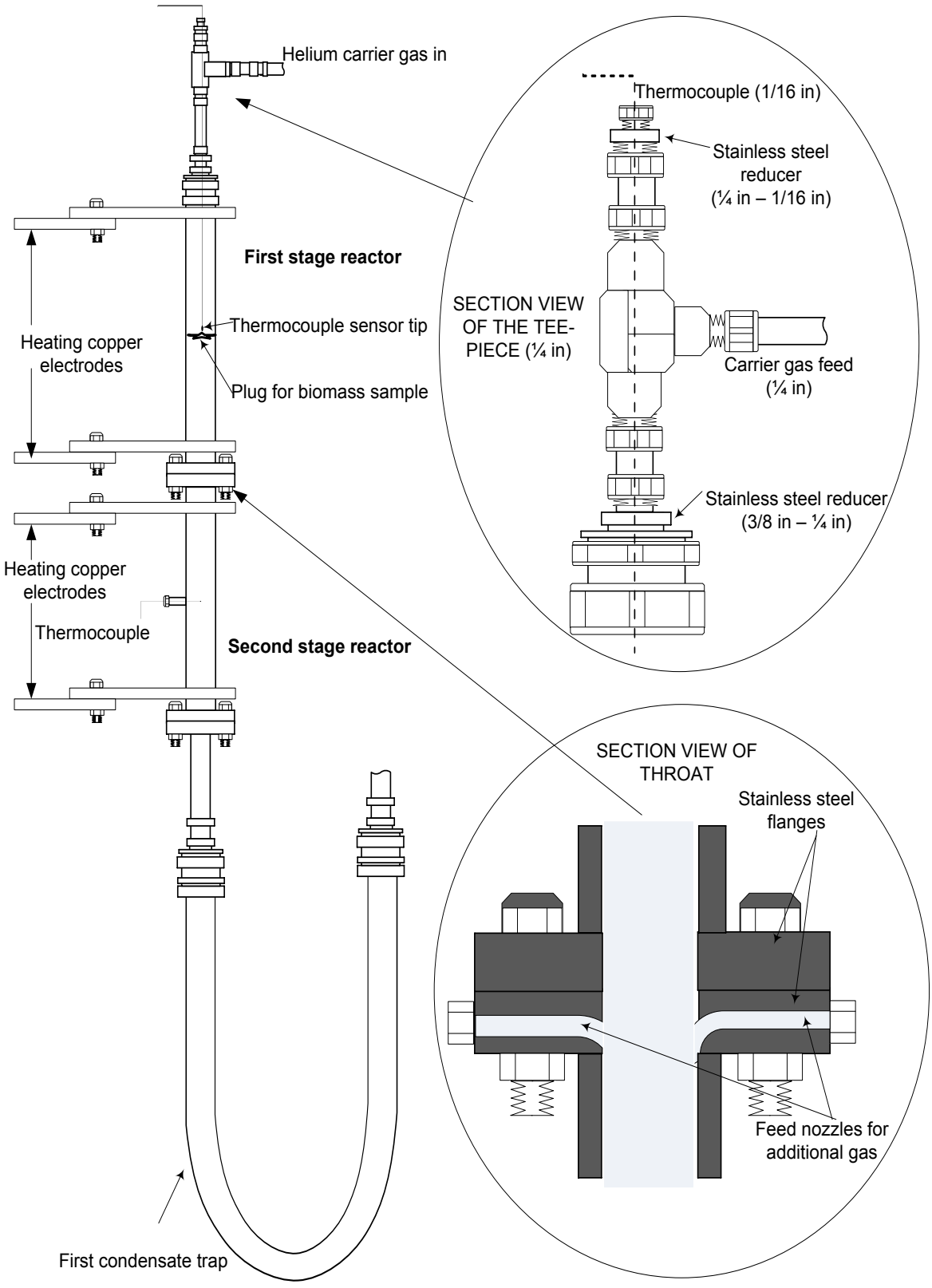


Figure 5:2: Lay-out of the Tow-stage Reactor in the Configuration used by Dabai [75]

5.2. Modification to the reactor

5.2.1. Introduction to causes for modification

A review of the previous reactor configuration indicated that relatively batch-like experiments could be performed using the original arrangement and there were severe experimental errors that could be reduced. Among the sources of the errors were; (i) the batch loading of samples in the reactor led to drastic changes in the rate of gas formation, (ii) the use liquid nitrogen for gas-liquid product separation led to capturing most of CO_2 and some of the other permanent gases which consequentially led to wrong online gas measurements, (iii) the use of additional connections for a secondary reactor, flanges and tapping into the reactor tube for gas nozzles and a thermocouple which led to increased risks of leaks and handling of the system and (iv) the use of incoloy reactor wall exposed to the reactions led to catalytic effects that may not have been accounted for.

5.2.2. Objectives for the reactor modification

The objectives for modifying the reactor were:

1. To achieve continuous operations at a regulated rate flow of reactants,

2. To minimise the process operation and reduce the number of connections on the reactor which as a result reduced the risks of gas leaks,

3. To successfully use a catalyst bed in the reactor and

4. To analyse all target product gases on-line while retaining all liquid products in the traps.

5. To eliminate the potential for the reactor wall from taking part in catalysing the process reactions.

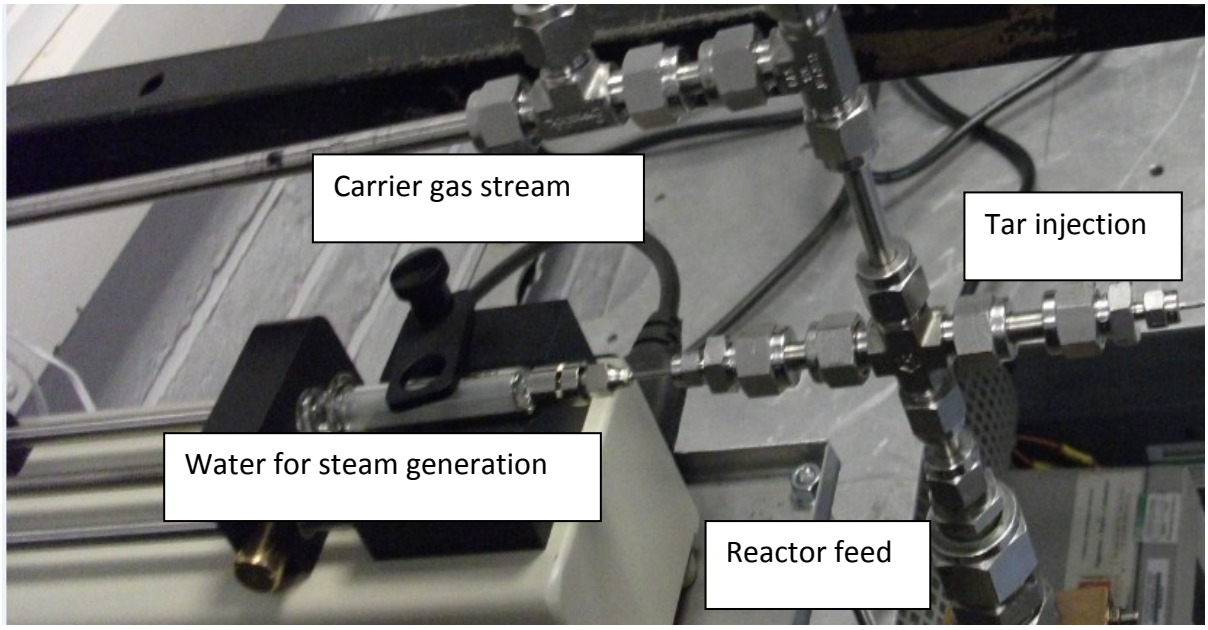


Figure 5:3: Initial Feedings Set-up

5.2.3. Material feeding / Introduction of Syringe Pumps

On first attempt the electric heater was removed and replaced by a heating tape to better effective heating. Two syringe pumps were introduced just above the inlet to the reactor. One pump was for steam injection and the other for tar injection. The streams connecting from the syringe pumps to the carrier gas steam leading the reactants into the reactor were both connecting from the sides, through a cross union fitting, joining the carrier gas at an angle of 90 degrees (as shown in Figure 5:**3**). A bed thermocouple was installed coming through the top of the union cross fitting, vertically through the feed main stream with its sensor-tip in the bed position. When the change was tested in a cold run, at 15 g/Nm³, only droplets of tar were produced at regular intervals but not continuously. When tar concentration in the stream was increased to 30 g/Nm³ and then 100 g/Nm³ by increasing the flow rate, the continuity of flow improved particularly at 100 g/Nm³. When temperature was applied at 50 °C around the reactor inlet using an S/C of 1 and tar concentrations of 15 g/Nm³, 30 g/Nm³ and 100 g/Nm³ tar clots were formed along the inlet lines, largely at 15 g/Nm³. The feed temperature was changed to 100 ^{o}C, 200 °C, 300 °C and 500 ^{o}C a large amount of tar deposited on the tube wall at the inlet (as shown in Figure 5:4) and on the thermocouple probe in the feeding region.

At 300 ^{o}C, tar deposition decreased, but carbonisation increased and at 500 ^{o}C it blocked the feed nozzle. A feed of tar at 15 g/Nm^{3} produced traces of syngas in the product gas. At 30 g/Nm^{3} small amounts of gas were detected in the product stream with pulsing readings and much fluctuations in the signal (Figure 5:6). At 100 g/Nm^{3} of tar in the feed a fairly steady syngas reading was achieved with a much better quality of the signal integrity (Figure 5:7). The signal shows that with time the signal decreased. This was because most of the tar was carbonising in the feed lines and along the thermocouple probe at the inlet. When the S/C was increased from 2 to 3, this significantly reduced the amount of carbon deposits and improved the tar feeding but still there was a substantial amount of carbon deposits on the walls at the inlet.

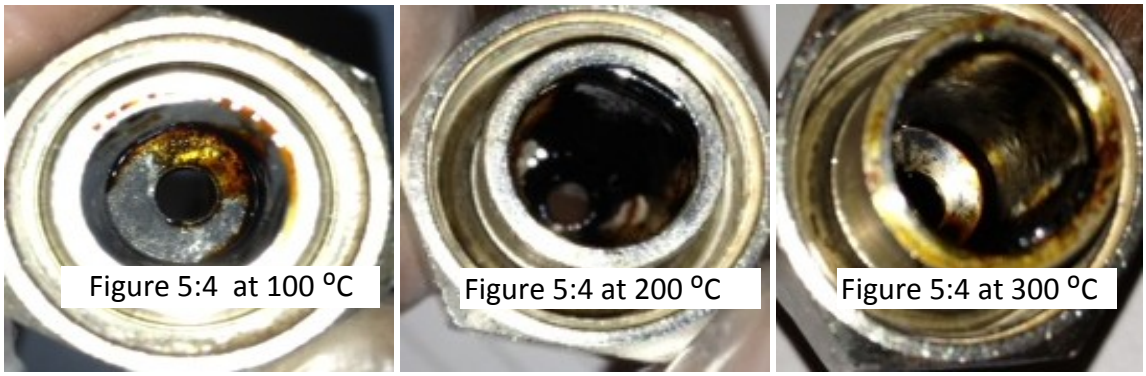


Figure 5:4: Tar Clots Deposited on the Inner Walls of the Feed Tube.

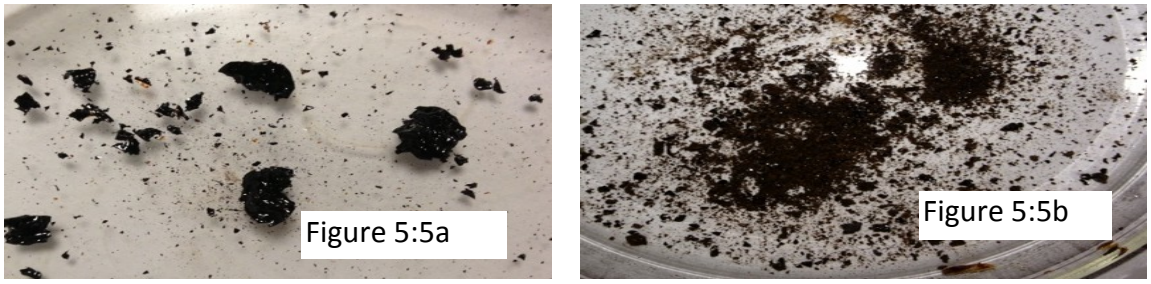


Figure 5:5: Recovered Carbon from the Feed Nozzle at 500 $^{\circ}$C

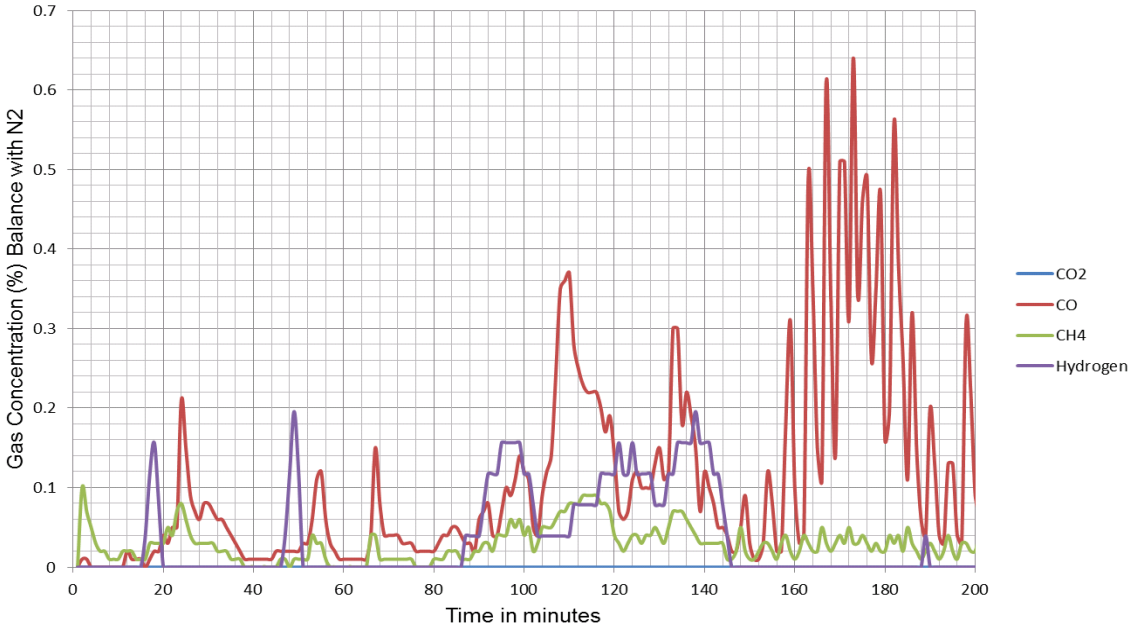


Figure 5:6: Signal to the Gas Analyser as Gas Concentration with Time during a Reaction at 600 °C with S/C =2 and Tar at 30g/Nm^3.

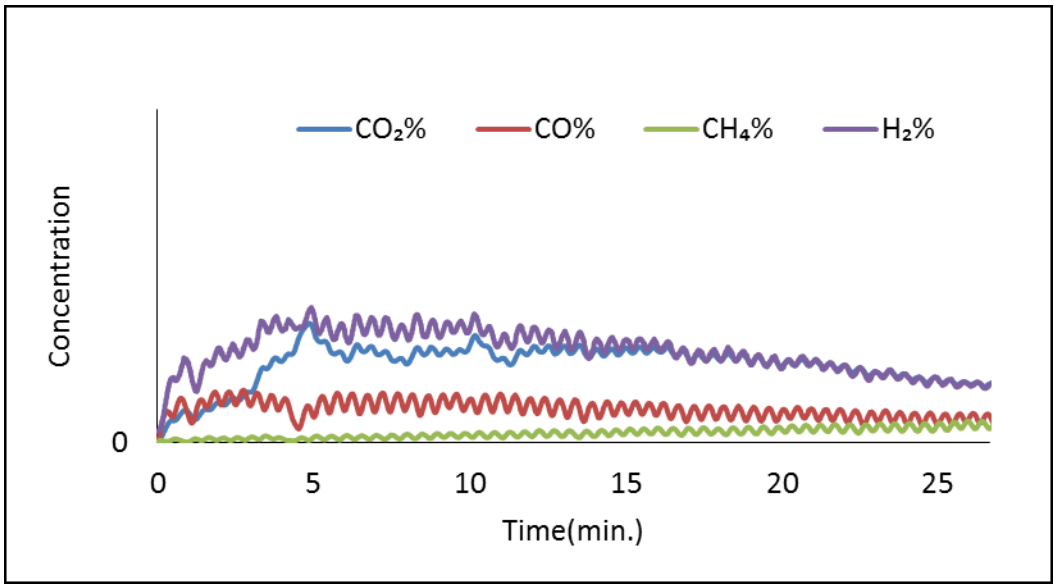


Figure 5:7: The signal to the Gas Analysers as Gas Concentration with Time during a Reaction at 600 °C with an S/C of 2 and Feed at 100 g/Nm³ of Tar.

5.2.4. Introduction of a Pre-conditioning Chamber

Cold and hot commissioning tests were undertaken feeding 30, 50 and 100 g/Nm³ of tar concentration. Of these data points, the 100 g/Nm^3 tar concentration presented promising results but not sufficient to complete the commissioning of the feeding section. Hot commissioning with a pre-conditioning chamber set at 300 °C and steam/carbon at 3, produced better carbon to gas/vapour conversion. Approximately 95% of carbon went through the SiC bed. This result together with literature supported the idea of using an S/C of 2 or 3 for applications in most of this study. To eliminate the pulsing signal and maintain a sustained steady gas concentration, the feed stream tar concentration was kept at 100g/Nm^3, the bed thermocouple was repositioned coming into the reactor bed from the exit stream of the reactor and a small bed of SiC was introduced in the preconditioning chamber. This successfully resolved the pulsing problem and efficiently vaporised the tar before entering the reaction bed. The advantages of using SiC were that it is inert and a good thermal conductor and improves thermal shock tolerance with the ability to survive and maintain integrity in the face of rapid temperature changes; the chosen particle sizes provided sufficient voids to enabled a continuous flow and an even discharge of a homogeneous vapour into the reactor. Other modifications included changing the tar feed line from side feed injection to vertical injection into the reactor and using a temperature of 350 °C in the conditioning chamber. This was based on Chapter 5 tar analysis. The results indicated that nearly fully evaporated was achieved, leaving only a tiny amount of carbon residue behind. The preconditioning chamber was therefore commissioned at conditions with an S/C of 3, a preheating temperature of 350 °C and tar concentration at 100 g/Nm³.

5.2.5. Relocating the Bed Thermocouple

At the reactor outlet, a male threaded 9.53 mm union was connected to a reducing male-female adapter. This adapter was linked to a Tee-piece male union with a 6.35 mm tube. The branched side of the Tee was connected to a 1.59 mm Type-K thermocouple running up to the centre of the reactor tube. The other end of the Tee-piece was connected to the first trap using a 6.35 mm to a 9.53 mm connector. The thermocouple

was purposely moved from the top to bottom in order to create room for the preconditioning section and improve the feed flow. Figure 5:8 illustrates the first set of modifications to the reactor configuration.

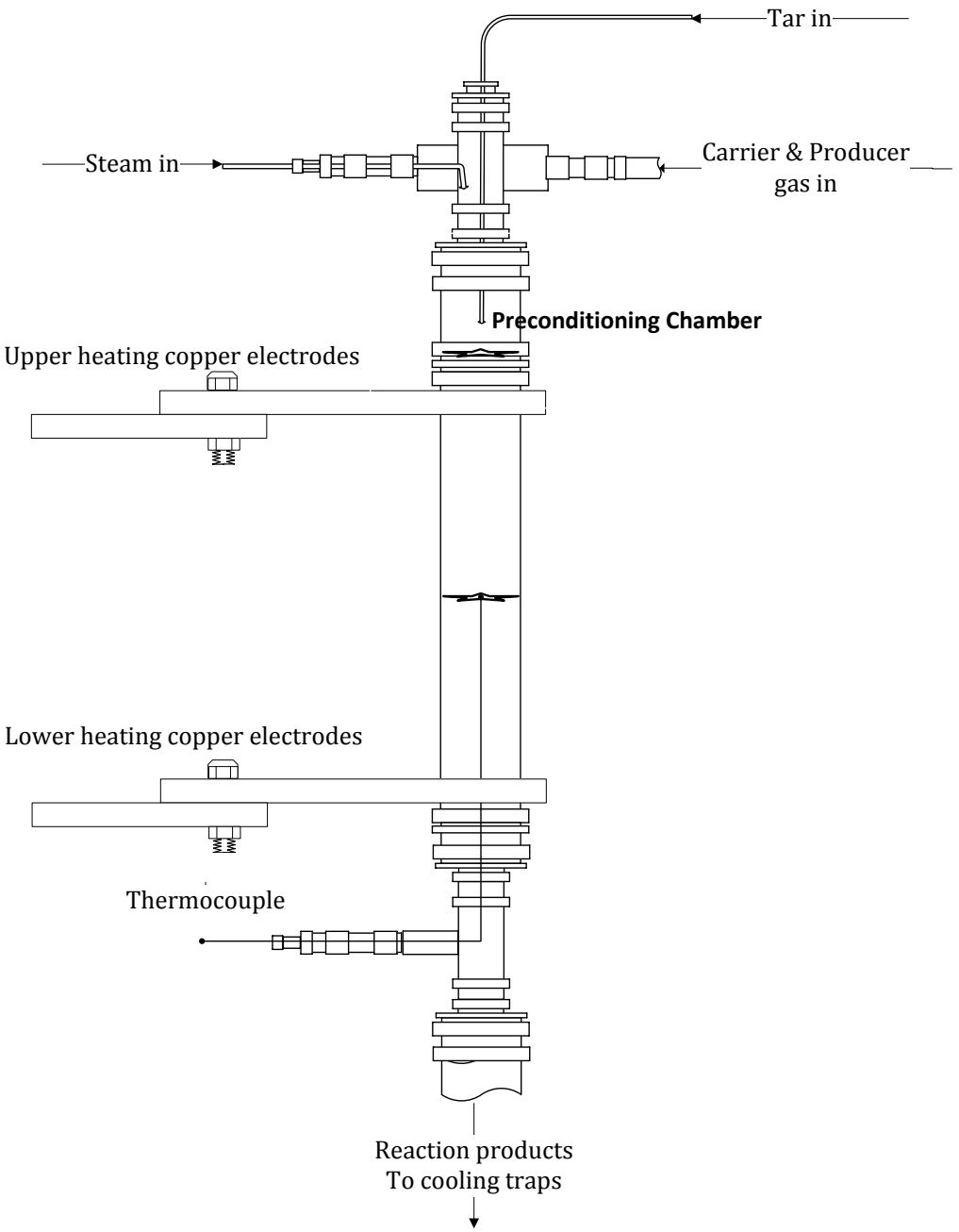


Figure 5:8: Reactor Design After the Primary Modifications.

5.2.6. Determining the Bed Position

The temperature along the reactor varied significantly with length. To determine the bed position, the region with the highest temperature along the reactor was identified. Two methods were employed: (I) a fixed temperature was set, half-way down on the outside body of the reactor tube and an adjustable thermocouple was placed at different lengths inside the reactor tube; (2) a new reactor with several thermocouples along the tube was designed as shown in Figure 5:10, Appendix 4 and Appendix 5. N_2 gas was passed through the system and when the external temperature was maintained for 15 minutes, repeated temperature measurements along the centre line of the reactor tube were recorded at various heights. Once the position with the highest temperature was determined, this was later used to place the catalyst bed. Figure 5:9 illustrate the temperature profile (obtained from the method several thermocouples fitted inside the reactor) along the reactor, with a set temperature causing a highest temperature of 1000 °C inside the reactor tube at 11 cm from the top of the reactor.

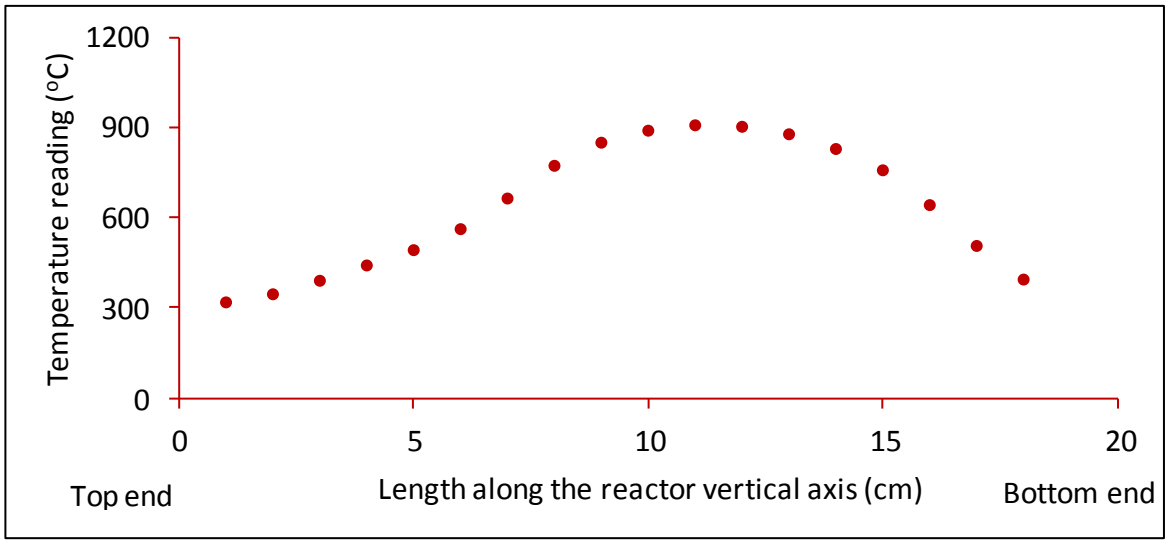


Figure 5:9: Temperature distribution Along the Vertical Axis of the Reactor Tube, with 0.209 L/min N2 Flow at 900 °C Bed Temperature.

Several repeats were carried out at various set temperature points and location of the set temperature thermocouple. All these measurements indicated the highest

temperature was obtained at 11cm down the reactor tube from the top. It was also observed that at 11 cm +/ - 2 cm, there was a negligible temperature gradient. Because of this even temperature distribution, the length between 9 cm and 13 cm down the tube was considered to be the best position to place the catalyst bed.

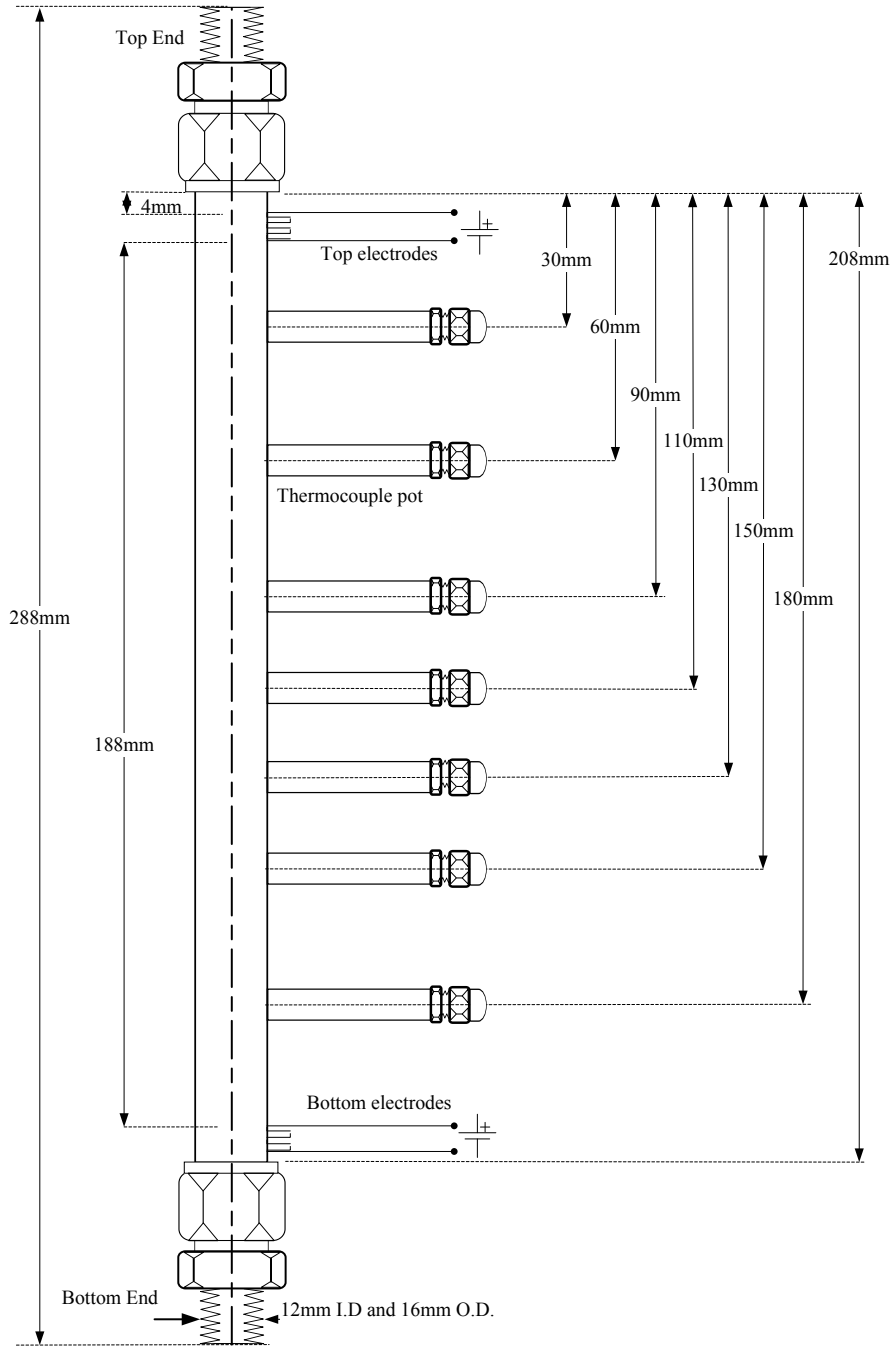


Figure 5:10: Reactor Tube with Multiple Thermocouple Points along Its Vertical Length.

5.2.7. Determining the effect of CO_2 on the Hydrogen analyser

The hydrogen analyser used in this project operated using the principle of thermal conductivity. Given that the fuel gases CH_4 and CO_2 have a significant thermal conductivity factor, the analyser was calibrated to measure H_2 in CO_2 and the hydrogen reading when CO_2 in N_2 is passed through, to correct for the influence of CO_2 gas. CH_4 conductivity factor is quite significant but based on literature, thermodynamic modelling and preliminary tests; the concentration of CH_4 in the product stream at the selected operating conditions for the experiments was insignificant. Therefore, the influence of CH_4 thermal conductivity on the H_2 analyser was neglected. A calibration curve for the hydrogen analyser was created from different mixtures and the correction factor was established from Figure 5:11 and Figure 5:12.

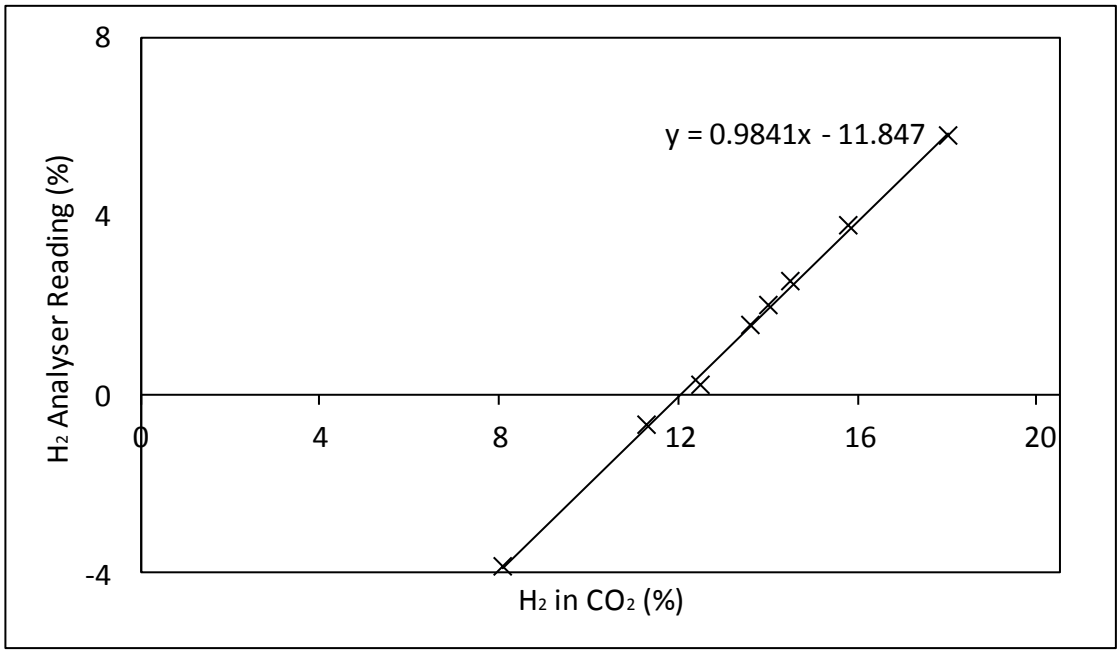


Figure 5:11: Calibration curve to estimate the hydrogen content in CO_2 and H_2 gas environment.

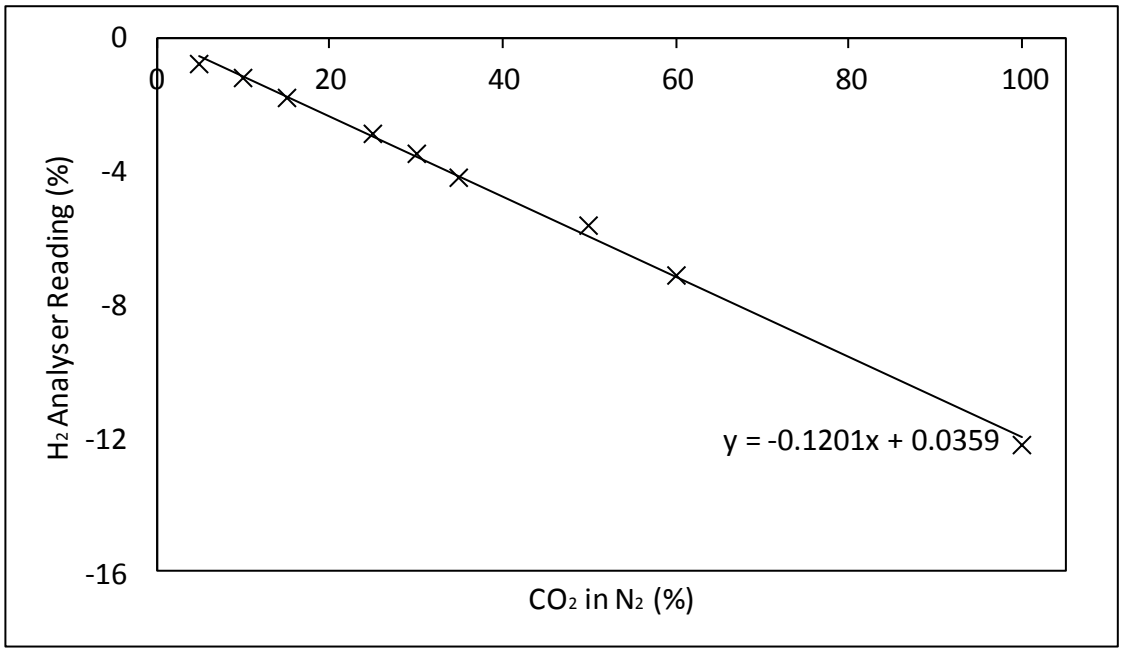


Figure 5:12: Calibration curve to Estimate the Hydrogen content in CO_2 and N_2 gas environment.

5.2.8. Determining an Appropriate Cooling Agent for the Second Trap

Previous users of the Hot-Rod reactor used liquid nitrogen to cool the gas and condense tar in the second trap. In this project, the impact of using liquid nitrogen was investigated and the results showed that most of CO_2 and CH_4 gases were retained in the second trap at near liquid nitrogen temperature.

Figure 5:13 illustrates the results of using liquid nitrogen compared to using dry-ice. After a thorough evaluation of the process, the second trap was placed in a Dewar filled with dry-ice. In addition, inline filters were placed after the second trap to filter out any tars in the gas. Both traps were filled with wire-mesh to improve their efficiency.

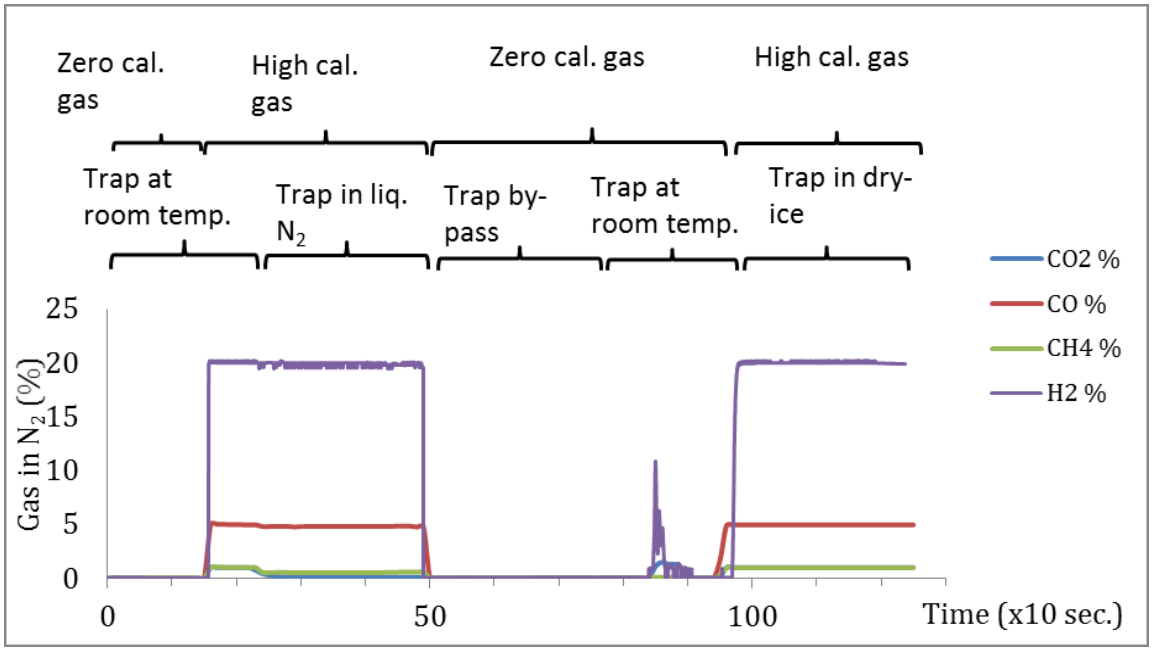


Figure 5:13: Calibration Gas Concentration in N_2 Detected by Analysers after Passing through Liquid Nitrogen or a Dry-Ice Condensate Trap

Table 5:1 shows a summary of the steps followed during the investigation of the effect of the different condensate baths content. Table 5:1 illustrates the dewar condensate material and gas passing through the trap at the respective times.

Table 5:1: Table describing the feeding times, feed composition and coolant in the Dewar

Time range (min.)	0 – 14	14 – 48	48 – 95		95 – 140
Feed gas	Zero cal.	High cal.	Zero cal.		High cal.
Time range (min.)	0 – 23	23 – 48	48 – 84	84 – 95	95 140
Dewar content	Empty	Liquid nitrogen	Empty & by-pass	Empty	Dry-ice

Zero cal. gas = N_2, High cal. gas = 1%CO_2, 5% CO, 1%CH_4 and 20% H_4 mixture in N_2.

Dry ice was found to be the most suitable medium that explicitly condensed all the tars that were contained in the product stream; dry-ice did not affect the concentration of hydrogen, carbon monoxide, carbon dioxide and methane which were measured using the online analyser. When liquid nitrogen was used, most of the CO_2 and CH_4 were retained in the traps resulting in inaccurate gas readings in the analysers.

5.2.9. Introducing a Quartz Glass Liner inside the Metallic Reactor Tube

This was the final modification on the reactor and it was based on the evaluation of the data from thermodynamic equilibrium model and literature knowledge. CH_4 is produced at temperatures below 550 ^oC. At 600 ^oC and above, CH_4 is not expected to be present in the products. However the experimental results, in particular, from the blank in an Incoloy reactor and Ni-catalyst tests in Chapter 4 indicate a significant amount of CH_4 in the products. This observation raised interests to investigate the cause to this behaviour. It was concluded that CH_4 is formed from thermal decomposition of tar but also comparing the gas formed in an Incoloy reactor to that in a quartz reactor, the metal alloy of the Incoloy reactor and the Ni-catalyst played a substantial part in promoting the methanation reaction, leading to the generation of CH_4 in the product stream. In order to eliminate the reactions catalysed by the reactor body, the reactor was modified by adding an internal quartz tube liner. The quartz tube isolated the reactants from contact with the reactor wall. The final modification of the reactor is illustrated in Figure 5**:14**.

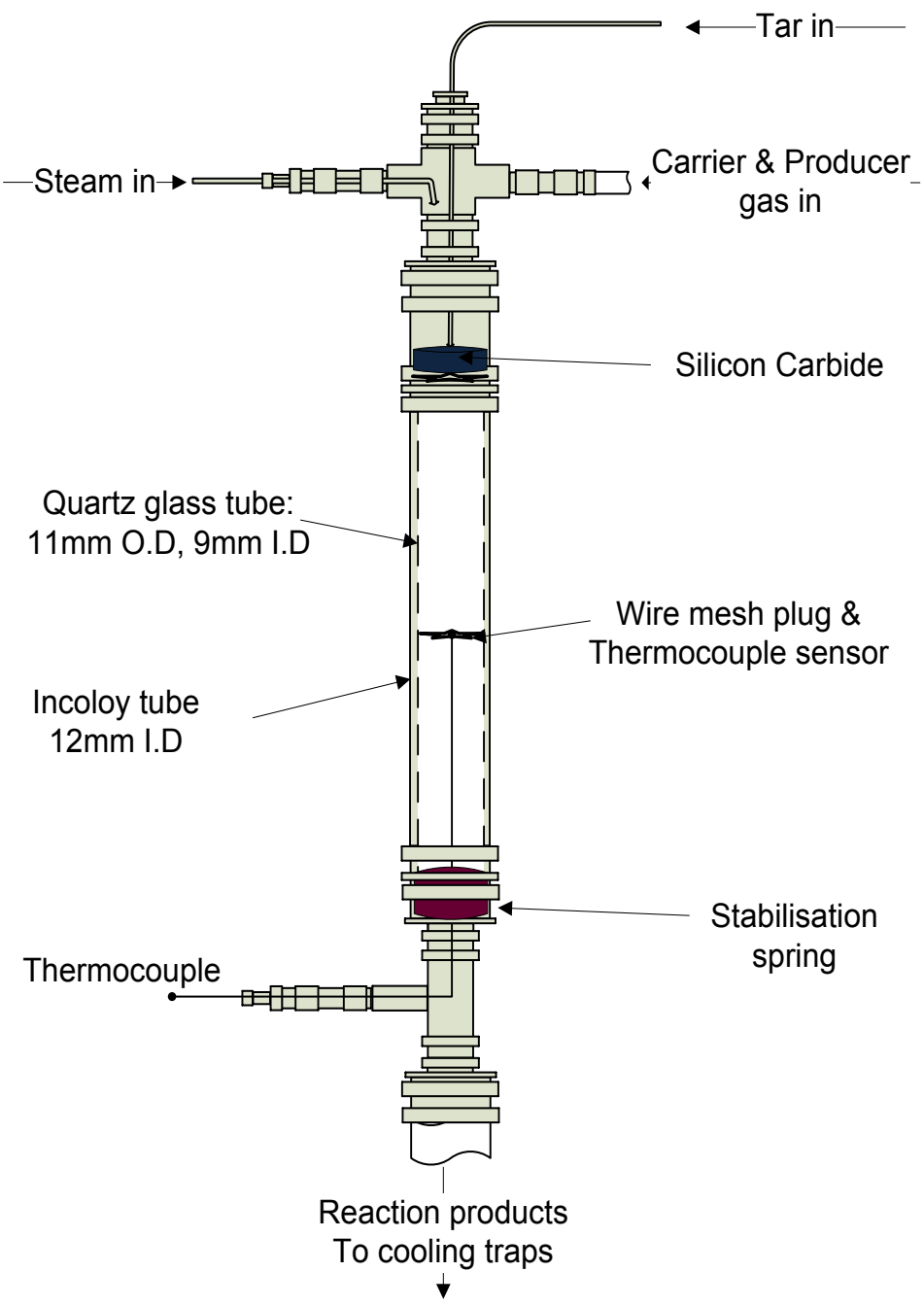


Figure 5:14: Final Design of the Process Reactor

5.3. Summary

The development of the reactor involved a considerable amount of thinking which required synthesising a series of options to eliminate undesirable behaviours but support the final design and develop a procedure for operation. After a thorough

consideration of the pros and cons of the previous reactor design and literature ideas a preferred design approach was used to modify the reactor and achieve a best fit to deliver the service required. At completion of modifying the reactor, separate parts of the reactor were sequentially commissioned. The commissioning exercise confirmed the ability to control or handle the reactor operation, the functionality of the reactor instruments and reliability of operation within a range of variables. The commissioning results were also used to approve the suitability for continuous operations of the reactor at different data points. Details on the final commissioning tests and operating procedures are given as part of the preliminary runs and experimental procedure. To sum up the modification and commissioning exercises provided the principal methodology to independently vary the steam to carbon ratios, regulate the tar concentration, maintain the pre-conditioning temperature at 350 ^{o}C and achieve a steady and measurable gas concentration in the analysers over an extensive period. Parts of the final arrangement of the reactor looks as shown in figures below:

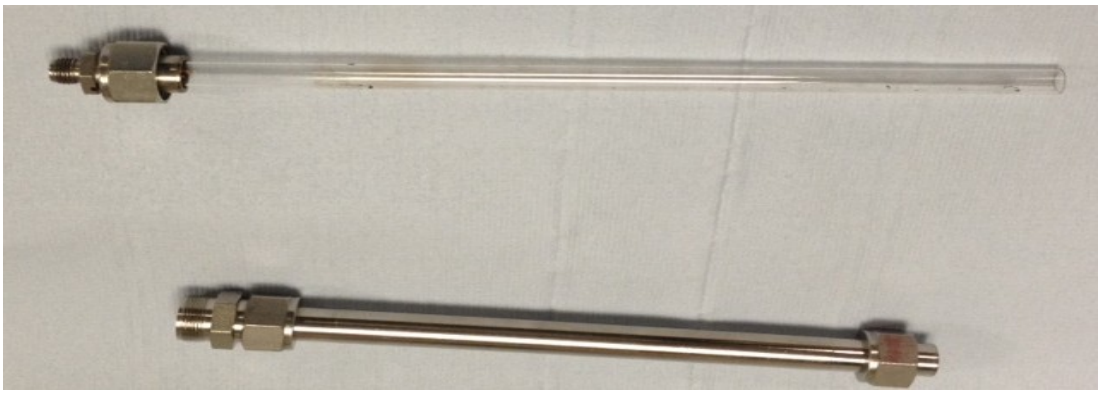


Figure 5:15: Quartz and Incoloy Reactor Tubes separately



Figure 5:16: Quartz Tube Lined Inside the Incoloy Tube

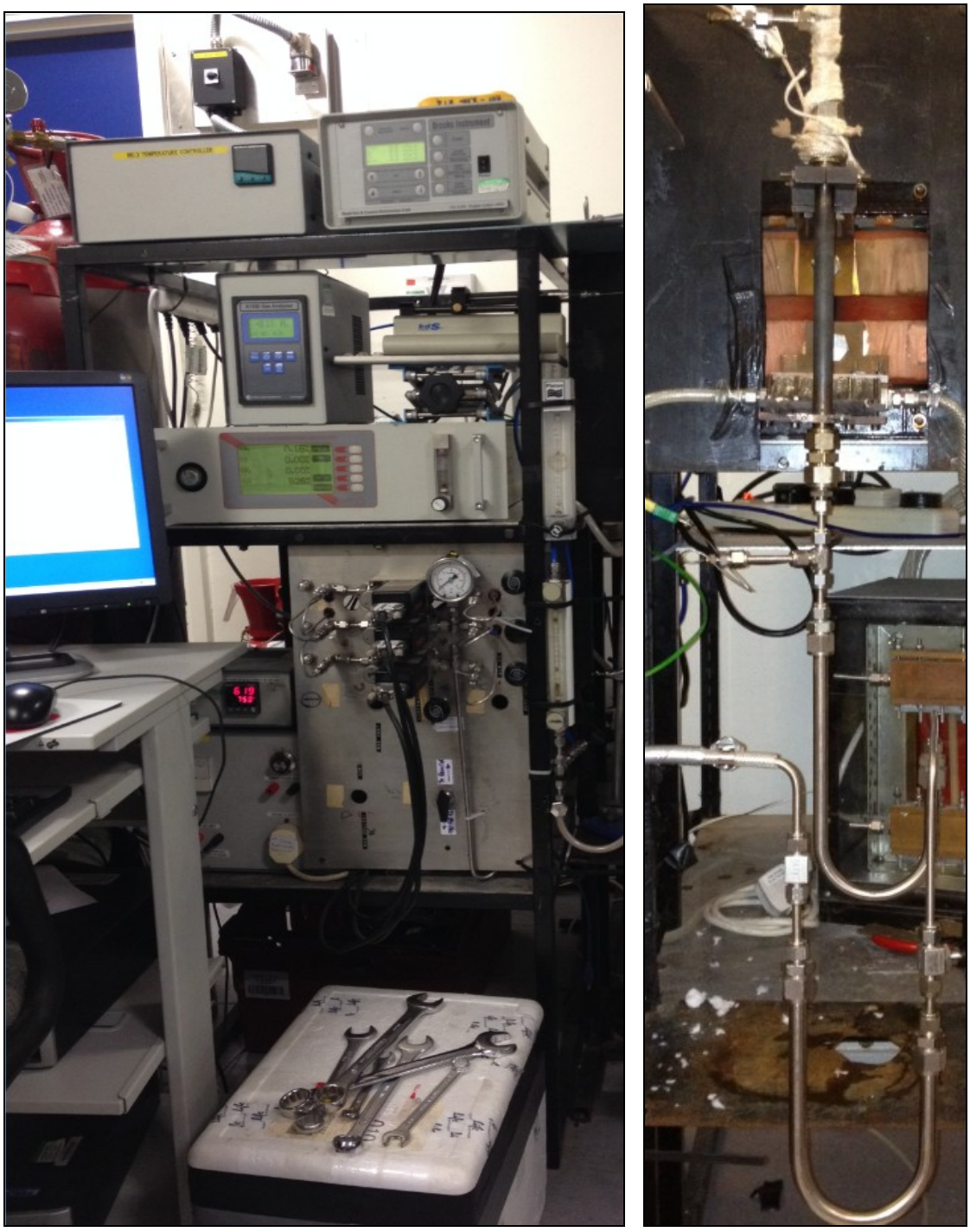


Figure 5:17: To the left is are the control equipment and to the right is the non lagged reactor connected to the condensate traps.

6. RESULTS AND DISCUSSION I: CONTRUST BETWEEN THE REACTOR BEFORE AND AFTER, AND TESTS AT HIGHER TEMPERATURES

The final modification of the reactor system, following the modifications to the condensate system and the feeding and preconditioning section, was the addition of a quartz tube liner inside the Incoloy tube. This was successfully accomplished and the majority of the project experiments were performed using this configuration.

This chapter presents a series of results from experiments aimed at tar destruction while making contrasts in performance of Pt-, Rh- and Ni-catalysts for tar cracking and reforming. Variables including (i) temperatures at 700 °C to 950 °C, [40] catalysts; Pt-, Rh- and Ni-catalyst, (iii) steam carbon ratios 1, 2 and 3, (iv) residence time by changing carrier gas flow rates at 0.209 L/min, 0.402 L/min, 0.603 L/min and 0.733 L/min and carrier gas composition using N_2 alone and a syngas mixture of 1%CO_2, 5%CO, 1%CH_4 and 20%H_2 were investigated. Some variables were eliminated in order to focus on a narrow range that would suite the further developments of the kinetics studies. Preliminary trial tests were performed in an Incoloy reactor tube and the quartz lined reactor tube. The preliminaries showed that the Incoloy wall has an impact on the reactions. The results in this section are mostly obtained from a quartz reactor and compared with thermodynamic calculations to assess how close the experimental reactions are towards equilibrium. In this study, non-catalysed and catalysed reactions were initially performed at 850 ^{o}C, 900 °C and 950 ^{o}C but later tests were performed either at 700 °C and or at 750 °C.

Non-catalysed thermal reactions are referred to as blank tests. These tests were used as a basis for studying the effect of the S/C, temperature and flow rates. Blank tests in the preliminary tests were performed at 850 ^{o}C, 900 ^{o}C and 950 ^{o}C. All blank tests were controlled by the basic thermal reactions, except the preliminary tests performed in an Incoloy reactor, it was identified that the Incoloy material catalysed the reactions. After modifying to a quartz liner, the blank tests were repeated to eliminate the Incoloy

material effect. The blank results with the lined reactor are compared with the simulated equilibrium results together with the catalytically controlled reactions.

Generally, biomass tars react to form char, soot, permanent gases and potentially secondary and tertiary tars [13]. This conversion involves a complex network of reactions, but most commonly, tar will gasify and reform following Equation 6-1 to Equation 6-6. Different catalysts can selectively influence different reactions and can therefore cause a suite of reactions to yield differing product compositions. The performances of thermal cracking and the catalysts are frequently linked to these reactions. In this project, the effect of the catalyst has been assessed by comparing their product results with the blank and the thermodynamic equilibrium calculations.

Gasification and gas reforming reactions:

Equation 6-1 Boudouard Reaction [68], [69]

$$C + CO_2 \leftrightarrow 2CO$$

Equation 6-2: Steam Reforming Reaction [70] or Solid Carbon Reaction [71]

$$C + H_2O \leftrightarrow CO + H_2$$

Equation 6-3: Methane Formation [72]

$$C + 2H_2 \leftrightarrow CH_4$$

Equation 6-4: Water Gas Shift Reaction [73]

$$CO + H_2O \leftrightarrow CO_2 + H_2$$

Equation 6-5: Methane Reforming Reaction [70]

$$CH_4 + H_2O \leftrightarrow CO + 3H_2$$

Equation 6-6: Methanation Reaction [70], [74]

$$CH_4 + 2H_2O \leftrightarrow CO_2 + 4H_2$$

6.1. The Contrast between the Reactor with and Without a Quartz Liner

Two sets of results were obtained under similar conditions using the unlined (Incoloy) and quartz lined reactors. The experimental results obtained including those in the preliminary studies show; more CH_4 and CO fractions were formed in an Incoloy tube reactor than those from a quartz reactor. This led to debate whether the reactor wall had some significant influence on the chemical reactions. This part of the study was therefore done to assess the impact of the Incoloy reactor wall, and the results are shown in Figure 6**:1**.

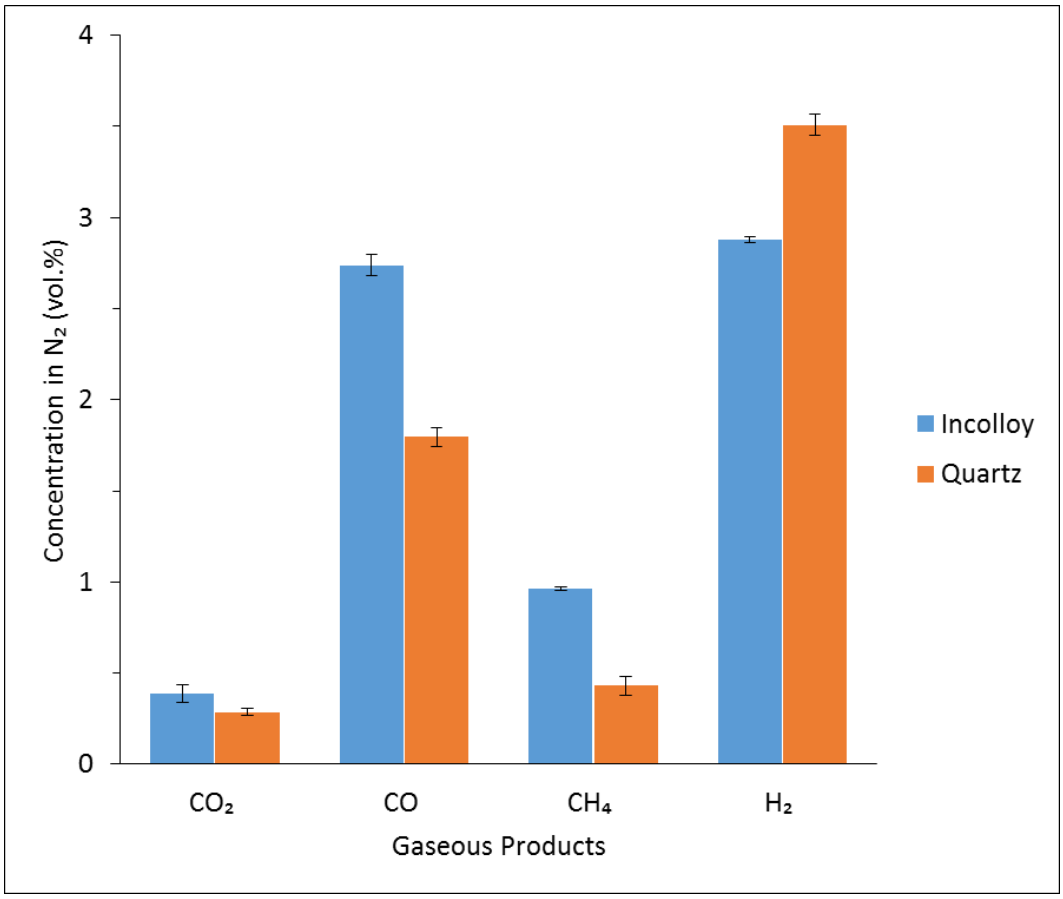


Figure 6:1: Comparisons of results from reaction in Incoloy & Quartz reactors at 900 °C with an S/C of 2.

Comparing the products from both reactors, carbon conversion in the Incoloy reactor was 65% compared to 58% in the quartz blank reactor. The concentrations of CO_2, CO

and CH_4 formed in the Incoloy reactor are higher than the concentrations obtained in the quartz lined tube reactor. Whereas, the concentration of H_2 formed in the quartz lined reactor is higher than the H_2 formed in the Incoloy tube reactor. This effect suggests an effect of the metal wall, which possibly led to a formation of hydrogenated compounds. It is therefore worth stating that the material in the Incoloy must have encouraged the conversion of carbon, the conversion of tar into methane and the overall gas formation.

6.2. Catalytic effect at 850 °C, 900 °C and 950 °C with an S/C 2 in a quartz reactor

The initial set-up of the reactor system was developed with an Incoloy reactor, which was used for the majority of the preliminary tests. After developing the reactor with control over the variables, a series of reproducible runs were performed and successfully integrated in the discussion. In this section, the results are discussed and later compared to the thermodynamics equilibrium calculations.

These tests were performed to investigate the effects of temperature on the reactions by examining the changes in the product suite. The experiments for each variable were repeated twice and their average was used to represent the data. During these tests the following operating conditions were selected; injecting tar at a rate of 100g/Nm^3, an S/C of 2, nitrogen carrier gas at 0.209 L/min, one gram of a catalyst per test and the reactor operating temperatures: 850 °C, 900 °C and 950 °C. Prior to adding the reactants to the reactor, the catalyst was reduced in 45%H_2/N_2 in situ at 900 ^oC for 1 hour. Once H_2 was switched off, the reactor was allowed to climatise in a N_2 only environment for 5 minutes.

Table 6:1: Summary of Gas Composition Formed During the Reactions of 100 g/Nm³ of Tar in 0.209 L/min of N_2 with Steam at an S/C of 2 under Pt-, Rh- and Ni-Based Catalyst at 850, 900 and 950 °C in a Quartz Reactor.

Operating Condition S/C = 2		Experimental Products					
		Gas Conc.(%) in N_2				Trap C-/Fed	H_2O
Catalyst	Temperature (°C)	CO_2	CO	CH_4	H_2	(%)	(g)
Pt	850	2.11	1.85	0.03	8.78	37	0.7
	Error	---	---	---	---	+/- 3	0.10
	900	1.93	1.87	0.01	8.99	32	0.9
	Error	---	---	---	---	+/- 2	0.05
	950	1.95	2.02	0.00	9.08	31	1.0
	Error	---	---	---	---	+/- 3	0.05
Rh	850	2.07	1.66	0.03	8.50	36	0.9
	Error	---	---	---	---	+/- 3	0.10
	900	2.04	1.97	0.00	9.54	32	0.8
	Error	---	---	---	---	+/- 2	0.10
	950	2.01	2.07	0.00	9.43	32	0.9
	Error	---	---	---	---	+/- 2	0.05
Ni	850	0.82	2.10	0.57	5.28	41	1.0
	Error	---	---	---	---	+/- 2	0.05
	900	1.12	2.74	0.42	6.41	29	0.8
	Error	---	---	---	---	+/- 2	0.10
	950	1.49	2.41	0.49	7.19	24	0.8
	Error	---	---	---	---	+/- 2	0.05

6.2.1. Hydrogen formation at 850 – 950 °C with S/C of 2

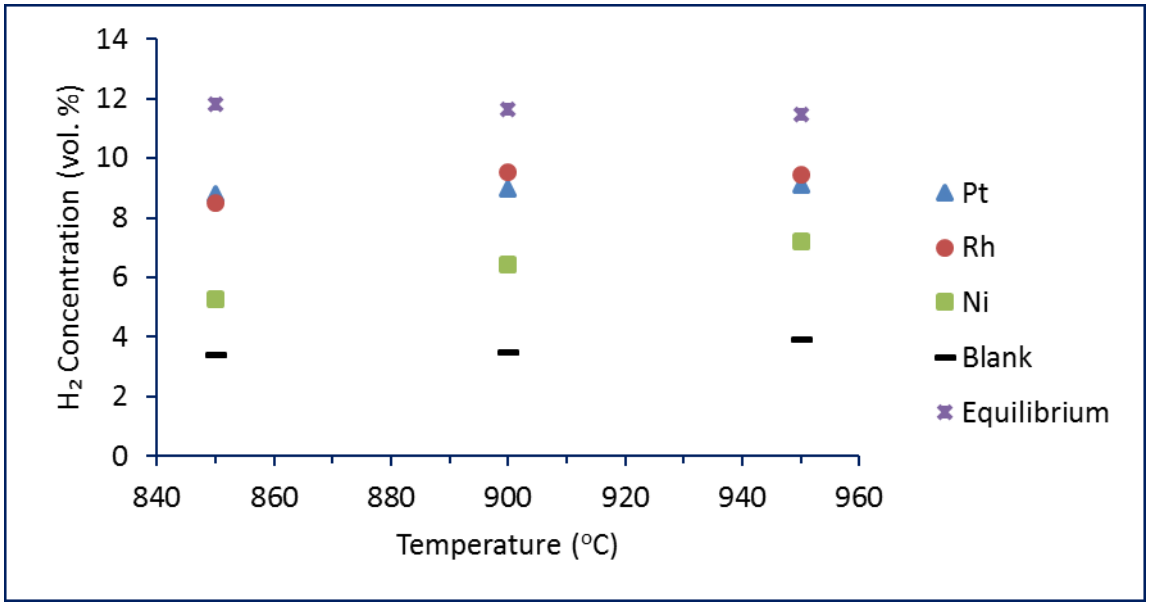


Figure 6:2: Hydrogen concentrations as a Function of Temperature, Formed during the Reactions of 100 g/Nm³ of Tar in 0.209 L/min N_2 with Steam at an S/C of 2 under Pt-, Rh- and Ni-catalysts at 850, 900 and 950 °C

Figure 6**:2** illustrates the trends of hydrogen obtained when reforming tar at 850 °C, 900 °C and 950 °C with steam of S/C of 2. During hydrogen formation, Pt- and Rh-catalysts closely approach equilibrium at higher temperatures. Ni-catalyst forms much lower H_2 fractions as well as the blank forms which forms even much lower H_2 fractions than Ni-catalyst. Overall, the H_2 yield from each test increased with increase in temperature. At 900 °C and above, the H_2 yield with Rh- and Pt-based catalysts is close to the equilibrium H_2 concentration than that from Ni-catalyst reactions. The hydrogen production with Ni- and Pt-based catalyst has been reported elsewhere and the results here are consistent with the trend reported by Lee et al. [75]. Compared to blank tests, all three catalysts increased hydrogen production when temperatures are increased from 850 °C to 950 °C.

All three catalysts promoted H_2 production. Rh- and Pt-based catalysts have a better hydrogen production activity than Ni-based catalyst at higher temperatures and an S/C of 2. This could be that Pt- and Rh-catalysts have a higher reforming activity.

6.2.2. Carbon monoxide formation at 850 – 950 °C with S/C of 2

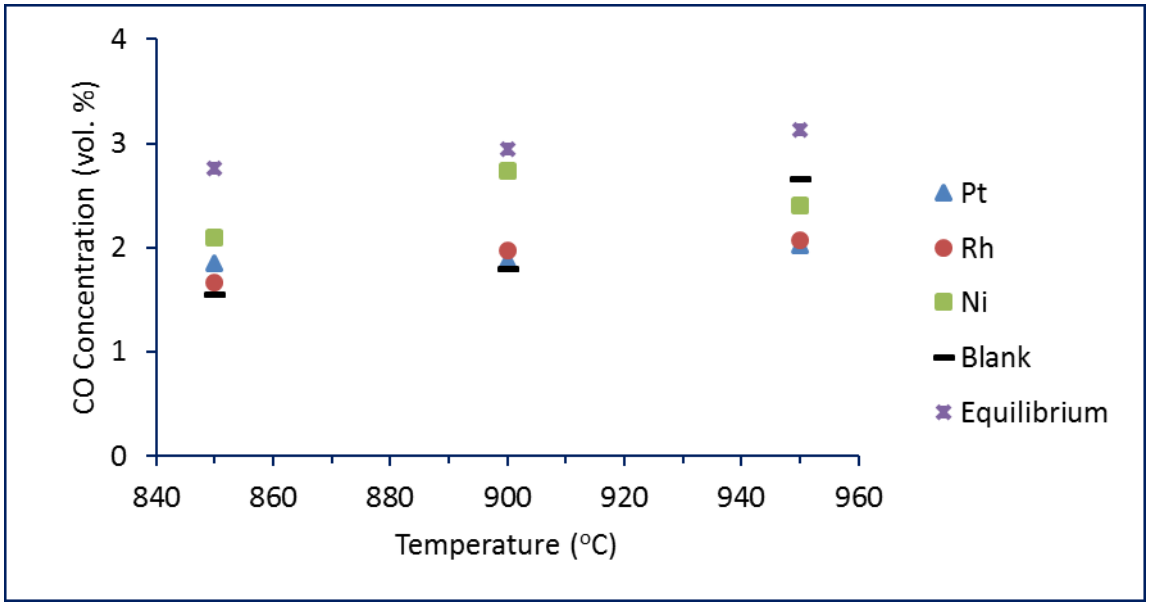


Figure 6:3: CO concentrations as a Function of Temperature, Formed during the Reactions of 100 g/Nm³ of Tar in 0.209 L/min N_2 with Steam at an S/C of 2 under Pt-, Rh- and Ni-catalysts at 850, 900 and 950 °C

Figure 6**:3** shows the concentration of CO after reforming tar at 850 °C, 900 °C and 950 °C with an S/C of 2. The figure shows that CO yield increases with temperature, except for Ni catalyst at 950 °C. CO production using Ni-based catalyst is relatively high in particular at 900 °C, this observation of a high CO volume concentration during Ni-catalyst conversions is consistent with a study by Lee et al. whose tests were performed for "hydrogen production by supercritical water gasification" at even a relatively lower temperature [75]. At 850 °C to 950 °C, the gas trend follows a simillar characteristic as that shown with the equilibrium. At 950 °C, the CO from the blank moves even closer to the equilibrium. Given CO in the blank run at 850 °C and 900 °C is slightly similar to that with the catalyst and at 950 °C is a lot closer to the equilibrium, exceeding that obtained during catalytic reforming, the reactions at about these temperatures could well be largely contolled by thermal-cracking.

6.2.3. Carbon dioxide formation at 850 – 950 °C with S/C of 2

At equilibrium CO_2 conversion was expected to decrease with increase in temperature. This is also shown in Figure 6**:4**.

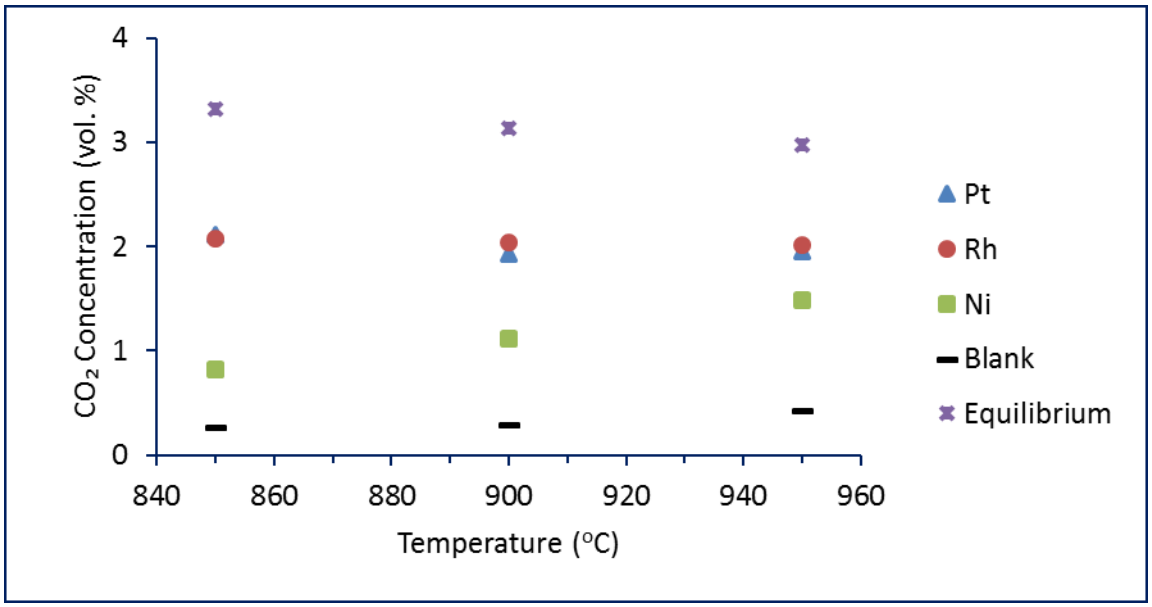


Figure 6:4: CO_2 Concentrations as a Function of Temperature, Formed during the Reactions of 100 g/Nm³ of Tar in 0.209 L/min N_2 with Steam at an S/C of 2 under Pt-, Rh- and Ni-catalysts at 850, 900 and 950 °C

The CO_2 formed during the Rh- and Pt-based catalysts experiments is closer to equilbrium and it appeared to follow the equilibrium trend, but CO_2 formed during the Ni-catalyst experiments could be under the influence of kinetic control. The practical experiments under kinetic control, it can be seen that an increase in CO_2 could occur with temperature and could tail off as equilibrium is approached. Inspite of the predicted behaviour, the CO_2 from the blank and Ni catalyst is noticeably below the predicted equlibrium.

As noted in equilibrium modelling and literature, the decomposition of tar produces an increasing amount of CO_2 at lower temperatures up until 500 °C and eventually CO_2 starts to drop at above 500 °C, whereas CO increases with temperature. A similar behaviour is noted with both the Rh- and Pt-catalyst. All catalysts promote CO

production at 850 °C and 900 °C and the CO formation was observed to increase with temperature, possibly due to increased carbon - to- CO_2 reactions.

6.2.4. Methane formation at 850 – 950 °C with S/C of 2

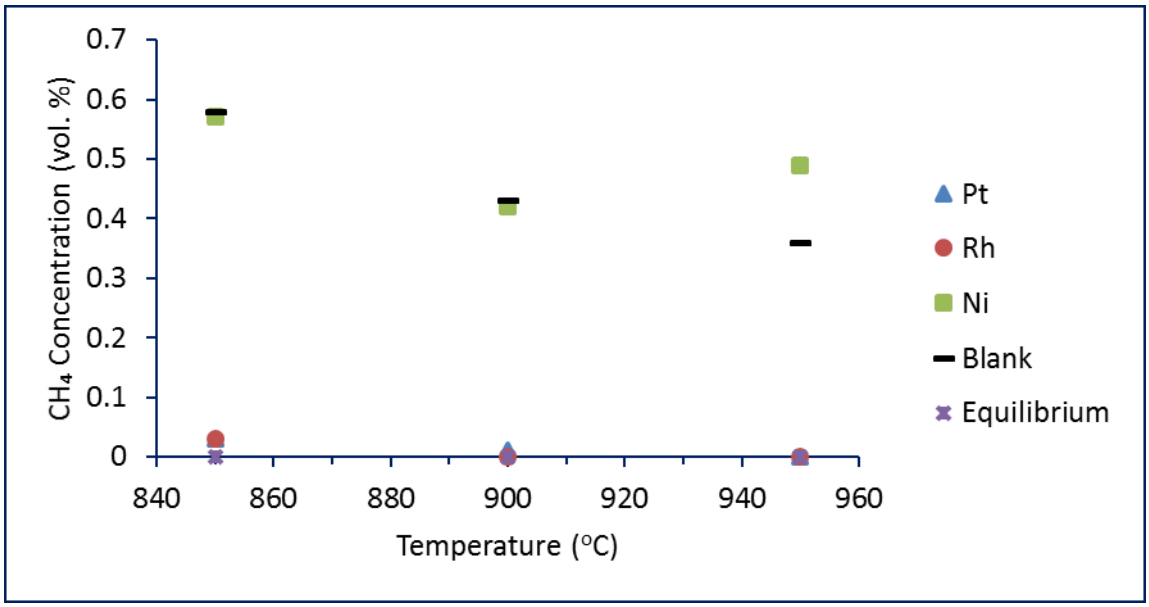


Figure 6:5: CH_4 concentrations as a Function of Temperature, Formed during the Reactions of 100 g/Nm³ of Tar in 0.209 L/min N_2 with Steam at an S/C of 2 under Pt-, Rh- and Ni-catalysts at 850, 900 and 950 °C

In Figure 6**:5**, no CH_4 is predicted at equilibrium and at high temperatures. The Pt- and Rh-catalyst results are consistent with this. At lower temperatures, these two catalysts show low levels of CH_4, suggesting that kinetics were a bit slow to reach equilibrium. The blank tests show the presence of more CH_4. The CH_4 fractions decrease markedly with temperature, although not to zero as a small amount is still noticable at increased temperatures. This shows that CH_4 is being formed through tar cracking and Ni-catalyst is not active enough to reform it completely. Also, the relatively low hydrogen yield and higher methane yield observed with Ni-based catalyst signifies that Ni-based catalysts promotes the activity of CH_4 production.

In summary, from the above individual gas analysis at 850 – 950 °C with an S/C of 2, a higher H_2 and CO_2 formation is observed from Rh- and Pt-based catalyst than the Ni-

based catalysts. This behaviour would indicate that the two former catalysts are more active for both H_2 and CO_2 formation. Generally Pt and Rh consistently stood out as good catalysts for methane reforming.

6.2.5. Carbon conversion at 850 – 950 °C and S/C of 2 in a Quartz Reactor

The results discussed here follow the reaction of tar and steam in a reactor without a preconditioning chamber. The major improved here was the addition of a quartz liner in the reactor tube. Experiments were performed at temperatures between 850 and 950 °C to investigate the effect of temperature on carbon conversion.

To monitor the conversion, a carbon balance across the system was performed. In each test 1 ml of tar containing 0.52 g of carbon was injected into the process. After each reaction, some of the carbon was collected in a liquid phase while the rest was converted to either gas or solid. The product gas was analysed on-line while the unconverted liquid to gas was collected in the traps and the solids were gathered from the reactor for gravimetric and further analysis. The amount of carbon converted to gas was calculated using the Equation 6-7 and Equation 6-8.

Equation 6-7: Carbon Converted to Gas

$$C_i = (X_i\ QT\ \rho_i\ MMc)/(MM_i*100)$$

Equation 6-8: Carbon Yield or conversion in %

$$Yield\ (\%) = (\Sigma C_i * 100\%)/(Cf)$$

Where C_i is the mass of carbon from either gas formed (Equation 6-7) or carbon collected from traps (Equation 6-8), Cf is the total carbon in the feed, X_i is the volumetric fraction or concentration of carbon dioxide or carbon monoxide or methane obtained from the gas analyser, QT is the total volumetric flow in the product stream, ρ_i is the density of carbon MMC is the molar mass of carbon and MM_i is the molecular mass of compound.

The catalyst activity determined the enhanced rate of conversion of tar into the gaseous products: CO_2, CO, CH_4 and H_2. To provide evidence of the catalysts' activity, the reaction path which was actively more favoured than the blank's reaction was investigated. With the aid of the thermodynamic equilibrium data the activity of the catalysts is compared with the gas data from the equilibrium model to determine how close the catalyst activity enabled equilibrium to be approached.

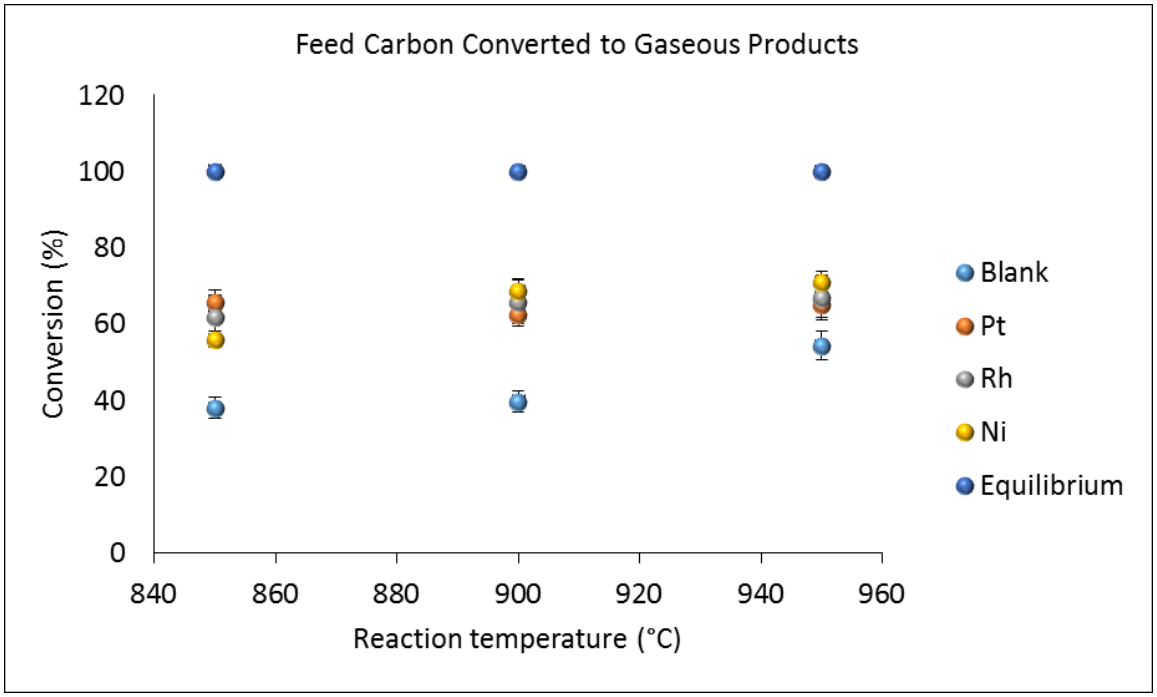


Figure 6:6: Carbon Converted to Gas Products in a Quartz Reactor as a Function of Temperature, Formed during the Reactions of 100 g/Nm³ of Tar in 0.209 L/min N_2 with Steam at an S/C of 2 under Pt-, Rh- and Ni-catalysts at 850, 900 and 950 °C

The activity of all three catalysts used in this study is relatively high compared to the blank experiments. The conversions with Pt-based catalyst at all three temperatures was near constant, the conversions with the Rh- and Ni-based catalyst increased with increasing temperature. At 850 °C, the conversions with Rh-, Pt- and Ni-based catalysts were 69%, 70% and 59% respectively and when the temperature was increased to 950 ^{o}C, the conversions with Rh- and Ni-catalyst increased to 72%, and 76% respectively

while Pt-catalyst conversion of carbon to gas remained the same. Rh-based catalysts are known for providing surface oxygen for oxidation of deposited carbon, but Ni-based catalyst was significantly more active in carbon conversion at temperatures above 900 °C than either Pt- or Rh-based catalysts. Ni-based catalyst is also active at CO_2 formation and the rate of its carbon conversion increased more significantly than the other two catalysts. At 850 °C Ni catalyst was less active than either of the two other catalysts but its activity increased significantly above that of Rh and Pt-based catalyst at 900 °C.

Generally, the non-catalysed reaction increased carbon conversion with temperature. The effect of temperature is less marked with catalysed reactions, but extents at lower temperatures are greater than without catalyst. By 950 °C, however, the non-catalysed reaction had begun to catch up with the catalysed conversion. It seems to be difficult to achieve 100% the equilibrium conversion. This could be due to unreactive char formation or insufficient time of reaction in the bed or due to insufficient steam.

6.3. Thermal-Cracking and Reforming of Tar at 700 – 950 °C with an S/C of 2

These tests were performed to investigate the effects of temperature during steam reforming of tar. No catalyst was used. The tests were performed at temperatures between 700 °C and 950 °C in a quartz lined reactor. The results are presented in Figure 6:7.

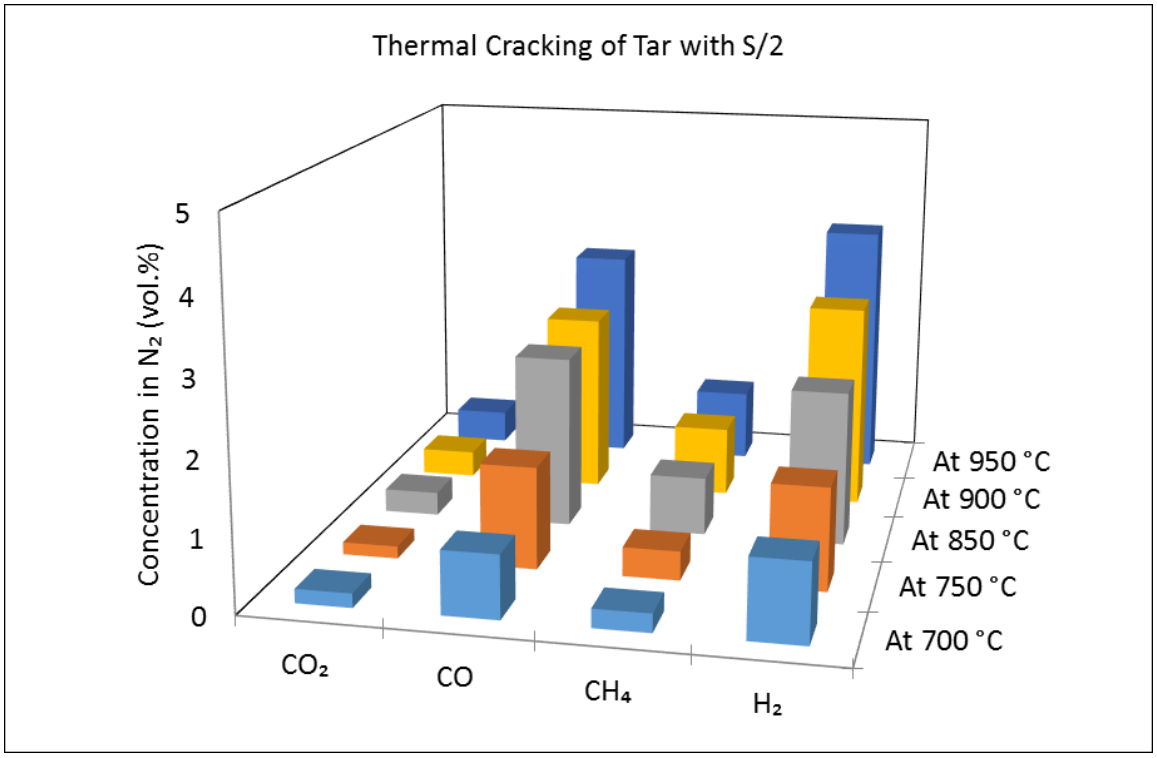


Figure 6:7: Gas Formation in 0.209 L/min of N_2 at 700 - 950 ^{o}C from Tar Reactions with Steam at an S/C of 2.

Observations from Figure 6**:7** show that at higher temperatures, higher volume fractions of H_2 and CO are formed. Overall gas fraction increases with temperature with only slight changes in CO_2 and CH_4. Comparing the gas fractions with the equilibrium model, the experimental results have similar trends with CO and H_2 but contradicting results with CO_2 and CH_4. No CH_4 was predicted in at equilibrium at these temperatures, but if any, for both CO_2 and CH_4 should be decreasing. These contradicting gas formations would imply that non-catalysed reactions did not reach full conversion. Evidence to support this argument is presented in the carbon analysis. At 700 °C, only 20% of the carbon injected into the process converted to gas. As temperature increased to 750, 850, 900 and 950 °C, the amount of carbon converted to gas increased to 30%, 54%, 89% and 69% respectively. With such large differences in carbon conversion between 700 to 950 °C it must be concluded that only a small amounts of carbon is converted to gas at lower temperatures. 50% conversion and above is achieved at temperatures above 800 ^{o}C. Jointly assessing the carbon conversion and gas formation,

it is possible that water-gas shift (Equation 6-4), Boudouard (Equation 6-1) and steam reforming (Equation 6-2) reactions effectively dominate the reactions as temperatures increase with ineffectively low methanation reactions occurring. Generally, the trend in carbon conversion follows that of the equilibrium model except that in equilibrium maximum conversions were achieved at such high temperatures.

6.4. Conclusions

At 950 ^{o}C, most of the tar that passed through the Pt-, Rh- and Ni- catalyst beds was converted to gas and as no carbon was collected in the traps, but a noticable amount of carbon was retained at top of the catalyst bed and in the line before the bed. Of the three catalyst when analysed under a microscope and analysed on a TGA, no carbon deposits were detected on the Rh catalyst. The low carbon convertion observed in a Rh experiment is a result of carbon lost on the walls of the reactor before the tar sample reached the bed.

Comparing the activities at the different temperatures, this data suggests that although all catalyst were very active, Ni activity was slow at lower temperatures than at higher temperatures. Pt- and Rh- based catalytic activities were mostly steady at all three temperatures. Of the three catalysts, Rh translates a much better conversion based on the the results later discussed from TGA and Microscopic analysis. When the temperature was increased there was a relatively much higher volume concentration of carbon monoxide and hydrogen mainly due to the waster gas shift reaction and lighter compounds such as methane decomposition; which are consistent with the observations and modeling reported by Balu et al. [71]. To study the activity of the catalyst at the same time minimising heating, the catalysts will be investigated at even much lower temperatures. This could also alow future work to determine the kinetics of the reactions.

During observations, nearly 20% of the tar injected into the process did not reach the reaction bed, and elsewhere the carbon deposited on the catalyst bed. One of the possible causes for this was due to insuficient steam in the process. For this reason,

steam in the feed was increased from an S/C of 2 to an S/C of 3 in the next set of experiming while narrowing down the operation range. The amount of silicon carbide in the preconditioning zone was reduced to minimise any carbon loss to the preconditioning chamber.

Generally, the non-catalysed reaction increased carbon conversion with temperature. The effect of temperature is less marked with catalysed reactions, but extents at lower temperatures are greater than without catalyst. By 950 ^{o}C, however, the non-catalysed reaction had begun to catch up with the catalysed conversion. It seems to be difficult to achieve 100% the equilibrium conversion. This could be due to unreactive char formation or insufficient time of reaction in the bed or due to unsufficient steam.

7. RESULTS AND DISCUSSION II: TAR REFORMING IN A QUARTZ LINED REACTOR AT 700 AND 750 °C UNDER DIFFERENT OPERATING VARIABLES

To make a definitive progress with the experiments, a thermodynamic equilibrium calculation was performed using a selected operating window. The results from tar cracking and reforming at 850°C, 900°C and 950°C showed that the reactions were mainly temperature controlled at temperatures of 900°C and above. It was therefore meaningful to explore a range of temperatures lower than 900°C to justifiably determine the activity of the catalysts.

In order to focus on a lower temperature range, the thermodynamic equilibrium calculations performed during preliminary trials are incorporated into this chapter. The thermodynamic data in this chapter include results from various temperatures and steam-to-carbon ratios within a selected range.

Another variable considered in this section is the use of model compounds guaiacol and toluene. These were investigated at a similar selected range of variables to validate the reliability of using model compounds in the study of catalysts activity. The results were together compared with the thermodynamic equilibrium calculations.

7.1. Thermodynamic Equilibrium Calculations to Validate the Operating Window

Like in Chapter 4 the thermodynamic equilibrium calculation were performed using a Gibbs free minimisation reactor in an Aspen Plus software. The results obtained from thermodynamic equilibrium calculation at 700 ^{o}C, 750 ^{o}C and 900 ^{o}C at an S/C of 1, 2 and 3 illustrated in Table 7:1.

Table 7:1: Thermodynamic Equilibrium Calculated Gas Data at 700°C, 750°C and 900°C at Different Steam-to-Carbon Ratios

Equilibrium modelling gas volume concentration diluted in nitrogen							
Operating Conditions		Product Gas Concentration (%)				Carbon	Water
	Temperature (^{o}C)	CO_2	CO	CH_4	H_2	(g)	H_2O (g)
No added steam	700	1.65	4.52	0.02	10.24	0.00	0.26
	750	1.50	4.69	0.00	10.13	0.00	0.27
	900	1.15	5.07	0.00	9.82	0.00	0.30
S/C = 1	700	3.22	2.86	0.00	11.70	0.00	0.86
	750	2.98	3.11	0.00	11.50	0.00	0.89
	900	2.41	3.72	0.00	10.98	0.00	0.95
S/C = 2	700	3.97	2.07	0.00	12.39	0.00	1.57
	750	3.74	2.32	0.00	12.18	0.00	1.60
	900	3.14	2.95	0.00	11.64	0.00	1.66
S/C = 3	700	4.40	1.61	0.00	12.79	0.00	2.32
	750	4.18	1.84	0.00	12.59	0.00	2.34
	900	3.61	2.45	0.00	12.07	0.00	2.40

The results show that CO and H_2O in the product stream increases with temperature whereas CO_2 decreases. The effect with temperature is similarly the same as reported in Chapter 4. Comparing individual gas at similar conditions but changing the steam content show that CO_2, H_2 and H_2O in the product steam increased with steam but CO decreases. Only traces of CH_4 were detected in calculations at 700 ^{o}C with without steam. At all other conditions in this calculated window, no CH_4 was detected. These results and trend are compared with the experimental results later in the chapter.

7.2. Pt-, Rh- and Ni-catalytic Reforming of Guaiacol and Toluene Mixture at 750 °C

Guaiacol was one of the compounds detected in higher concentrations during the GC-MS analysis of the tar sample. It was mixed with toluene and the mixture was used as a

model compound for evaluating the catalyst performance in tar destruction, but also compares the catalyst activity in model tar and a biomass tar reforming.

The experiments with model compounds were performed after the final modification, in quartz lined reactor. These tests were performed by mixing Guaiacol with Toluene at 50% volume fractions of each. The reactor was operated at 750 ^{o}C, an S/C of 3 in N_2 as a carrier gas at 0.206 L/min. The gas fractions from tests with each of the catalysts are shown in Figure 7**:1**.

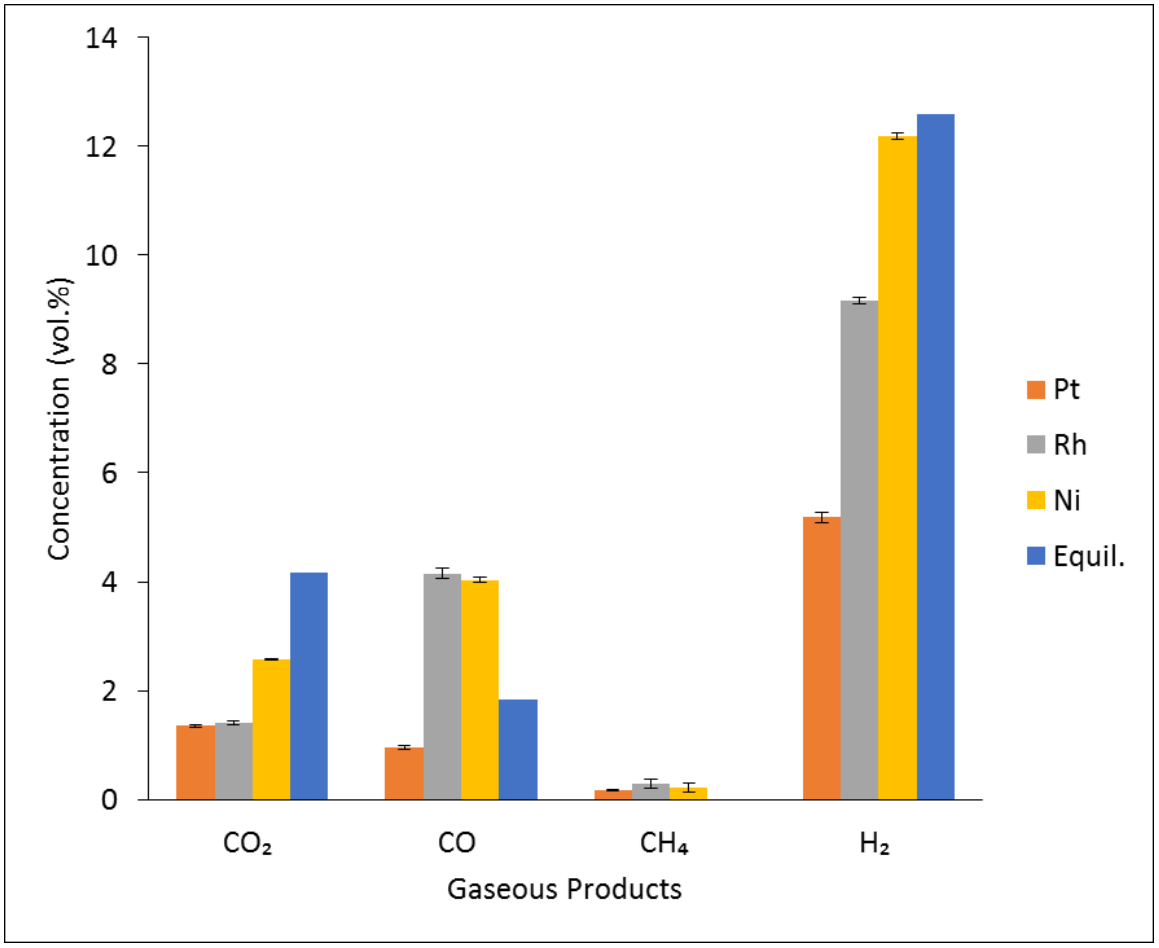


Figure 7:1: Reforming of 100 g/Nm³ of 50% Guaiacol and 50% Toluene with an S/C of 3 in 0.209 L/min at 750 °C

The gas formation with model compounds shows that Ni has a better carbon conversion, with 100% of carbon from the feed converted to gas. In Pt and Rh bed reactions, 84% and 40% of carbon was converted to gas. A significant amount of soot

and carbon was observed in the reactor after each test with model compounds, except with Ni-catalyst. A similar behaviour was observed elsewhere in literature [76] when studying the effect of tar-contaminated syngas on solid oxide fuel cell anode materials from which it was suggested that Toluene would increase the amount of carbon during operations at 700 °C and above.

Although this test was also aimed at obtaining the amount of liquid products to complete the mass balance, it was not practically easy to separate the liquid products from the extraction solvent (chloroform-methanol mixture or Chloroform on its own) given also the liquid products may have reformed into other unidentified compounds.

By comparing the gaseous product distribution, Ni and Rh formed relatively the same amount of CO and more than twice that from Pt. Pt and Rh formed relatively the same amount of CO_2 but Ni formed more than 1.5 times of the CO_2 from either Pt or Rh. H_2 formation in the Ni-catalyst bed was very close to equilibrium and higher than that from Rh and Pt. Overall, the Ni bed has a much better activity than either Rh or Pt in reforming the mixture of 50% Guaiacol in Toluene model compounds at these conditions.

7.3. Thermal- and Catalytic Cracking and Reforming of Tar

In gasification, some operations are performed without using catalysts or adding steam. The outcomes from such operations vary broadly, depending on the feedstock and the conditioning of the reactants, as there is little modulation of the process. Keeping all variable the same, a blank run was used to assess how effective the catalysts are.

In this study, the three catalysts are investigated to study their reaction activity and the products favoured by each catalyst's reaction pathways. The tests were performed at temperatures of 700 °C and 750 °C, established from the conclusions drawn from the preliminary tests. Such temperatures were not expected to affect the catalysts since all three catalysts are based on Al_2O_3 as a primary support, which is not chemically affected by heat. Other varied parameters included the steam-to-carbon ratios from 1 to 3 and feed gas flow rates and feeding with a mixture of syngas. All tests were performed with

a tar concentration of 100 g/Nm^3 and each test was repeated at least twice to account for errors and reliability of data. In the main body of this report, averages of these results are reported and the discrete data and error assessments are reported showing the averages of the gas concentrations.

7.4. The Effects of Adding Steam to the Reactants in a Quartz Reactor at 750 °C

Steam addition with the biomass tar plays an important role in the reformation reactions. Often the amount of steam in the reactant is controlled by either drying the feed during preconditioning or by adding steam to the reactor. In these tests steam was added to the process and expected to reduce carbon deposition on the catalyst. This is because the metal oxides used in the catalysts' design have a higher affinity for water and are effective at dehydration. Additional steam was varied based on the amount of carbon in the feed tar sample. Tests were performed with Steam-to-Carbon molar ratios (S/C) of 1, 2 and 3 and tests without adding steam. Show the gas results. Table 7:2 and Table 7:3 show the gas results obtained from reactions without steam compared to those with S/C of 1 – 3.

Table 7:2: Product Formation from Tar Cracking at 750 °C without Steam

	Gas (in vol. %), water (vol. %) and carbon (g %) products at 750 ^{o}C, From feed at 0.209L/min N_2, 100 g/Nm^3 tar, with and without steam.							
No steam								
	Blank %	Error	Pt %	Error %	Rh %	Error %	Ni %	Error %
CO_2 in N_2	0.17	0.04	0.75	0.04	0.50	0.04	0.51	0.02
CO in N_2	1.50	0.07	1.68	0.07	4.41	0.04	3.05	0.09
CH_4 in N_2	0.41	0.03	0.39	0.03	0.40	0.05	0.25	0.01
H_2 in N_2	1.31	0.04	3.46	0.04	6.59	0.10	5.28	0.16
H_2O	0.7	0.05	0.8	0.05	0.7	0.05	0.7	0.00
C - gas	33	2	45	5	84	4	60	4
C - Trapped	62	14	51	9	11	23	35	18

Table 7:3: Products Formation from Tar Reforming Without Steam and With Steam of an S/C Ratios of 1 -3 and Catalyst at 750 °C

	Gas (in vol. %), water (vol. %) and carbon (g %) products at 750 ^{o}C, From feed at 0.209L/min N_2, 100 g/Nm^3 tar, with and without steam.							
S/C = 2								
	Blank %	Error	Pt %	Error %	Rh %	Error %	Ni %	Error %
CO_2 in N_2	0.17	0.01	1.29	0.08	---	---	1.08	0.03
CO in N_2	1.37	0.16	1.49	0.20	---	---	2.07	0.06
CH_4 in N_2	0.39	0.07	0.35	0.03	---	---	0.32	0.02
H_2 in N_2	1.37	0.04	5.33	0.11	---	---	5.58	0.14
H_2O	1.2	0.05	1.3	0.05	---	---	1.2	0.15
C - gas	30	8	51	10	---	---	56	3

C - Trapped	59	20	54	10	---	---	37	15
S/C = 3								
	Blank %	Error %	Pt %	Error %	Rh %	Error %	Ni %	Error %
CO_2 in N_2	0.17	0.01	1.53	0.17	1.55	0.18	1.57	0.10
CO in N_2	1.44	0.11	1.56	0.17	4.40	0.22	2.28	0.12
CH_4 in N_2	0.40	0.04	0.35	0.00	0.16	0.03	0.30	0.06
H_2 in N_2	1.34	0.07	5.26	0.51	9.47	0.32	6.71	0.21
H_2O	1.4	0.15	1.3	0.10	1.1	0.15	1.1	0.35
C - gas	32	5	56	11	99	14	67	9
C - Trapped	61	5	39	11	0	0	30	9

CO_2 only increased with increase in process steam during all catalysed experiments. No differences are observed with CO_2 in the blank results. Comparing the data to the equilibrium model, CO_2 would increase when H_2O is increased following the Water-Gas Shift reaction, suggesting that carbon conversion may be improved or carbon from CO or CH_4 is being used up. The consistent results in CO_2 form the blank would suggest that the reaction here did not reach the equilibrium. CO and CH_4 fluctuate irregularly but the overall carbon conversion increases. Overall, when steam was increased in the feed material, the dry gas formation and carbon conversion increased.

7.5. Effects of Changing Residence Time

Experiments at different feed flow rates were performed to investigate the effect of the residence time which would support future develops of the reaction kinetics. In order to investigate residence time effect, the flow through the reactor was primarily determined based on the bed size, using a residence time of 0.36 seconds. Prior to the reactions in these tests, the catalyst bed was heated to 900 ^oC in nitrogen. At 900 °C, the catalyst was activated in 45%H_2/N_2 for one hour. After activation, the bed temperature was changed to a steady temperature of 750 ^oC and the gas mixture was

switched to N_2 at 0.209 l/min, 0.402 l/min, 0.603 l/min and 0.733 l/min, thus reducing the bed residence time from 0.36s to 0.19s, 0.13s and 0.10s respectively. Steam at a steam-to-carbon ratio of 3 and tar at 100 g/Nm^3 were injected into the reactor and products were collected as described in the experimental procedure. The gas results are presented in Figure 7:2, Figure 7:3, Figure 7:4, and Figure 7:5.

Table 7:4: Gas formation and Carbon Balance at Different Flow Rate

Gas concentration (vol% in N_2) and carbon trapped from reforming 100 g/Nm³ of tar with an steam at an S/C of 3 tar in Nitrogen at 750 °C								
q = 0.209 l/min								
	Blank	Error	Pt	Error	Rh	Error	Ni	Error
CO_2	0.17	0.01	1.53	0.17	1.55	0.18	1.57	0.10
CO	1.44	0.11	1.56	0.17	4.40	0.22	2.28	0.12
CH_4	0.40	0.04	0.35	0.00	0.16	0.03	0.30	0.06
H_2	1.34	0.07	5.26	0.51	9.47	0.32	6.71	0.22
C - Gas	32	5	56	11	98	14	67	27
C - Trap	61	5	39	4	0	0	30	9
q = 0.402 l/min								
	Blank	Error	Pt	Error	Rh	Error	Ni	Error
CO_2	0.14	0.04	1.19	0.06	1.62	0.03	1.76	0.04
CO	1.42	0.14	1.52	0.02	4.56	0.47	1.98	0.05
CH_4	0.39	0.05	0.43	0.01	0.33	0.03	0.25	0.01
H_2	0.72	0.09	3.59	0.14	8.72	0.21	6.24	0.23
C - Gas	31	8	51	3	104	18	65	10
C - Trap	60	8	42	6	0	0	34	6
q = 0.603 l/min								
	Blank	Error	Pt	Error	Rh	Error	Ni	Error

CO_2	0.15	0.00	0.83	0.06	1.64	0.35	1.27	0.11
CO	1.48	0.01	1.61	0.15	3.78	0.34	2.14	0.06
CH_4	0.42	0.02	0.46	0.08	0.35	0.14	0.35	0.05
H_2	0.65	0.02	2.43	0.21	8.10	0.58	4.43	0.35
C - Gas	32	1	47	10	93	28	61	7
C - Trap	64	5	48	4	0	0	31	8
q = 0.733 l/min								
	Blank	Error	Pt	Error	Rh	Error	Ni	Error
CO_2	0.18	0.04	0.72	0.09	1.30	0.11	---	---
CO	1.57	0.03	1.78	0.12	3.50	0.02	---	---
CH_4	0.53	0.04	0.56	0.06	0.47	0.08	---	---
H_2	0.73	0.10	2.46	0.09	6.69	0.20	---	---
C - Gas	36	4	49	9	36	7	---	---
C - Trap	---	---	---	---	---	---	---	---

The data in Table 7:**4** is summarised in Figure 7:**2** to Figure 7:**5** below. From observations across the data in the table also presented in the figures below, all catalysts functionality indicate CO_2 and H_2 formation decrease with decrease in residence time, that is to say; increase in carrier gas flow rate, while CO slightly fluctuates and CH_4 slightly increase. Comparing the catalysed results to non-catalysed results, relatively a substantial amount of tar was converted to gas in the catalysed experiments. Only very small amount of gases are formed in the non-catalysed experiments with formation of each remaining almost the same for the different investigated residence times.

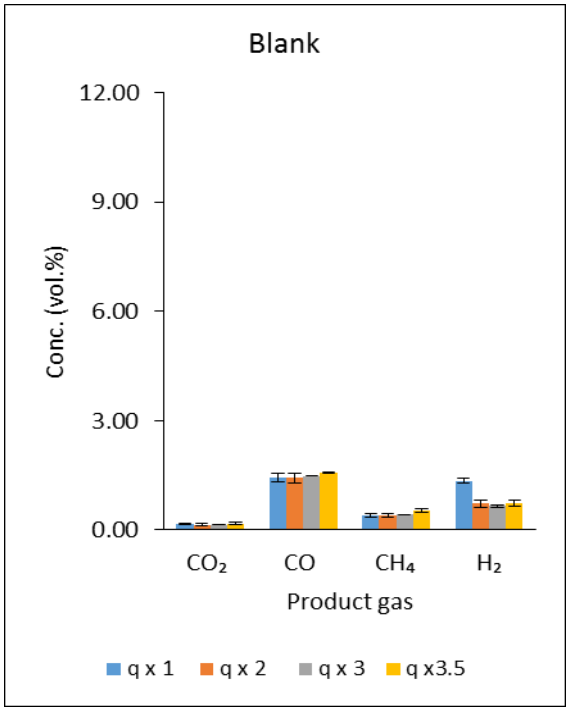


Figure 7:2: Thermal reaction

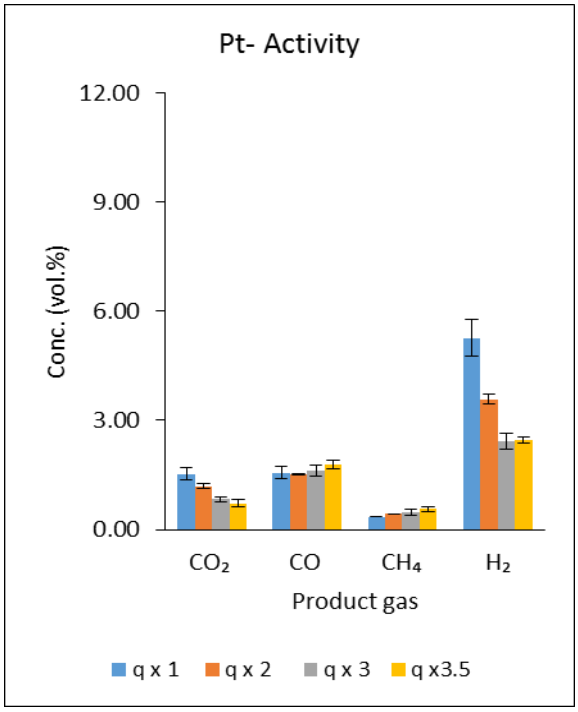


Figure 7:4: Pt-catalyst activity

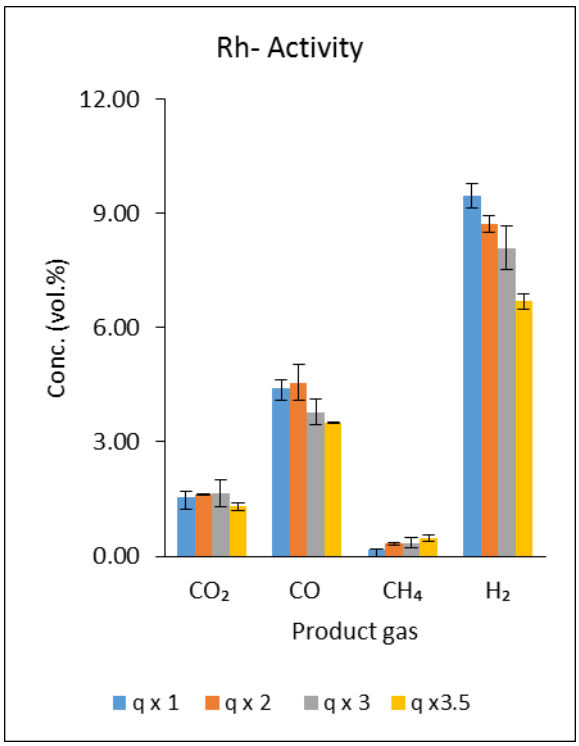


Figure 7:3: Rh-catalyst activity

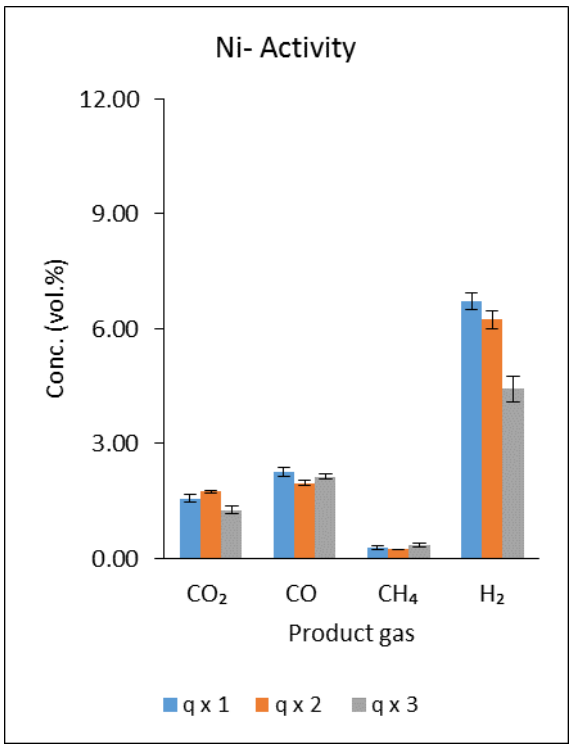


Figure 7:5: Ni-catalyst activity

7.6. Effects of Adding Hydrogen

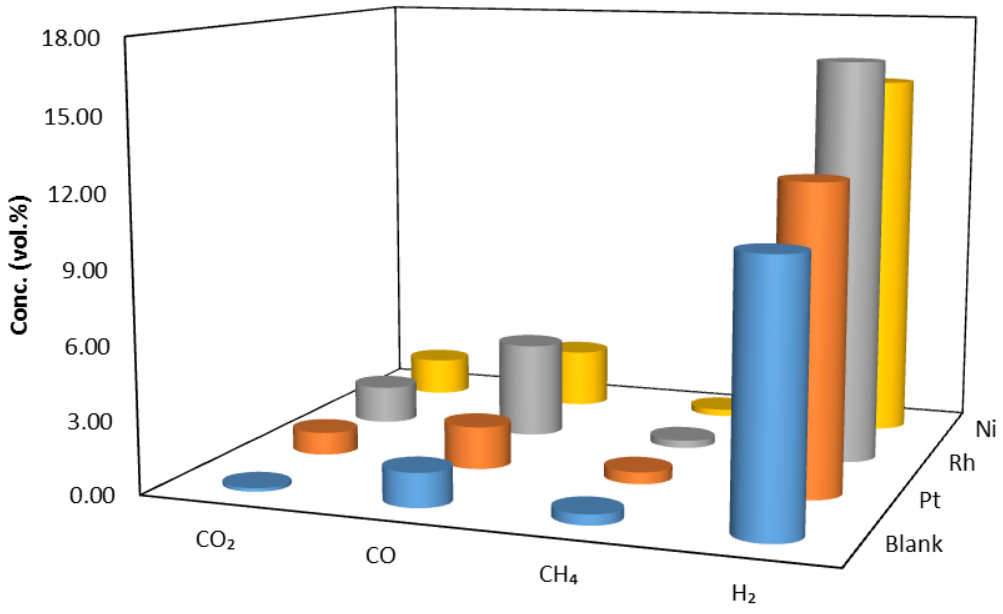
In a set of experiments, hydrogen gas was added in the feed stream with expectations that it would hydrogenate any polyunsaturated compounds in feedstock and consequently, with the presence of active catalysts, improve the conversion of feedstock to permanent gas products. During each of these tests, 10% H_2 in N_2 was fed into the reactor together with tar and steam. Prior to the reactions, the catalyst was reduced and after reduction the gas mixture was switched to 10%H_2/N_2 at 0.627 l/min and the bed temperature was reduced to 750 ^oC. Once a steady temperature was achieved, steam and tar were injected into the reactor at an S/C of 3 and 100 g/Nm³ respectively. Following a similar procedure described in products collection and analysis, the resultant permanent gases and carbon composition gathered are presented in Figure 7**:6**.

Table 7:5: Gas and Carbon Formation in an Increased H_2 Concentration environment

	0.627 l/min 10 H_2%/N_2 at 700 ^oC with an S/C = 3, 100 g/Nm³							
Products	Blank	Error %	Pt	Error %	Rh	Error %	Ni	Error %
CO_2 in N_2	0.15	0.02	0.65	0.07	1.83	0.17	---	---
CO in N_2	1.28	0.05	1.61	0.16	3.59	0.32	---	---
CH_4 in N_2	0.37	0.05	0.47	0.03	0.31	0.03	---	---
H_2 in N_2	11.19	0.13	11.96	0.91	16.69	0.25	---	---
H_2O	1.40	0.2	1.40	0.1	1.1	0.2	---	---
C – to – gas	28	10	44	6	92	9	---	---
C – trapped	59	32	47	19	2	65	---	---
0.627 l/min 10 H_2%/N_2 at 750 ^oC with an S/C = 3, 100 g/Nm^3								
	Blank	Error %	Pt	Error %	Rh	Error %	Ni	Error %
CO_2 in N_2	0.14	0.02	0.94	0.15	1.57	0.27	1.57	0.17

CO in N_2	1.40	0.20	1.76	0.08	3.96	0.37	2.45	0.04
CH_4 in N_2	0.44	0.05	0.49	0.02	0.32	0.01	0.29	0.07
H_2 in N_2	10.70	0.26	12.52	0.28	16.65	0.04	15.34	0.37
H_2O	1.30	0.46	1.37	0.20	1.15	0.25	1.55	0.25
C – to – gas	31	7	51	8	94	9	70	12
C – trapped	59	17	44	13	0	0	25	14

The data at 750 ^{o}C in the table above is further illustrated in Figure 7:6. A detailed discussion of the results in Table 7:5 is presented in the paragraph below Figure 7:6.



	CO_2	CO	CH_4	H_2
Blank	0.14	1.40	0.44	10.70
Pt	0.94	1.76	0.49	12.52
Rh	1.57	3.96	0.32	16.65
Ni	1.57	2.45	0.29	15.34

Figure 7:6: Gas Product and Catalytic Activity in H_2 Rich N_2 Environment

The gas products and carbon obtained from a H_2 rich carrier gas containing 10% H_2 as shown in Table 7:5 and Figure 7:6 are compared with the results in Table 7:6 which were obtained at the same conditions but without the added 10% H_2 in the carrier gas.

Firstly, comparing the results at 700 and 750 ^{o}C, there are only small differences in carbon conversion and in gas formation. For instance, the difference in carbon converted to gas during the blank, Pt and Rh reactions are 2.94%, 7.53% and 1.25% respectively. This suggests that changing the temperature from 700 ^{o}C to 750 ^{o}C during reactions in a H_2 rich environment only had a slight influence on the products provided all other variables were kept constant. Comparing the result with and without added H_2 but with all other variables kept constant, the conversion fluctuates with the catalyst present. Pt and Ni increased carbon conversion by 4% and 9% respectively. Rh conversion remained the same whereas the blank tests reduced carbon to gas conversion by 1% in the presence of the added hydrogen. In the case of gas formation, the tests with added H_2 show that CH_4 and H_2 slightly increased except with the Rh catalyst. This increase in CH_4 would suggest that both Ni and Pt catalyst have a relatively higher potential to dissociate H_2 into hydrogen atoms leading to the formation of other light branched chain hydrocarbons. The results from the blank runs show only a small difference in carbon conversion and hydrogen formation remains almost the unchanged.

Table 7:6: Product gas and Carbon Formation at 750 ^{o}C, S/C 3 in 0.627 l/min N_2

	0.627 l/min N_2 at 750 ^{o}C with an S/C = 3, 100 g/Nm^3							
Products	Blank	Error	Pt	Error	Rh	Error	Ni	Error
CO_2 in N_2	0.15	0.00	0.83	0.06	1.64	0.35	1.27	0.11
CO in N_2	1.48	0.01	1.61	0.15	3.78	0.34	2.14	0.06
CH_4 in N_2	0.42	0.02	0.46	0.08	0.35	0.14	0.35	0.05
H_2 in N_2	0.65	0.02	2.43	0.21	8.10	0.58	4.43	0.35
C – to – gas	32	1	47	10	93	28	61	7
C – trapped	64	5	48	4	0	0	31	8

Comparing the amount of carbon-to-gas from tests with and without added hydrogen, little differences can be recognised and can be neglected since the volumes gathered all fall within the error margins. Similarly, the same for the amount of carbon gathered

from the traps. However literature suggest that the addition of H_2 would potentially lead to a carbon-free regime, a similar account described by Cheng et al. when using hydrogen as a gasifying agent in glycerol-steam reforming [77].

7.7. Effects of Adding a Syngas Mixture

All the above results show cracking and reforming of tar in a N_2 or N_2 and H_2 environment, but a typical gasifier is a syngas rich environment. The experiments discussed in this section were designed to mimic a syngas rich environment as in a typical gasifier under operation at conditions gathered from the earlier variables as the best operating conditions. Prior to feeding the sample, the catalyst was activated as in the previous experiments. At the end of activating the catalyst, the carrier gas was switched to a syngas mixture containing 1%CO_2, 5% CO, 1%CH_4 and 20% H_2 in N_2 and left for 5 minutes to stabilise. Steam at an S/C of 3 and tar at 100 g/Nm^3 were then added into the reactor, in total 1.1145 grams of carbon were available for the reactions. The flow into the reactor was maintained at 0.209 l/min and 0.402 l/min for individual runs. The gas formation and carbon conversions are presented in Figure 7**:7** , Figure 7**:8** and Table 7**:7**.

The gas formation and carbon conversion are compared with tests performed in N_2 only under similar operating conditions. Unlike from most of the test runs performed, the carbon recovered from syngas added experiments was not recorded or measured.

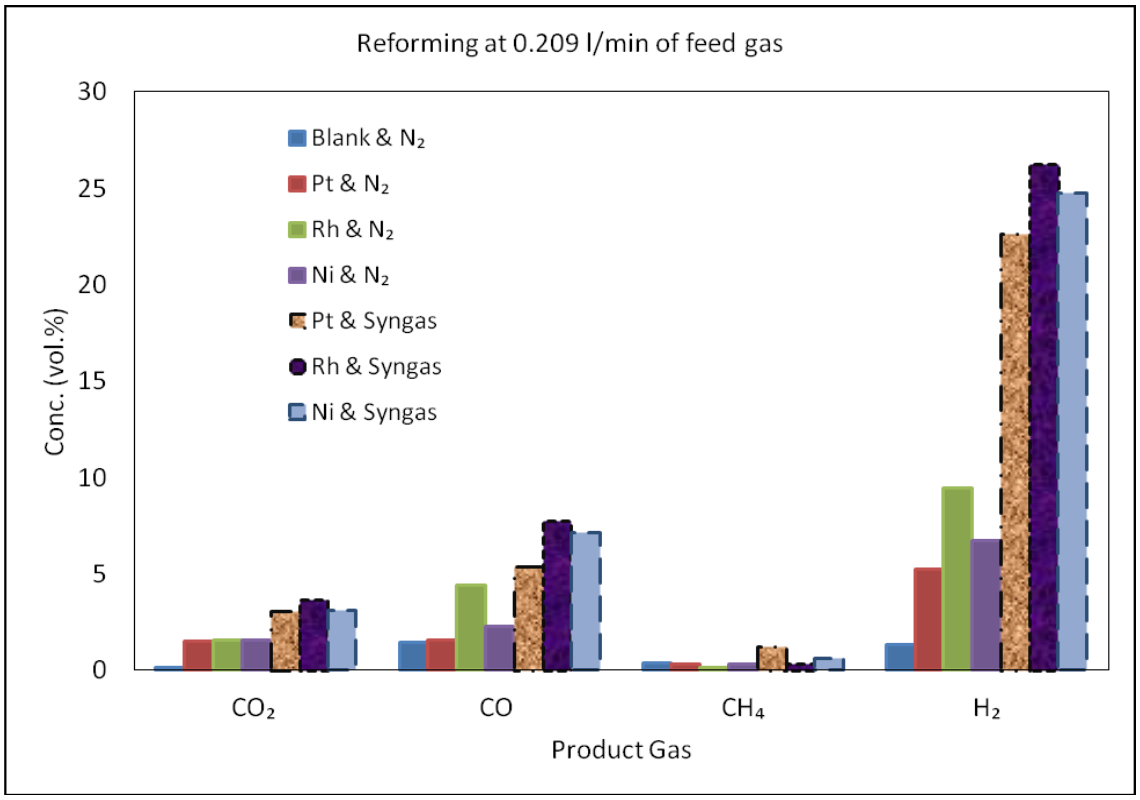


Figure 7:7: Reforming of Tar in Syngas and N_2 at 0.209 l/min

Figure 7:7 above shows the product gas concentrations obtained from experiments with and without bottled syngas added to the feed. The results are further discussed in the following paragraphs after Table 7:7 comparing the data from operation at different residence time as a result of increasing the flow rate.

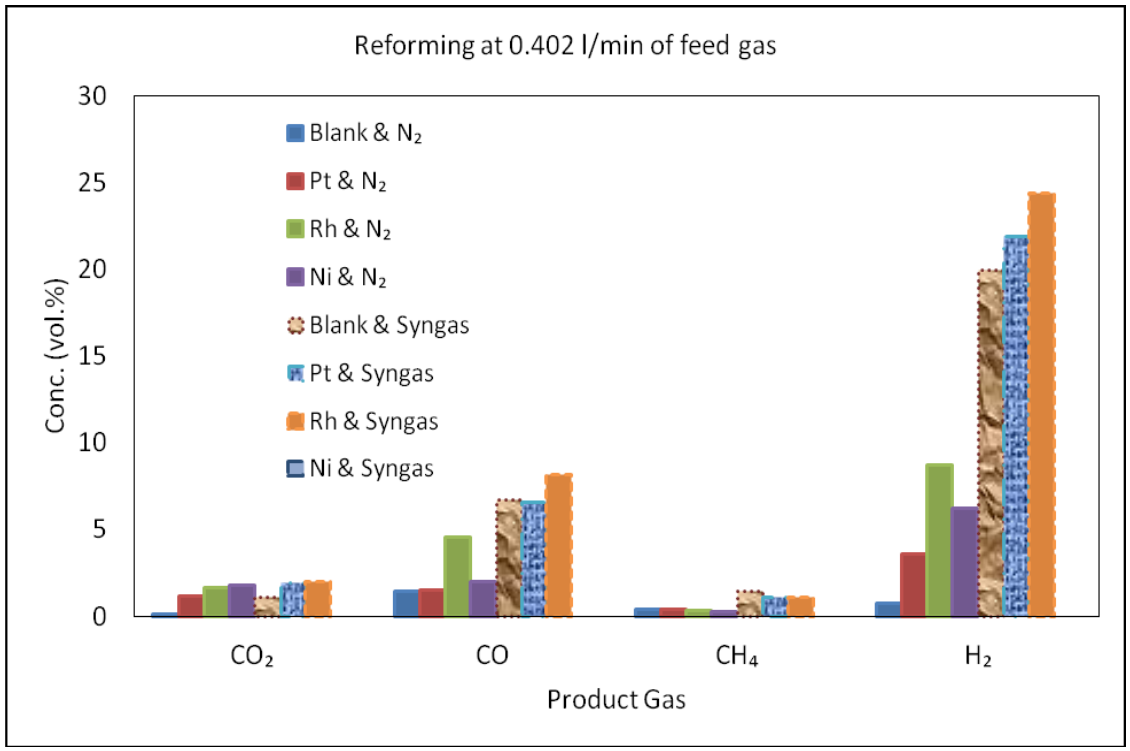


Figure 7:8: Reforming in Syngas at 0.402l/min

Figure 7:8 above follows Figure 7:7 under similar feed mixtures and operation but with increased flow rate, hence different residence time. The trends presented in Figure 7:7 and Figure 7:8 are summarised in Table 7:7 and discussed in the paragraphs that follow Table 7:7.

Table 7:7: Reforming tar at S/C of 3 in 0.209 l/min and 0.409 l/min N_2 at 750 °C

	Gas concentration (vol%) and carbon trapped from reforming 100 g/Nm³ of tar with an steam at an S/C of 3 tar in N_2 carrier gas at 750 °C										
	q = 0.209 l/min						**q = 0.402 ml/min**				
	CO_2	CO	CH_4	H_2	C (%)		CO_2	CO	CH_4	H_2	C
Blank	0.17	1.44	0.40	1.34	61+/-5		0.14	1.42	0.39	0.72	60+/-8
Pt	1.53	1.56	0.35	5.26	39+/-4		0.83	1.61	0.46	5.26	42+/-6
Rh	1.55	4.40	0.16	9.47	0		1.62	4.56	0.33	8.72	0
Ni	1.08	2.07	0.32	5.58	30+/-9		1.57	2.28	0.30	6.71	34+/-6

The trends in Figure 7**:7**, Figure 7**:8**, Figure 7**:9** and Table 7**:7**; the gas formation within a syngas environment are mostly identical to those seen within N_2 only carrier gas, but the gas formed in a syngas environment by difference is lower than that observed in N_2 only. Overall within the syngas enriched environment at a flow rate of 0.402 l/min a significant amount of CO_2 was formed that almost double by increasing the flow from 0.209 l/min. CO decreases as the low rate for both gases are increased. That is to say, at 0.402 l/min, CO decreased from 6.62% and 8.20% to 5.39% and 7.76% under the influence of Pt and Rh reactions respectively. Such a characteristic may suggest that the reactants did not have a sufficient time to completely reform at higher flow rates and overall, the conversion was not strongly improved.

Looking at the blank tests, the addition of syngas to the process strongly improved the carbonaceous gas formation together with carbon conversion. Further evidence can be drawn from Figure 7**:9**, which indicated the carbon conversions to gaseous products. Generally, carbon conversion was further achieved at the addition of syngas in the process, specifically in the blank, Pt and Ni reactions.

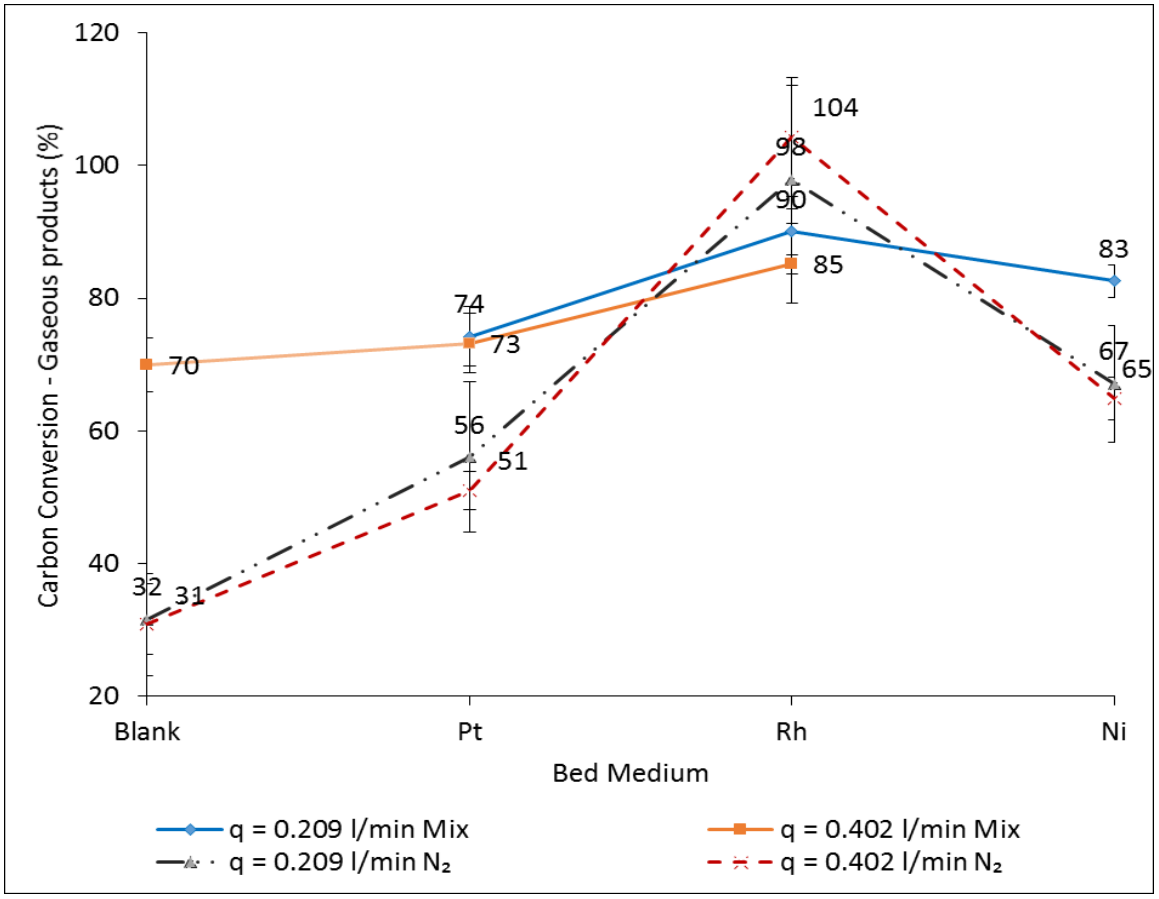


Figure 7:9: Carbon Conversion to Carbon in Product gas in a syngas mixture and in N_2 only

7.8. Summary

This chapter has dealt with reforming tar under different variables, investigating the destruction of tar from gasification. The results and discussion show a development from equilibrium modelling to preliminary tests and finally to the final practical tests. The preliminary tests were used to verify the suitability of the process design, and the equilibrium model was used to predict the performance of the experimental. The practical experiments were performed at a sequence of integrated variables in order to improve the process of tar destruction.

The key variables investigated include cracking at various temperatures, reforming with Pt, Rh and Ni catalyst, reforming in various steam concentration, addition of H_2 and a syngas mixture in the process and changing the reaction residence time. For each

variable, data for gas formation, liquid products and solid were collected. This data was used as a basis for the carbon balance, and credibility of the results was achieved by performing repeated test, gathering information on errors and comparing matching results. The outcomes of each of the variables are disclosed in the conclusion chapter.

The use of model compounds does not reflect the realistic performance of the catalyst. As it was observed, carbon conversions with model compounds were inconsistent with those from the real tar. Since the conversion for model compounds was high, it can be that there are more refractory compounds in the model compounds. Also Ni activity on model compounds forms a larger H_2 fraction than Rh, yet all results from biomass tar indicate Rh as a better catalyst for H_2 formation and carbon conversion. At 850 and above, Rh converted more than 95% carbon from the feed biomass tar to gaseous products and no tar was seen in the traps, but only 85% of carbon in the model compound was converted to gas. Ni converted 60% of carbon in biomass tar to gas as opposed to 100% of the carbon in model compound. For over the duration of the tests, Ni deactivated within the initial 30 minutes into the experiment with biomass tar yet during the model compound reforming, Ni activity stayed steady throughout the entire run time. This suggests that model tars are not a good representative of biomass tars and studies of tar in syngas should be investigated with genuine biomass tar.

Measurements from all tests indicate Rh is a much better catalyst for reforming tar and has a steady activity for over longer periods of runs. Ni is very active and its performance with model compounds is unattainable but it rapidly deactivates with biomass tar. Pt is relatively better in steady state activity than Ni but not better than Rh.

8. RESULTS AND DISCUSSION III: THE ANALYSIS FOR SPENT CATALYSTS AND BY-PRODUCTS

In chapter 6, the gas formation and amount of carbon collected in the traps was presented but the details on the catalyst and by-products were not argued. This chapter presents an analysis of the spent catalyst and the liquid products corresponding to the gas products. The aim for this analysis is to provide detailed information that strength evidence to the gas formation and as what that happens to the reactants.

8.1. Analytical Techniques Employed

The analytical techniques employed include: (i) the use of the thermogravimetric analysis (TGA) to determine the carbon deposited on the catalyst, [40] the use of a scanning electron microscope (SEM) to investigate the changes in the morphology of the catalyst, (iii) a Raman analysis to determine the nature of carbon deposits and (iv) the use gas chromatography-mass spectrometry (GC-MS) used to examine nature of the liquids in the formed. The discussions on the results in this chapter interlink with a combination of the different analytical techniques employed.

8.1.1. Thermogravimetric Technique

A TGA was used to determine the amount of carbon deposits on the spent catalyst after the reforming reactions. The TGA equipment used is a Perkin-Elmer TGA type. During the analysis, approximately 5 mg of the sample were placed on a TGA pan and combusted from 50 °C to 900 °C at a rate of 10 °C/min in 40 mL/min of air. The amount of carbon was calculated as the difference between the initial stabilised weight and the final stabilised weight of the sample.

In order to validate amount of carbon obtained from the difference, a fresh catalyst was also examined on the TGA following the same conditions and the weight loss of the catalyst was deduced. From the raw data, the derivative of the weight loss of the fresh and spent catalyst was integrated in the temperature region were carbon deposited. The weight loss of the fresh catalyst was deducted from the weight loss of the spent

catalyst to estimate the actual weigh of carbon deposits. And the areas under the plot of the fresh and spent catalysts of the same suite were compared to establish the percentage of the corresponding area from carbon deposits.

8.1.2. Scanning Electron Microscopy, Raman and GC-MS techniques

During the SEM analysis, a catalyst pellet was selected at random as a representative of the entire catalyst sample. Because of this, the analysis is predicted to carry a significant margin of error but this was reduced by taking multiple images of different samples. In the analysis, a representative catalyst was placed on a specimen chamber and mounted on a rigid gold coated sticker to improve the electronic conductivity of the specimen holder. The equipment was operated and images were taken at various magnifications.

For both the Roman and GC-MS analysis, support was obtained from laboratory assistants. The analytical results from fresh material are compared with spent and by-products below. Different results were obtained from each change of variables as it's expressed in the discussions that follow.

8.2. Spent Catalysts and Trapped Liquids

8.2.1. Trapped Liquids

Figure 8:1 shows two distinctive liquids that were trapped in the product stream. The first trap collected liquid that condensed in Ice- water and the second trap condensed all remaining liquid in the product stream. Only very small amounts of liquids were collected. So, in order to gather a reasonable volume for further analysis, a trial run was performed for 3 hours. The analysis of the liquids products were then analysed in a GC-MS and FTIR, and the results are shown below.

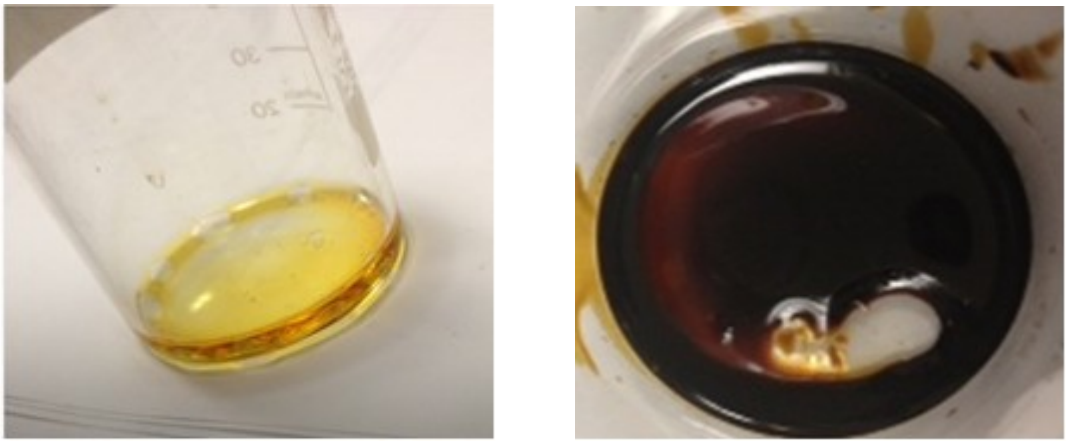


Figure 8:1: Liquid Products in Collected in Tar Traps; Orange - Yellowish from the first trap and Dark Brown to Black in the Second Trap, from Reforming Tar at 750 °C with S/C of 3 in 0.209 L/min of N_2.

8.2.2. GC-MS analysis of Liquid Products

All liquid were collected in tar traps as described in chapter 3 and 5 but in very small quantities. A representative sample was analysed using a GC-MS. The GC-MS temperature was set at 300 °C as the maximum temperature in the GC-MS coulmn used. All GC-MS analysed results are attached in Appendix 1 and Appendix 2.

For only the non-catalysed tests performed at 750 ^{o}C with S/C at 3 an FTIR analysis was performed to identify the difference between the compound in the feed tar and those trapped tar. The transmitted spectra are illustrated in Figure 8:2. FTIR analysis shows there were slight variations in transmission among the feed tar and the trapped tar spectra. Between 500 and 700 cm^{-1} the transmission of tar from the dry-ice trap exceeds that of tar from the Ice-water trap and tar of the feed. Between 900 and 1750 cm^{-1} the transmission of feed tar exceeds that of the trapped tars. The trapped tar spectra between 800 and 2000 cm^{-1} are virtually identical, whereas between 3000 and 3800 cm^{-1} the transmission for dry-ice condensate exceeds the others, followed by that of the Ice-water condensate and lowest is that of the feed tar. These variations indicate that below 700 cm^{-1} there were lighter compounds formed and trapped in the traps than the compounds in the feed. In the range between 700 to 1700 cm^{-1} most

compounds were converted to gas. Above 3000 cm^{-1}, heavier compounds were reformed and trapped in the condensate traps.

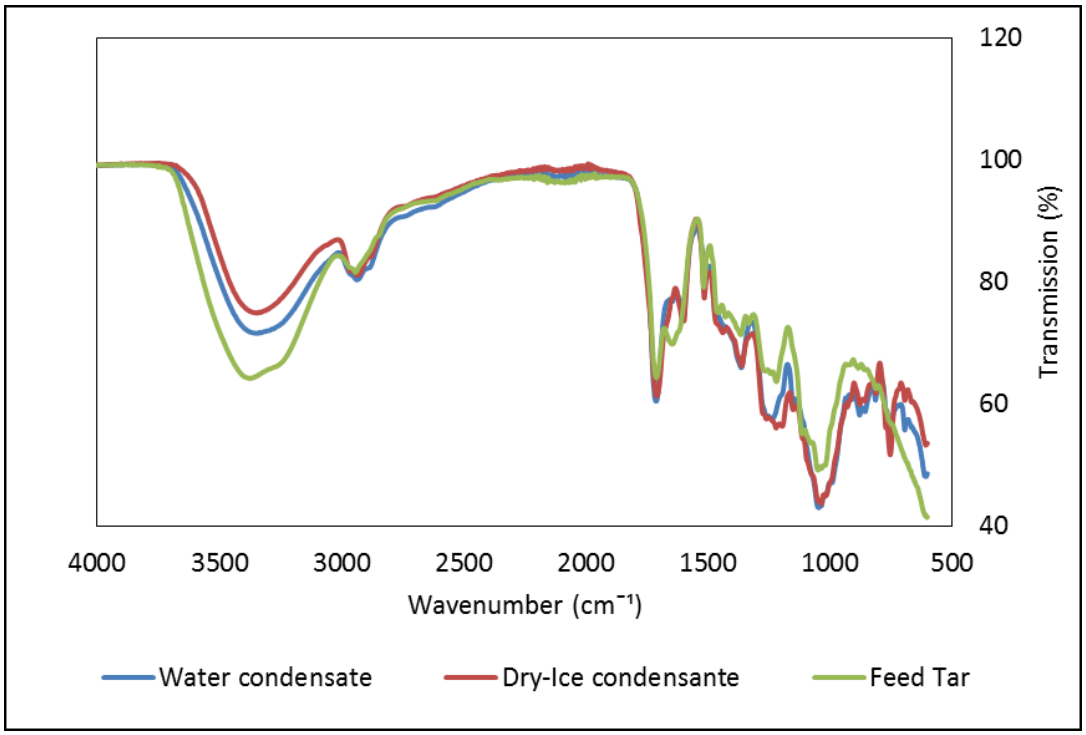


Figure 8:2: Liquids FTIR Transmission Spectra

8.2.3. Analysis of the Fresh Pt, Rh and Ni-catalyst

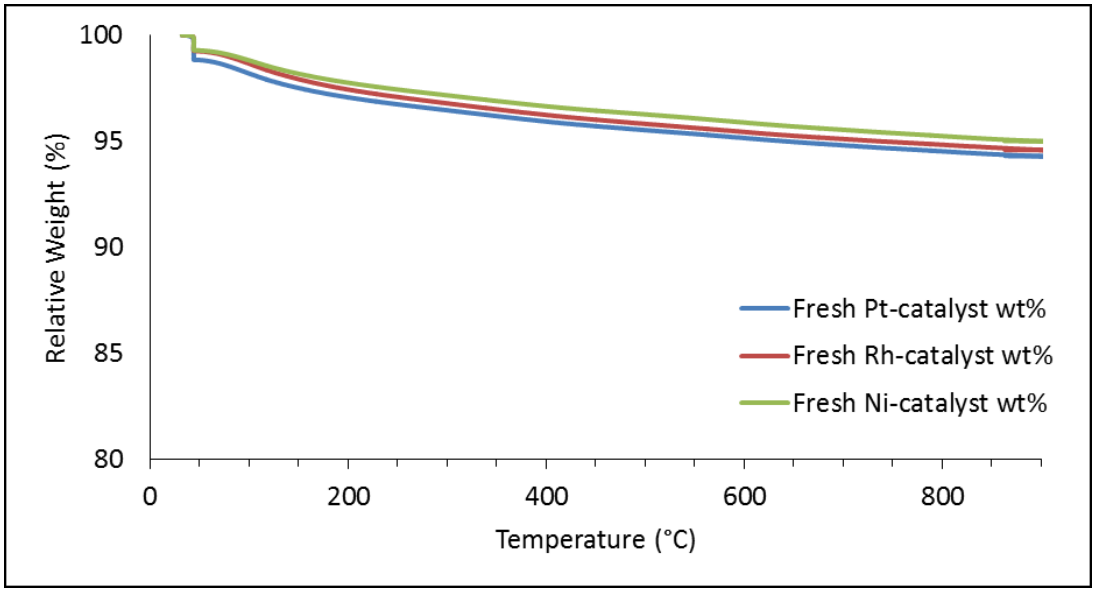


Figure 8:3: TGA for carbon decomposition from Fresh Pt-, Rh- and Ni-catalyst

The data presented in Figure 8:3 shows how the relative weight of fresh catalysts changed with temperature. One would expect this to be relatively constant after the loss of moisture quotient under 100 °C but this continued weight loss could be a result of change in the physical properties of catalyst. However, all three catalysts were investigated for their thermal stability and discovered to functionally remain stable even at 950 °C. The discussion of the results in this study uses 95% as a reference point for other thermogravimetric analysis of the spent catalyst to account for the weight loss in the actual catalyst.

The fresh catalyst was analysed using a Scanning Electron Microscopy (SEM) for both morphological study and detection of the elements' composition. Analysis of the fresh catalyst showed identical elements as specified in the materials section (section 3.1.1.2). The microscopic imaging of the fresh was used as a basis reference for the spent catalyst. Figure 8:4, Figure 8:5 and Figure 8:6 show the morphological imaging of the three fresh catalysts.

As specified in chapter 3, all catalysts have the same support but different active metal. BET analysis also showed that all catalyst had similar characteristics.

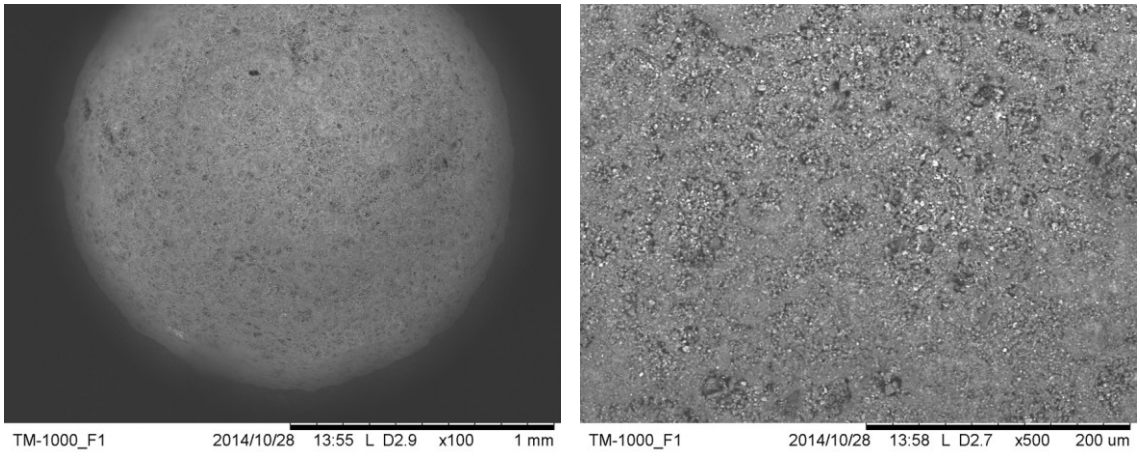


Figure 8:4: SEM Imaging of Fresh Pt-catalyst

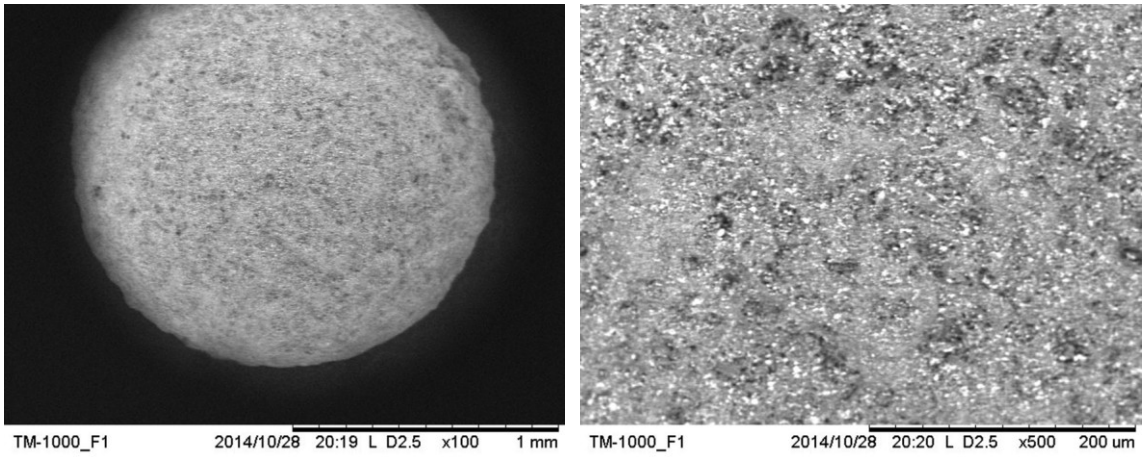


Figure 8:5: SEM Imaging of Fresh Rh-catalyst

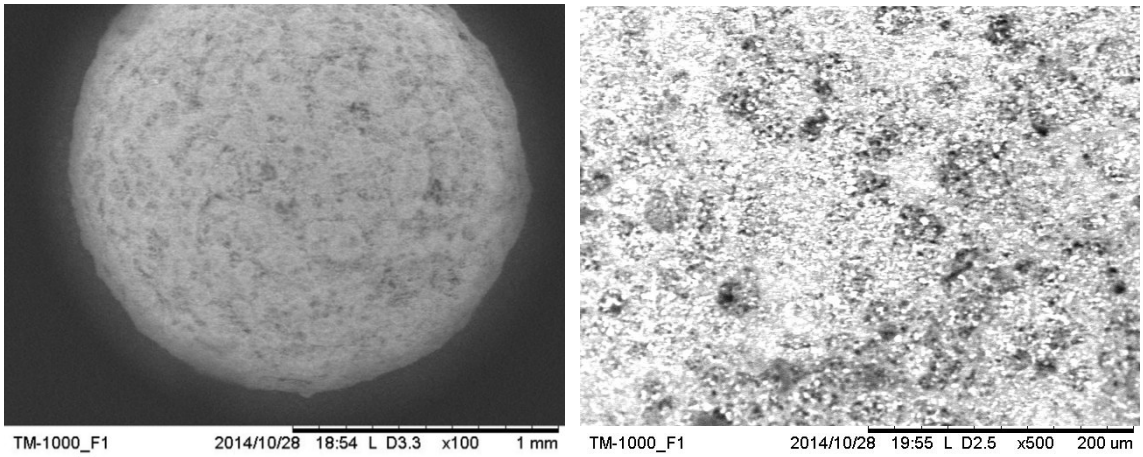


Figure 8:6: SEM Imaging of Fresh Ni-catalyst

8.2.4. Results Analysis of By-products from Model Compounds.

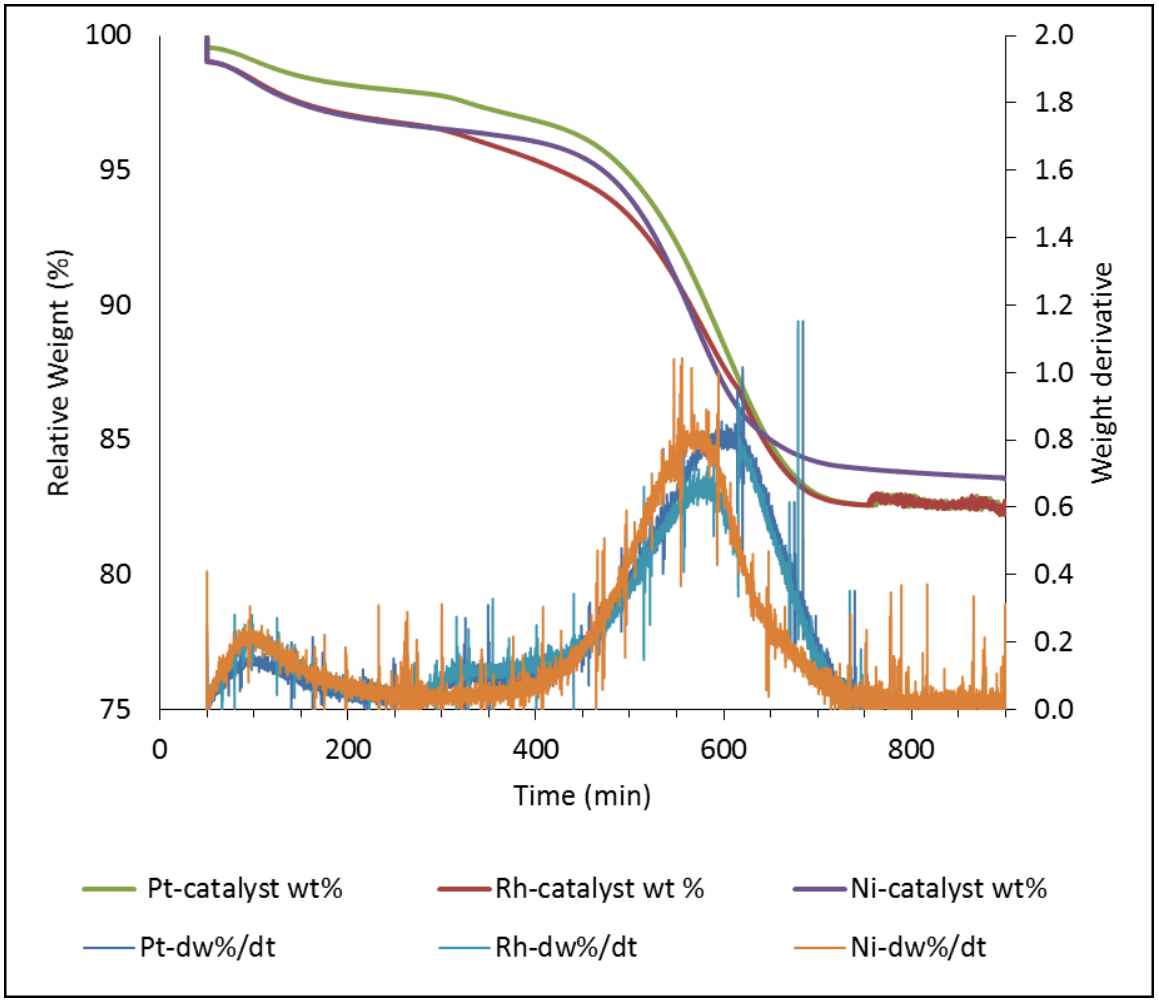


Figure 8:7: TGA for carbon decomposition from Spent Pt-, Rh- and Ni-catalyst in Model Compounds

Figure 8:7 indicates that above 200 °C, the catalyst samples start to drop in weight and at about 700 °C, the samples weights remain steadily constant. This analysis and considering the relative weight loss in the fresh catalyst denote that the amount of carbon deposits can be deduced as 12% (95%-82.5%). Since all three catalyst weight loss start and finish at the same weighting, it would suggest that the all contained the same amount of deposits after being used under the same conditions.

Figure 8:8, Figure 8:9 and Figure 8:10 show the catalyst activity in reforming the mixture of guaiacol and toluene. All three catalysts activity produced a steady gas formation all

the way through the entire period of the trial run. Among the three, Ni-catalyst formed a higher concentration of gases and its carbon conversion was relatively higher than Rh and Pt (Chapter 6).

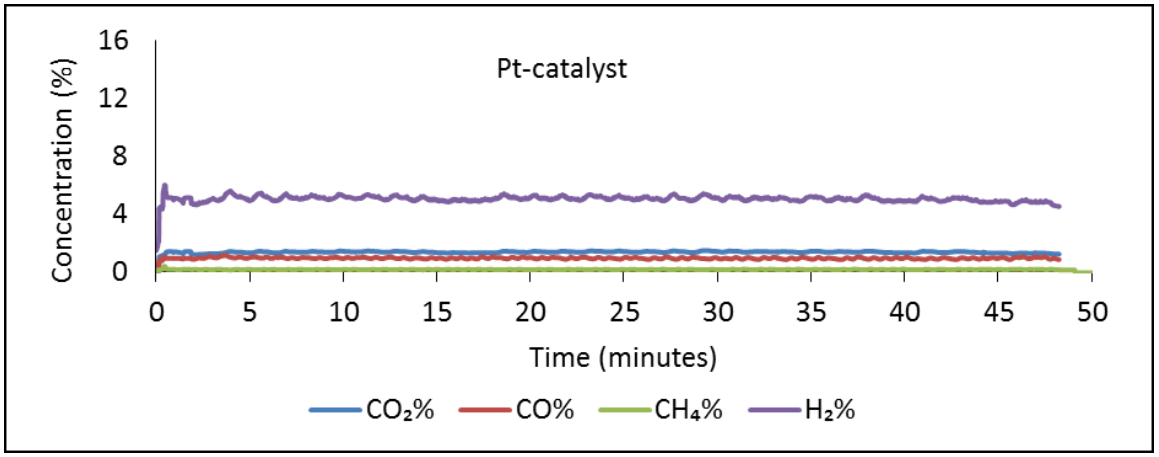


Figure 8:8: Gas Concentration in 0.209 L/min of N_2 under Pt-catalyst Activity at 750 °C from 50% Guaiacol / Toluene Reforming Reactions with Steam at an S/C of 3

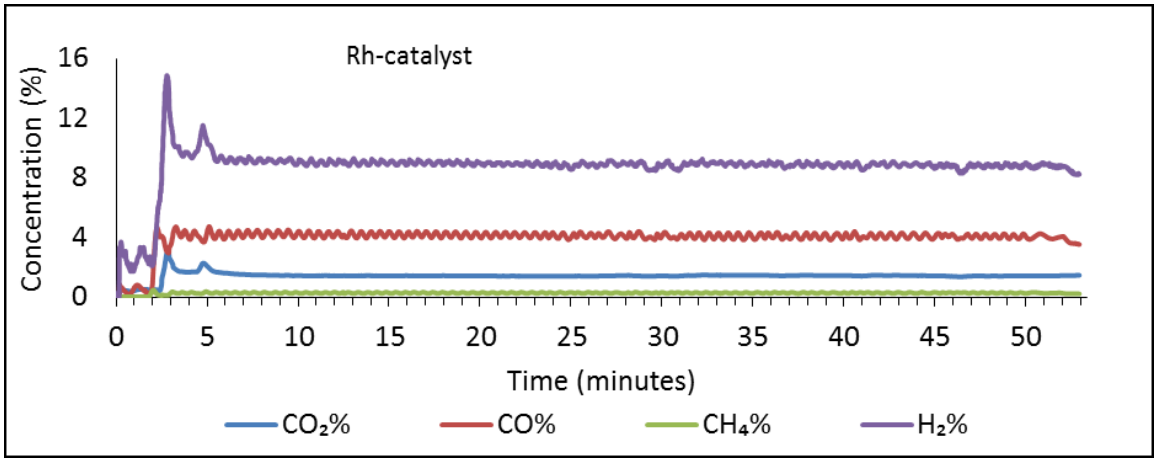


Figure 8:9: Gas Concentration in 0.209 L/min of N_2 under Rh-catalyst Activity at 750 °C from 50% Guaiacol / Toluene Reforming Reactions with Steam at an S/C of 3

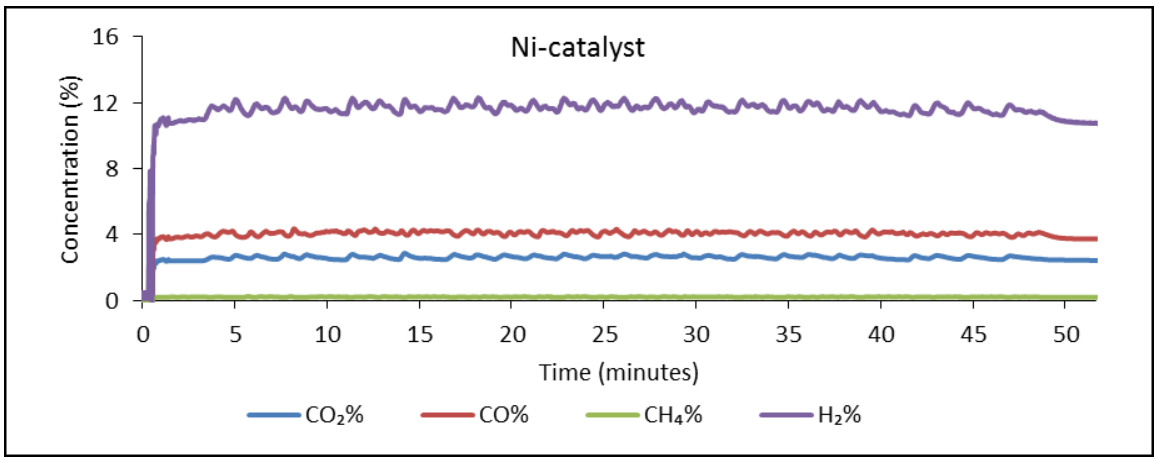


Figure 8:10: Gas Concentration in 0.209 L/min N_2 under Ni-catalyst Activity at 750 °C from 50% Guaiacol/Toluene Reforming Reactions with Steam at an S/C of 3

8.2.5. Results Analysis of Biomass Tar By-products when Using Pt-catalyst

After trial tests with module compounds, the catalyst activity was tested in a biomass environment and the results are compared. In order make comparative judgment, most of the tests with tar were performed at similar operating conditions as the model compounds, but at times with slight deviations were applied to assess the reactions dependence on the variables. The figures below illustrate the TGA, gas analysers and SEM results analysis.

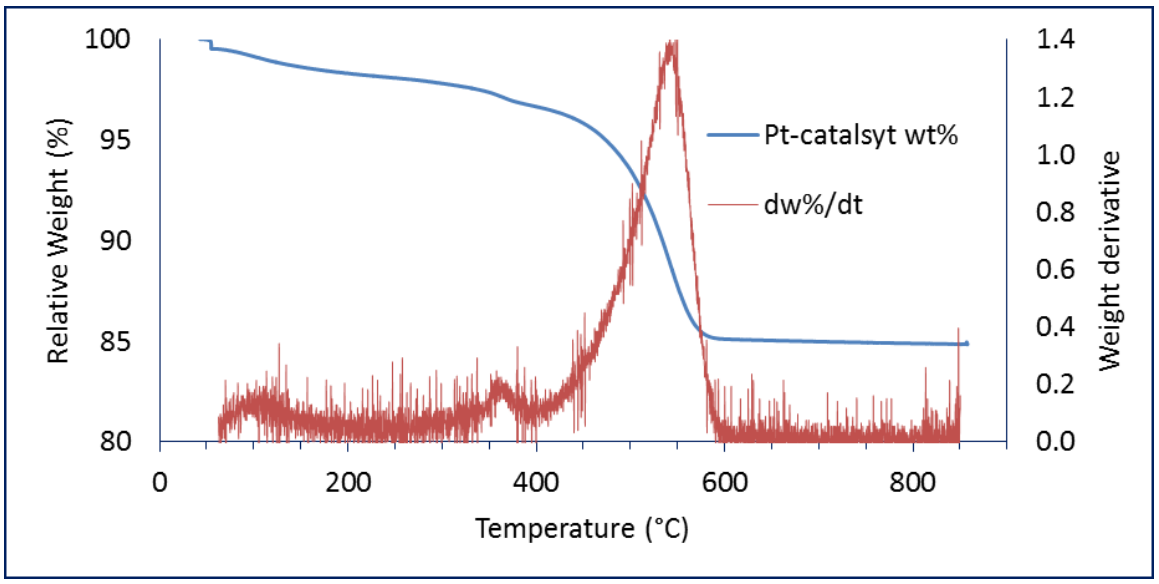


Figure 8:11: TGA for Carbon Decomposition from Spent Pt-Catalyst from Reactions of Biomass-Derived Tar at 750 °C and an S/C Of 3

Changing trial run steam to carbon ratio

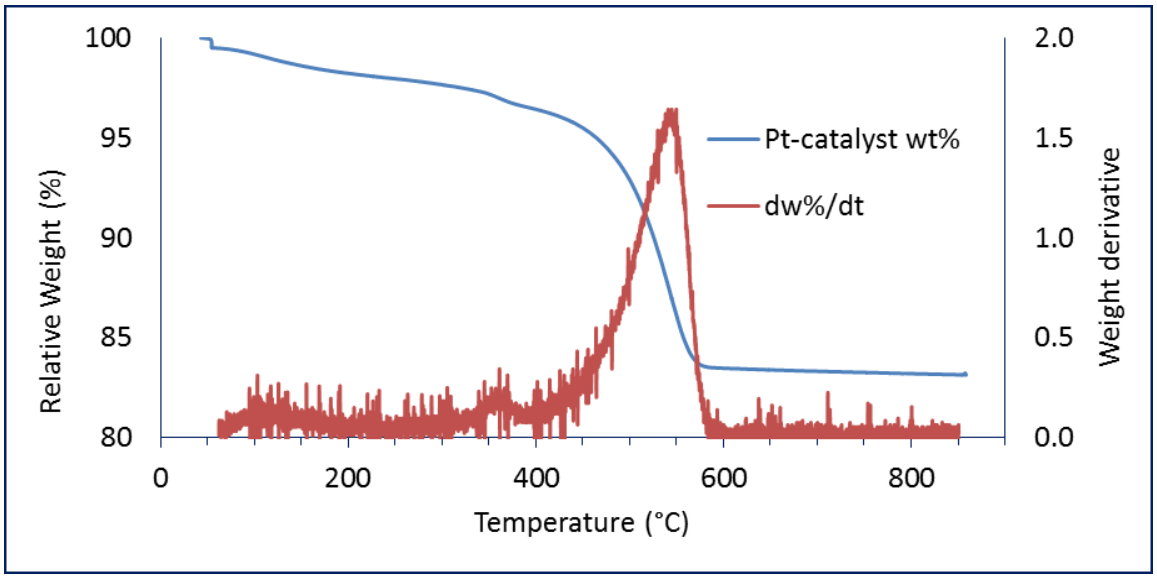


Figure 8:12: TGA for Carbon Decomposition from Spent Pt-Catalyst from Reactions of Biomass-Derived Tar at 750 °C and an S/C of 2

Figure 8:11 and Figure 8:12 show that the addition of steam reduced carbon formation on the catalyst. This trend supports the evidence of the gas fractions formation under the same catalyst. Carbon dioxide and hydrogen fractions increased in the products while carbon monoxide fractions decreased when steam was added. When each of relative weights loss in Figure 8:11 and Figure 8:12 is compared with those in Figure 8:7, the biomass-derived tar deposited less carbon content on the catalyst compared to that with the model compounds. The respective weight losses are 9% and 12% in and S/C of 3 (Figure 8:11) and an S/C of 2 (Figure 8:12).

Changing trial run temperature

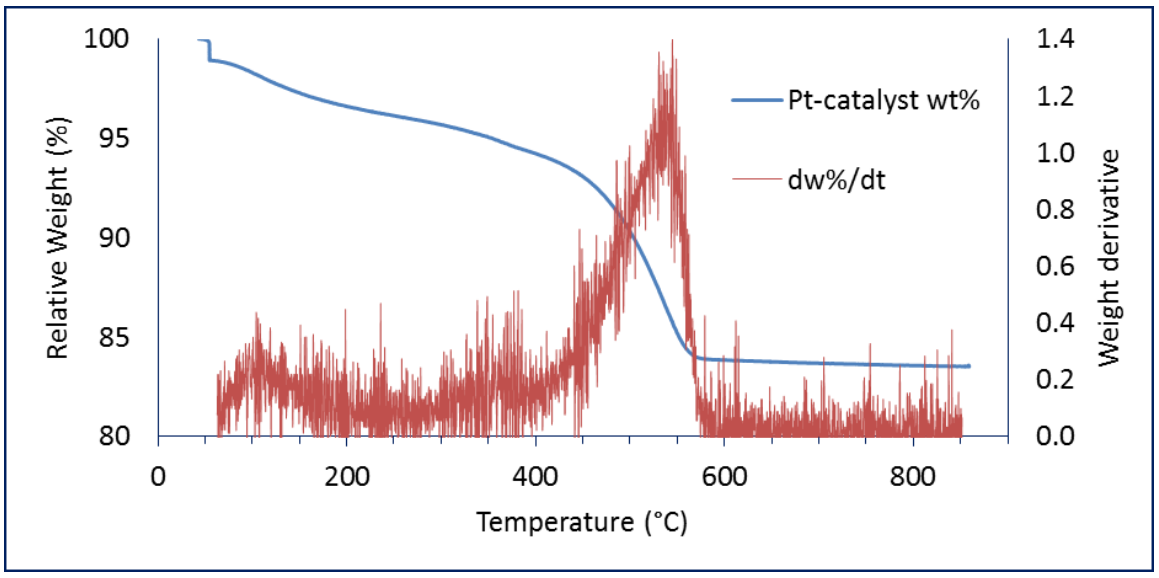


Figure 8:13: TGA for Carbon Decomposition from Spent Pt-Catalyst from Reactions of Biomass-Derived Tar at 700 °C and an S/C Of 3

Figure 8:13 shows carbon deposits at 700 °C. Comparing the results with those at 750 °C (Figure 8:11), carbon deposits increased at lower temperature. Similarly these features correlate well with the gas formation. With the exception of CH_4, each of the other gaseous fractions increased with increase in temperature and vice versa. Generally, this trend suggests carbon conversion is also dependent on the reaction temperature, similar does the carbon recovered from the traps (Chapter 5).

Effect of adding syngas

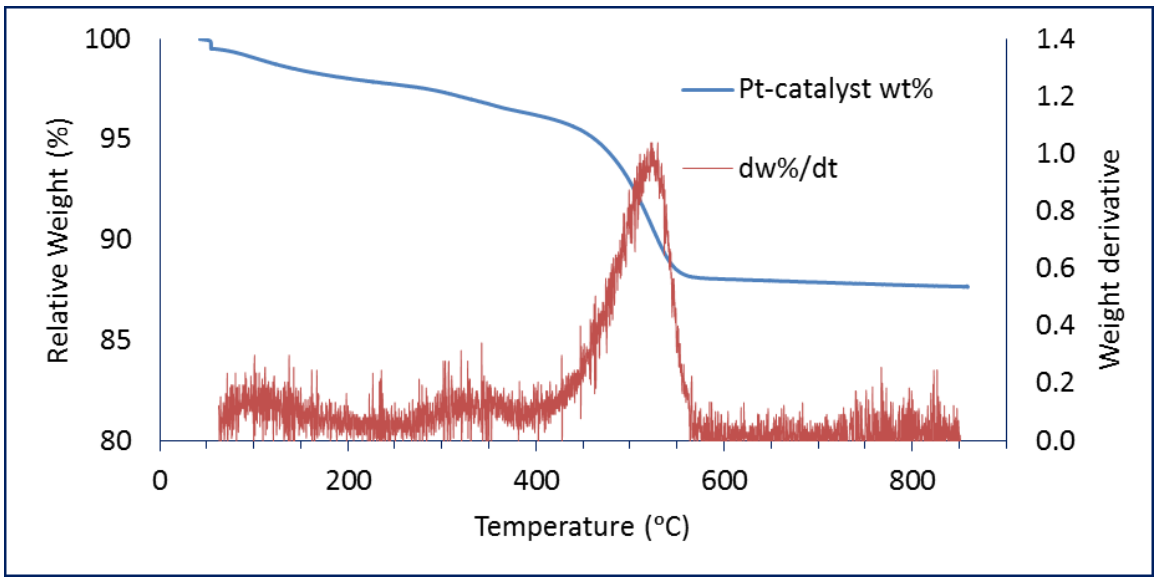


Figure 8:14: TGA for Carbon Decomposition from Spent Pt-Catalyst from Reactions of Biomass-Derived Tar at 750 °C and an S/C of 3 in Syngas Mixture

Figure 8:14 shows nearly 6.5% (minus 5% of thermal effect) relative carbon weight was deposited on the Pt-catalyst at these conditions. Comparing these results with those presented in Figure 8:11, it suggest that the addition of "this" hydrogen rich syngas reduces carbon deposits on the catalyst. Compiling data for the gas formation, liquid products and carbon conversion discussed in Chapter 5, there are more liquid products in the product stream and the carbon conversion is relatively at added syngas than just in N_2 at similar test conditions. This observation would suggest that adding such a syngas mixture reduces carbon deposition but does not necessary promote gas formation. Instead it possibly promotes the hydrogenation reactions, forming other tar compounds, hence the more carbonaceous liquids gathered in the trap.

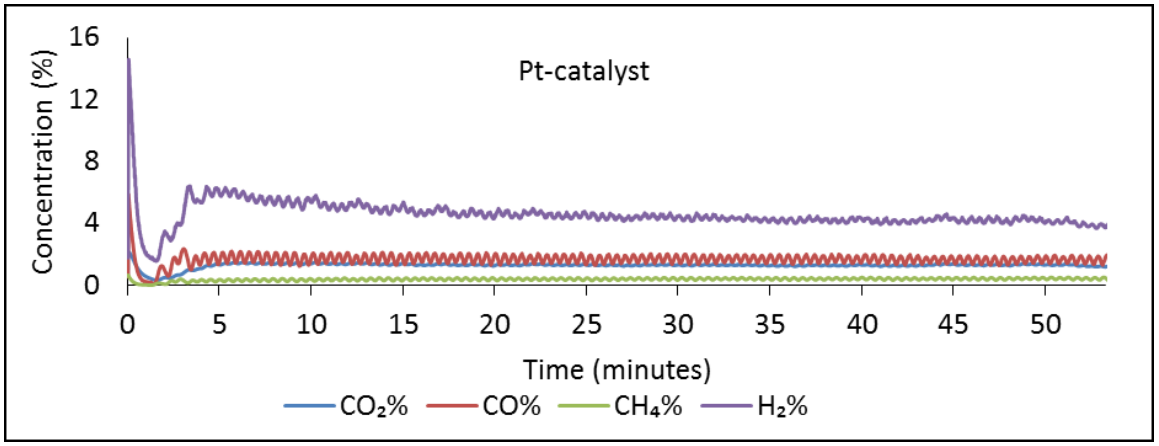


Figure 8:15: Gas Concentration in 0.209 L/min of N_2 under Pt-catalyst Activity at 750 °C from Biomass-derived Tar Reforming Reactions with Steam at an S/C of 3

Figure 8:16 shows the Rh-catalyst activity in tar conversion over the period of the test run. Across the period of the test, the figure shows the catalyst's rate of gas formation was consisted but to a small magnitude its activity in H_2 formation was progressively reducing. Comparing this data with the results from model compounds (Figure 8:8), the results suggest that Pt-catalyst delivers a higher carbon conversion and gas formation with tar than with model compounds, however, a better consistent activity is achievable with model compounds.

Effects of injecting tar directly into the bed

A trial run involving feeding tar directly into the catalyst bed was performed to investigate how the catalyst would behave. The trial test differs from the above run only that in this test the pre-conditioning chamber was removed.

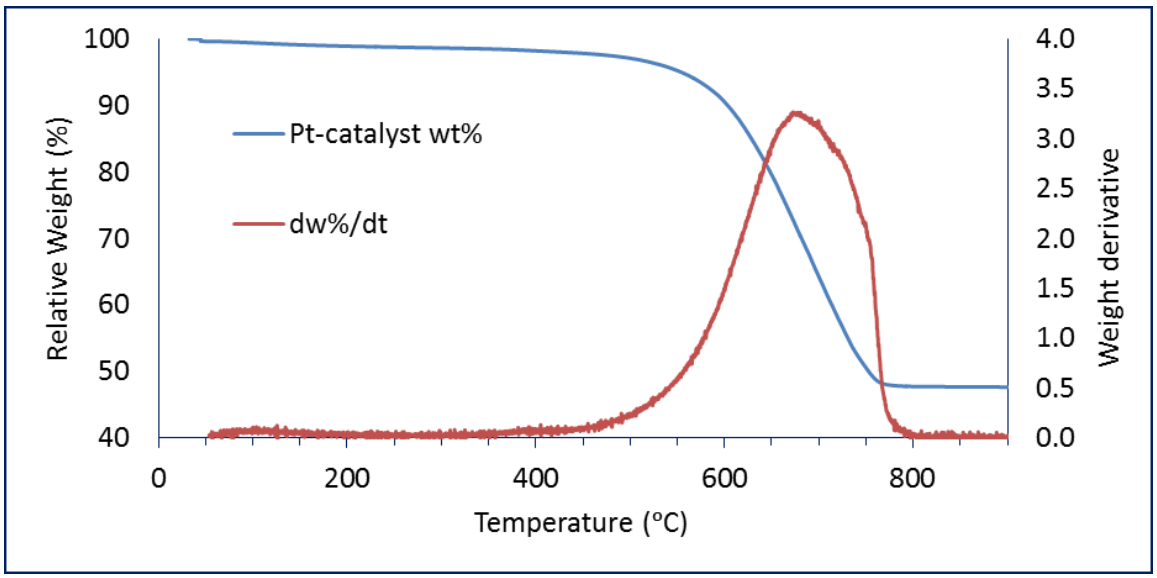


Figure 8:16: TGA for Carbon Decomposition from Spent Pt-Catalyst from Reactions of Biomass-Derived Tar at 900 °C and an S/C of 2 Direct Feed without Pre-conditioning

The results show that when tar was directly injected into the catalyst bed a larger deposition of carbon on the catalyst was formed. If compared with the carbon conversion in blank tests, the results show only a slight improvement in conversion was achieved. Considering the high temperature used, this test is not viable to employ in anyway. Figure 8:18 shows carbon deposition on the catalyst, which resulted into fouling. The difference between Figure 8:18 and Figure 8:17 show the importance of conditioning the feed before the bed.

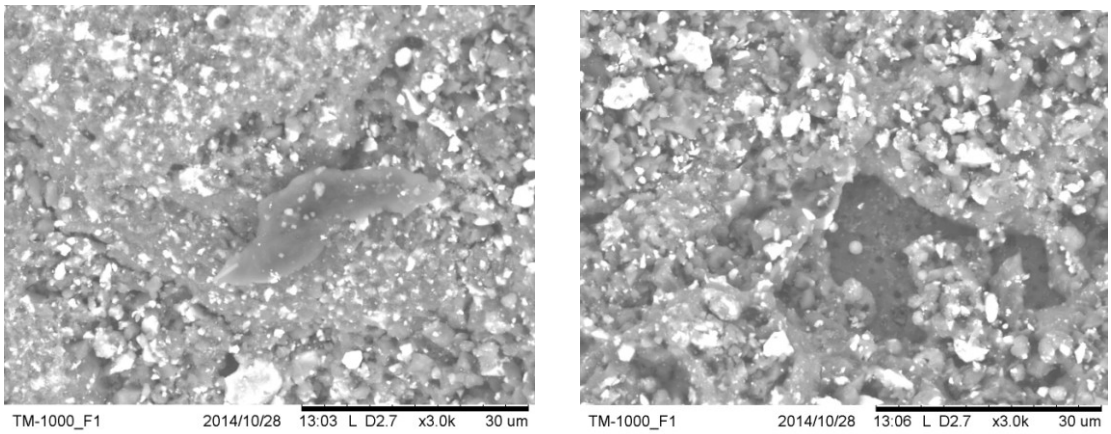


Figure 8:17: SEM Analysis Showing Carbon Deposition on Pt-catalysts at 750 °C, an S/C of 3

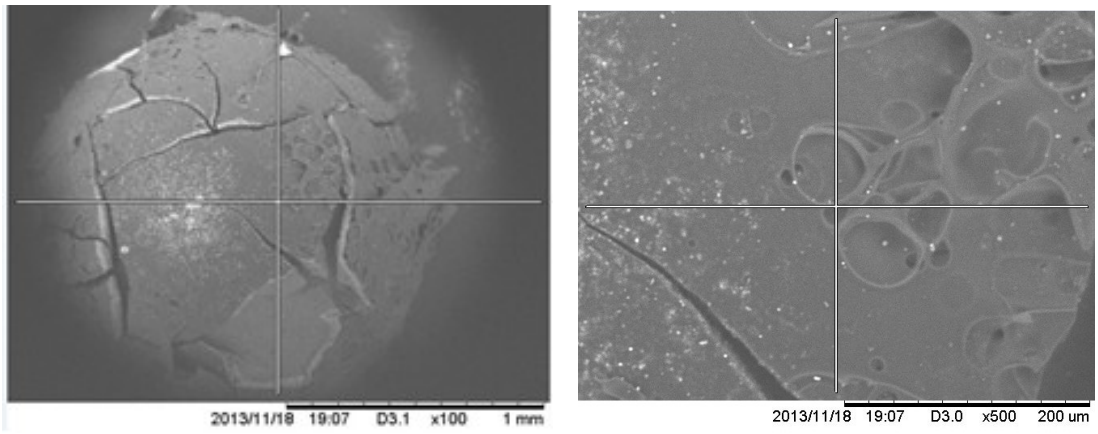


Figure 8:18: SEM Analysis Showing Fouling in Pt-catalysts at 900 °C and an S/C of 2 (without a preconditioning chamber)

8.2.6. Results Analysis of Biomass Tar By-products when Using Rh-catalyst

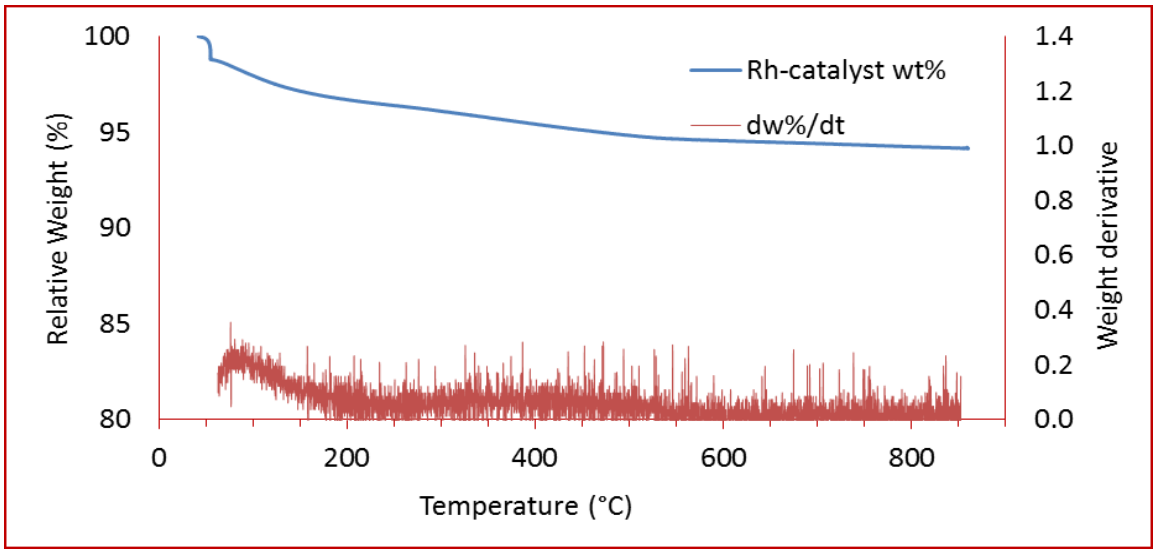


Figure 8:19: TGA for Carbon Decomposition from Spent Rh-Catalyst from Reactions of Biomass-Derived Tar at 750 °C and an S/C of 3

Figure 8:19 shows the relative weight of spent Rh-catalyst with temperature after. When deductions for the catalyst's thermal effect Figure 8:3 are considered, there are doubtfully no deposits measured. Cross linking this result with the catalyst activity in Figure 8:21, the Rh-catalyst activity remained consistently steadily and high in carbon conversion, suggesting it has a high resistance to coking, with supporting evidence from the SEM analysis (Figure 8:22).

Rh-catalyst's activity dependence on steam

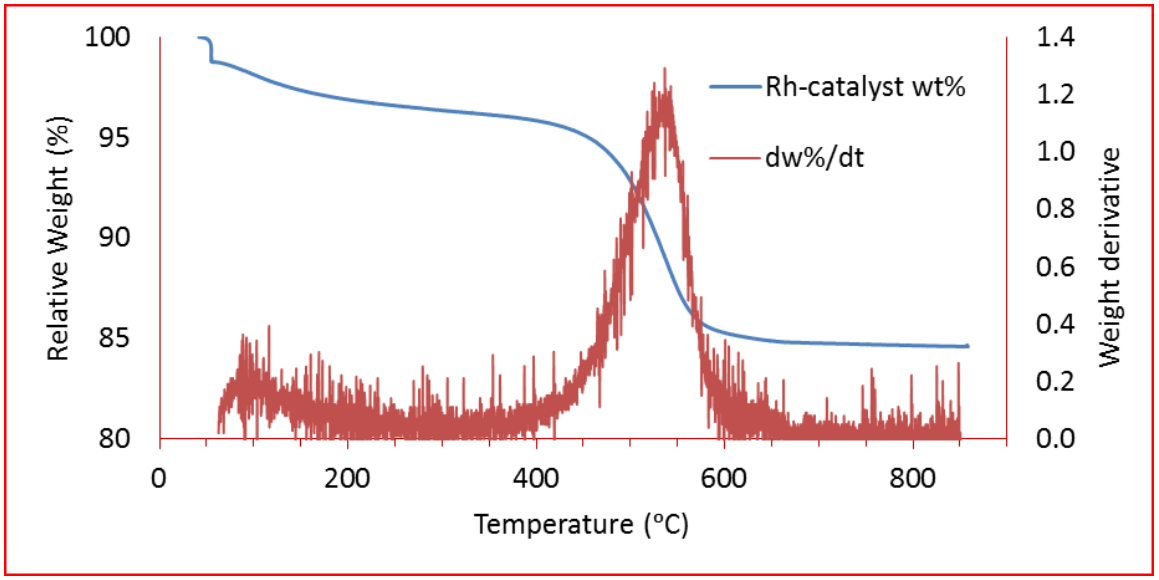


Figure 8:20: TGA for Carbon Decomposition from Spent Rh-Catalyst from Reactions of Biomass-Derived Tar at 750 °C and No Steam

Figure 8:20 shows that the Rh-catalyst coked in the absence of added steam. Nearly 10% of the catalyst was carbon deposits on the catalyst during the trial run. This shows that steam played a vital role in carbon reforming. In spite of the harsh conditions, Rh-catalyst still shows it has a somewhat high resistance to carbon deposits.

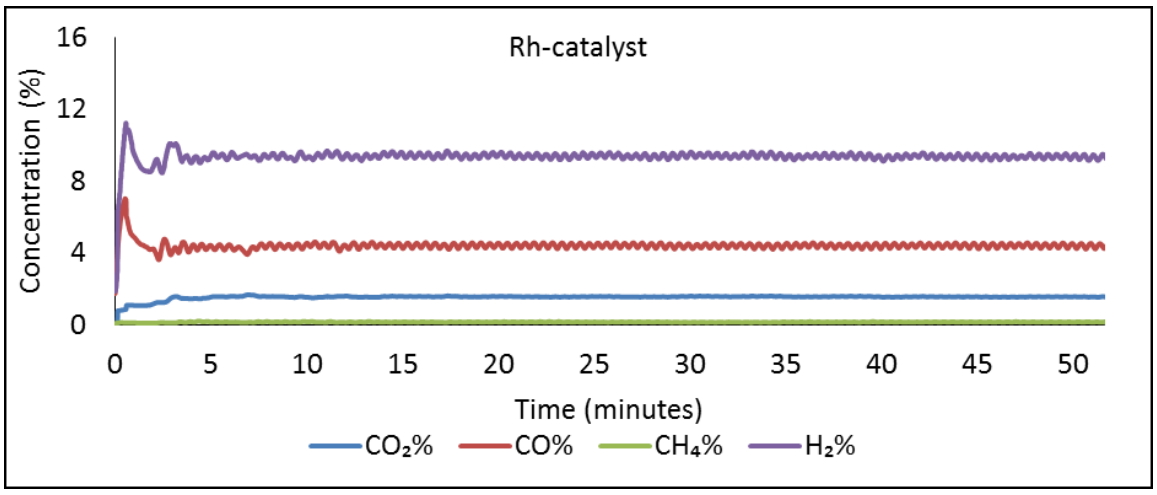


Figure 8:21: Gas Concentration in 0.209 L/min of N_2 under Rh-catalyst Activity at 750 °C from Biomass-derived Tar Reforming Reactions with Steam at an S/C of 3

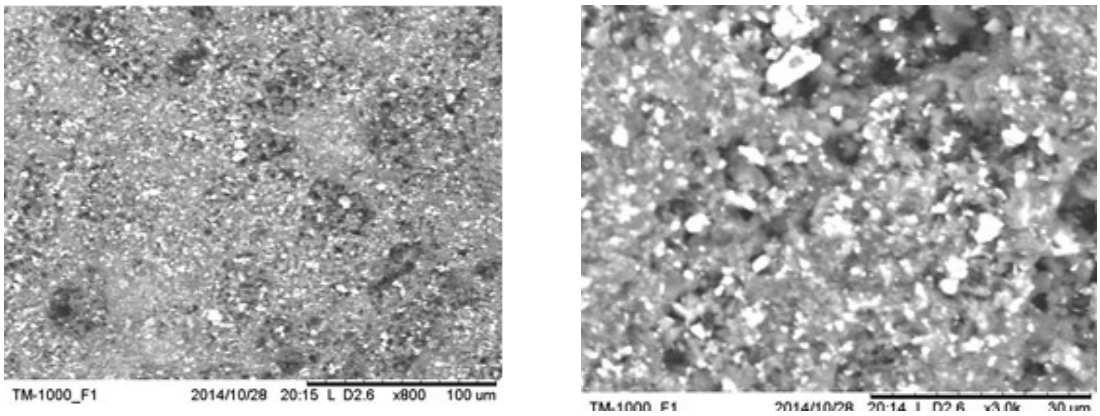


Figure 8:22: SEM Analysis for Recovered Rh-catalysts after Biomass-derived Tar Reforming Reactions with Steam at an S/C of 3 in 0.209 L/min N_2 at 750 °C.

8.2.7. Results Analysis of Biomass Tar By-products when Using Ni-catalyst

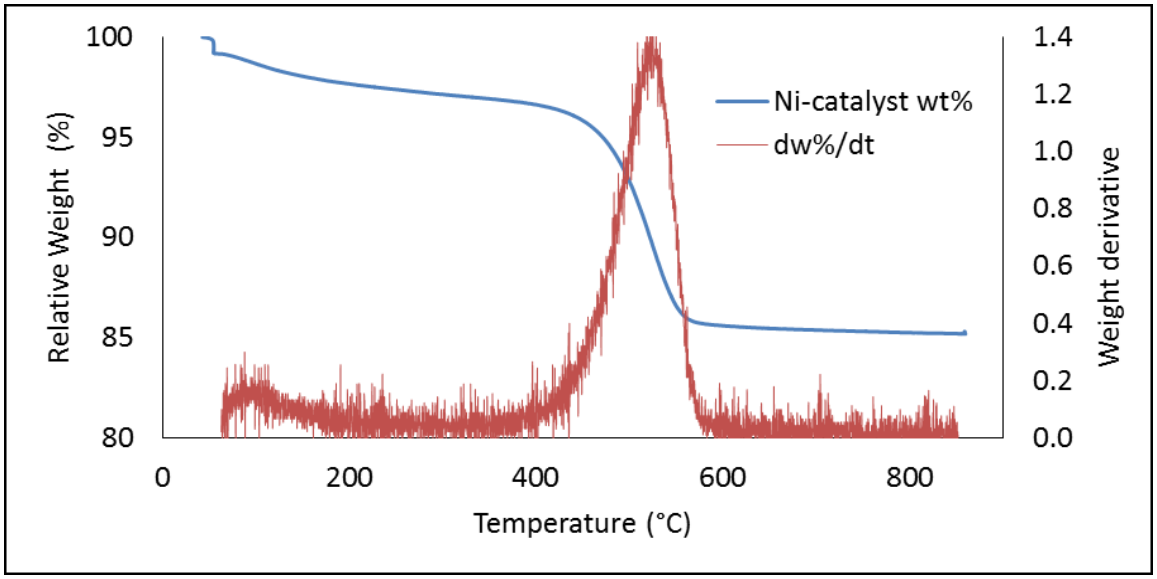


Figure 8:23: TGA for carbon decomposition from Spent Ni-catalyst from reactions of biomass-derived tar at 700 °C and an S/C of 3

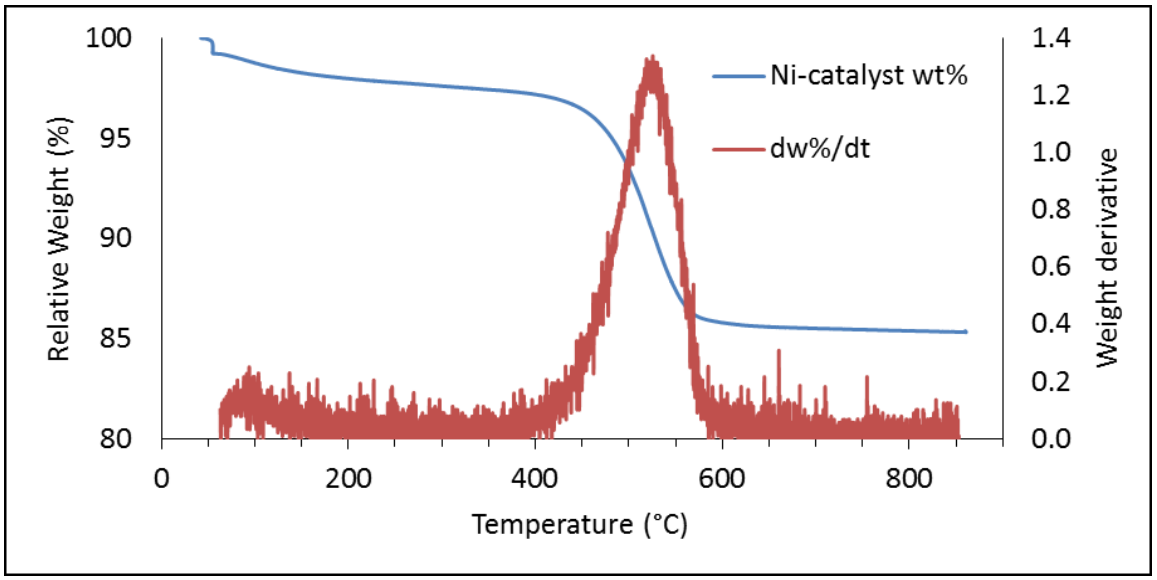


Figure 8:24: TGA for Carbon Decomposition from Spent Ni-Catalyst from Reactions of Biomass-Derived Tar at 750 °C and an S/C Of 3

In Figure 8:24 shows 9% (minus 5% thermal effect) weight loss from the Ni-catalyst. When compared with the Rh-catalyst, which almost has no carbon deposits detected, the Ni-catalyst cokes. With reference to gas fractions in Figure 8:25 and carbon

deposition on catalyst in Figure 8:26, the Ni-catalyst has a high activity but rapidly decays with a build-up of a carbon layer on its surface (Figure 8:26). Although in the initial 15 minutes of the reaction the Ni-catalyst is very active, its rate of deactivation raises concerns over its durability and resistance to deactivation. While performing some of the Ni-catalyst experiments; after 30 minutes into the trial tests the reactor was irregularly observed to induce a back pressure build-up in the lines. This implied that the bed had been blocked and visual checks at the end proved evidence of carbon build-up on top of the catalyst bed.

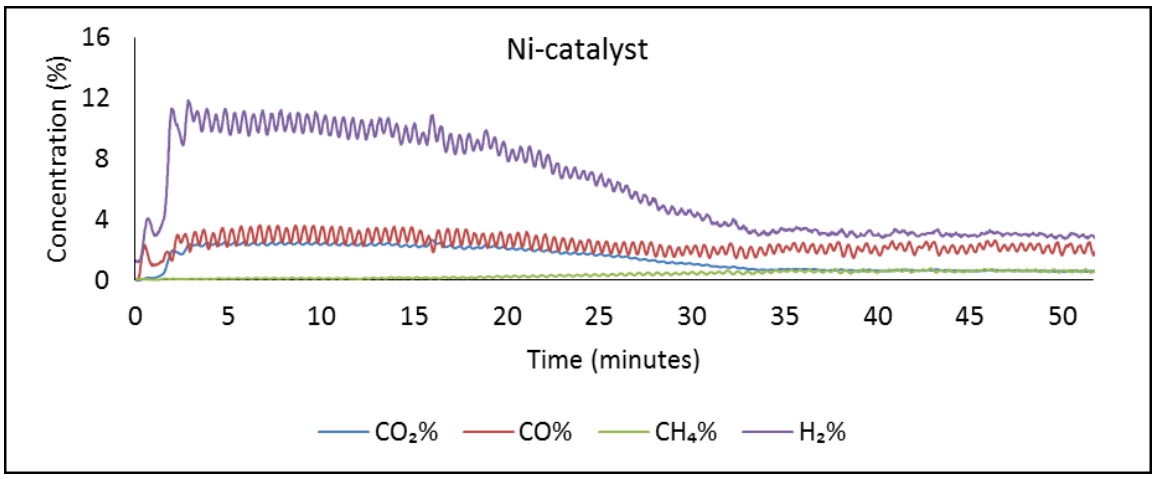
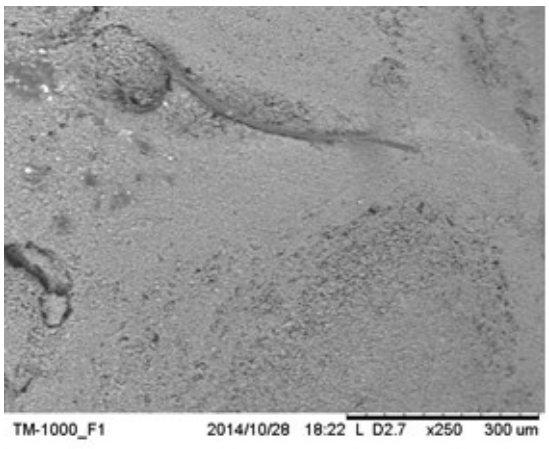


Figure 8:25: Gas formation in 0.209 L/min N_2 at 750 °C with an S/C of 3 with Ni-catalyst



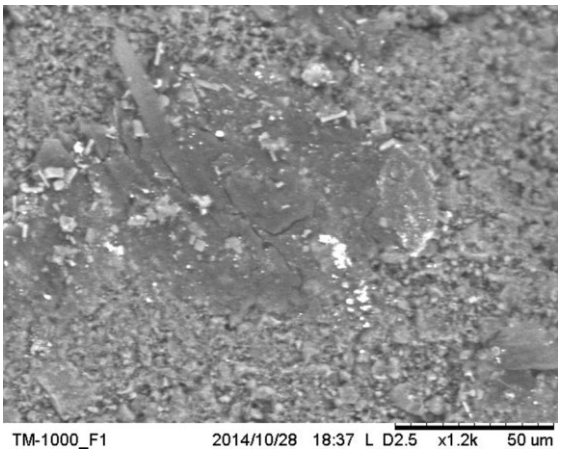


Figure 8:26: SEM Analysis Showing Carbon growth on Ni-catalysts at 750 °C, with an S/C of 3

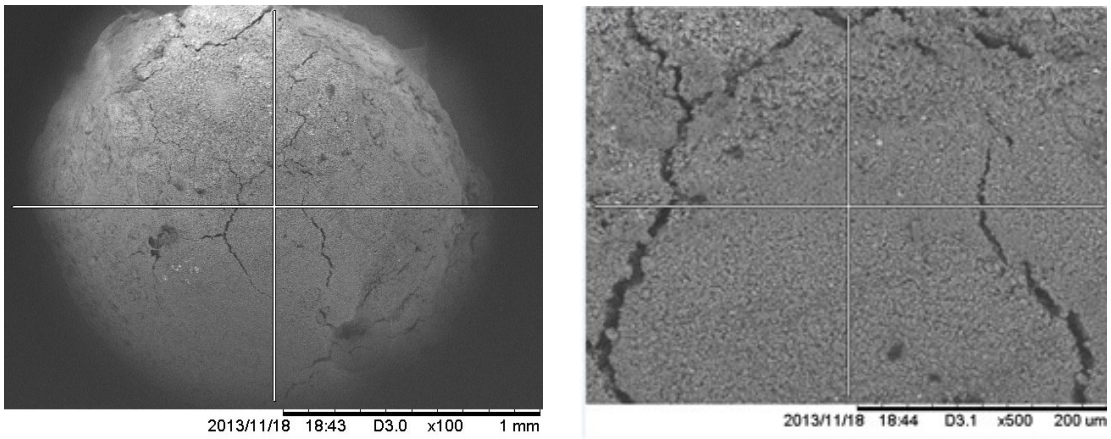


Figure 8:27: SEM Analysis Showing Fouling in Pt-catalysts at 900 °C and an S/C of 2 (without a preconditioning chamber)

With the exception of the Ni-catalyst performance in steam reforming of model compounds, which demonstrated to be active and resistant to deactivation, when the Ni-catalyst was used for steam reforming of biomass tar it easily deactivated. This observation is similar what Effendi et al. [72] reported when reforming CH_4-CO_2 in a fixed bed and fluidised bed reactor. Effendi demonstrated and concluded that carbon deposits mainly contained two C-O and C-C bond species.

8.2.8. Carbon conversion to Gas in a Quartz Reactor at 750 °C with Steam at an S/C of 3

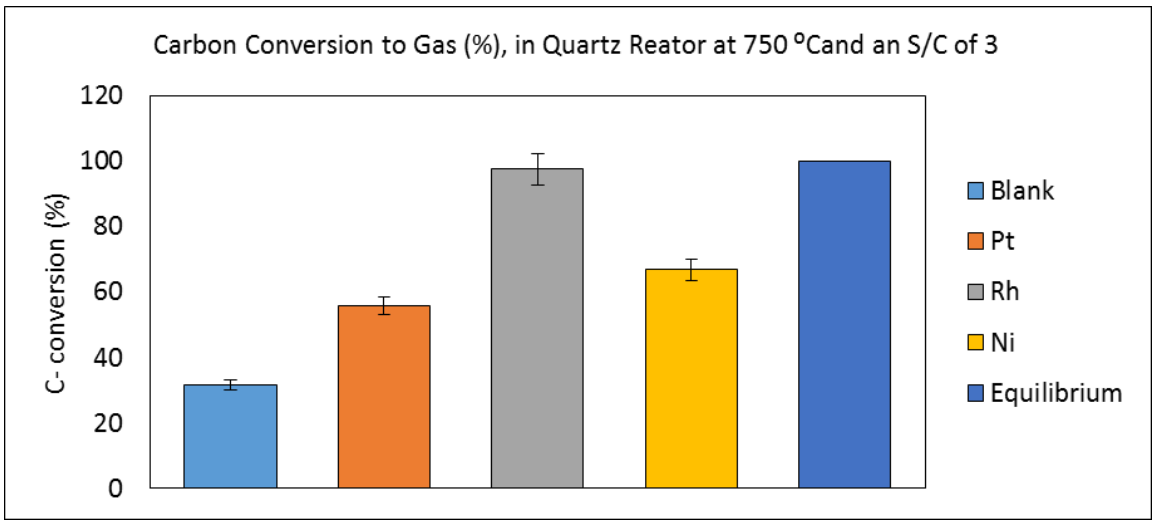


Figure 8:28: Mass Conversion of Carbon to Gas at 750 °C from Reforming 100 g/Nm³ of Tar with Steam at an S/C of 3

Figure 8:28 shows the overall carbon yield in the product stream for the different bed catalyst including the analysis from the blank and simulation. The tar sample fed in the reaction for each reaction contained 0.52g of carbon. Of the feed carbon, 32%, 57%, 97% and 67% was converted to gas for the blank, Pt-catalyst, Rh-catalyst and Ni-catalyst reactions respectively.

Comparing the C-conversions with the equilibrium results which show a full C-conversion, the Rh-catalyst nearly achieved the equilibrium conversion, with 97% C-conversion. The Ni-catalyst was good at conversion but its activity was observed to drop rapidly after the initial 30 minutes into the test. Pt-catalyst on another had converted less carbon at these conditions but its activity was observed to stay steady throughout the run time. All three catalysts' carbon conversion to gas is evident distinguishable when compared with the blank, which only converted 32% of the carbon in the feed to gas.

8.3. Raman Analysis

A sample of a catalyst was selected at random to analyse the nature of carbon deposits. All representative samples were chosen from trial runs operated in 0.209 L/min N_2, with an S/C of 3 at 750 °C. For each sample there was only a small amount of carbon for analysis, so, for some analysis such as with Rh, a small crack off the catalyst was sampled. During the analysis, the sample was compressed in a small window and analysed at atmospheric conditions.

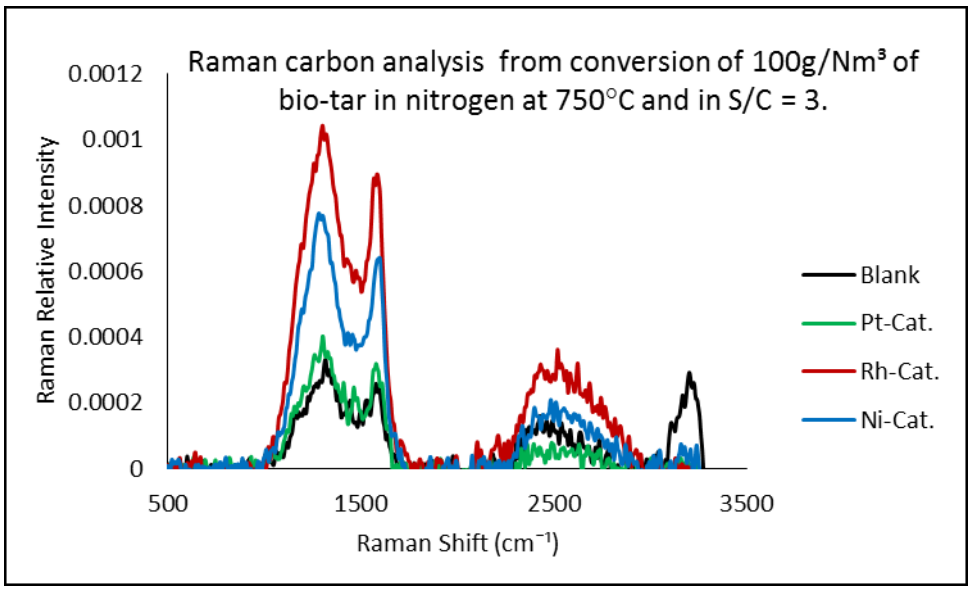


Figure 8:29: Raman Analysis for Carbon Deposited on the Individual Catalyst Recovered from the Reactions of Biomass-Derived Tar Reforming with Steam of an S/C of 3 in 0.209 L/min N2 at 750 °C

The carbon spectrum from Raman analysis shows that for all carbon peaks appear in the same shifts. The intensity of each peak in this case may not give a realistic interpretation of carbon content but the peaks correlate with the nature of carbon. In this case the carbon from all catalysts was graphite in nature. The most eluded peaks appear at about 1500 cm^{-1}, which represents a G-band nature of carbon which also can appear at around 2500 cm^{-1}, commonly referred to as the Graphite carbon.

8.4. FTIR analysis

FTIR analysis was performed was performed to understand the functional groups within the feed material and the products. The two were compared to indentify the change in chemistry of material after being exposed to operational conditions.

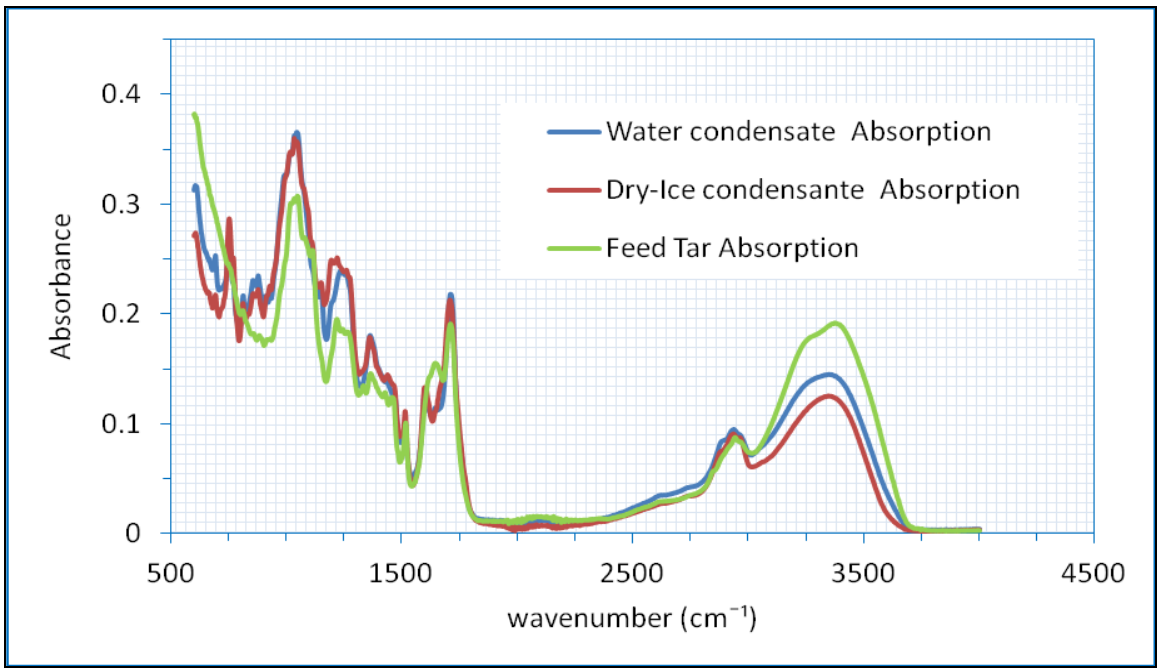


Figure 8:30: FTIR Spectra of Tar Analysis from Feedstock and By-Products Collected In the Identified Condensate Traps

Qualitative analysis of the results showed that the chemical composition of tar changed mostly among the compounds below a wavenumber of 2000 cm^{-1}. When the spectra peaks were referenced to the standards for infrared absorption bands to determine the functional groups, it was evident that when the ratio of steam to carbon ration was increased, the compounds contained more oxygenated compounds. This was particularly more pronounced in samples from tests with steam to carbon ratios of 3.5 and above. Figure 8.30 above for example illustrates a strong peak between 1000 – 1300 cm-1, which reflects the presence of esters or ethers or alcohols, a strong broad peak between 3230 – 3550 cm^{-1}, which shows a likely presence of phenols, alcohols or hydrogen bond.

9. CONCLUSIONS.

Literature studies show that the conversion of waste material to syngas has gained a particular interest to the energy market but even so, the conversion efficiency of carbonaceous material to gaseous products is highly demanded for in the refinery industry. The conversion of carbonaceous materials to gases is essential to refineries so that high efficient production can be achieved and the energy demands can be met at little cost and under safe production measures. Gases can easily be transported around and can be synthesised into a target product.

The syngas composition leaving different types of gasifiers can be categorised into three groups; the major constituents including H_2O and permanent gases H_2, CO_2 and CO, a rage of tar compounds, contaminants such as sulphur and the heavy metal compounds that come from ash. Hence the main barrier to efficient syngas production is gas cleaning which requires removing tar and heavy metals in a more production effective means.

Tar was defined as a complex mixture of condensable hydrocarbons, and commonly a by-product from gasification or pyrolysis of biomass, coal and other waste matter. It can contain compounds with one to several carbon rings and traces of: O, N, Cl and S. It can be categorised into primary, secondary and tertiary tars and classified as: GC-undetectable, heterocyclic, light and heavy PAH compounds. The majority of biomass or coal originated tars are benzene, toluene and naphthalene.

Mostly the operational factors including temperature, gasifier design, pressure, residence time and gasifying agents influence the nature and amount of tar products. The temperature distinctly influences the heating rate, and higher heating rates result in decrease of tar and CO_2, and increase of H_2 and CO contents. Tars are believed to form between 200 ^{o}C to 1100 ^{o}C. At increasing temperature primary tars crack first followed on by the secondary and then tertiary. The entrained and downdraft gasifiers are thought to be the most effective gasifiers. On average, downdraft gasifiers have an output of < 1 g/Nm^3 tar and a typical gas product of 15% H_2, 24% CO, 11% CO_2, 2% CH_4

and 48% N_2 on dry basis. Operating pressures < 10 bars are more suitable since high pressures result in high PAH concentrations in products, and a conversion shift to higher temperatures. Among the possible gasifying agents, steam is thought to influence the production of gas with a relatively high calorific heating value (i.e. higher H_2 and CO content), oxygen would produce a much higher calorific gas but also it is suggested that oxygen should be avoided in storage tanks where it can react with hydrocarbon radicals in the bulk hydrocarbons to produce peroxy radicals which propagate free-radical polymerisation reaction that subsequently lead to fouling. Air is the other gasifying agent, although it is considered to dilute the gas with nitrogen and with potential to form NOx at temperatures. The NOx compounds can react with ammonia to form NOx ammonium salts or with dienes to form NOx gums. These two NOx products are known to be explosive when warmed up if no action is taken to remove them.

For tar reduction, generally in the interest of reducing costs during tar cracking, catalysts are preferable over higher temperatures. The catalyst so far used can be applied either in the gasifier matter (primary catalyst) or in a separate reactor as secondary catalysts. Secondary catalysts are preferable over the primary ones because it is hard to recover the primary catalysts. Among the catalysts explored, the ones containing Co, Ni and Rh are thought to have a better performance but commonly, Ni-based catalysts are mostly utilised due to nickel's sufficient performance, abundance and low cost. Carbon formation on Ni-based catalysts can be minimised using alkali promoters such as CaO, MgO and K_2O.

Contaminants:

Tar formation is mostly governed by complex mechanisms that do not reach the state of thermodynamic equilibrium while other compounds are a result of thermodynamics. There have been various attempts to eliminate tar from syngas among which very high temperatures have been used, for example using a plasma arc at 1200 – 6000 ^{o}C, using catalysts and modulating the various operating parameters: - steam content, oxygen content, and residence time. Most of these attempts are extremely costly and possess very high operational challenges.

This study focused on tar destruction and maximisation of syngas formation at reduced risk operations and at a rational production cost. To tackle the challenges that stumble upon the process of tar destruction, this study investigated some of the measures already under taken but also inventively investigated the use of a newly innovated catalyst. The catalyst was developed at Johnson Matthey plc (a world leading catalyst industry) and designed to functionally improve the conversion of tar to permanent gases. In order to examine and produce sufficient evidence that verifies the performance of theses catalysts, a well-structured and broadened testing approach was undertaken, involving operations at various temperatures, steam-to-carbon ratios, reaction environment and residence time, in a well refined reactor design. The results from each set of tests are compared with equilibrium model results to gather the effectiveness and closeness of the catalyst functionality to equilibrium.

Sulphur-based contaminants are often introduced from the feedstock. During reactions, most sulphur species are converted into hydrogen sulphide (H_2S), an acid that can cause corrosion problems in used wall material and poisoning of the catalyst. For instance, for H_2S is in contact with iron in the walls, iron corrosion would occur leading to a formation of iron sulphides. Literature shows that sodium hydroxide (NaOH) has been used to remove sufficient amounts of H_2S in a process that forms sodium hydrosulphide (NaHS). The NaHS is removed from the process and purged into a wastewater treatment.

Heavy metal contaminants are also reported to be of a serious concern of which arsenic and mercury are the considered to be the most prominent. In literature, these metals are heavily linked to the poisoning of the catalyst and pose serious health concerns if discharged to the environment. At high temperatures, the arsenic species crack and combine with alkyl radicals to form heavy organometallic compounds and arsine (AsH3).

Effect of adding silicon carbide and a preconditioning zone: It was identified that during feeding high-molecular compounds (including Fulvenes which often entangle in fouling) accumulate and deposit onto the internals for the lines through radical polymerisation. This caused fouling and plugging issues which decreased the process

efficiency and created handling issues at the feed point. As one of the most critical modifications, the addition of the preconditioning zone resolved one of the most challenging physical features when dealing with tar in heated streams. The preconditioning chamber incorporated a critical study of the suitable feed condition and required the addition of SiC as a good heat transfer medium which, together with a choice of 350 ^{o}C heating temperature, facilitated the vaporisation and flow of tar through the reactor. Otherwise without this in place, it was observed that most of the tar caused fouling and carbonisation along the feed line and hindered advances with the reaction studies. SiC was ideal for this application because of its properties which would benefit in high temperature stability, effectiveness in heat transfer and ability to improve thermal heat tolerance.

Effect of modifying the reactor internal wall from incoloy to quartz: To prevent contamination of the bed activity, the inside wall of the reactor was modified from an Incoloy to a quartz. This amendment eliminated the activity of the Incoloy material from influencing the reaction pathway of the reactants. In fact, the reactor wall effect was identified when comparing the blank experimental results to those predicted in the equilibrium models. To elaborate on this development, the equilibrium model predictions do not show any methane formed at temperatures above 600 ^{o}C. The same argument is reported in most gasification literature and if otherwise only a small amount of methane would prevail at high temperatures. However, from the experimental tests in the blank reactor a significant amount of methane was observed. By principle, the reactions in the blank test were particularly driven by temperature and the compounds in the products should reflect that predicted in thermodynamic models. Depending on the process conditions, the equilibrium state was not reached during the blank experiments and this was reflected by the overall gas volumetric composition produced. When the temperature was increased, the overall gas volumetric composition increased, and simultaneously the amount of tar in the product stream decreased. This behaviour is similar to what is reported in literature [15].

On translating conclusions from equilibrium modelling, literature survey and knowing that incoloy contains a distinctive amount of Ni, this would justify the basis of the CH_4 formation in an Incoloy reactor. It is understood that CH_4 would have formed primarily from branched chains on the tar compounds or from the methanation reactions. With Ni present in the incoloy, this would be problematic to determine the functionality of catalyst in an Incoloy reactor. Consequently, a quartz liner was introduced and the results show that this modification successfully solved the problem. The role of the quartz tube was to prevent the Incoloy material from participating in the reactions. In fact, the results show that with nickel catalysts, there were distinctive traces of methane present compared to the compounds formed with platinum and rhodium, where there was noticeably no methane formed. This could be thought that the rhodium and platinum catalysts were able to reform methane but Ni did not and possibly Ni boosted the formation of CH_4.

Connectively, the installation of a quartz tube aligned with the prevention of corrosion in the reactor. In previous studies a 316 stainless still had been used for similar tests but due to the nature of the operating conditions, corrosion could have been a likely problem to face. In such scenario faced by corrosion, the reactor would lose its material strength, or develop pit holes and ultimately cause safety risks. A choice of using incoloy was of more advantage compared to stainless steel but equally incoloy had previously shown signs of rusting, which directly would jeopardise the intelligence of the reactor design and the integrity or quality of the work investigated. By creatively installing a quartz tube, such issues were eliminated and fouling at the inlet section and collation in the reactor. In addition, the reactor was continuously monitored for maintenance.

Effect of using dry ice as a cooling medium instead of using liquid nitrogen: Dry-ice temperature is around -78.5 ^{o}C while that of liquid nitrogen is -196 ^{o}C. Among the gaseous products of interest to measure were CO, CO_2, H_2 and CH_4 with properties: CO melts at -205 ^{o}C and boils at -191.5 ^{o}C, CO_2 melts at -56.5 ^{o}C and sublimes at -78.45 ^{o}C, H_2 melts at -259 ^{o}C and boils at -252.9 ^{o}C while CH_4 melts at -182.5 ^{o}C and boils at -161.5 ^{o}C [78], it is clear that CO_2 would be condensed in the condensate traps when liquid

nitrogen was used as a cooling agent. Experimentations showed that CO_2 condensed and froze in the line which eventually restricted gas flow and eventually blocked the pipe line. For this reason, dry-ice was a found to be effective and suitable material to use for gas cooling.

The effect of temperature: The catalysed and non-catalysed reactions were performed at atmospheric pressure in a quartz plug reactor at temperatures between 700, 750, 850, 900 and 950 °C to demonstrate the effect of temperature. The increase of temperature in all experiments, as predicted from literature and thermodynamic modelling, led to high gas yields. Simultaneously, the amounts of liquids thought to be formed due to further cracking and enhanced reactions with the gasifying medium were reduced. Taking other variables in account, it is observed that increase in temperature increased the overall gas yield, which could be due to increased steam reforming and cracking of tar and heavier hydrocarbons.

Varying temperature data points led to changes in the gas composition, and congruently the selectivity changed. Thermodynamic results at temperatures above 700^{o}C show that the selectivity of H_2 and CO increases with temperature. This also agrees with literature [79]. Reversely, the selectivity of CO_2 decreases with increase in temperature, which matches with thermodynamic model results but it can be found elsewhere reported that CO_2 remained constant [79]. No CH_4 was notices at such high temperatures. Whilst no carbon was left unconverted, it can be concluded that temperature changes the product selectivity, favouring discrete reactions from the same reactants concentration.

Interpreting the results from the non-catalysed tests it can be concluded that at 750^{o}C and above the ratio of the permanent gases at each temperature data point changed. This agrees with the thermodynamic model results and a similar trend was observed in the catalytic reaction at temperatures between 700^{o}C and 900^{o}C. Hence it can be concluded that at temperatures lower than 900^{o}C there are some heterogeneous reaction of char with steam as also reported by Franco et al. [79] and/or endothermic reactions involving secondary and tertiary tars.

In the catalytic reactions at data points between 900^{o}C and 950^{o}C there was marginal differences to distinguish the trend within each catalyst. Most of tar was converted to permanent gases and the gas composition remained constant within the margin of error. It is assumed that at temperatures above 950^{o}C there is no variation in gas composition. This can imply or even lead to conclusion that at these reaction conditions (catalyst at 900^{o}C and above) there was no further tar reforming but all heavy compounds reform to yield permanent gaseous products only.

Effects of steam to carbon ratio: Steam was increased from no steam to a steam to carbon ratio of 3 in 1 step increments. From observations discussed in the earlier chapters it is clear that steam increased the carbon conversion (reduces or eliminates the formation of carbon in the bed), enhanced dry gas yield and significantly increased H_2 formation. This agrees with literature [80] giving conclusions obtained from a case study of an "absorption-enhanced steam gasification of biomass for hydrogen production". Similarly literature [81] shows that S/C or temperature improved carbon conversion and enhanced dry gas yield. In general, increasing the steam in the process increases the gas yield but however when an S/C of 3.5 was used, there was less gas CO produced than at an S/C of 3. More CO_2 and H_2O were generated in the products while only a slight increase of H_2 was observed. When tar conversion to gas at an S/C of 2 was compared with that at an S/C of 3, there was a distinctive increase in gas formation and the calorific value of the gas increased with steam. One can argue that the precise S/C lays somewhere between 2 and 3. In some minor tests a further increase of steam to carbon ratio to 4 was experimented and it was found that the rise in steam slightly increased in H_2, increased in CO_2 and tar oxygen containing components but CO decreased. This behaviour could largely be explained by steam partial pressure in the system. As a result, this led to the formation of –COOH and functional groups and somewhat favouring the formation of CO_2 and H_2.

Effect of catalysts: The ratio of steam to carbon was varied but in most experiments it was set at 3. As it was predicted that gas yield increased with temperature, it is thought that in the presence of a catalyst increased the rate of gas formation but also selectively

influenced the gas composition. The individual catalysts formed different compositions of permanent gases and CO_2, CO and CH_4 gases formed had a strong correlation with the carbon conversion. By contrast, Rh-catalyst is very active at carbon conversion and has a much higher gas formation, almost near to equilibrium. At 900°C, Rh-catalyst shows it has the ability to attain complete tar elimination. Rh-catalyst also exhibited good stability (which agrees with what is reported in literature [55]), and activity, without showing arguably any form of decay and carbon deposition. Pt-catalyst was equally stable as Rh but its activity was relatively slower particularly at lower temperatures (700°C and 750°C) as opposed to its activity at higher temperatures (900°C and 950°C). At lower temperatures, carbon growth was observed on the Pt-catalyst surface, which elaborated the reason behind its slow activity at lower temperature. Ni-catalyst is very active, in fact even more active than the Pt-catalyst but unlike the stability Rh- and Pt- catalyst possess, Ni-catalyst quickly deactivates, developing a larger layer of carbon on its surface. The gradual deposition of carbon on the Ni-catalyst easily led to blockages in the reactor. It is because of this carbon deposition that the Ni-catalyst's ability to carbon conversion is considered low. Comparing the results with equilibrium, all catalysts displayed better results, nearing equilibrium with increase in temperature but in terms of stability and durability the rhodium catalyst has a much better performance. The addition of steam improved the conversion and longevity of the catalyst performance. As the steam to carbon ration in the feed was increased the amount of carbon deposition reduced. This agrees with other literature studies which involved the use of Ni/Al_2O_3 in steam reforming of a model biogas in fixed and fluidized bed reactors [74].

Overall, the application of the rhodium and platinum metal catalyst in the process showed a significant potential to lead technologies in converting tar to useful fuel gas and stating the potential application of the catalyst in the chemical industry. Both catalyst, mostly the rhodium catalyst, showed viable results with successfully efficiently and highly selectively cracking and reforming tar to syngas. All three catalysts are magnificently thermally stable demonstrating that they have a strong interaction with the metal support and consequently can be reduced at high temperatures and for

operation that require low temperature operations they can hold for temperature runaway.

All tests showed a higher H_2 content in the gas formed. The selectivity of CO also increased with temperature and was near equilibrium with the Rh-base catalysts. Nearly no tar in the product stream was seen where Rh-base catalyst was used and low tar concentrations were recorded where Pt-base catalyst was used, significantly at lower temperatures. Whereas CH_4 was still seen in Ni-based catalyst, only traces could be detected where either Rh-based or Pt-based catalysts were used. The amount and type of depositions on spent catalyst could not be precisely determined because it was considerably small but all depositions were found to be only influenced by the type of a catalyst and the amount of steam available for the reaction. To sum up, the Rh-based catalyst product a better quality gas with a higher heat value than either of the Pt- and Ni-base catalyst.

Effect of using model compounds rather than biomass tar as feed material: The use of model compounds showed a discrepancy in catalytic performance and the nature of solids formed and composition of product gases. The results from thermal steam reforming of a combination of model compound guaiacol and toluene showed a significant amount of soot (an amorphous carbon) and not graphite like carbon in the reactor tube whereas biomass tar produced mostly graphite like carbon with little or no soot. Also the catalyst performance in gas formation from model tar reformation disagrees with the gas composition formation from reforming biomass tar. Since the two materials behave different, this affirms that realistic hypothesises or claims including kinetic studies of biomass gasification cannot be legitimately determined or represented using model compounds.

More supporting evidence is extracted from studying the activity of the catalyst within reforming model compounds and biomass tar. The results from the two materials show significant differences enough to challenge most speculated similarities. For instance, in this study, the Ni catalyst excelled in reform model compounds to permanent gases, retained its activity for an elongated period while, at a steady rate converting more than

99.99% carbon in the feed to permanent gases, however, when it's activity is compared with reactions in the biomass tar only 68% carbon was converted to gas and the catalytic activity depreciated within minutes. In contrast, even though Ni performed excellently in model compounds, it rapidly died off in biomass tar yet the Rh performed better in converting biomass tar yielding a consistent gas composition at a steady rate.

Future work that will certainly be a great benefit to this work is to develop a kinetic model for the reactions involved. In this work, there is sufficient amount of information that has been generated to cover the data required in kinetic development. This will potentially close the biggest challenge on tar reactions. Other studies that can be of great contribution need to cover an analysis and characterisation of the full spectrum of the tar compounds recovered in the product stream (tar trap). This will require performing longer tests and making modifications to the traps to allow caption of larger amount of tar. Longer runs will be desirable since for most of the experiments performed during this study, lasting just about 54 minutes, mostly tar traces to small amount if not nothing were generated. By increasing the experimental period more tar can be collected ideally sufficient for further analysis. The residue tar from the individual variables can also be characterised with various techniques including; for example, a size exclusion chromatography (SEC) and a UV-fluorescence spectroscopy, shown elsewhere. For instance, the listed techniques have been employed to characterise asphaltenes from various crude oils to compare the retention times for solvents and the relative magnitudes of the aromatic rings respectively [82]. Similar techniques were used to illustrate the presence of large molecules in a solution during the study of the effect of catalysts deactivation on hydrocracking heavy hydrocarbon liquids [83]. With such characterisation the effect of the individual variables for insistence the catalyst on particular tar compounds can be justified.

More future work can also be done on application of this kind of catalyst on a larger scale. Industries often face a challenge to reduce catalysts especially catalysts that require high temperatures to be reduced. Since the nature of the catalyst applied in this

project required high temperatures, investigations should be considered to know how reduction can be achieved on large scale plants with larger beads.

REFERENCES

1. BP *BP Energy Outlook 2035*. BP Energy Outlook, 2015.

2. Bridgwater, A.V., *Advances in Thermochemical Biomass Conversion.* Vol. 1.

3. Lee, T.-w., *Method of preparing carbon thin film, and electronic device and electrochemical devices each including the carbon thin film*. 2012: US.

4. Basu, P., *Tar Production and Destruction*, in *Biomass Gasification Design Handbook*. 2010, Academic Press: Boston. p. 97-116.

5. Li, C. and K. Suzuki, *Tar property, analysis, reforming mechanism and model for biomass gasification--An overview.* Renewable and Sustainable Energy Reviews, 2009. **13**(3): p. 594-604.

6. Phuphuakrat, T., T. Namioka, and K. Yoshikawa, *Tar removal from biomass pyrolysis gas in two-step function of decomposition and adsorption.* Applied Energy, 2010. **87**(7): p. 2203-2211.

7. Hosoya, T., H. Kawamoto, and S. Saka, *Pyrolysis gasification reactivities of primary tar and char fractions from cellulose and lignin as studied with a closed ampoule reactor.* Journal of Analytical and Applied Pyrolysis, 2008. **83**(1): p. 71-77.

8. Li, X.T., et al., *Biomass gasification in a circulating fluidized bed.* Biomass and Bioenergy, 2004. **26**(2): p. 171-193.

9. Saidur, R., et al., *A review on biomass as a fuel for boilers.* Renewable and Sustainable Energy Reviews, 2011. **15**(5): p. 2262-2289.

10. Anis, S. and Z.A. Zainal, *Tar reduction in biomass producer gas via mechanical, catalytic and thermal methods: A review.* Renewable and Sustainable Energy Reviews, 2011. **15**(5): p. 2355-2377.

11. Hasler, P. and T. Nussbaumer, *Sampling and analysis of particles and tars from biomass gasifiers.* Biomass and Bioenergy, 2000. **18**(1): p. 61-66.

12. Abu El-Rub, Z., E.A. Bramer, and G. Brem, *Review of Catalysts for Tar Elimination in Biomass Gasification Processes.* Industrial & Engineering Chemistry Research, 2004. **43**(22): p. 6911-6919.

13. Milne TA, E.R., Abatzoglou N. , *Biomass gasifier "tars": their nature, formulation, and conversion.*, M. TA, Editor. 1998, Golden: Colarado, USA.

14. Devi, L., K.J. Ptasinski, and F.J.J.G. Janssen, *A review of the primary measures for tar elimination in biomass gasification processes.* Biomass and Bioenergy, 2003. **24**(2): p. 125-140.

15. Marcos Millan, F.D., Nigel Paterson, Paul Fennel, and Rafael Kandiyoti *Tar Formation and Destruction in a Fixed-Bed Reactor Simulating Downdraft Gasification: Equipment Development and Characterization of Tar-Cracking Products* Energy Fuels 2010 **24** p. 4560-4570

16. Leibold, H., A. Hornung, and H. Seifert, *HTHP syngas cleaning concept of two stage biomass gasification for FT synthesis.* Powder Technology, 2008. **180**(1-2): p. 265-270.

17. Bridgwater, A.V., *Catalysis in thermal biomass conversion.* Applied Catalysis A: General, 1994. **116**(1-2): p. 5-47.

18. Ponzio, A., S. Kalisz, and W. Blasiak, *Effect of operating conditions on tar and gas composition in high temperature air/steam gasification (HTAG) of plastic containing waste.* Fuel Processing Technology, 2006. **87**(3): p. 223-233.

19. Kinoshita, C.M., Y. Wang, and J. Zhou, *Tar formation under different biomass gasification conditions.* Journal of Analytical and Applied Pyrolysis, 1994. **29**(2): p. 169-181.

20. Liu, H., et al., *Effect of Additives on Catalytic Cracking of Biomass Gasification Tar over a Nickel-Based Catalyst.* Chinese Journal of Catalysis, 2010. **31**(Compendex): p. 409-414.

21. Mermelstein, J., M. Millan, and N.P. Brandon, *The interaction of biomass gasification syngas components with tar in a solid oxide fuel cell and operational conditions to mitigate carbon deposition on nickel-gadolinium doped ceria anodes.* Journal of Power Sources, 2011. **196**(11): p. 5027-5034.

22. Abu El-Rub, Z., E.A. Bramer, and G. Brem, *Experimental comparison of biomass chars with other catalysts for tar reduction.* Fuel, 2008. **87**(10-11): p. 2243-2252.

23. Cao, Y., et al., *A novel biomass air gasification process for producing tar-free higher heating value fuel gas.* Fuel Processing Technology, 2006. **87**(4): p. 343-353.

24. van der Drift, A., J. van Doorn, and J.W. Vermeulen, *Ten residual biomass fuels for circulating fluidized-bed gasification.* Biomass and Bioenergy, 2001. **20**(1): p. 45-56.

25. Hernández, J.J., G. Aranda-Almansa, and A. Bula, *Gasification of biomass wastes in an entrained flow gasifier: Effect of the particle size and the residence time.* Fuel Processing Technology, 2010. **91**(6): p. 681-692.

26. Manyà, J.J., et al., *Influence of gas residence time and air ratio on the air gasification of dried sewage sludge in a bubbling fluidised bed.* Fuel, 2006. **85**(14-15): p. 2027-2033.

27. Bridgwater, A.V., *The technical and economic feasibility of biomass gasification for power generation.* Fuel, 1995. **74**(5): p. 631-653.

28. Sadhukhan J., N.K.S., Shah, N. And Simons, H.J., *Heat integration strategy for economic production of CHP from biomass waste.* . Energy & Fuels, 2009. **23**(10): p. 5106 - 5120.

29. Sadhukhan J., N.K.S., Martinez-Hernandez E. , *Biorefineries and Chemical Processes*. Design, Integration and Sustainability Analysis. 2014, Chichester: Wiley.

30. Herbet J. Setzer, E.S.K., East Hampton; John AS Bett, Hamden, , *Steam Reforming Catalysts* in *Google Patents* 1988: United States p. 1.

31. Lim, M.T. and Z. Alimuddin, *Bubbling fluidized bed biomass gasification--Performance, process findings and energy analysis.* Renewable Energy, 2008. **33**(10): p. 2339-2343.

32. Basu, P., *Gasification Theory and Modeling of Gasifiers*, in *Biomass Gasification Design Handbook*. 2010, Academic Press: Boston. p. 117-165.

33. Knight, R.A., *Experience with raw gas analysis from pressurized gasification of biomass.* Biomass and Bioenergy, 2000. **18**(1): p. 67-77.

34. Sutton, D., B. Kelleher, and J.R.H. Ross, *Review of literature on catalysts for biomass gasification.* Fuel Processing Technology, 2001. **73**(3): p. 155-173.

35. Gates, B.C., et al., *George C.A. Schuit 1910-2001*, in *Advances in Catalysis*. 2002, Academic Press. p. xix-xxi.

36. Zhou, J., et al., *Biomass-oxygen gasification in a high-temperature entrained-flow gasifier.* Biotechnology Advances, 2009. **27**(5): p. 606-611.

37. Gil, J., et al., *Biomass gasification in atmospheric and bubbling fluidized bed: Effect of the type of gasifying agent on the product distribution.* Biomass and Bioenergy, 1999. **17**(5): p. 389-403.

38. Qin, Y.-H., J. Feng, and W.-Y. Li, *Formation of tar and its characterization during air-steam gasification of sawdust in a fluidized bed reactor.* Fuel, 2010. **89**(7): p. 1344-1347.

39. Umeki, K., et al., *High temperature steam-only gasification of woody biomass.* Applied Energy, 2010. **87**(3): p. 791-798.

40. Wang, L., et al., *Catalytic performance and characterization of Ni-Fe catalysts for the steam reforming of tar from biomass pyrolysis to synthesis gas.* Applied Catalysis A: General, 2011. **392**(1-2): p. 248-255.

41. Kim, Y.H., et al., *A simulation study on gas-to-liquid (natural gas to Fischer-Tropsch synthetic fuel) process optimization.* Chemical Engineering Journal, 2009. **155**(1-2): p. 427-432.

42. Niemantsverdriet, J.W., *Case Studies in Catalyst Characterization*, in *Spectroscopy in Catalysis*. 2007, Wiley-VCH Verlag GmbH & Co. KGaA. p. 251-295.

43. Göransson, K., et al., *Review of syngas production via biomass DFBGs.* Renewable and Sustainable Energy Reviews, 2011. **15**(1): p. 482-492.

44. Richards, G.N. and G. Zheng, *Influence of metal ions and of salts on products from pyrolysis of wood: Applications to thermochemical processing of newsprint and biomass.* Journal of Analytical and Applied Pyrolysis, 1991. **21**(1-2): p. 133-146.

45. Garcia, L., et al., *Catalytic steam reforming of bio-oils for the production of hydrogen: effects of catalyst composition.* Applied Catalysis A: General, 2000. **201**(2): p. 225-239.

46. Dou, B., et al., *Catalytic cracking of tar component from high-temperature fuel gas.* Applied Thermal Engineering, 2003. **23**(17): p. 2229-2239.

47. Xu, C., et al., *Recent advances in catalysts for hot-gas removal of tar and NH3 from biomass gasification.* Fuel, 2010. **89**(8): p. 1784-1795.

48. Swierczynski, D., et al., *Steam reforming of tar from a biomass gasification process over Ni/olivine catalyst using toluene as a model compound.* Applied Catalysis B: Environmental, 2007. **74**(3-4): p. 211-222.

49. Liu, H., et al., *Effect of Additives on Catalytic Cracking of Biomass Gasification Tar over a Nickel-Based Catalyst.* Chinese Journal of Catalysis, 2010. **31**(4): p. 409-414.

50. Caballero M A. Coella J, A.M., Gil J. , *Biomass gasification with air in a fluidized bed, Hot gas cleanup with selected commercial and full-size nickel-based catalysts.* . Industrial & Engineering Chemistry Research, 2000(39): p. 1143-1154.

51. Dou B, P.W., Ren J, Chen B, Hwang J, Yu T-U *Removal of tar components over cracking catalysts from high temperature fuel gas.* . Energy Conversion and Management 2008 (49): p. 2247-2253.

52. Hongzhang, D., et al., *Surface features and catalytic performances of platinum/alumina and platinum-rhenium/alumina catalysts for n-heptane conversion prepared by metal carbonyl complexes.* Applied Catalysis, 1991. **78**(1): p. 1-14.

53. E.G, D., *Studies in surface science and catalysis, volume 29 : Metal clusters in catalysis edited by B.C. Gates, L. Guczi and H. Knözinger, Elsevier Science Publishers, Amsterdam, 1986, xxvii + 648 pages, ISBN 0-444-42682-5, price US $84.75/ Dfl. 195.00.* Journal of Molecular Catalysis, 1987. **43**(1): p. 138-139.

54. Chen, Y., et al., *Sulphur-resistant character of Titania-supported Platinum catalysts.* Applied Catalysis, 1990. **63**(1): p. 107-115.

55. Polvinen, R., et al., *The effect of Pt–Rh synergism on the thermal stability of rhodium oxide on pure alumina and Ce–ZrO2-modified alumina-supported catalysts.* Journal of Catalysis, 2004. **226**(2): p. 372-381.

56. Hu, G., et al., *Steam gasification of apricot stones with olivine and dolomite as downstream catalysts.* Fuel Processing Technology, 2006. **87**(5): p. 375-382.

57. Pelovski, Y., I. Dombalov, and V. Petkova, *Mechano-chemical Activation of Dolomite.* Journal of Thermal Analysis and Calorimetry, 2001. **64**(3): p. 1257-1263.

58. Makó, É., *The effect of quartz content on the mechanical activation of dolomite.* Journal of the European Ceramic Society, 2007. **27**(2-3): p. 535-540.

59. Di Felice, L., et al., *Catalytic biomass gasification: Simultaneous hydrocarbons steam reforming and CO2 capture in a fluidised bed reactor.* Chemical Engineering Journal, 2009. **154**(1-3): p. 375-383.

60. Álvarez-Rodríguez, R. and C. Clemente-Jul, *Hot gas desulphurisation with dolomite sorbent in coal gasification.* Fuel, 2008. **87**(17-18): p. 3513-3521.

61. Vassilatos, V., et al., *Catalytic cracking of tar in biomass pyrolysis gas in the presence of calcined dolomite.* The Canadian Journal of Chemical Engineering, 1992. **70**(5): p. 1008-1013.

62. Zhang, R., Y. Wang, and R.C. Brown, *Steam reforming of tar compounds over Ni/olivine catalysts doped with CeO2.* Energy Conversion and Management, 2007. **48**(1): p. 68-77.

63. Young, R.C.T.a.B.C., *A Comparison of Zeolite and Dolomite as Gasification Tar-Cracking Catalysts* in *Energy & Environmental Research Center* University of North Dakota Grand Ford Forks

64. Zhang, G., et al., *CO2 reforming of CH4 in coke oven gas to syngas over coal char catalyst.* Chemical Engineering Journal, 2010. **156**(3): p. 519-523.

65. Min, Z., et al., *Catalytic reforming of tar during gasification. Part II. Char as a catalyst or as a catalyst support for tar reforming.* Fuel, 2011. **90**(7): p. 2545-2552.

66. Wang, D., W. Yuan, and W. Ji, *Char and char-supported nickel catalysts for secondary syngas cleanup and conditioning.* Applied Energy, 2011. **88**(5): p. 1656-1663.

67. Barbero, E.J., *Introduction to composite materials design*. 2010: CRC press.

68. Calo, J.M. and M.T. Perkins, *A heterogeneous surface model for the "steady-state" kinetics of the boudouard reaction.* Carbon, 1987. **25**(3): p. 395-407.

69. Lahijani, P., et al., *Conversion of the greenhouse gas CO2 to the fuel gas CO via the Boudouard reaction: A review.* Renewable and Sustainable Energy Reviews, 2015. **41**: p. 615-632.

70. Guan, G., et al., *Catalytic steam reforming of biomass tar: Prospects and challenges.* Renewable and Sustainable Energy Reviews, 2016. **58**: p. 450-461.

71. Balu, E., U. Lee, and J.N. Chung, *High temperature steam gasification of woody biomass – A combined experimental and mathematical modeling approach.* International Journal of Hydrogen Energy, 2015. **40**(41): p. 14104-14115.

72. Effendi, A., et al., *Characterisation of carbon deposits on Ni/SiO2 in the reforming of CH4–CO2 using fixed- and fluidised-bed reactors.* Catalysis Communications, 2003. **4**(4): p. 203-207.

73. Guo, L., et al., *Mechanisms of the water–gas shift reaction catalyzed by carbonyl complexes M(CO)6 (M = Mo, W).* International Journal of Hydrogen Energy.

74. Effendi, A., et al., *Steam reforming of a clean model biogas over Ni/Al2O3 in fluidized- and fixed-bed reactors.* Catalysis Today, 2002. **77**(3): p. 181-189.

75. Lee, I.-G., et al., *Hydrogen production by supercritical water gasification of valine over Ni/activated charcoal catalyst modified with Y, Pt, and Pd.* International Journal of Hydrogen Energy, 2015. **40**(36): p. 12078-12087.

76. Boldrin, P., M. Millan-Agorio, and N.P. Brandon, *Effect of Sulfur- and Tar-Contaminated Syngas on Solid Oxide Fuel Cell Anode Materials.* Energy & Fuels, 2015. **29**(1): p. 442-446.

77. Cheng, C.K., S.Y. Foo, and A.A. Adesina, *Thermodynamic analysis of glycerol-steam reforming in the presence of CO2 or H2 as carbon gasifying agent.* International Journal of Hydrogen Energy, 2012. **37**(13): p. 10101-10110.

78. Airliquide. *http://encyclopedia.airliquide.com/Encyclopedia.asp?LanguageID=11&CountryID=19&Formula=CO2&btnFormula.x=0&btnFormula.y=0&GasID=0&UNNumber=&EquivGasID=45&VolLiquideBox=&MasseLiquideBox=&VolGasBox=&MasseGasBox=&RD20=29&RD9=8&RD6=64&RD4=2&RD3=22&RD8=27&RD2=20&RD18=41&RD7=18&RD13=71&RD16=35&RD12=31&RD19=34&RD24=62&RD25=77&RD26=78&RD28=81&RD29=82#GeneralData*. 2013 [cited 2016 29/05/2016].

79. Franco, C., et al., *The study of reactions influencing the biomass steam gasification process ☆.* Fuel, 2003. **82**(7): p. 835-842.

80. Wei, L., et al., *Absorption-enhanced steam gasification of biomass for hydrogen production: Effect of calcium oxide addition on steam gasification of pyrolytic volatiles.* International Journal of Hydrogen Energy, 2014. **39**(28): p. 15416-15423.

81. Mazumder, J. and H.I. de Lasa, *Catalytic Steam Gasification of Biomass Surrogates: Thermodynamics and Effect of Operating Conditions.* Chemical Engineering Journal.

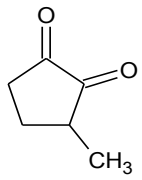
82. Leyva, C., et al., *Chemical characterization of asphaltenes from various crude oils.* Fuel Processing Technology, 2013. **106**: p. 734-738.

83. Millan, M., et al., *Effect of Catalyst Deactivation and Reaction Time on Hydrocracking Heavy Hydrocarbon Liquids.* Energy & Fuels, 2007. **21**(3): p. 1370-1378.

Appendix

Appendix 1: Compounds Detected from GC-MS Analysis of Fresh Tar

3-methylcyclopentane-1,2-dione

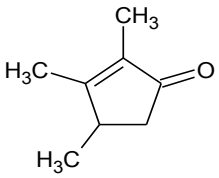


Molecular Formula: $C_6H_8O_2$

Formula Weight: 112.12652

Density: 1.102 ± 0.06 g/cm^3

2,3,4-trimethylcyclopent-2-en-1-one

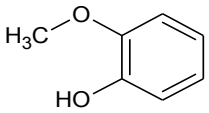


Molecular Formula: $C_8H_{12}O$

Formula Weight: 124.18028

Density: 0.923 ± 0.06 g/cm^3

2-methoxyphenol

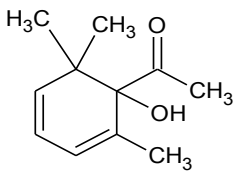


Molecular Formula: $C_7H_8O_2$

Formula Weight: 124.13722

Density: 1.109 ± 0.06 g/cm^3

1-(1-hydroxy-2,6,6-trimethylcyclohexa-2,4-dien-1-yl)ethanone

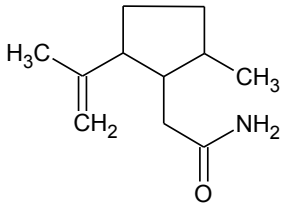


Molecular Formula: $C_{11}H_{16}O_2$

Formula Weight: 180.24354

Density: 1.023 ± 0.06 g/cm^3

2-[2-methyl-5-(prop-1-en-2-yl)cyclopentyl]acetamide

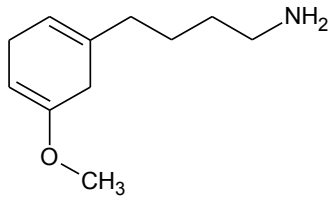


Molecular Formula: $C_{11}H_{19}NO$

Formula Weight: 181.27466

Density: 0.941 ± 0.06 g/cm^3

4-(5-methoxycyclohexa-1,4-dien-1-yl)butan-1-amine

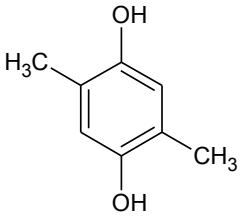


Formula Weight: 181.27466

Molecular Formula: $C_{11}H_{19}NO$

Density: 0.96 ± 0.1 g/cm^3

2,5-dimethylbenzene-1,4-diol

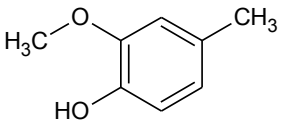


Molecular Formula: $C_8H_{10}O_2$

Formula Weight: 138.1638

Density: 1.162 ± 0.06 g/cm^3

2-methoxy-4-methylphenol

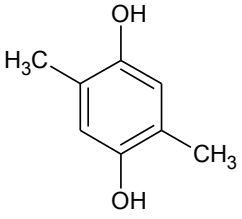


Formula Weight: 138.1638

Molecular Formula: $C_8H_{10}O_2$

Density: 1.078 ± 0.06 g/cm^3

2,5-dimethylbenzene-1,4-diol

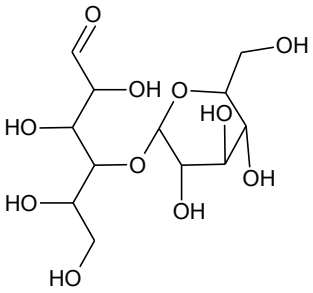


Molecular Formula: $C_8H_{10}O_2$

Formula Weight: 138.1638

Density: 1.162 ± 0.06 g/cm^3

2,3,5,6-tetrahydroxy-4-{[3,4,5-trihydroxy-6-(hydroxymethyl)tetrahydro-2*H*-pyran-2-yl]oxy}hexanal

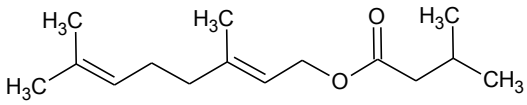


Formula Weight: 342.29648

Molecular Formula: $C_{12}H_{22}O_{11}$

Density: 1.68 ± 0.1 g/cm^3

(2*E*)-3,7-dimethylocta-2,6-dien-1-yl 3-methylbutanoate

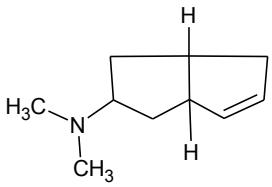


Formula Weight: 238.36574

Molecular Formula: $C_{15}H_{26}O_2$

Density: 0.893 ± 0.06 g/cm^3

N,*N*-dimethyl-1,2,3,3a,4,6a-hexahydropentalen-2-amine

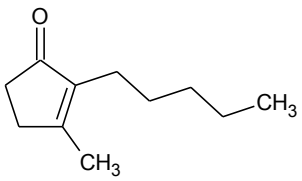


Formula Weight: 151.24868

Molecular Formula: $C_{10}H_{17}N$

Density: 0.95 ± 0.1 g/cm^3

3-methyl-2-pentylcyclopent-2-en-1-one

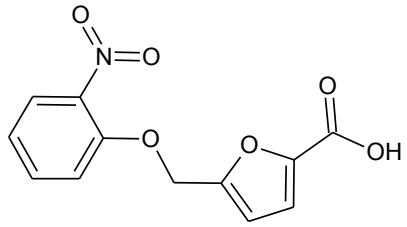


Molecular Formula: $C_{11}H_{18}O$

Formula Weight: 166.26002

Density: 0.915 ± 0.06 g/cm^3

5-[(2-nitrophenoxy)methyl]furan-2-carboxylic acid



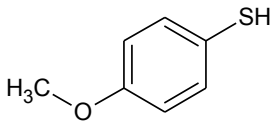
Molecular Formula: $C_{12}H_9NO_6$

Formula Weight: 263.20296

Nominal Mass: 263 Da

Density: 1.451 ± 0.06 g/cm^3

4-methoxybenzenethiol



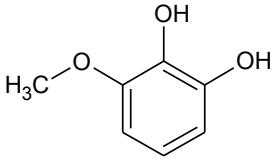
Molecular Formula: C_7H_8OS

Formula Weight: 140.20282

Nominal Mass: 140 Da

Density: 1.112 ± 0.06 g/cm^3

3-methoxybenzene-1,2-diol

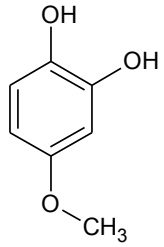


Formula Weight: 140.13662

Molecular Formula: $C_7H_8O_3$

Density: 1.270 ± 0.06 g/cm^3

4-methoxybenzene-1,2-diol

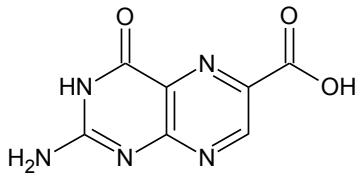


Molecular Formula: $C_7H_8O_3$

Formula Weight: 140.13662

Density: 1.270 ± 0.06 g/cm^3

2-amino-4-oxo-3,4-dihydropteridine-6-carboxylic acid

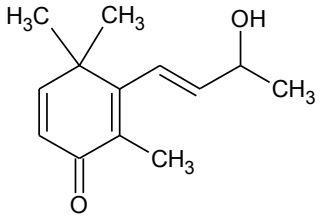


Formula Weight: 207.1463

Molecular Formula: $C_7H_5N_5O_3$

Density: 2.16 ± 0.1 g/cm^3

3-[(1*E*)-3-hydroxybut-1-en-1-yl]-2,4,4-trimethylcyclohexa-2,5-dien-1-one

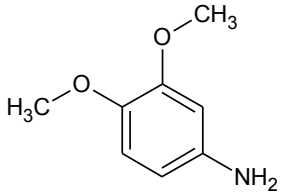


Molecular Formula: $C_{13}H_{18}O_2$

Formula Weight: 206.28082

Density: 1.062 ± 0.06 g/cm^3

3,4-dimethoxyaniline

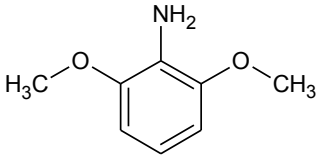


Formula Weight: 153.17844

Molecular Formula: $C_8H_{11}NO_2$

Density: 1.096 ± 0.06 g/cm^3

2,6-dimethoxyaniline

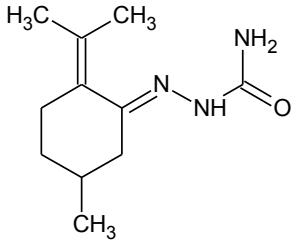


Formula Weight: 153.17844

Molecular Formula: $C_8H_{11}NO_2$

Density: 1.096 ± 0.06 g/cm^3

(2*E*)-2-[5-methyl-2-(propan-2-ylidene)cyclohexylidene]hydrazinecarboxamide

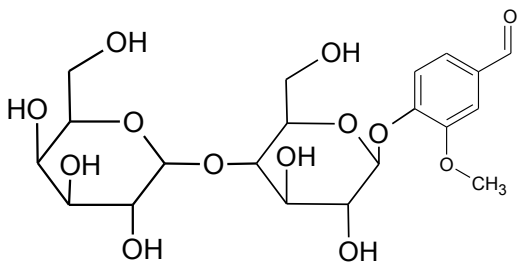


Molecular Formula: $C_{11}H_{19}N_3O$

Formula Weight: 209.28806

Density: 1.14 ± 0.1 g/cm^3

Vanillin lactoside

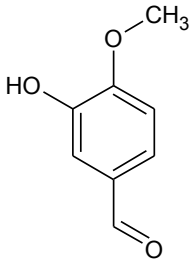


Formula Weight: 476.42852

Molecular Formula: $C_{20}H_{28}O_{13}$

Density: 1.61 ± 0.1 g/cm^3

3-hydroxy-4-methoxybenzaldehyde

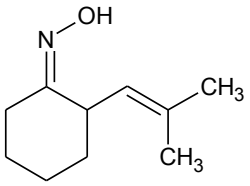


Formula Weight: 152.14732

Molecular Formula: $C_8H_8O_3$

Density: 1.231 ± 0.06 g/cm^3

(1*Z*)-*N*-hydroxy-2-(2-methylprop-1-en-1-yl)cyclohexanimine

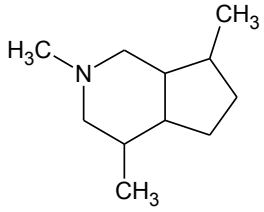


Formula Weight: 167.24808

Molecular Formula: $C_{10}H_{17}NO$

Density: 1.01 ± 0.1 g/cm^3

2,4,7-trimethyloctahydro-1*H*-cyclopenta[*c*]pyridine

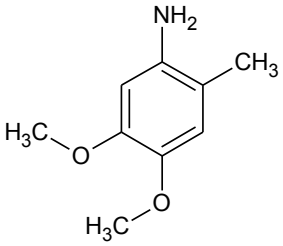


Formula Weight: 167.29114

Molecular Formula: $C_{11}H_{21}N$

Density: 0.872 ± 0.06 g/cm^3

4,5-dimethoxy-2-methylaniline

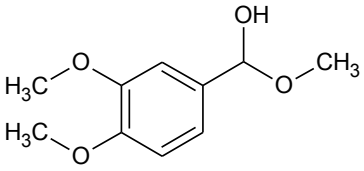


Molecular Formula: $C_9H_{13}NO_2$

Formula Weight: 167.20502

Density: 1.071 ± 0.06 g/cm^3

(3,4-dimethoxyphenyl)(methoxy)methanol / 3,4-dimethoxy-Benzaldehyde, methoylmonoacetal

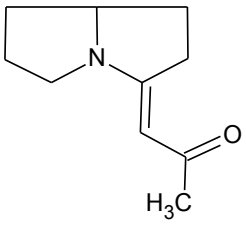


Molecular Formula: $C_{10}H_{14}O_4$

Formula Weight: 198.21576

Density: 1.133 ± 0.06 g/cm^3

(1*E*)-1-(hexahydro-3*H*-pyrrolizin-3-ylidene)propan-2-one

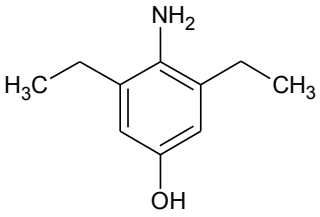


Molecular Formula: $C_{10}H_{15}NO$

Formula Weight: 165.2322

Density: 1.07 ± 0.1 g/cm^3

4-amino-3,5-diethylphenol

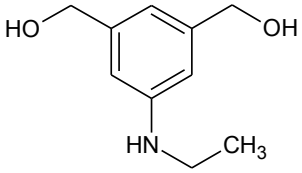


Molecular Formula: $C_{10}H_{15}NO$

Formula Weight: 165.2322

Density: 1.060 ± 0.06 g/cm^3

[5-(ethylamino)benzene-1,3-diyl]dimethanol / N-ethyl-3,5-di(hydroxymethyl)-Aniline

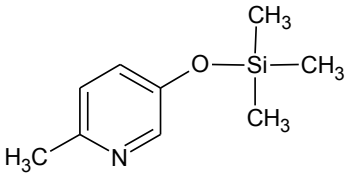


Molecular Formula: $C_{10}H_{15}NO_2$

Formula Weight: 181.2316

Density: 1.184 ± 0.06 g/cm^3

3-Trimethylsilyloxy-6-methylpyridine

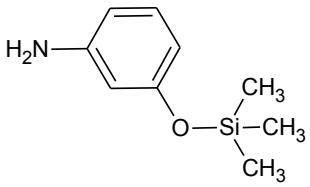


Molecular Formula: $C_9H_{15}NOSi$

Formula Weight: 181.307

Density: 0.945 ± 0.06 g/cm^3

3-Trimethylsilyloxyaniline

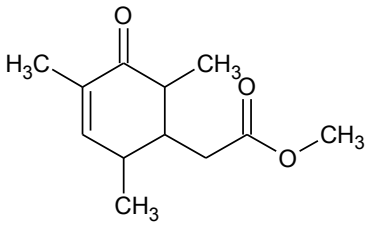


Formula Weight: 181.307

Molecular Formula: $C_9H_{15}NOSi$

Density: 0.982 ± 0.06 g/cm^3

methyl (2,4,6-trimethyl-5-oxocyclohex-3-en-1-yl)acetate

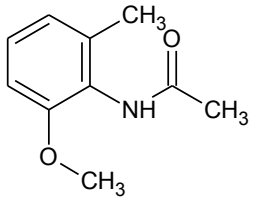


Molecular Formula: $C_{12}H_{18}O_3$

Formula Weight: 210.26952

Density: 0.992 ± 0.06 g/cm^3

N-(2-methoxy-6-methylphenyl)acetamide

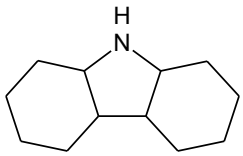


Molecular Formula: $C_{10}H_{13}NO_2$

Formula Weight: 179.21572

Density: 1.100 ± 0.06 g/cm^3

dodecahydro-1*H*-carbazole / Docecahydrocarbazole

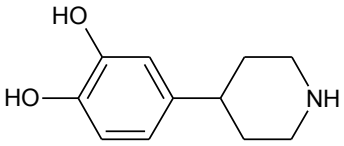


Formula Weight: 179.30184

Molecular Formula: $C_{12}H_{21}N$

Density: 0.950 ± 0.06 g/cm^3

4-(piperidin-4-yl)benzene-1,2-diol

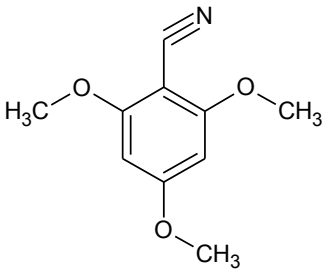


Molecular Formula: $C_{11}H_{15}NO_2$

Formula Weight: 193.2423

Density: 1.181 ± 0.06 g/cm^3

2,4,6-trimethoxybenzonitrile

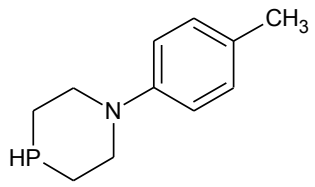


Molecular Formula: $C_{10}H_{11}NO_3$

Formula Weight: 193.19924

Density: 1.15 ± 0.1 g/cm^3

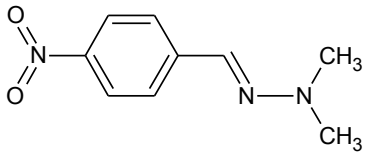
1-(4-methylphenyl)-1,4-azaphosphinane



Molecular Formula: $C_{11}H_{16}NP$

Formula Weight: 193.225202

(2*E*)-1,1-dimethyl-2-(4-nitrobenzylidene)hydrazine

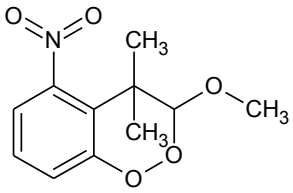


Molecular Formula: $C_9H_{11}N_3O_2$

Formula Weight: 193.20254

Density: 1.14 ± 0.1 g/cm^3

3-methoxy-4,4-dimethyl-5-nitro-3,4-dihydro-1,2-benzodioxine

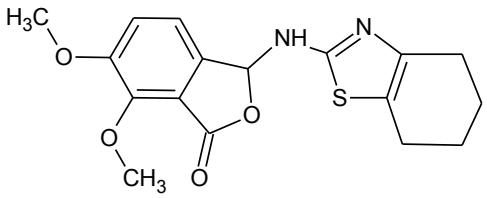


Molecular Formula: $C_{11}H_{13}NO_5$

Formula Weight: 239.22462

Density: 1.29 ± 0.1 g/cm^3

6,7-dimethoxy-3-(4,5,6,7-tetrahydro-1,3-benzothiazol-2-ylamino)-2-benzofuran-1(3*H*)-one

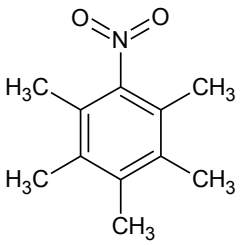


Molecular Formula: $C_{17}H_{18}N_2O_4S$

Formula Weight: 346.40082

Density: 1.393 ± 0.06 g/cm^3

1,2,3,4,5-pentamethyl-6-nitrobenzene



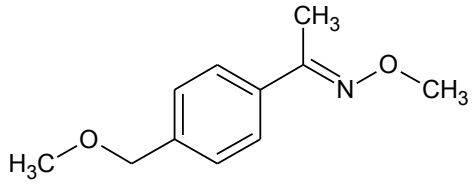
Molecular Formula: $C_{11}H_{15}NO_2$

Formula Weight: 193.2423

Density: 1.057 ± 0.06 g/cm^3

(1*E*)-*N*-methoxy-1-[4-(methoxymethyl)phenyl]ethanimine

/ Alpha-methyl-N-methoxy-4-(methoxymethyl)-Benzaldimine

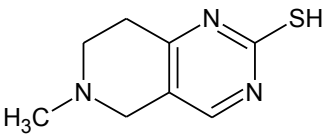


Molecular Formula: $C_{11}H_{15}NO_2$

Formula Weight: 193.2423

Density: 0.98 ± 0.1 g/cm^3

6-methyl-5,6,7,8-tetrahydropyrido[4,3-*d*]pyrimidine-2-thiol

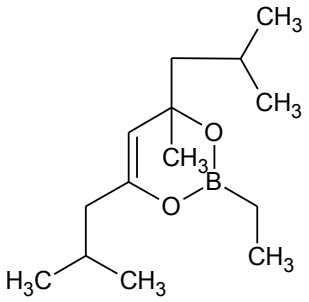


Molecular Formula: $C_8H_{11}N_3S$

Formula Weight: 181.25804

Density: 1.238 ± 0.06 g/cm^3

4H-1,3,2-Dioxaborin, 2-ethyl-4,6-bis(2-methylpropyl)-

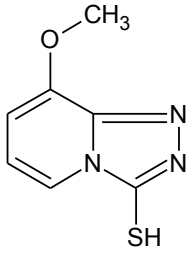


Molecular Formula: $C_{14}H_{27}BO_2$

Formula Weight: 238.17398

Density: 0.88 ± 0.1 g/cm^3

8-methoxy[1,2,4]triazolo[4,3-*a*]pyridine-3-thiol

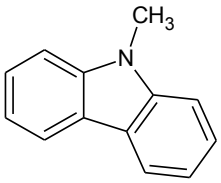


Formula Weight: 181.21498

Molecular Formula: $C_7H_7N_3OS$

Density: 1.47 ± 0.1 g/cm^3

9-methyl-9*H*-carbazole

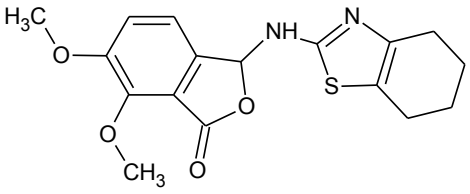


Molecular Formula: $C_{13}H_{11}N$

Formula Weight: 181.23314

Density: 1.09 ± 0.1 g/cm^3

6,7-dimethoxy-3-(4,5,6,7-tetrahydro-1,3-benzothiazol-2-ylamino)-2-benzofuran-1(3*H*)-one

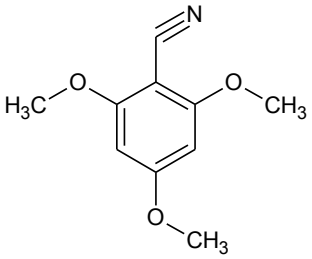


Formula Weight: 346.40082

Molecular Formula: $C_{17}H_{18}N_2O_4S$

Density: 1.393 ± 0.06 g/cm^3

2,4,6-trimethoxybenzonitrile

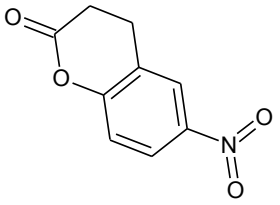


Molecular Formula: $C_{10}H_{11}NO_3$

Formula Weight: 193.19924

Density: 1.15 ± 0.1 g/cm^3

6-nitro-3,4-dihydro-2*H*-chromen-2-one

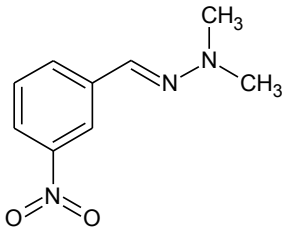


Molecular Formula: $C_9H_7NO_4$

Formula Weight: 193.15618

Density: 1.423 ± 0.06 g/cm^3

(2*E*)-1,1-dimethyl-2-(3-nitrobenzylidene)hydrazine

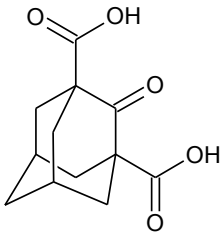


Molecular Formula: $C_9H_{11}N_3O_2$

Formula Weight: 193.20254

Density: 1.14 ± 0.1 g/cm^3

2-oxotricyclo[3.3.1.1^{3,7}]decane-1,3-dicarboxylic acid

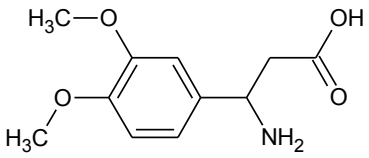


Molecular Formula: $C_{12}H_{14}O_5$

Formula Weight: 238.23656

Density: 1.588 ± 0.06 g/cm^3

3-amino-3-(3,4-dimethoxyphenyl)propanoic acid

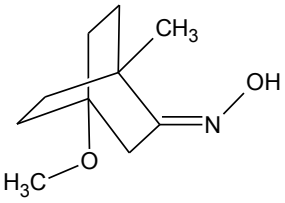


Molecular Formula: $C_{11}H_{15}NO_4$

Formula Weight: 225.2411

Density: 1.212 ± 0.06 g/cm^3

(2*Z*)-*N*-hydroxy-4-methoxy-1-methylbicyclo[2.2.2]octan-2-imine

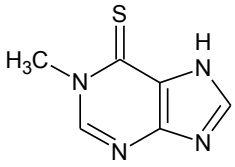


Molecular Formula: $C_{10}H_{17}NO_2$

Formula Weight: 183.24748

Density: 1.19 ± 0.1 g/cm^3

1-methyl-1,7-dihydro-6*H*-purine-6-thione

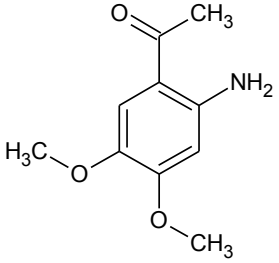


Molecular Formula: $C_6H_6N_4S$

Formula Weight: 166.20364

Density: 1.58 ± 0.1 g/cm^3

1-(2-amino-4,5-dimethoxyphenyl)ethanone

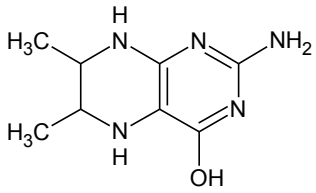


Molecular Formula: $C_{10}H_{13}NO_3$

Formula Weight: 195.21512

Density: 1.139 ± 0.06 g/cm^3

2-amino-6,7-dimethyl-5,6,7,8-tetrahydropteridin-4-ol

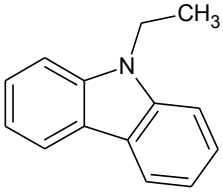


Molecular Formula: $C_8H_{13}N_5O$

Formula Weight: 195.22172

Density: 1.255 ± 0.06 g/cm^3

9-ethyl-9*H*-carbazole

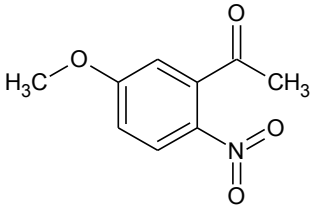


Molecular Formula: $C_{14}H_{13}N$

Formula Weight: 195.25972

Density: 1.07 ± 0.1 g/cm^3

1-(5-methoxy-2-nitrophenyl)ethanone

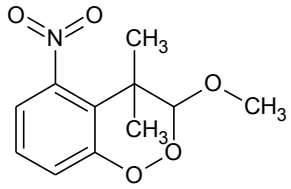


Formula Weight: 195.17206

Molecular Formula: $C_9H_9NO_4$

Density: 1.244 ± 0.06 g/cm^3

3-methoxy-4,4-dimethyl-5-nitro-3,4-dihydro-1,2-benzodioxine

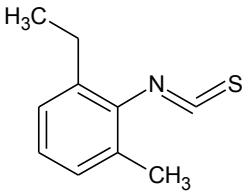


Molecular Formula: $C_{11}H_{13}NO_5$

Formula Weight: 239.22462

Density: 1.29 ± 0.1 g/cm^3

1-ethyl-2-isothiocyanato-3-methylbenzene

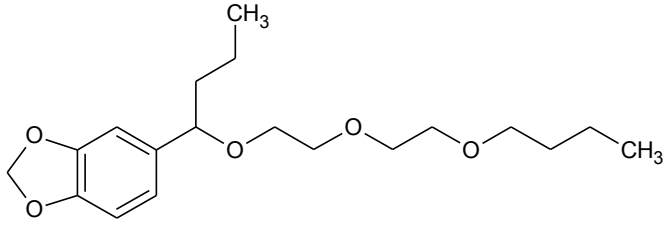


Molecular Formula: $C_{10}H_{11}NS$

Formula Weight: 177.26604

Density: 1.00 ± 0.1 g/cm^3

1,3-Benzodioxole, 5-[1-[2-(2-butoxyethox)ethoxy]butyl]-

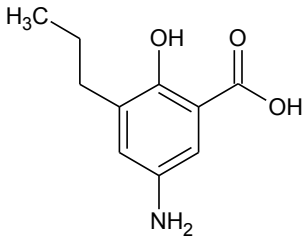


Molecular Formula: $C_{19}H_{30}O_5$

Formula Weight: 338.4385

Density: 1.063 ± 0.06 g/cm^3

5-amino-2-hydroxy-3-propylbenzoic acid

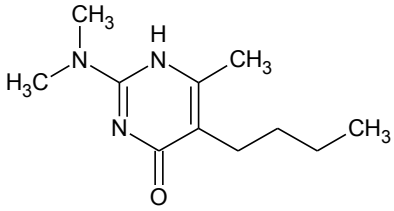


Molecular Formula: $C_{10}H_{13}NO_3$

Formula Weight: 195.21512

Density: 1.284 ± 0.06 g/cm^3

5-butyl-2-(dimethylamino)-6-methylpyrimidin-4(1*H*)-one

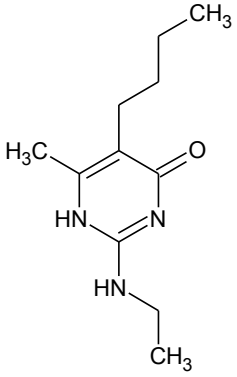


Molecular Formula: $C_{11}H_{19}N_3O$

Formula Weight: 209.28806

Density: 1.07 ± 0.1 g/cm^3

5-butyl-2-(ethylamino)-6-methylpyrimidin-4(1*H*)-one

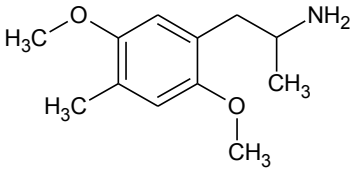


Molecular Formula: $C_{11}H_{19}N_3O$

Formula Weight: 209.28806

Density: 1.10 ± 0.1 g/cm^3

1-(2,5-dimethoxy-4-methylphenyl)propan-2-amine

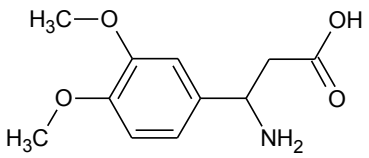


Molecular Formula: $C_{12}H_{19}NO_2$

Formula Weight: 209.28476

Density: 1.010 ± 0.06 g/cm^3

3-amino-3-(3,4-dimethoxyphenyl)propanoic acid

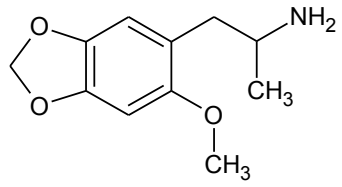


Molecular Formula: $C_{11}H_{15}NO_4$

Formula Weight: 225.2411

Density: 1.212 ± 0.06 g/cm^3

1-(6-methoxy-1,3-benzodioxol-5-yl)propan-2-amine

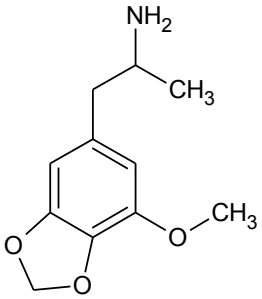


Molecular Formula: $C_{11}H_{15}NO_3$

Formula Weight: 209.2417

Density: 1.175 ± 0.06 g/cm^3

1-(7-methoxy-1,3-benzodioxol-5-yl)propan-2-amine



Molecular Formula: $C_{11}H_{15}NO_3$

Formula Weight: 209.2417

Density: 1.175 ± 0.06 g/cm^3

Appendix 2: GC-MS Sample Emitted Spectra

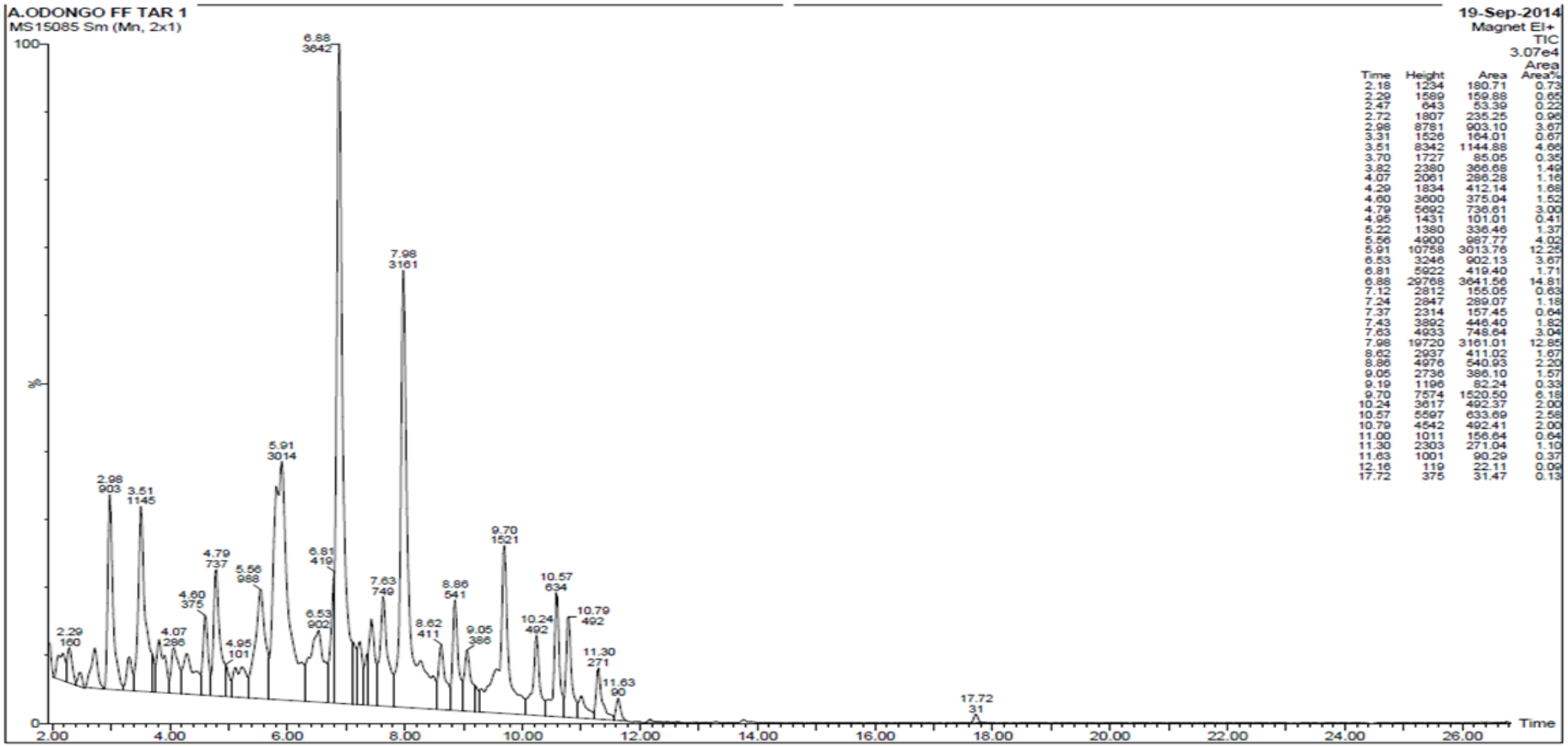


Figure 0:1: GC-MS Analysis of Biomass Tar for the Reactants Feed

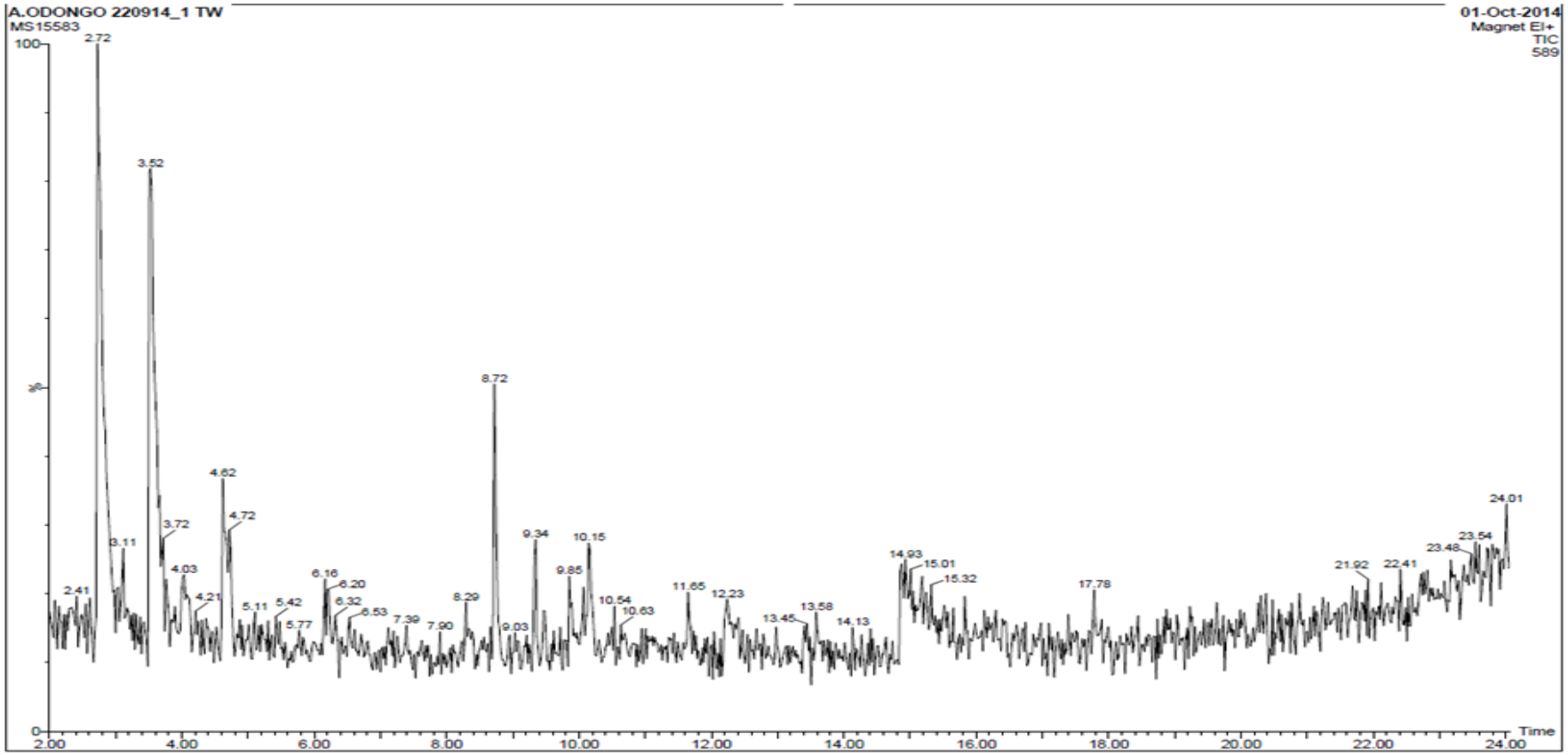


Figure 0:2: GC-MS Analysis of Liquid Products Recovered in the Dry-Ice Condensate Trap from Reforming Guaiacol and Toluene in an S/C of 3 at 750 °C using Rh-catalyst.

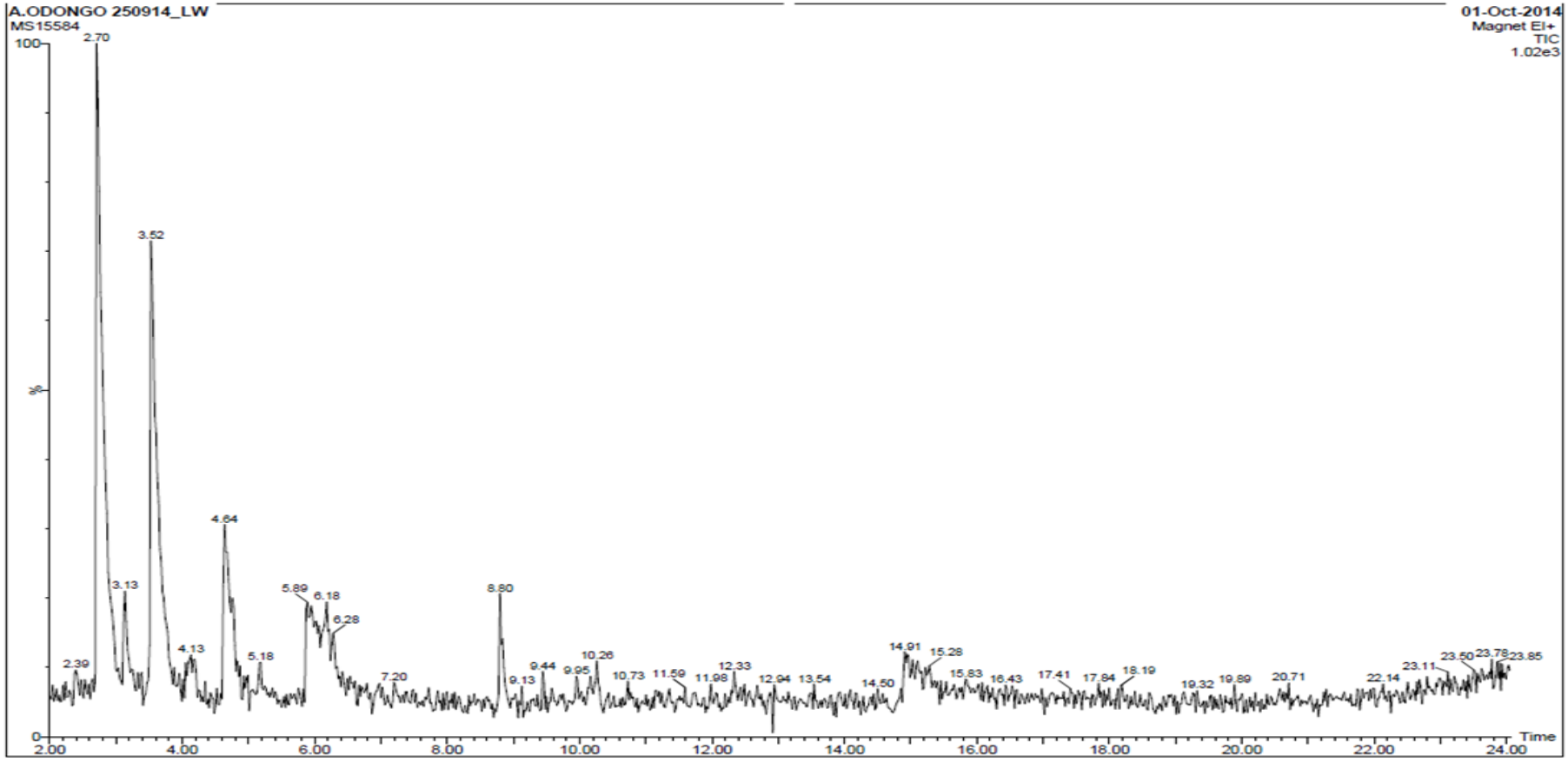


Figure 0:3: GC-MS Analysis of Liquid Products Recovered in the Ice-Water Condensate Trap from Reforming Guaiacol and Toluene in an S/C of 3 at 750 °C using Rh-catalyst

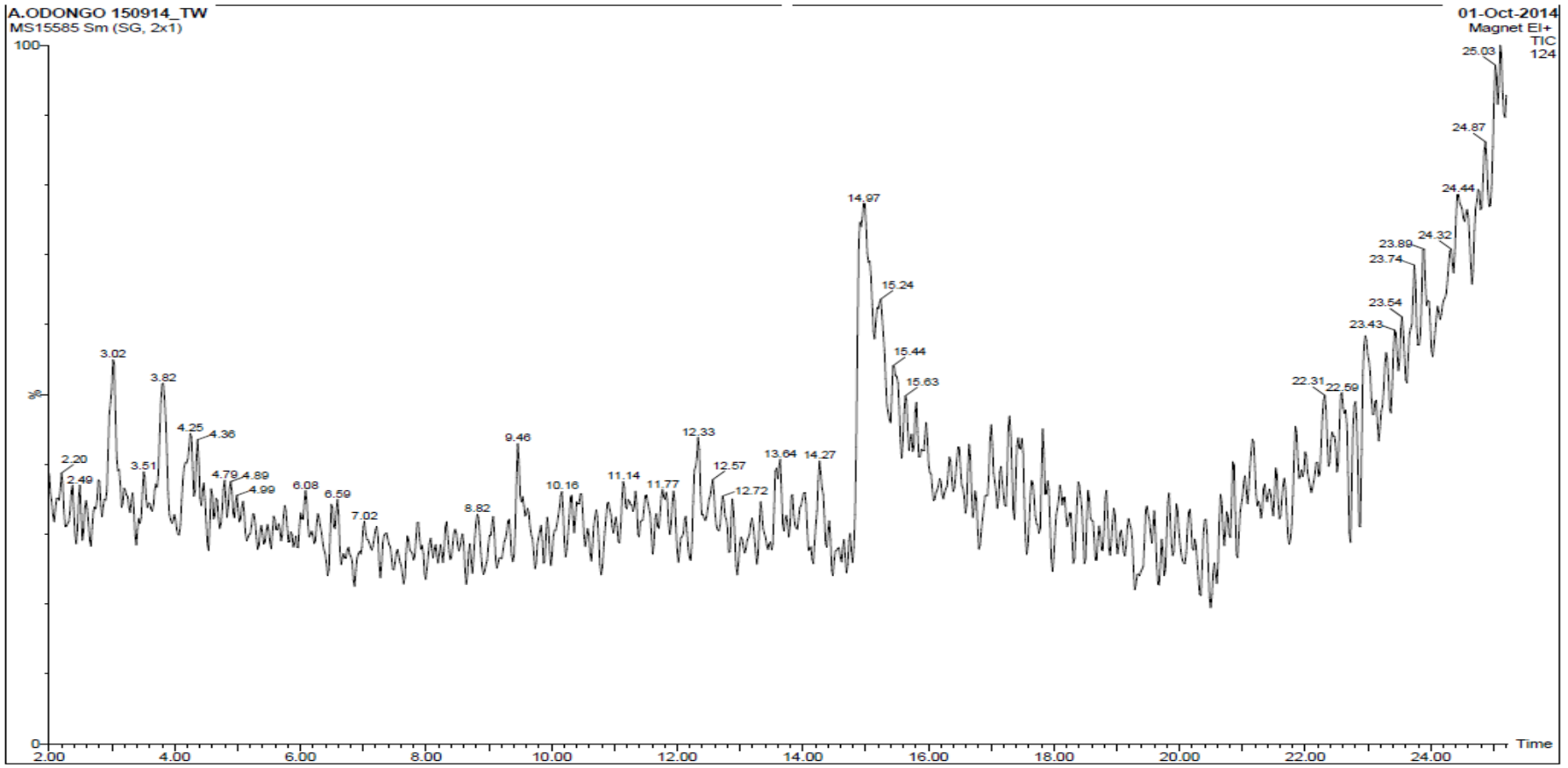


Figure 0:4: GC-MS Analysis of Liquid Products Recovered in the Dry-Ice Condensate Trap from Reforming Tar in an S/C of 3 and 1%CO_2, 5%CO, 1%CH_4 and 20%H_2 at 750 °C using Rh-catalyst

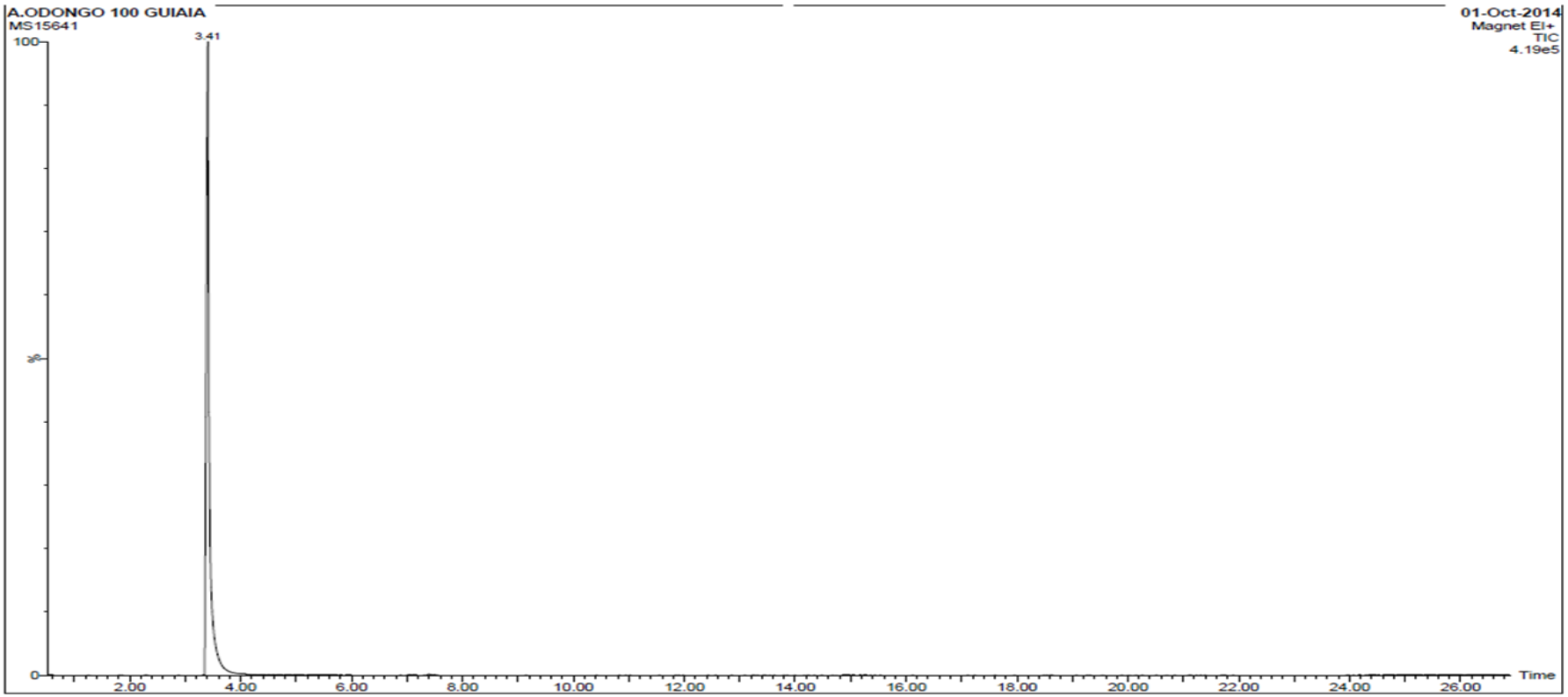
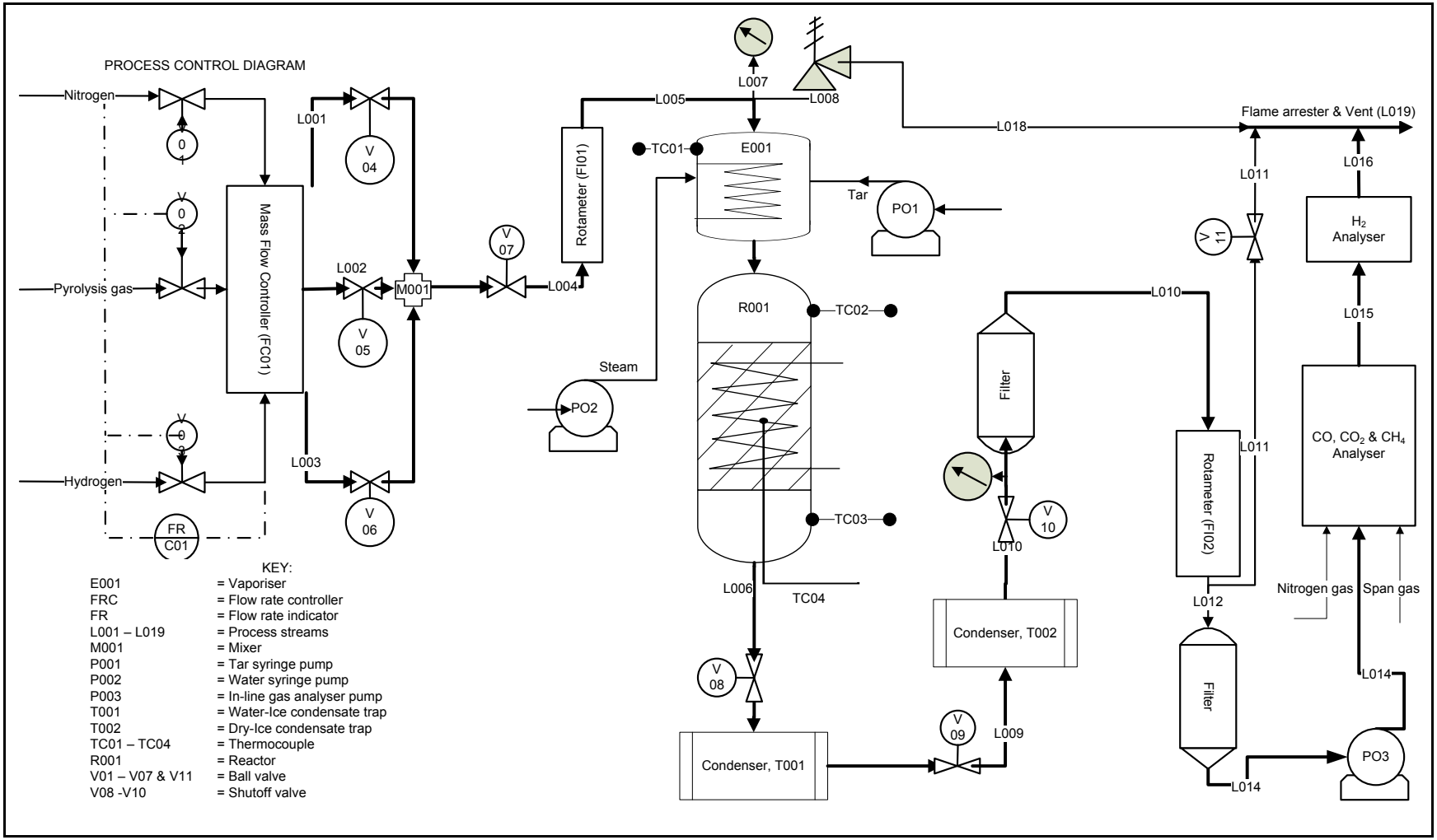


Figure 0:5: GC-MS Analysis of Guaiacol only Before Reaction

Appendix 3: Detailed Process Flow Diagram



Appendix 4: Fatigue Assessment of Reactor Vessel

To ensure the integrity of the reactor tube design against the risk of gross plastic deformation and incremental collapsing, the material minimum thickness was calculated. The derived thickness also includes the corrosion allowance, the thinning allowance due to forming and negative tolerance permitted by material temperatures and pressure. The tabulated thickness is increased by a scale factor of 3.5 to account for these uncertainties.

Design pressure: During operation of the reactor, internal pressure can be exerted, but most of the experiments in experiments are conducted at atmospheric pressure. To allow for operations at various pressures and pressure fluctuations, the reactor is designed for pressure loadings of up to 1MPa. This pressure is relatively much higher than the maximum that exist in the reactor during operation and higher than the maximum pressure which can be attained by the relieve valve.

Design loading: The effect of localised stress caused by supporting rings and external supporting electrodes were careful considered during the construction of the rig. The upper side of the reactor tube is clamped on fixed electrode that supports most of the vessel weight, whilst the lower end of the reactor tube is clamped to electrodes attached to flexible flat copper braided wires which give the allowance for both thermal expansion and contraction of the vessel.

Design temperature: In the computations, a stress maximum temperature used is 1000 °C which is 11.1% more than the actual desired maximum metal operating temperatures. This is intended to allow an adequate margin to cover uncertainties in temperature fluctuations such as those induced from exothermic reactions.

Pipe-work based on specification; Reactor vessels minimum thickness with internal pressure loading:

$$e = \frac{pD_i}{2f - p} = \frac{1MPa * 12mm}{2 * 10MPa - 1MPa} = 0.63mm$$

Where: e is the minimum thickness; p is the internal design pressure, D_i is the tube internal diameter and *f* is the nominal design stress. The value of "*f*" used here correlates to the design stress factor at a given temperature for a number of hours.

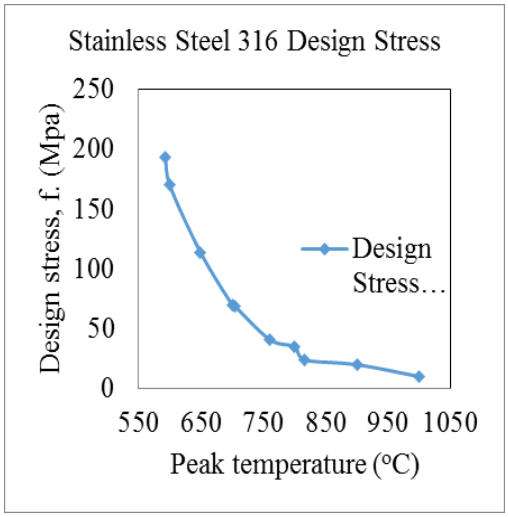
Summary of tabulated parameters:

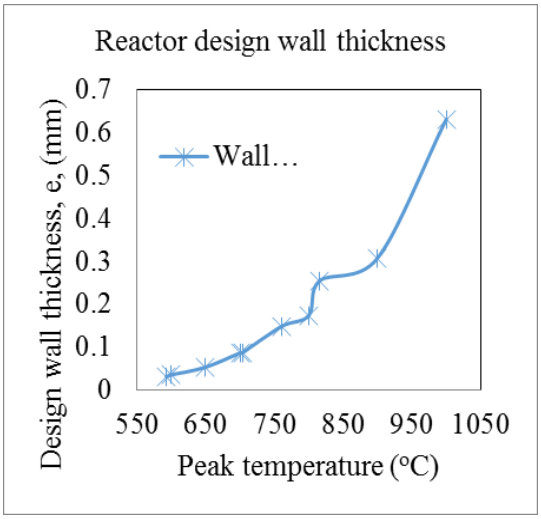
Parameters	Calculated parameters	Constructed reactor parameters
Design pressure	*p* = 10 bar	= 4 bar max. used
Design temperature	T = 1000 °C	= 950 °C max.
Wall thickness	e = 0.63mm	=2.2 mm (scaled up by 3.5)
Wall design stress	*f* = 10 MPa for 10000hr	

Table representing the Rupture-Strength Values for Stainless Steel 316 and the calculated wall thickness

Temperature	**Design stress (f) in Mpa for Stainless Steel 316**	**e**
(°C)	10,000 h	(mm)
593	193	0.031
600	170	0.035
649	114	0.053
700	70	0.086
704	69	0.088
760	41	0.148
800	35	0.174
816	24	0.255
900	20	0.308
1000	10	0.632

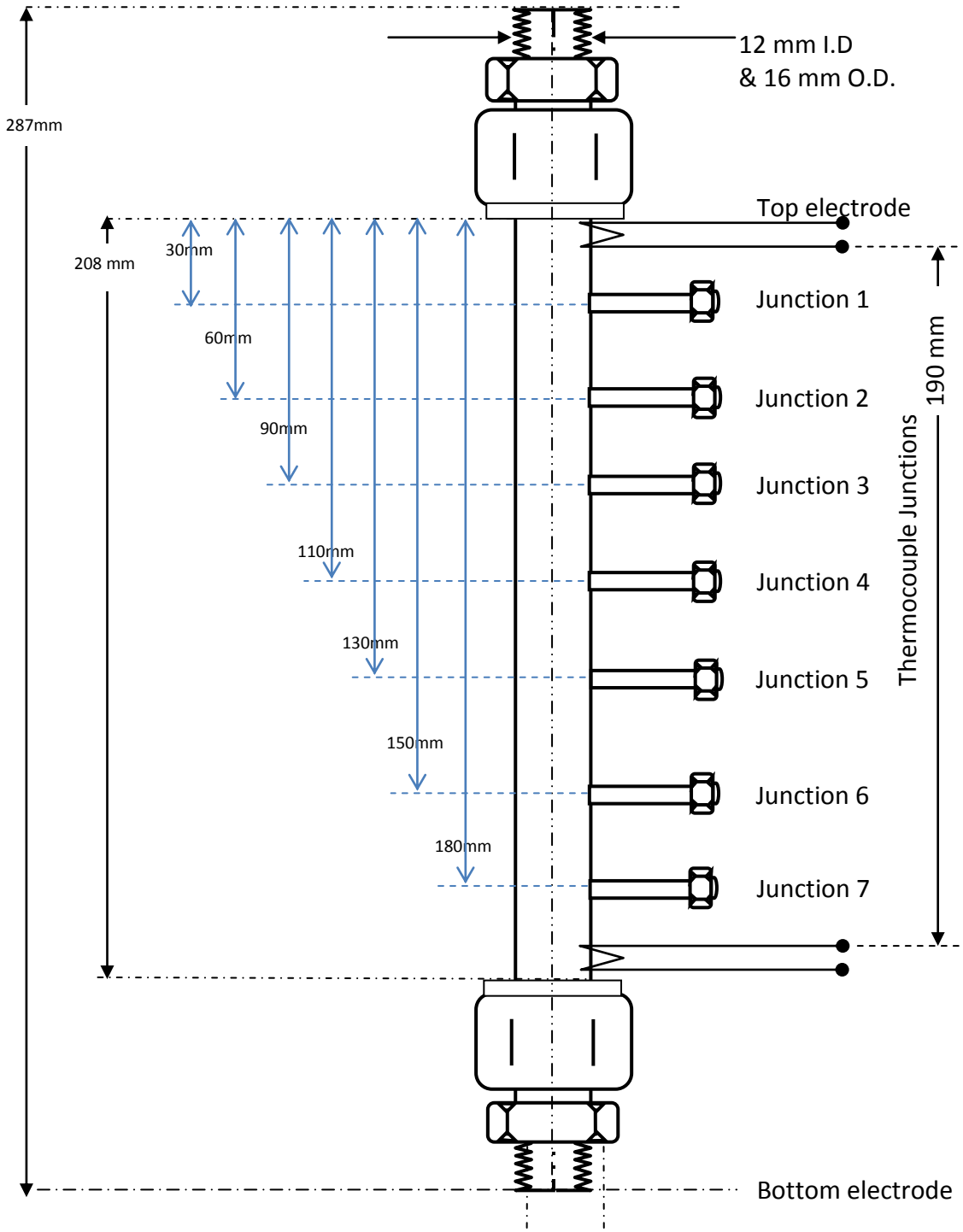
Design criteria: Comparisons of the adequacy design of this reactor is made with a similar incoloy800HT reactor tube previously used for the same purpose. The vessel size, thickness, geometry and operating conditions including the intended service life were put in consideration. The vessel requires periodic inspections after every 15 hours of use to monitor its condition. Given the reactor is operated at extreme temperatures and frequently subjected to temperature cycling, the Do/Di of the reactor constructed is greater than 1.3 (based on the mean diameter rules). This is to account for a factor of safety against gross plastic deformation and the reactor is only operated relatively low pressures. Also these conditions should allow a maximum design life for 10,000 hours. At no more than these conditions should the reactor be used any further.





Graphs of design stress and corresponding wall thickness at peak temperatures.

Appendix 5: General Arrangement of Thermocouples Along the Reactor

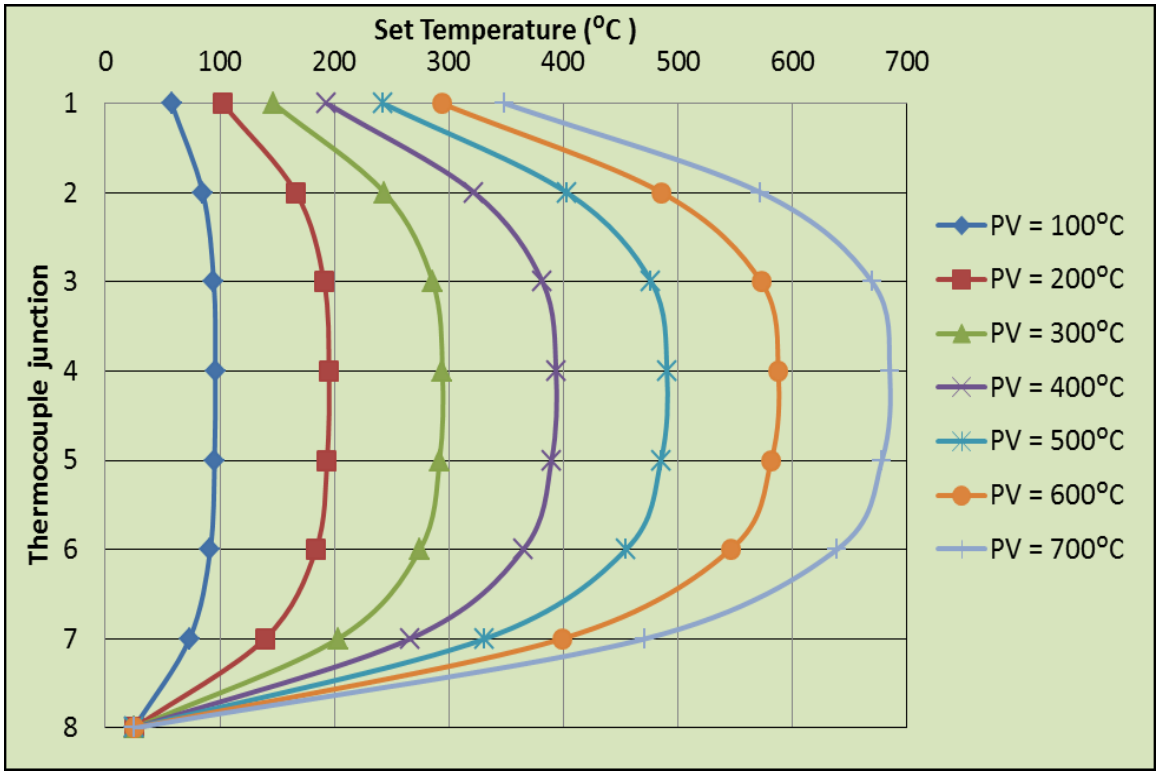


Dimensions for the scale up of the reactor and side thermocouples

Appendix 6: Heat conduction in the gas inside the heated reactor tube.

Practical approach:

Temperature profile recorded by the individual thermocouple junctions at various set temperatures



Comparision of temperatures between Metal only and with a Quartz tube reactor recorded at various thermocouple junctions and at set temperatures between 100 – 700 °C inclusive.

	SP	PV	Junct 1	Junct 2	Junct 3	Junct 4	Junct 5	Junct 6	Junct 7	Cold Junct
Metal	100	100	57	85	94	96	95	91	73	24
Quartz	100	100	53	77	89	93	95	93	84	25
	Differ.		4	8	5	3	0	-2	-11	-1
Metal	200	200	102	166	191	195	193	184	139	25

Quartz	200	200	94	154	184	192	194	189	156	26
	Differ.		8	12	7	3	-1	-5	-17	-1
Metal	300	331	147	244	286	294	292	275	203	25
Quartz	300	611	140	233	279	291	292	281	226	26
	Differ.		7	11	7	3	0	-6	-23	-1
Metal	400	471	193	322	382	394	390	365	266	25
Quartz	400	400	188	314	375	390	390	372	291	26
	Differ.		5	8	7	4	-0	-7	-25	-1
Metal	500	609	243	403	477	490	485	455	331	25
Metal	600	749	294	486	573	588	582	546	399	25
Metal	700	861	349	573	670	685	678	639	471	25
SP = Set Point, PV = Process Valuable, Junction = Thermocouple Junction.										

Theoretical approach for gas temperature at the various length of the tube:

The temperature distribution in the gas flowing though the tube can be explained by both conduction and radiation. In tubular gas preheating systems in a pipe, the raised temperature gas is obtained though heating the cylindrical gas. Assuming that heat transfer takes place by conduction from the walls of the tube within the gas in an axial direction, mass flow of the gas in an axial direction, and by the variables: mean flow rate (υ), mean gas density (ρ), mean gas thermal conductivity (k), inlet temperature (T_o), overall heat transfer coefficient (h) and mean heat capacity (C_p), the temperature of the gas along the length of the tube taking small lengths (z) can be determined using the approach bellow, assuming for each small segment the temperature of the cylindrical wall is maintained the same at T_w.

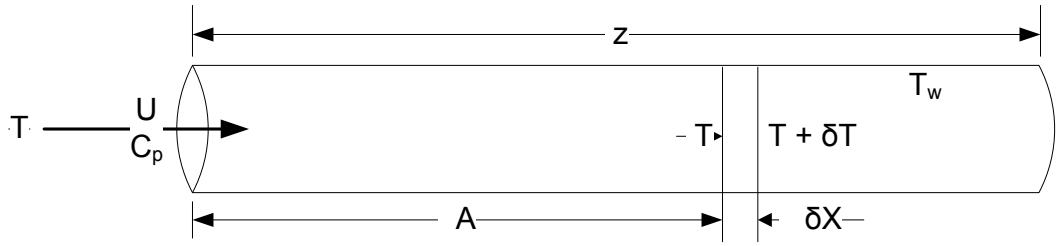


Figure 0:6: Heated Cylindrical Tube for Gas Heating

Using the symbols in the diagram given above and where A is the cross-sectional area of the pipe and d its diameter, the heat balance is derived from:

By conduction:

Input $-kA(dT)/(dx)$ Output: $-kA(dT)/(dx) + (d(-kA(dT)/(dx))dx)\delta x$

By mass flow:

Input: $u\rho C_pT$ Output: $u\rho C_p(T+((dT)/(dx))\delta x)$

Wall heat transfer:

Input: $\pi dh(T_w-T)\delta x$ Output: ---

At steady state the accumulation is zero.

Therefore:

$$-kA(dT)/(dx) + u\rho C_pT + \pi dh(T_w-T)\delta x = -kA(dT)/(dx) + (d(-kA(dT)/(dx))dx)\delta x + u\rho C_p(T+((dT)/(dx))\delta x)$$

Rearranging,

$$(d^2T)/(dx^2) - ((u\rho C_p)/(kA))*((dT)/(dx)) + ((\pi dh)/(kA))*(T_w-T) = 0$$

Substituting for $T_w-T = t$,

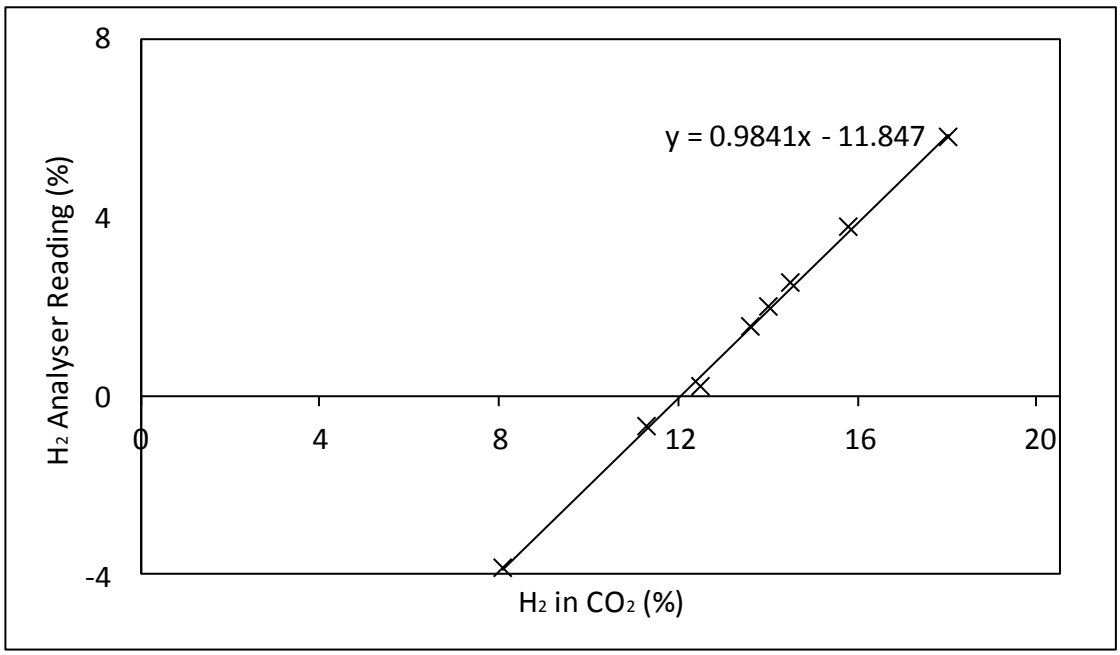
$$(d^2t)/(dx^2) - ((u\rho C_p)/(kA))*((dt)/(dx)) + ((\pi dh)/(kA))*t = 0$$

The temperature at each point can be obtained by deriving the second derivative and solving the equation say by separating the variables and using the variable conditions. The axial heat distribution can be found using “The Laplace Transformation” approach. A highest temperature was achieved in the centre of the tube.

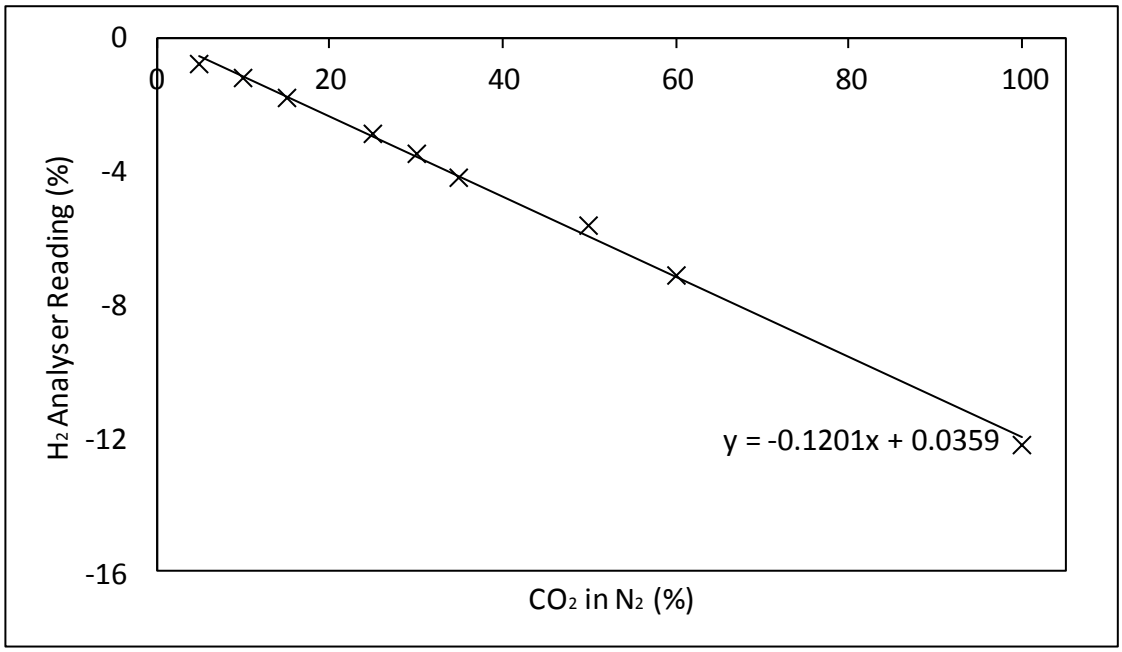
Appendix 7: Hydrogen Analyser Calibration

Determining the effect of CO_2 on the Hydrogen analyser

The hydrogen analyser used in this project operated using the principle of thermal conductivity. Given that the fuel gases CH_4 and CO_2 have a significant thermal conductivity factor, the analyser was calibrated to measure H_2 in CO_2 and the hydrogen reading when CO_2 in N_2 is passed through, to correct for the influence of CO_2 gas. CH_4 conductivity factor is quite significant but based on literature, thermodynamic modelling and our preliminary tests, the concentration of CH_4 in the product stream at the selected operating conditions for the experiments was insignificant. Therefore, the influence of CH_4 thermal conductivity on the H_2 analyser was neglected. A calibration curve for the hydrogen analyser was created from different mixtures and the correction factors were established from the graphs below.



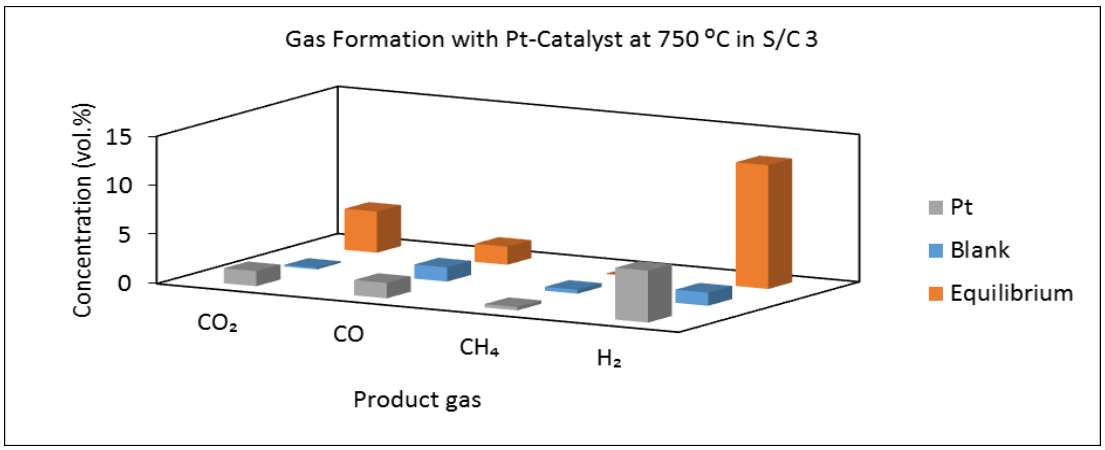
Calibration curve to estimate the hydrogen content in CO_2 gas in H_2 on the hydrogen analyser read.



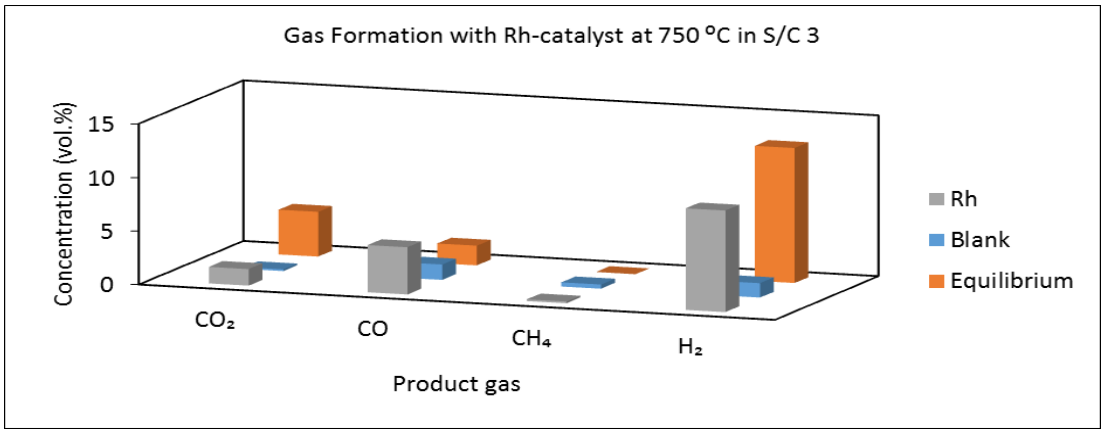
Calibration curve to estimate the hydrogen analyser reading when passing through carbon dioxide gas in nitrogen.

Appendix 8: Graphs Illustrating Gas Formation

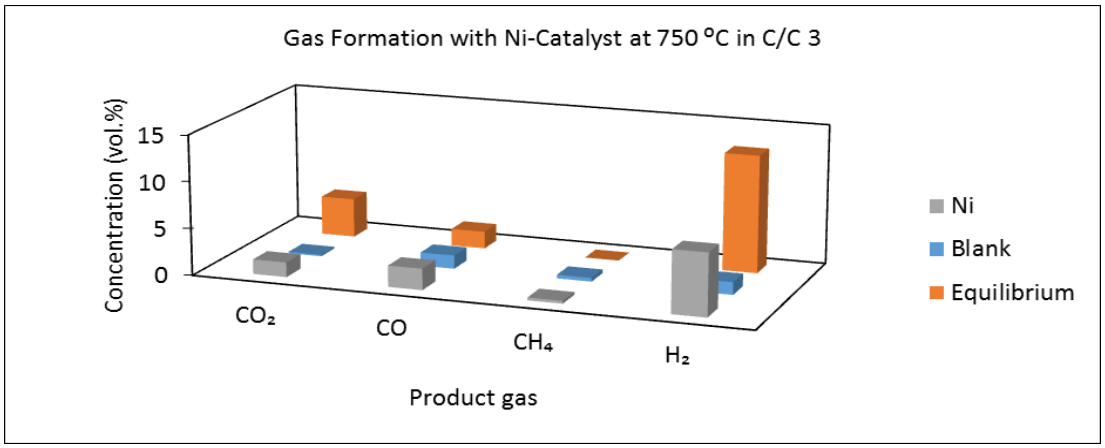
Graphs showing the gaseous results with the individual catalysts from experiments operated at 750 ^{o}C, S/C of 3 in N_2 carrier gas.



Gas Formation in N_2 with Pt-Catalyst at 750 ^{o}C

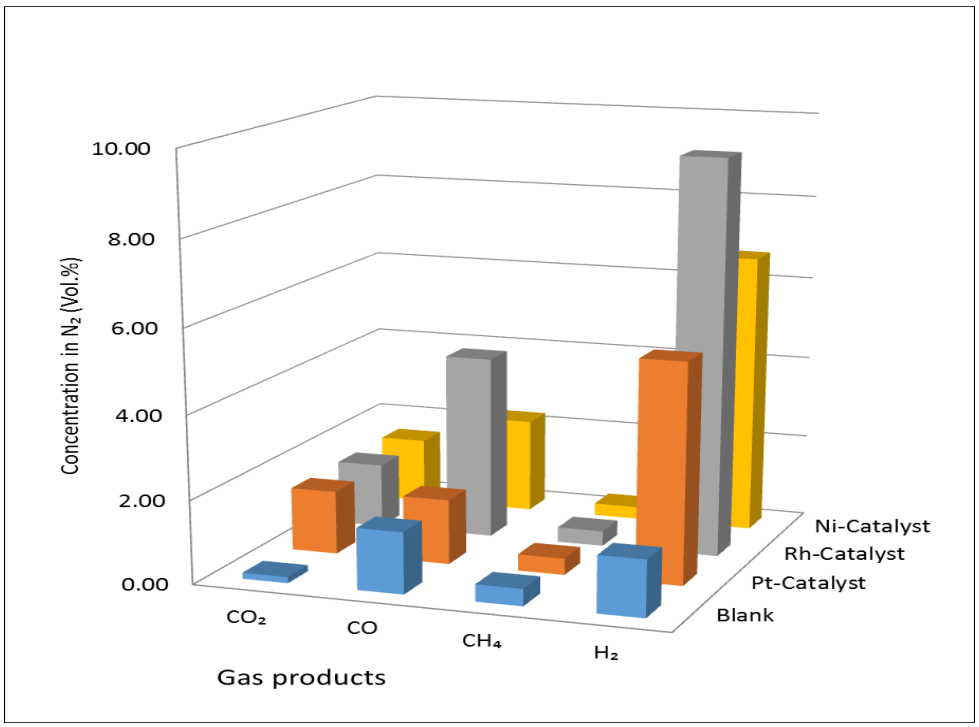


Gas Formation in N_2 with Rh-Catalyst at 750 ^{o}C



Gas Formation in N_2 with Ni-Catalyst at 750 ^{o}C

Combined gas results at 750 ^{o}C, S/C of 3 in N_2 carrier gas.



Gas Formation in an S/C of 3 at 750 ^{o}C with Pt, Rh and Ni catalyst.

Appendix 9: Graphical representation for data from Increasing S/C and Temperature.

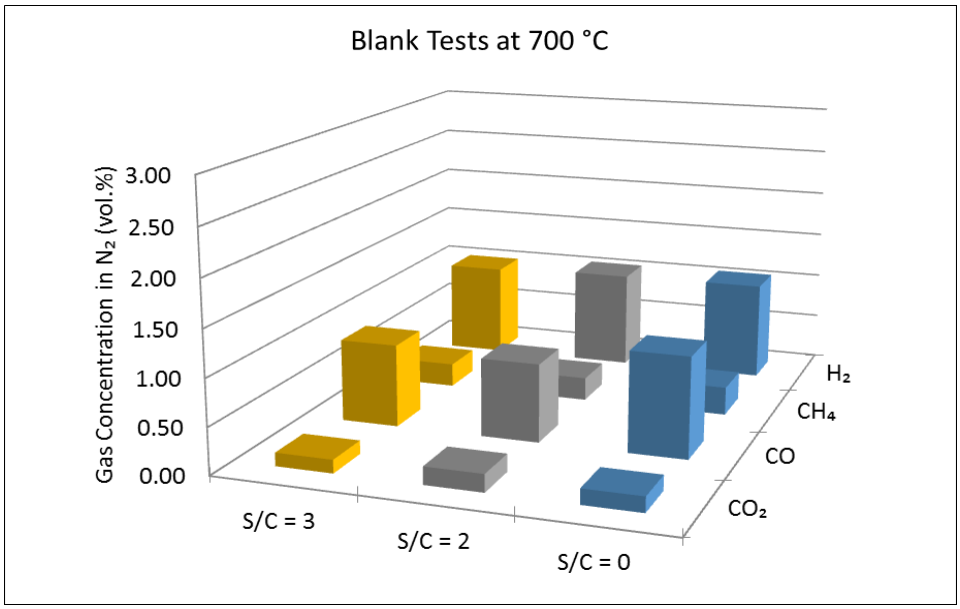


Figure 0:7: Gas Formation in N_2 due to the Effects of steam –to-carbon ratio at 700 °C

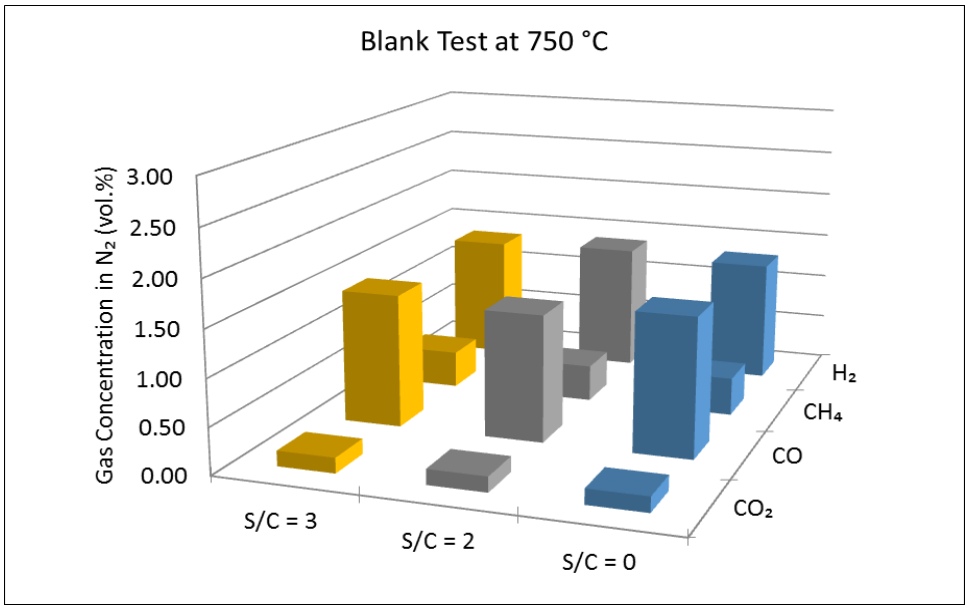


Figure 0:8: Gas Formation in N_2 due to the Effects of steam –to-carbon ratio at 750 °C

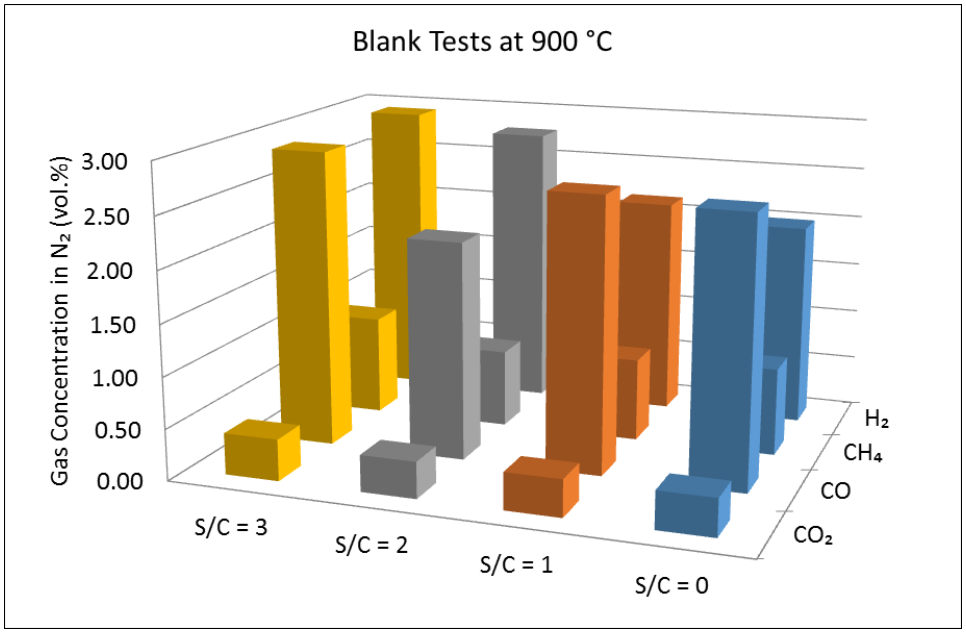


Figure 0:9: Gas Formation in N_2 due to the Effects of steam –to-carbon ratio at 900 °C